

I. A Unified Analysis of Converters  
with Resonant Switches

II. Input-Current Shaping for  
Single-Phase Ac-Dc Power Converters

Thesis by  
Stephen D. Freeland

In Partial Fulfillment of the Requirements  
for the Degree of  
Doctor of Philosophy

California Institute of Technology  
Pasadena, California

1988  
(Submitted October 20, 1987)

© 1988

Stephen D. Freeland

All Rights Reserved

*to my parents*

## Acknowledgements

I wish to thank my advisor, Professor R. D. Middlebrook, for the freedom to choose research topics, for his encouragement, and most of all for the excellent example he has set as a professor, a speaker, and as a writer.

I gratefully acknowledge the financial support of the National Science Foundation (graduate research fellowship), of Caltech (graduate teaching and research fellowships), of the ARCS Foundation (for two much-appreciated fellowships), and of the following corporations who supported my graduate research fellowships: Boeing Electronics, EG&G Almond Instruments, GTE Communication Systems, IBM, Merlin Gerin, Rockwell International, and Southern California Edison.

Every graduate of the Power Electronics Group owes a debt to his predecessors, who have left behind a well-organized laboratory, useful computer programs, and helpful hints on many procedures necessary for completing papers and theses. Thanks go to Zhe Zhang and Ramaswamy Mahadevan for developing graphics software and  $\text{\LaTeX}$  files that have been invaluable in the preparation of this thesis. I also wish to thank the members of the Power Electronics Group for helpful discussions, suggestions, and of course friendships. Special thanks must go to Billy Lau for his patient help with numerous computer and mathematical impasses.

Finally, this thesis could never have become a reality without the love and support of all my family and most especially that of my wife Janice and daughter Megan.

## Abstract

### Part I:

Quasi-resonant converters are a family of single-switch resonant dc-dc converters featuring zero-current or zero-voltage switching. Recognition of the topological structure uniting these resonant converters—and the rectangular-wave (PWM) converters on which they are based—leads to general models of their dc and low-frequency ac behavior.

An expression is derived that yields the dc conversion ratio of a quasi-resonant converter in terms of the well-known conversion ratio of the underlying PWM topology. A small-signal, low-frequency dynamic model is developed whose parameters also incorporate the PWM conversion ratio. The dc and ac models reveal that any quasi-resonant converter with a full-wave resonant switch has dc and low-frequency behavior identical to that of its PWM parent, with switching-frequency control replacing duty-ratio control. Converters with half-wave resonant switches behave more like PWM converters in discontinuous conduction mode or with current programming, exhibiting lossless damping in the small-signal model and output resistance at dc.

Although quasi-resonant converters come in an astounding variety of topologies, the dc (and to a large extent ac) behavior of these converters depends only on the underlying PWM topology and the class of resonant switch, and is unchanged by movement of the resonant reactances to various alternative positions.

### Part 2:

The distorted input-current waveforms of nonlinear electronic loads cause interference and lead to poor utilization of the utility power line, a situation that is rapidly becoming intolerable with the increased application of electronic loads. *Input-current shaping*, also known as power-factor improvement, addresses the problem of improving current

waveforms drawn from the power line. This study is restricted to single-phase ac-dc power conversion systems.

Current-shaping circuits are shown to fall into just a few categories with common features and limitations. In addition to the more common buck- and boost-based current-shaping converters, a class of circuits with “automatic” current shaping is presented and analyzed. A set of rules is derived for determining whether a particular dc-dc converter topology is suitable for use as a current-shaping ac-dc converter, and the rules are used to judge the suitability of several resonant converter topologies for this application. A new, low-cost converter is suggested that combines input-current shaping, isolation, and fast output-voltage regulation.

Input-current shaping requires that a converter store significant energy, leading to unfortunate size and weight restrictions. Additional implications of stored energy are examined, along with several methods of reducing the energy storage. It is shown that the ability of a current-shaping converter to regulate its output voltage is severely restricted as a result of the energy requirement. The methods and implications of introducing isolation to a shaping ac-dc converter are also studied.

# Contents

<b>Acknowledgements</b>	<b>iv</b>
<b>Abstract</b>	<b>v</b>
<b>I A Unified Analysis of Converters with Resonant Switches</b>	<b>1</b>
<b>1 Introduction</b>	<b>3</b>
<b>2 A Survey of Quasi-Resonant Converters</b>	<b>7</b>
2.1 The Quasi-Resonant Family of Converter Topologies . . . . .	7
2.2 Examples of Quasi-Resonant Topologies . . . . .	9
2.3 Control of Quasi-Resonant Converters . . . . .	15
2.4 Previous Methods of Analysis . . . . .	16
<b>3 The Resonant Switch in Its Environment</b>	<b>21</b>
3.1 Basic Approach . . . . .	21
3.2 Switching in PWM Converters . . . . .	23
3.3 Resonant Switches . . . . .	27
3.4 The Small-Ripple Approximation . . . . .	37
3.5 Averages of the Resonant-Switch Waveforms . . . . .	40
<b>4 Dc Analysis of Quasi-Resonant Converters</b>	<b>45</b>
4.1 Dc Conversion Ratio . . . . .	45
4.2 Relation to PWM Conversion Ratio . . . . .	51
4.3 Output Resistance . . . . .	51

<b>5</b>	<b>Small-Signal Analysis of Quasi-Resonant Converters</b>	<b>57</b>
5.1	Modelling Goal . . . . .	57
5.2	A Low-Frequency Model for the Resonant Switch . . . . .	59
5.3	Small-Signal Circuit Model . . . . .	62
5.4	Interpretation of the Small-Signal Model . . . . .	65
5.5	An Example . . . . .	70
5.6	Effects of the Resonant Reactances . . . . .	74
<b>6</b>	<b>Extensions of Resonant Switches</b>	<b>77</b>
6.1	Zero-Voltage Resonant Switches . . . . .	77
6.2	Multiple Conduction Cycles . . . . .	83
6.3	Converters with Transformers . . . . .	84
6.4	Converters with Multiple Switches . . . . .	86
<b>7</b>	<b>Experimental Verification</b>	<b>91</b>
7.1	Dc Measurements . . . . .	91
7.2	Small-signal Measurements . . . . .	93
7.3	Modulators for Frequency-Controlled Converters . . . . .	103
<b>8</b>	<b>Conclusion</b>	<b>109</b>
<b>II</b>	<b>Input-Current Shaping for Single-Phase Ac-Dc Power Converters</b>	<b>111</b>
<b>9</b>	<b>Introduction</b>	<b>113</b>
<b>10</b>	<b>The Input-Current Problem</b>	<b>119</b>
10.1	Definitions and Conventions . . . . .	119
10.2	The Capacitor-Input Filter . . . . .	123
<b>11</b>	<b>Input-Current Quality and Power Factor</b>	<b>127</b>
11.1	Power Factor . . . . .	127
11.2	Other Measures of Current Quality . . . . .	133



11.3 Sine Wave or Proportional Current? . . . . .	134
<b>12 Passive Current-Shaping Methods</b>	<b>139</b>
12.1 Inductor-Input Filter . . . . .	140
12.2 Resonant-Input Filter . . . . .	148
12.3 Ferroresonant Transformer . . . . .	153
12.4 Tuned Filters . . . . .	155
<b>13 Active Shaping Methods</b>	<b>161</b>
13.1 Buck-Based Topologies . . . . .	162
13.2 Boost-Based Topologies . . . . .	171
13.3 “Automatic” DCM Shapers . . . . .	182
<b>14 Using Dc-Dc Converters in Shaping Applications</b>	<b>193</b>
14.1 Environment of a Shaping Converter . . . . .	193
14.2 Necessary Conditions for Shaping . . . . .	197
14.3 Automatic Current Shaping . . . . .	200
14.4 Resonant Converters as Shapers . . . . .	202
<b>15 Energy Storage</b>	<b>213</b>
15.1 Minimum Stored Energy . . . . .	213
15.2 Energy Storage Methods . . . . .	214
15.3 Implications of Stored Energy . . . . .	220
<b>16 Isolation and Voltage Regulation</b>	<b>223</b>
16.1 Output Voltage Regulation . . . . .	223
16.2 Isolation . . . . .	237
<b>17 Conclusions</b>	<b>245</b>
<b>A Proofs of Topological Theorems</b>	<b>249</b>
<b>B Averaging and Its Effect on Low-Frequency Information</b>	<b>253</b>
B.1 Definition of Averaging . . . . .	254

B.2 Analysis of Averaging . . . . .	255
B.3 Example of Failed Averaging . . . . .	257
B.4 Example of Successful Averaging . . . . .	258
B.5 Conclusion . . . . .	258
<b>References</b>	<b>259</b>

**Part I**

**A Unified Analysis of Converters  
with Resonant Switches**



## Chapter 1

# Introduction

Making power converters smaller and lighter has always been a major goal of power electronics. It was in fact the need for lightweight, highly efficient converters in aerospace applications that stimulated the initial development of switched-mode power conversion. Reactances—capacitors and magnetic devices—account for a large part of the weight and volume of a switching converter, and these devices must shrink before a converter can be made significantly lighter or smaller. The size of reactive elements is determined chiefly by the switching frequency, and consequently methods of increasing converter operating frequencies have lately received a great deal of attention.

Until recently, semiconductor devices were the bottleneck preventing higher switching frequencies. Transistors turned OFF so slowly that operation above 100 kHz was impractical. With the continual improvement of power switching transistors, and in particular the recent introduction of power MOSFET devices, the speed of the semiconductor switch is no longer the limiting factor. Instead, parasitic effects such as transformer leakage inductance and transistor junction capacitance now limit the switching frequency in conventional (PWM) power converters.

*Resonant converters* [1,2,3] are power converters with quasi-sinusoidal waveforms, as opposed to the nearly rectangular waveforms of PWM converters. With quasi-sinusoidal waveforms, a resonant converter is insensitive to many of the parasitics that preclude high frequencies in more conventional topologies. In fact, some resonant topologies are able to use these same parasitics to advantage. Resonant converters therefore show great promise as a means of achieving higher switching frequencies, and experimental converters operating at radio frequencies have already been reported in the literature [3].

Dozens of PWM converter topologies are known, but until recently designers of resonant converters had only a few topologies available to them. A new class of dc-to-

dc resonant converters, first introduced in [4], changes this situation. The methods of [4] allow one to change any single-switch PWM converter into a “quasi-resonant” (or “resonant-switch”) converter by simple modification of the PWM topology. From each PWM converter, several different quasi-resonant converters can be constructed, so that now the designer may choose from more varieties of resonant than of PWM topologies!

Indeed, the many combinations of quasi-resonant topologies and operating modes can easily become confusing, and analyzing the behavior of each different variation soon becomes tedious. Despite their apparent differences, however, a common characteristic unites the various quasi-resonant converters: each is a modification of a PWM dc-to-dc converter topology. These PWM topologies are well-understood. Their dc and ac behavior is derived and interpreted without undue difficulty. More important, the behavior of PWM topologies is familiar to design and system engineers.

Analysis of resonant converters is traditionally difficult, with no practical alternatives to numerical analysis on a computer. The treatment of quasi-resonant converters presented here, however, has such attractive features as simplicity, clarity, and generality—features usually found only in models of PWM converters. It is no coincidence that the new quasi-resonant converter models share the advantages of their PWM counterparts. This useful feature is instead a direct result of treating the quasi-resonant converters as descendants of PWM topologies, rather than as “new” circuits.

The following chapters use the PWM heritage of quasi-resonant converters as the basis of a general dc and ac analysis. Instead of analyzing each converter separately, the fundamental principle behind these converters—the operation of the resonant switch—is studied first. The behavior of a particular resonant switch is then combined with the familiar characteristics of a parent PWM converter to yield a model for the corresponding quasi-resonant converter.

Chapter 2 briefly reviews quasi-resonant topologies and some techniques previously used to analyze resonant converters. Chapter 3 studies the behavior of a resonant switch in an environment representing a general PWM converter. In Chapter 4, a model of the resonant switch is used to find the dc conversion characteristics of quasi-resonant converters. These results have implications concerning the ability to operate converters in paral-

lel. Chapter 5, using the same resonant-switch model, derives approximate small-signal ac circuit models of quasi-resonant converters. Some extensions of the resonant-switch concept are considered in Chapter 6, where the modifications necessary to account for these extensions in the dc and ac analyses are given. Chapter 7 contains experimental results that confirm the validity of the approximate models derived in earlier chapters. Conclusions concerning the behavior of quasi-resonant converters and the means of modeling these topologies are given in Chapter 8.

Two notational conventions should be mentioned here. First, the term "PWM" (pulse-width modulation), is used to distinguish "conventional" converters from resonant or quasi-resonant converters. A PWM converter, for the present purposes, is a converter with approximately rectangular (often called "quasi-square wave") waveforms. Such converters are assumed to operate in the continuous conduction mode, so that the ripple voltages and currents in the reactive elements are small. Second, "quasi-resonant converter" is the name given to a complete power converter using resonant-switch technology. The term "resonant switch" refers to the configuration and operation of semiconductor switches and reactive elements that together produce quasi-sinusoidal waveforms. When a resonant switch is embedded in a PWM converter, the resulting circuit is called a quasi-resonant converter.

The approach used here is both simple and general as a result of the approximations used in the analysis. The price of using these approximations is a loss of accuracy under certain conditions, although both the arguments in Chapter 3 and the experimental results of Chapter 7 suggest that the approximations are well-justified in light of usual design practices. The cost of using approximations is far outweighed by the benefits of generality and simplicity, and the fact that these leave the engineer with an intuitive understanding of his design.

Numerical analysis and computer simulation will always be available for accurate evaluation of a particular converter's behavior. The models developed in this part provide an alternative: analytical tools for analyzing and, above all, understanding, quasi-resonant converters.





## Chapter 2

# A Survey of Quasi-Resonant Converters

Quasi-resonant converters were first introduced as a family in [4] with only two topological varieties of resonant switch. Since that time, new switch topologies have been steadily added, along with different methods of operation within a given topology. At least half a dozen varieties of resonant switch can currently be formed from any PWM converter, so that the total number of possible converters is very large indeed.

This chapter gives an overview of quasi-resonant converters, beginning with a discussion of the evolution of this converter family in Section 2.1. Section 2.2 presents examples of some of the many varieties of converters with resonant switches, while control of these converters is outlined in Section 2.3. In Section 2.4, published dc analyses of quasi-resonant converters are reviewed, and some possible methods of dynamic analysis are considered.

### 2.1 The Quasi-Resonant Family of Converter Topologies

The idea of a family of quasi-resonant converters came from considering two apparently different converters, those of [5] and [6]. Both of these converters exhibit the novel and useful feature of having the transistor switch turn both ON and OFF into zero current. This feature allows operation at higher frequencies as a result of reduced switching losses. In addition, the transformer leakage inductance, usually responsible for producing dangerous voltage spikes on the switches, instead has no qualitative effect and in fact can aid in generating the resonant waveforms.

The authors of [4] recognized that the principles underlying [5] and [6] could be applied to a variety of PWM converters, and in [4] they presented a family of converters characterized by two varieties of resonant switch, the “M-type” and the “L-type.”

The new family of converters was given the name “quasi-resonant” to distinguish them from continuously-resonating converters, such as those discussed in [1] and [2]. The two resonant switches described in [4] would later be classified as half-wave, zero-current, sinusoidal-wave switches.

It was soon realized that the resonant switch in [5] did not correspond to either of the half-wave switches of [4], but rather was a member of a new class of resonant switch—the “full-wave” switch [7]. The topological difference between the half- and full-wave switches is small, but the behavior of the two is very different. Most significantly, converters with full-wave switches exhibit no load-dependence in their conversion ratio, while half-wave converters are heavily load dependent. As shown in later chapters, half-wave switches add lossless damping to the converter dynamics, while full-wave converters behave very nearly like their (undamped) PWM parents.

The next addition to the quasi-resonant converter family came from application of duality principles to the zero-current switches. The result was a set of converters that turn both ON and OFF into zero voltage [8]. The main advantage of this technique is that the converter is insensitive to the parasitic drain-to-source (or collector-to-emitter) capacitance of the switching transistor, and in fact the capacitance can in some cases be used to produce the needed resonance. The dual of the zero-current resonant switch is called the zero-voltage resonant switch, and it too comes in half-wave and full-wave versions.

Finally, rules describing the most general resonant-switch topologies were published in [9]. Application of these rules brought recognition of several new ways of implementing previously known resonant switches, and it also led to the discovery of another species of resonant switch. All the “old” resonant switches were labeled “sinusoidal-wave” while the new versions were “square-wave” switches. A resonant switch, and the corresponding quasi-resonant converter, can therefore have any combination of the following characteristics: half-wave or full-wave, zero-current or zero-voltage, square-wave or sinusoidal-wave. Several topological variations of each of the resulting eight combinations also exist.

## 2.2 Examples of Quasi-Resonant Topologies

The buck topology is used in this section to illustrate qualitatively the several different varieties of resonant switches. The examples given are intended only to illustrate the qualitative behavior of the converters. Quantitative analysis is given in following chapters.

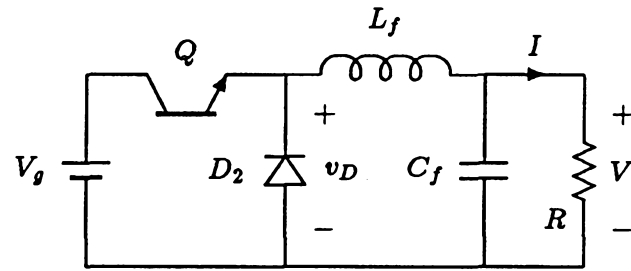
### PWM Buck Converter

The PWM buck converter appears in Fig. 2.1(a), with the pertinent waveforms shown in Fig. 2.1(b). All components are considered ideal, and in particular the transistor and diode have no ON voltage drops or switching losses.

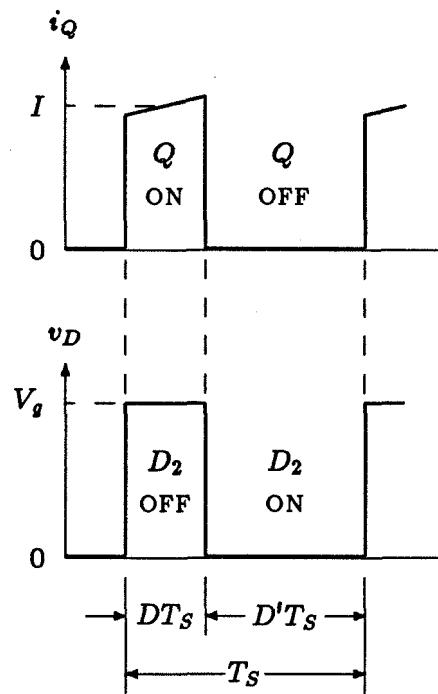
When the transistor  $Q$  is ON, the input voltage  $V_g$  is applied across the filter consisting of  $L_f$ ,  $C_f$ , and the load  $R$ . When  $Q$  is OFF, the diode  $D_2$  is ON, and the filter has zero volts across its input. If the inductor and capacitor are large enough that the filter corner frequency is much less than the switching frequency, then only the dc component of the rectangular voltage applied to the filter reaches the load. The output voltage then equals the average of the voltage waveform across the diode, and hence the conversion ratio  $V/V_g$  is equal to the transistor duty ratio  $D$ . To the extent that the inductor ripple current is small, both the transistor current and diode voltage waveforms are rectangular. The transistor must carry its full ON current immediately after turning ON, and it must interrupt this current upon turning OFF.

### Zero-Current, Sinusoidal-Wave Resonant Switches

A quasi-resonant buck converter using a zero-current, sinusoidal-wave resonant switch is shown in Fig. 2.2(a). In forming the resonant switch, diode  $D_1$  has been added to transistor  $Q$  and resonant elements  $L_r$  and  $C_r$  have also been added. The current and voltage waveforms of this converter, shown in Fig. 2.2(b), are quasi-sinusoidal. The resonant switch is called "zero-current" because the transistor current is zero when the transistor first turns ON, and the current afterward rises with a finite slope, in contrast to the PWM buck converter. The transistor turns OFF into zero current as the resonant circuit brings the current back to zero automatically. The losses incurred during the



(a)



(b)

Figure 2.1: The PWM buck converter (a), and its switch waveforms (b).

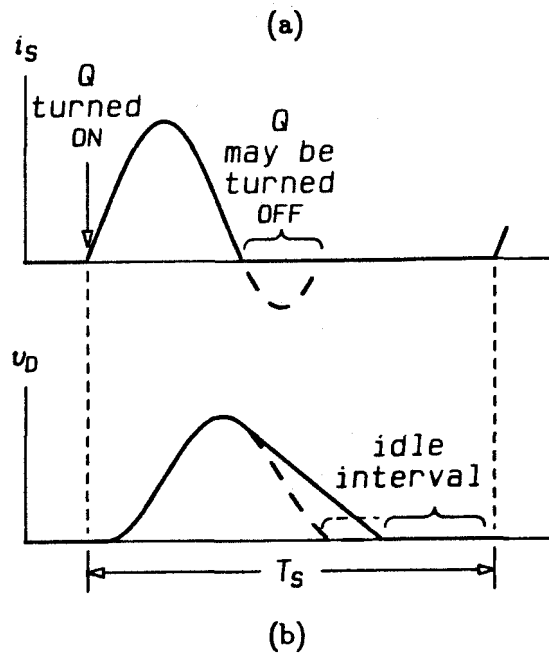
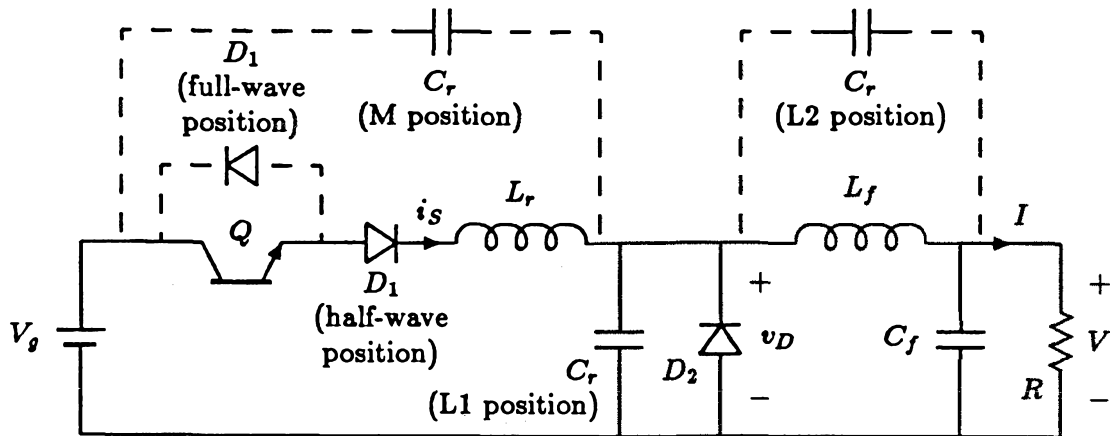


Figure 2.2: (a) A buck converter with a zero-current, sinusoidal-wave resonant switch. Dashed lines indicate alternate component positions as described in the text. (b) Waveforms of the half-wave (solid lines) and full-wave (dashed lines) zero-current resonant switch.

switching transitions are therefore much less than in the case of the PWM converter.

Diode  $D_1$  and transistor  $Q$  form a two-quadrant switch. When  $D_1$  is in *series* with  $Q$ , as shown with solid lines in Fig. 2.2(a), the switch is two-quadrant in voltage, and turns OFF when the current  $i_S$  first reaches zero. Diode  $D_1$  prevents the current  $i_S$  from falling below zero, as shown by the solid curve of Fig. 2.2(b). The transistor can be turned OFF with zero current at any time while  $D_1$  is blocking. This configuration is called a *half-wave* switch, because the current  $i_S$  completes slightly more than one-half of a sinusoidal cycle before being interrupted.

If instead  $D_1$  is in *parallel* with  $Q$ , as shown by dashed lines in Fig. 2.2(a), the resulting switch is two-quadrant in current. The switch current  $i_S$  is interrupted by  $D_1$  upon reaching zero from below, as shown in the dashed curve of Fig. 2.2(b). Once again,  $Q$  can be turned OFF at any time during the interval while  $D_1$  is blocking. This resonant switch is called a *full-wave* switch, as  $i_S$  completes nearly a full cycle at the resonant frequency.

Again assuming that the corner frequency of the  $L_f$ - $C_f$ - $R$  filter is much lower than the switching frequency, the output voltage is the average of the voltage  $v_D$  across the diode  $D_2$ , and in this case is a rather complicated function of the switching frequency and the values of the resonant elements  $L_r$  and  $C_r$ . The conversion ratio also depends on the load in the case of the half-wave switch. This is in contrast to the PWM buck converter in which the conversion ratio is independent of both switching frequency and the load. Surprisingly, in light of the small visible difference between the half- and full-wave waveforms of Fig. 2.2(b), the full-wave switch has the desirable characteristic of producing a conversion ratio virtually independent of the load.

The particular resonant-switch topology indicated by the solid lines of Fig. 2.2(a) is labeled "L1-type" in [9]. In any quasi-resonant converter, the capacitor  $C_r$  may occupy one of several positions. Two alternative locations in the buck topology are indicated by dashed lines in Fig. 2.2(a), labeled "L2" and "M" according to the convention of [9]. Practical considerations make some capacitor locations preferable to others. For example, the "L2" location allows resonant-frequency currents in the capacitor  $C_f$  and therefore produces more resonant-frequency noise in the load voltage than do the other

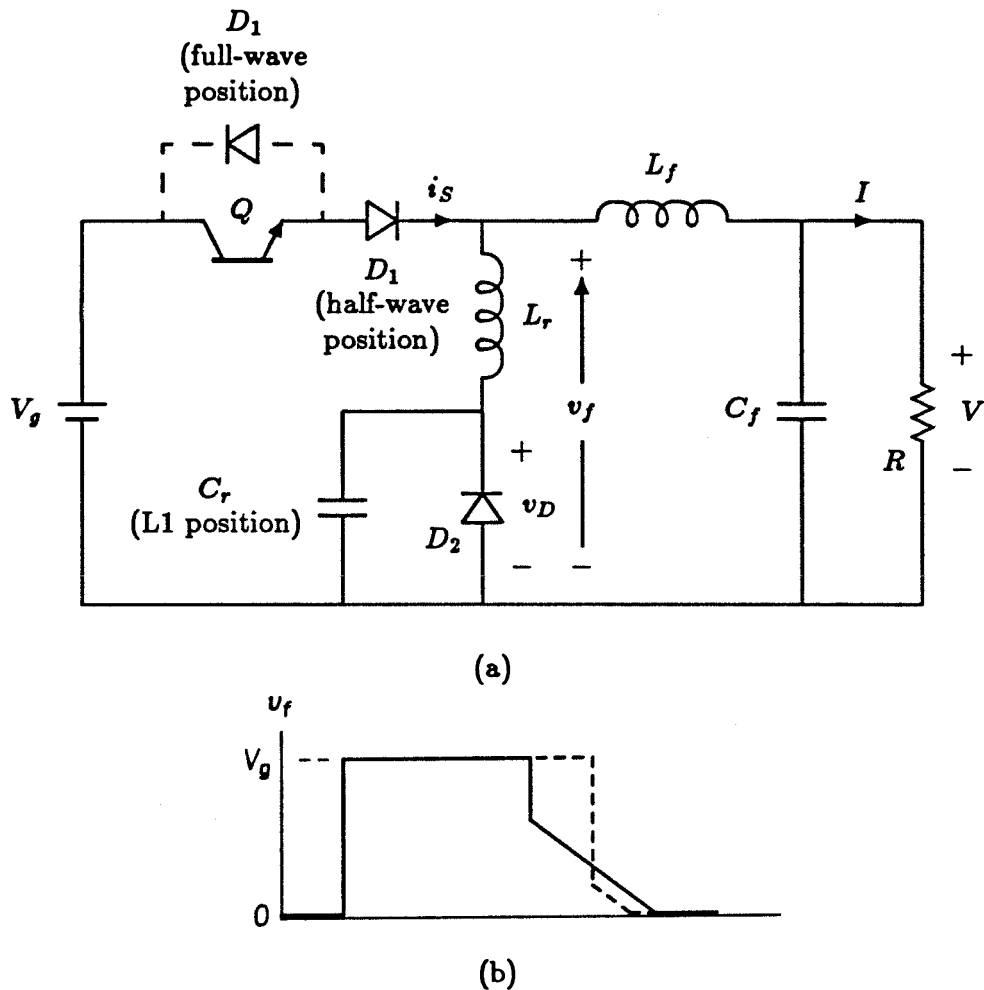


Figure 2.9: A buck converter with a zero-current, square-wave resonant switch (a). The voltage applied to the output filter is a rectangular waveform (b). Dashed lines indicate locations and waveforms corresponding to a full-wave switch.

two configurations. An important result, derived in Chapter 4, is that all the topological variations of a quasi-resonant converter ( $L_1$ ,  $L_2$ ,  $M$ , etc.) produce the same voltage conversion ratio,  $V/V_g$ .

### Square-Wave Switches

Moving the resonant inductor from its location in Fig. 2.2(a) to that of Fig. 2.3(a) produces a square-wave resonant switch, also of the zero-current variety. The waveforms  $i_S$  and  $v_D$  are unchanged but now the voltage  $v_f$  across the output filter—in this case

the combined voltages of  $L_r$  and  $D_2$ —is quasi-rectangular, as shown in Fig. 2.3(b). In the sinusoidal-wave converter of Fig. 2.2(a),  $v_f$  is equal to  $v_D$ , the sinusoidal waveform of Fig. 2.2(b). Despite the visible differences between these two  $v_f$  waveforms, both have the same average value, and hence the voltage conversion ratio is the same for the sinusoidal-wave and square-wave resonant switches. The square-wave switch, like the sinusoidal-wave variety, has both half-wave and full-wave variations and allows several locations of the resonant capacitor  $C_r$ . The full-wave location of  $D_1$  and the corresponding waveform of  $v_f$  are indicated by dashed lines in Fig. 2.3.

### Zero-Voltage Switch

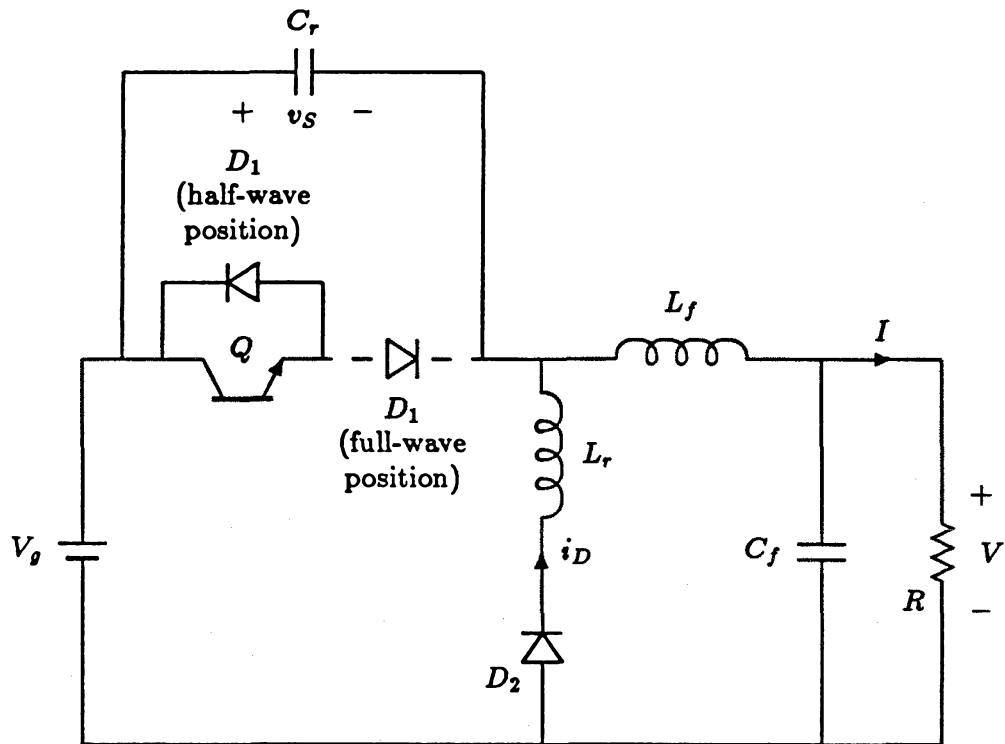
Figure 2.4 illustrates the zero-voltage resonant switch, with the sinusoidal-wave variety shown. In this configuration, the transistor switch turns both ON and OFF into zero voltage. The switch waveforms have the same shapes as those of the zero-current converters in Figs. 2.2 and 2.3, but current and voltage are interchanged. Like the zero-current resonant switch, the zero-voltage switch can be either half-wave or full-wave. The latter case is indicated by dashed lines in Fig. 2.4. An advantage of the half-wave configuration is that the capacitance of the transistor itself can be used as part (or all) of the resonant capacitor. In the PWM buck converter, the energy in this capacitance is lost every time the transistor turns ON, a serious drawback at high switching frequencies.

Zero-voltage resonant switches also come in square-wave configurations and with the usual freedom to place the resonant capacitor and inductor in any of several possible locations.

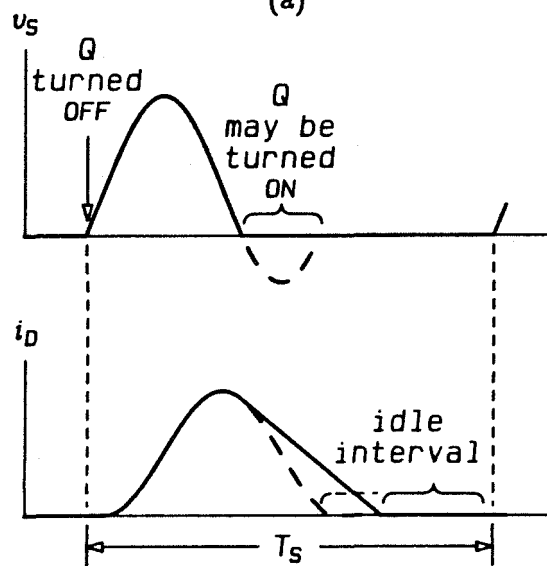
## 2.3 Control of Quasi-Resonant Converters

A quasi-resonant converter must be controlled by varying the switching frequency. As seen from the discussion of Section 2.2 and the waveforms of Fig. 2.2(b), once a zero-current switch is turned ON, the waveforms progress without benefit of any control until the cycle is complete and the switch again reaches the idle state ( $i_S$  and  $v_D$  both zero). The time taken for the cycle to evolve and the switch to return to its idle state is a function of many parameters, but the important thing is that there is no direct





(a)



(b)

Figure 2.4: (a) A buck converter with a zero-voltage, sinusoidal-wave resonant switch. (b) Switch waveforms of the half-wave (solid curves) and full-wave (dashed curves) zero-voltage resonant switch.

control over this time. The current  $i_S$  is interrupted by  $D_1$ , and  $Q$  must be turned OFF while  $D_1$  is blocking, so that the turn-OFF of  $Q$  cannot be a control variable. The only way to regulate a zero-current quasi-resonant converter—to exercise control over its output voltage—is to choose the time when the idle period is ended and the switch  $S$  is turned ON. This is equivalent to controlling the length of the idle interval, or to controlling the switching frequency. A similar situation is found in PWM converters using constant ON-time control.

For zero-voltage converters, the resonant cycle is initiated by turning OFF the switch. The switch must be turned back ON at a time determined by the evolution of the resonant-switch waveforms. Here again, one has no direct control over the OFF time of the switch, and the switching frequency is the only available control variable.

## 2.4 Previous Methods of Analysis

The reason for turning the PWM switch into a resonant switch is to produce quasi-sinusoidal switch waveforms, with corresponding lower switching loss. The waveforms of Figs. 2.1 through 2.4 show that replacing a PWM switch with a resonant switch changes considerably the “internal” behavior of a power converter. What does such a substitution do to the “external” behavior, such as the voltage conversion ratio and the input and output impedances? The designer of a quasi-resonant converter, and the system engineer who specifies it, must understand the converter’s dc and dynamic behavior.

Expressions for the dc conversion ratio of several quasi-resonant converters are available [4,7,8], but the dynamics of these converters are not known analytically. This section reviews the existing dc analyses of quasi-resonant converters, and considers the suitability of different methods of dynamic analysis.

### 2.4.1 Dc Analysis

Included in [4], [7], and [8] are expressions for the dc conversion ratio  $M = V/V_g$  of three quasi-resonant converters, those based on the buck, boost, and buck-boost PWM topologies. These expressions are found by equating the input energy with the output energy over a single switching cycle. Unfortunately  $M$  is an implicit function of the load

and the switching frequency, but then this is not surprising since other resonant converters also have implicit conversion ratios [10]. The equations describing the conversion ratio of a quasi-resonant converter are relatively simple compared to those in [10].

The dc analyses of [4]–[8] are made tractable by the assumption that certain reactive elements in the converter (excluding the resonant inductor and capacitor) have constant voltages or currents. This assumption limits the resonant switch to a second-order circuit and allows relatively simple calculation of the switch waveforms. An equivalent assumption is used in Chapter 3 of this part. What Chapter 3 has to offer is not more accurate expressions, but a more general and convenient dc analysis, with the ability to find the conversion ratio of *any* quasi-resonant converter given the form of resonant switch used and the well-known conversion ratio of the underlying PWM topology.

#### 2.4.2 Ac Analysis Methods

Dynamic (or ac) analysis of power converters is a difficult task because the circuits involved are nonlinear (with respect to the control variables) and time-varying. Large-signal analysis is extremely difficult analytically, and is usually restricted to computer simulation. Small-signal analysis, however, is sometimes analytically possible given certain simplifying approximations. A small-signal analysis is useful for studying the effects of small perturbations and stability about an operating point.

State-space averaging [11], perhaps the most popular method of analytical dynamic analysis for switching converters, cannot be used with resonant converters of any kind. State-space averaging assumes that the converter states have small, or at least linear, ripple waveforms. This is equivalent to requiring that the switching frequency be much higher than the natural frequencies of the networks formed by each position of the switches. Resonant converters, however, by definition have quasi-sinusoidal waveforms in the resonant reactances. These waveforms violate the small-ripple approximation and invalidate the averaging step that makes state-space averaging such a general and convenient analysis method.

## Vorpérian's Method for Resonant Converters

In a small-signal dynamic analysis of the series and parallel resonant converters [12], Vorpérian uses a dynamic modeling method that circumvents the limitations of state-space averaging. In that work, the state-space matrix equations describing each interval of a switching period are written, and the *averages* of the desired output quantities are expressed in terms of the state variables. These equations are perturbed and the small-signal assumption then allows linearization of some (but not all) of the exponential matrices. (The linear-ripple assumption of state-space averaging allows linearization of *all* exponential matrices). Vorpérian's method results in a linear discrete system giving the small-signal variations of the average of the output quantities over each switching period. Vorpérian predicted the frequency response of his converters by replacing the transform variable  $z$  of the discrete system with  $e^{j\omega T_s}$ , with  $F_s = 1/T_s$  the steady-state switching frequency. For frequencies  $\omega/2\pi$  much less than the switching frequency, however, the discrete averages of the outputs might be taken to constitute continuous variables, and the resulting model would be continuous as well as linear.

Vorpérian's method suffers from one great disadvantage—complexity. Calculation of the ac response requires evaluation of exponential matrices whose order is the number of reactances in the converter. The analysis therefore must be performed numerically on a computer. This leads to two problems. First, some of the states in a resonant converter—the “resonant” variables—change rapidly, while others—the “filter” variables—change much more slowly. This separation of the system time constants makes numerical evaluation of the exponential matrices difficult. Second, and much more important, the numerical analysis is of little help in leading the designer to an understanding of how individual components affect the converter performance.

The great complexity of Vorpérian's dynamic model stems from something of an inconsistency in the assumptions behind the dc and the ac models. In the dc analysis, the nonresonant reactances of the converter are assumed to have small ripple. This approximation is abandoned in the ac analysis, and instead the full power—and complexity—of exponential matrix equations is brought to bear on every reactance in the converter.

Vorpérian's method potentially gives very accurate results because it allows for large

ripple in all the reactances, but the method leaves the designer wishing for a simpler approach. Such an approach might be less accurate, but would use simple analytic expressions or circuit models to provide insight and understanding and therefore be a useful design tool.

### Resonant-Cell Method

Another resonant converter topology is the class-E dc-to-dc converter [3,13]. This converter, a modification of a switching radio-frequency amplifier, uses a resonant inverter to generate sinusoidal currents. These currents are rectified and filtered to accomplish dc-to-dc conversion. The transistor in a class-E converter turns both ON and OFF into zero voltage, much like a zero-voltage resonant switch. Because the class-E converter cell feeds a filter with sinusoidal currents, the analysis is quite a bit more complicated than for the resonant switch, which feeds reactances having nearly dc voltages and currents.

Small-signal ac analysis of a class-E converter is undertaken in [13]. The key to the method is the separation of the converter elements into two kinds—those with high-frequency, resonant waveforms, and those with small-ripple, quasi-dc waveforms. The analysis proceeds by assuming dc quantities in the small-ripple elements, calculating the complicated, rapidly-varying waveforms in the high-frequency elements, and then evaluating the *averages* of these waveforms. The average values are expressed as a function of the “external” quasi-dc quantities, and these expressions are perturbed and linearized as functions of the dc quantities and the switching frequency (the control variable for this converter). The high-frequency elements are then absorbed into a “cell,” a network of controlled sources with variations of the external dc quantities as inputs and the perturbations of the average resonant waveforms as outputs. This cell is embedded in the external network of filter elements with small ripple, resulting in a linear model of the entire converter. At frequencies well below the switching frequency, the discrete averages of the cell’s outputs may be considered as continuous waveforms, and the resulting model is both linear and continuous.

The separation of the converter into large- and small-ripple elements, which forms

the basis of this analysis method, relies on an approximation, certainly, but one that is usually satisfied in practice. Failure to invoke this approximation means that any analysis must be done on a computer, either as numerical evaluation of matrix equations, or as direct simulation of the converter.

While Vorpérian's method is potentially more accurate, it provides much less insight than the more approximate method of [13]. In addition, numerical difficulties caused by the separation of time constants in the converter may ultimately result in worse accuracy than from an approximate method that removes the high-frequency time constants by averaging.

The small-signal ac characteristics of quasi-resonant converters will be studied in Chapter 5 using a method closely related to that of [13]. Chapter 5 also uses a circuit-oriented approach, putting the information gained from manipulating equations back into the circuit model of the resonant switch.

## Chapter 3

# The Resonant Switch in Its Environment

Quasi-resonant converters can of course be analyzed from first principles, with each entire converter considered as a new and separate entity. The objective here, however, is to demonstrate and make use of the relation between PWM and quasi-resonant converters. With that goal in mind, each quasi-resonant converter is treated as the result of a topological modification of a PWM converter, emphasizing the *similarities* rather than the *differences* between the two converter classes.

Sections 3.1 and 3.2 consider the process of switching in PWM converters. Topological rules are derived governing the relation of the PWM switch to the reactances in the converter. In Section 3.3, these rules are combined with similar conditions for resonant switches to yield the behavior of any resonant switch. The important result of this section is that all topological variations of a resonant switch produce the same *average* effects. The result is significant because average quantities form the basis of the dc and ac analyses in following chapters. The expressions for the averages of the resonant-switch variables are derived in Section 3.5.

### 3.1 Basic Approach

Switched-mode power converters are nonlinear, time-varying systems with discontinuous structure. In most converters, the semiconductors alone are responsible for these unfortunate properties; if the semiconductor switches are opened or shorted, a well-behaved linear network is left behind. The switches cannot in practice be removed—they are essential to the power conversion process—but they can be *conceptually* separated and treated apart from the rest of the converter. This approach proves useful in studying PWM converters, and it is indispensable when studying quasi-resonant converters.

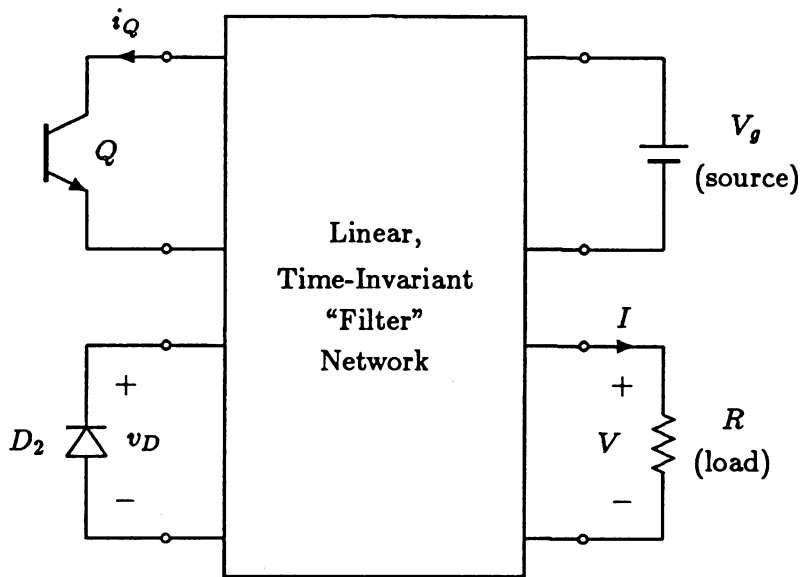


Figure 3.1: View of a PWM converter as a linear network connected to the source, load, and semiconductor switches.

Separation of the switch from the rest of a PWM converter is illustrated in Fig. 3.1. The figure illustrates pictorially that any PWM converter (with a single transistor and rectifier) may be considered as a linear network driven by the source voltages  $V_g$ , the diode voltage waveform  $v_D$ , and by the transistor current waveform  $i_Q$ . The switch waveforms  $v_D$  and  $i_Q$  are not independent. They are functions of the control scheme and the waveforms within the linear network, so that the perspective of Fig. 3.1 may not always be useful for directly determining the converter input, output, or control properties. Figure 3.1 nevertheless represents a powerful means of viewing the role of switching in a PWM converter, and the role the linear network plays in filtering the switching waveforms.

When the focus shifts to resonant switches in Section 3.3, it will be seen that the model of Fig. 3.1 applies equally to quasi-resonant converters. The conceptual separation of switch and linear network is the foundation of the dc and ac analyses of quasi-resonant converters in following chapters. The model of Fig. 3.1 should therefore be kept in mind, for it is a pictorial representation of the philosophy underlying the following treatment of both PWM and quasi-resonant converters.



## 3.2 Switching in PWM Converters

While any PWM converter may be transformed into a quasi-resonant converter, the models developed in later sections require a slightly restricted class of PWM converters. Section 3.2.1 explains the restrictions needed for the discussion of PWM switch operation in Section 3.2.2.

### 3.2.1 Definition of a PWM Converter

PWM converters come in many varieties, some “basic” and some more complicated. Although many of the more complex topologies can be converted into quasi-resonant converters, the basic function and behavior of quasi-resonant converters is best understood by restricting discussion to relatively simple PWM converters. The class of converters allowed is set forth in the following definition.

**Definition 1:** A PWM converter is a dc-to-dc power converter with 100% ideal efficiency, consisting of *only* the following elements:

1. A single transistor  $Q$ .
2. A single diode rectifier  $D_2$ .
3. An input voltage source,  $V_g$ , with small voltage ripple.
4. Linear capacitors with small ripple voltages.
5. Linear inductors with small ripple currents. No coupling is allowed.
6. A load,  $R$ , which is either in a loop of capacitors and possibly  $V_g$ , or is in a cut-set of inductors (this establishes small ripple voltage and current at the load).

“Ideal efficiency” means the efficiency when all components are ideal. In particular, the transistor and diode are assumed to have negligible switching and conduction losses. The restriction to a single transistor and diode, and the no-coupling requirement of item 5, are imposed to clarify the arguments that follow. They may be removed in certain cases. Chapter 6 gives an example of a quasi-resonant converter based on a PWM converter with multiple switches and magnetic coupling.

The small-ripple restrictions of items 4, 5, and 6 above form the heart of the present analysis. For the present, they are included without justification in the definition of a PWM converter. The validity and implications of the small-ripple approximation are discussed at length in Section 3.4.

Note that the load of item 6 need not be a linear resistance. At dc, the load has a dc voltage  $V$  and dc current  $I$  whose ratio is the *dc* load resistance, denoted  $R$ . Under small-signal modulation, the slope of the load  $V$ - $I$  characteristic defines the *small-signal* load resistance,  $R_L$ , which will differ from  $R$  for a nonlinear load.

The terms “PWM converter” or “PWM switch” will henceforth refer to PWM converters that satisfy the six requirements above.

### 3.2.2 Operation of the PWM Switch

From the six restrictions in the definition of a PWM converter, several conclusions can be drawn, concerning both the topology and the behavior of a PWM switch. The topological results are expressed in the following two theorems. Proofs are given in Appendix A.

**Theorem 1:** *The transistor  $Q$ , the diode  $D_2$ , and a set of capacitors with total voltage  $V_{\text{off}}$  form a loop. The source  $V_g$  may also be included in the loop, with its voltage included in  $V_{\text{off}}$ .*

**Theorem 2:** *The transistor  $Q$ , the diode  $D_2$ , and a set of inductors with total current  $I_{\text{on}}$  form a cut-set.*

The buck converter of Fig. 2.1 clearly satisfies Theorems 1 and 2. In that circuit, the loop of Theorem 1 contains  $Q$ ,  $D_2$ , and  $V_g$ , while  $Q$ ,  $D_2$ , and  $L_f$  form the cut-set of Theorem 2.

Kirchhoff’s voltage law for the loop of Theorem 1 gives

$$v_Q + v_D = V_{\text{off}} , \quad (3.1)$$

where  $V_{\text{off}}$  is positive by choice of the loop orientation. When  $Q$  is ON,  $v_Q = 0$  and  $v_D$  must be  $V_{\text{off}}$ . When  $D_2$  is ON,  $Q$  supports  $V_{\text{off}}$ . Kirchhoff’s current law for the cut-set

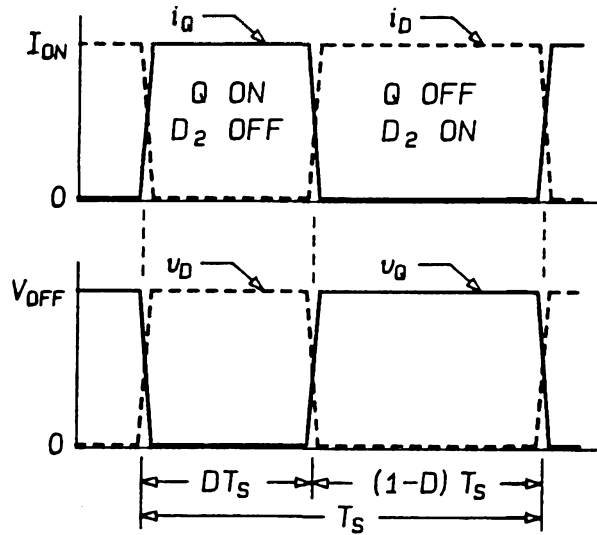


Figure 3.2: Switching waveforms in a PWM converter.

of Theorem 2 may be written

$$i_Q + i_D = I_{on}, \quad (3.2)$$

where  $I_{on}$  is positive by choice of the cut-set orientation. When  $Q$  is OFF,  $i_Q$  is zero, so that  $i_D$  must equal  $I_{on}$ . Similarly, when  $D_2$  is OFF,  $i_D$  is zero and the transistor current is equal to  $I_{on}$ .

For 100% efficient power conversion, the transistor and diode must operate in the switched mode, *i.e.*, they must be either ON, with zero voltage (ideally), or OFF, with zero current. This fact, together with Eqs.(3.1) and (3.2), implies that either the transistor or diode, but not both, must be ON at any given time. This in turn reveals that the PWM converter has only two states, one with  $Q$  ON and  $D_2$  OFF, and the other with  $Q$  OFF and  $D_2$  ON. The duty ratio  $D$  is defined as the fraction of a switching period (the interval between each turn-ON of the transistor) in which the transistor is ON.

The waveforms of Fig. 3.2 summarize these results. The transistor and rectifier voltages and currents are rectangular. When either device is ON it carries current  $I_{on}$ , and when OFF it is subject to a voltage  $V_{off}$ . The device currents are constant during the ON-time because they are supplied by a constant current source—the one or more “stiff” inductors that provide  $I_{on}$ . Similarly, the OFF voltages are constant at  $V_{off}$  because they are imposed by the input voltage source and/or a series of “stiff” capacitors, each

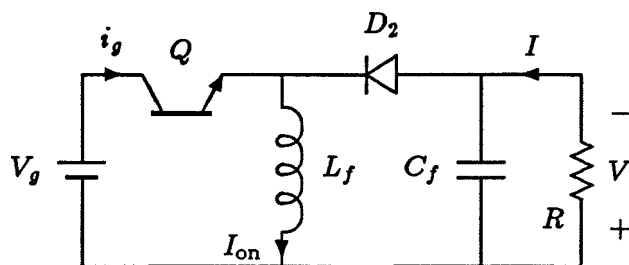


Figure 3.3: The buck-boost PWM converter.

of which have small ripple voltage. The transistor and rectifier switch the current  $I_{on}$  and the voltage  $V_{off}$  between themselves to create the rectangular waveforms of Fig. 3.2. (Note that the diode current is defined as positive when entering the *negative* voltage terminal of the device. This is contrary to the usual convention but still yields valid circuit equations. The convention was violated for the convenience of making both the diode current and voltage positive.)

The quantities  $I_{on}$  and  $V_{off}$  are easily found for any PWM converter by assuming constant currents in all the inductors and constant voltages on the capacitors. Assume the transistor is ON and find its current. This value is  $I_{on}$ , and the voltage across the diode, with the transistor still ON, is  $V_{off}$ . For example, in the PWM buck converter of Fig. 2.1, when the transistor  $Q$  is ON, the diode  $D_2$  sustains a voltage  $V_g$  while  $Q$  carries the inductor current. The voltage  $V_{off}$  is therefore  $V_g$ , generated by the input voltage source. The inductor  $L_f$  provides the current  $I_{on}$ , which equals the average load current  $I$ .

As a further example, consider the buck-boost converter of Fig. 3.3. In this converter, the inductor acts as a current source of value  $I_{on}$ , while the voltage  $V_{off}$  is generated by the input voltage source  $V_g$  in series with the output capacitor.

Usually, one will need to know  $I_{on}$  and  $V_{off}$  in terms of the source and load voltages and average currents. These quantities are found using the duty ratio of the switch and two facts: the average voltage on all inductors and the average current in all capacitors are both zero. For example, in the buck-boost converter of Fig. 3.3, the average input

current  $I_g$  is  $DI_{\text{on}}$  and the average output current  $I$  is  $D'I_{\text{on}}$ , with  $D' = 1 - D$ . Thus,

$$I_{\text{on}} = \frac{I}{D'} = \frac{I_g}{D}. \quad (3.3)$$

Since the average voltage on the inductor must be zero,  $DV_g - D'V = 0$  and hence

$$V_{\text{off}} = V + V_g = \frac{V_g}{D'} = \frac{V}{D}. \quad (3.4)$$

### 3.3 Resonant Switches

A quasi-resonant converter is formed by modifying the switching process in a PWM converter. This is done by replacing the PWM transistor and diode with a “resonant switch.” The action of zero-current resonant switches is analyzed in this section. The analysis is extended to include zero-voltage switches in Chapter 6.

#### 3.3.1 Rules Governing Zero-Current Resonant Switches

Three general rules governing the formation of zero-current resonant switches were presented in [9] and justified in terms of the desired behavior of the switch. For example, Rule 3 of [9] requires the resonant capacitor  $C_r$  and the diode  $D_2$  to form a loop that may also include voltage sources or capacitors with small voltage ripple. This ensures that  $C_r$  returns to a fixed voltage every time  $D_2$  turns ON. Of the three rules of [9], only two are necessary; any two of the rules imply the third.

For the present discussion, a quasi-resonant converter will be defined by the two topological rules of the following definition. These requirements will then be used to derive the switch waveforms and the behavior of quasi-resonant converters.

**Definition 2:** A PWM converter is transformed into a zero-current quasi-resonant converter by replacing the transistor  $Q$  with a two-quadrant switch  $S$ , and by adding a resonant inductor  $L_r$  and capacitor  $C_r$  according to the following two rules:

**Rule 1:** *The diode  $D_2$ , the resonant capacitor  $C_r$ , and a (possibly empty) set of capacitors and voltage sources form a loop.*

**Rule 2:** *The two-quadrant switch  $S$ , the resonant inductor  $L_r$ , and a (possibly empty) set of inductors form a cut-set.*

The original reactances of the PWM converter must continue to have small ripple in the quasi-resonant converter.

Rule 1 above is equivalent to Rule 3 of [9], but Rule 2 has no analog in [9]. While the two rules above are presented without justification, it is evident that Rule 1 ensures that the diode voltage will be continuous. Rule 2 likewise prevents discontinuous currents in the switch  $S$ .

The two-quadrant switch  $S$  may have one of two forms illustrated in Fig. 3.4. For zero-current resonant switches, a two-quadrant-in-voltage switch, shown in Fig. 3.4(a), produces what is called a half-wave resonant switch. When a two-quadrant-in-current switch replaces the PWM transistor, as in Fig. 3.4(b), the result is a full-wave switch. The following chapters will show that the distinction between half- and full-wave switches is perhaps the most important determinant of a quasi-resonant converter's behavior.

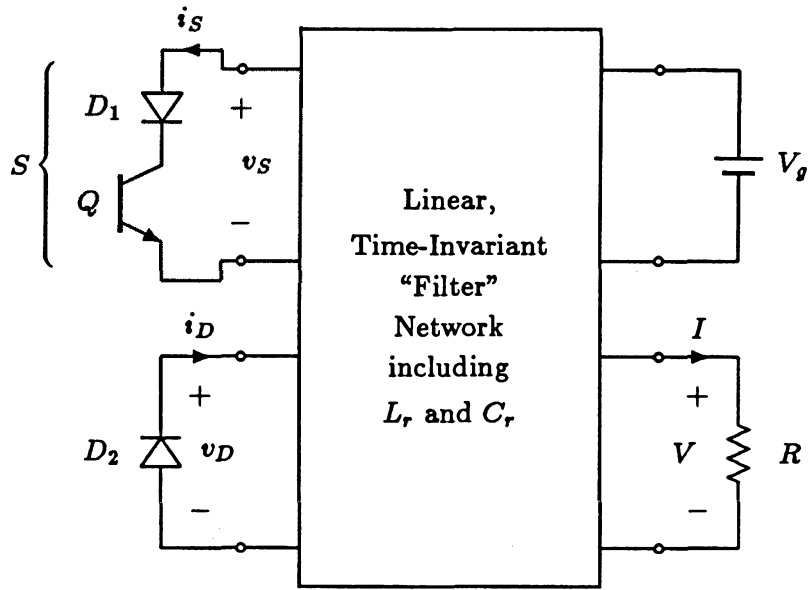
The quasi-resonant converter models of Fig. 3.4 correspond to Fig. 3.1 for PWM converters, with the switch separated from the linear network that makes up the rest of the converter. The linear network for a quasi-resonant converter is the *same* as that for its parent PWM converter, excepting the addition of  $L_r$  and  $C_r$ .

Rules 1 and 2 above determine acceptable locations for  $L_r$  and  $C_r$ . For example,  $C_r$  may always be placed across the diode  $D_2$ , since this forms a loop satisfying Rule 1. Similarly,  $L_r$  may always be in series with the switch  $S$  since these two elements then form a cut-set satisfying Rule 2.

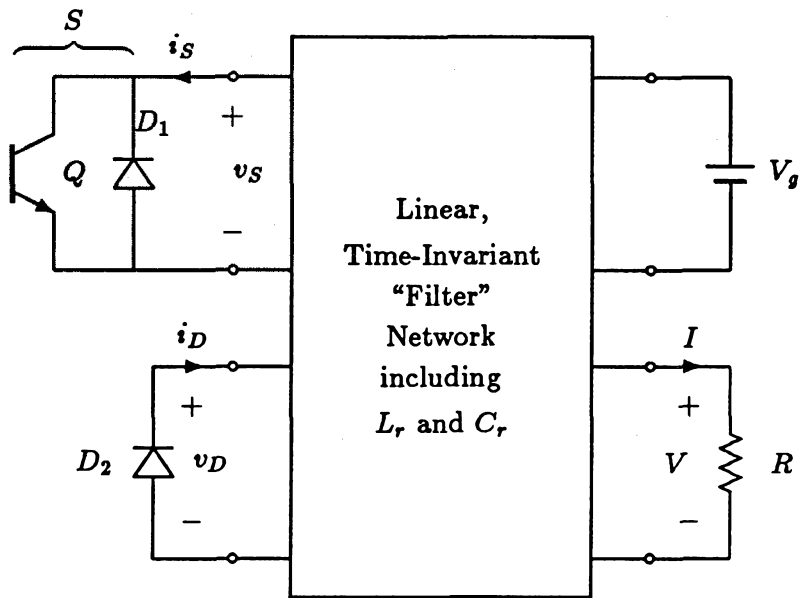
For evaluating the resonant-switch waveforms, however, it is convenient to derive two other topological relations from Rules 1 and 2. These are given in the following two theorems.

**Theorem 3:** *In a zero-current quasi-resonant converter, the elements  $S$ ,  $D_2$ ,  $L_r$ , and the elements producing the voltage  $V_{off}$  together form a loop.*

**Theorem 4:** *In a zero-current quasi-resonant converter, the elements  $S$ ,  $D_2$ ,  $C_r$ , and the inductors producing  $I_{on}$  together form a cut-set.*



(a)



(b)

Figure 3.4: Two kinds of zero-current resonant switch, half-wave (a) and full-wave (b). These figures, like Fig. 3.1, show the switches as external elements connected to a linear network.

The theorems are proved in Appendix A.

Theorem 3 implies that the resonant inductor is inserted in *series* into the  $Q$ - $D_2$ - $V_{off}$  loop of the original PWM converter. Theorem 4 likewise implies that  $C_r$  is added in *parallel*, connecting the two sub-networks separated by the cut-set  $Q$ - $D_2$ - $I_{on}$  of the original PWM converter. The fact that  $L_r$  is an element added in *series*, while  $C_r$  is added in *parallel* will prove useful in later analysis.

Application of Kirchoff's laws to the loops and cut-sets of Rules 1 and 2 and to Theorems 3 and 4, with appropriate choice of orientation, yields the following relations:

$$v_D = v_C + V_{dc} \quad (3.5)$$

$$i_S = i_L + I_{dc} \quad (3.6)$$

$$v_S + v_D + v_L = V_{off} \quad (3.7)$$

$$i_S + i_D - i_C = I_{on} . \quad (3.8)$$

The two quantities  $V_{dc}$  and  $I_{dc}$  are determined by the small-ripple elements included in the loop of Rule 1 and cut-set of Rule 2. Only the fact that  $V_{dc}$  and  $I_{dc}$  are small-ripple is important; their actual values are of no consequence.

Equations (3.5) through (3.8) are used in the next section to derive the resonant-switch waveforms, and to show that these waveforms are independent of the various allowed locations of  $L_r$  and  $C_r$ .

### 3.3.2 Operation of the Resonant Switch

The operation of the resonant switch during a single switching cycle is divided into four intervals as indicated in Table 3.1. To assist in understanding the switch operation, a quasi-resonant buck converter is presented in Fig. 3.5 along with the equivalent networks of the circuit for each of the sub-intervals in a switching period. The example of this figure demonstrates visually, for one particular case, why the switch and diode turn ON and OFF, and how the switch waveforms evolve.

The most important result of this section, however, is the fact that the waveforms  $i_S(t)$  and  $v_D(t)$  are the *same*, regardless of the underlying PWM topology or the location of  $L_r$  and  $C_r$ . While Fig. 3.5 is used as an illustration, the switch operation is derived



Interval	Name	Switch State	
		$S$	$D_2$
Initial State	Idle	OFF	ON
$0 < t < T_1$	Charging	ON	ON
$T_1 < t < T_2$	Resonant	ON	OFF
$T_2 < t < T_3$	Discharging	OFF	OFF
$T_3 < t < T_S$	Idle	OFF	ON

Table 3.1: The resonant switch takes on four different states during each switching period.

using only Equations (3.5) through (3.8).

As a means of simplifying the equations describing the resonant switch, define

$$\omega_0 \equiv \frac{1}{\sqrt{L_r C_r}} \quad (3.9)$$

$$R_0 \equiv \sqrt{L_r / C_r} . \quad (3.10)$$

The frequency  $F_0 = \omega_0 / 2\pi$  is the resonant frequency and  $R_0$  the characteristic resistance of the resonant tank formed by  $L_r$  and  $C_r$  during the resonant interval. Also define

$$\rho \equiv \frac{R_0 I_{on}}{V_{off}} . \quad (3.11)$$

A dimensionless quantity,  $\rho$  may be considered akin to the  $Q$  factor of a series resonant circuit. The smaller the dc load resistance  $R$ , the larger the ratio  $I_{on}/V_{off}$  and the larger  $\rho$  will be. It will shortly be shown that  $\rho$  must always be less than unity to enable operation in the desired mode.

### Initial State

Suppose the switch  $S$  is OFF and the diode  $D_2$  is ON, so that  $i_S$  and  $v_D$  are both zero. With these values in Eqs.(3.5) and (3.6),

$$v_C = -V_{dc} \quad (3.12)$$

$$i_L = -I_{dc} , \quad (3.13)$$

showing that the resonant current and voltage are fixed by the small-ripple values  $V_{dc}$  and  $I_{dc}$ , and implying that  $i_C$  and  $v_L$  are zero. The converter is in the idle state, with no change in the resonant variables.

In the example of Fig. 3.5, both  $V_{dc}$  and  $I_{dc}$  are zero, so that  $v_C$  and  $i_L$  are both zero in the idle state of Fig. 3.5(b).

**Charging Interval:  $0 < t < T_1$**

At  $t = 0$ , the switch  $S$  is turned ON, bringing  $v_S$  to zero. The diode remains ON during this interval and hence  $v_C$  does not change and  $i_C$  is zero. The evolution of the waveforms during this interval is described by

$$v_L = V_{off} \quad (3.14)$$

$$i_S + i_D = I_{on} \quad (3.15)$$

$$i_S = i_L + I_{dc} . \quad (3.16)$$

Differentiation of Eq.(3.16) and substitution from Eq.(3.14) yields

$$\frac{di_S}{dt} = \frac{di_L}{dt} = \frac{1}{L_r} V_{off} , \quad (3.17)$$

which has the solution

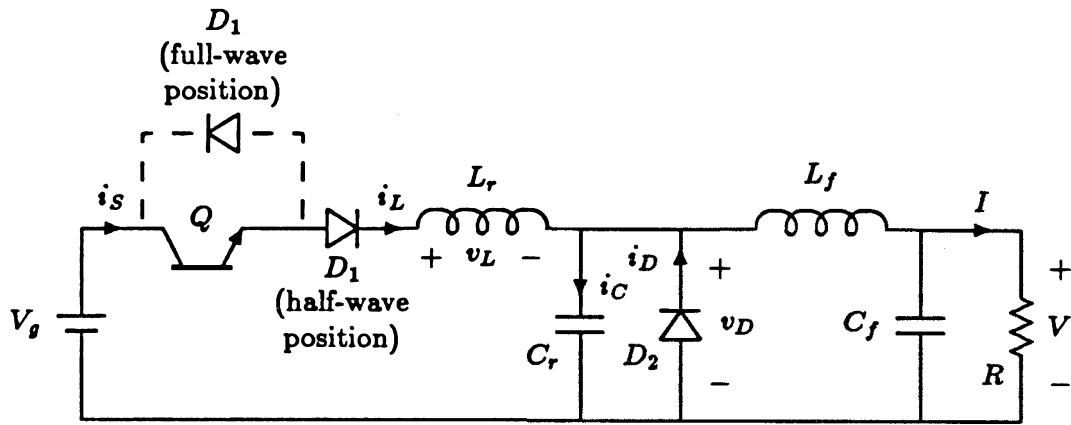
$$i_S(t) = I_{on} \frac{1}{\rho} \omega_0 t . \quad (3.18)$$

In Fig. 3.5(c), the inductor  $L_r$  is connected directly across the voltage source  $V_\theta$ , leading to the linearly increasing current of Eq.(3.18).

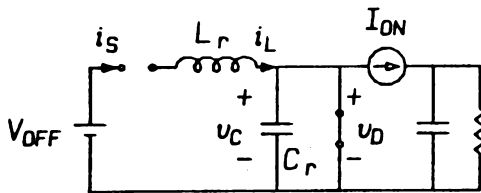
Equation (3.15) requires that as  $i_S$  rises,  $i_D$  must fall. The charging interval ends when  $i_D$  falls to zero and  $D_2$  turns OFF. In the example of Fig. 3.5, the current in  $L_r$  increases linearly, while the diode  $D_2$  carries the difference between  $I_{on}$  and  $i_L$ . When  $i_L$  reaches  $I_{on}$ ,  $D_2$  carries no current and turns OFF. The diode current reaches zero and the charging interval ends at time  $T_1$ , given from Eq.(3.18) by

$$\omega_0 T_1 = \rho . \quad (3.19)$$

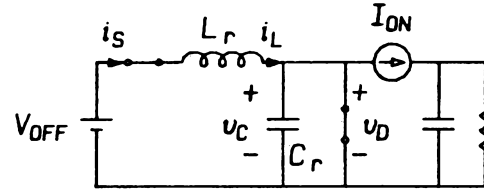
At the end of this interval,  $i_S = I_{on}$  and  $i_L = I_{on} - I_{dc}$ . Refer to Fig. 3.6 for an illustration of the waveforms described by the equations above.



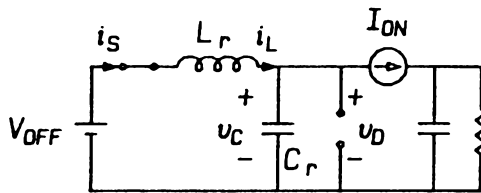
(a)



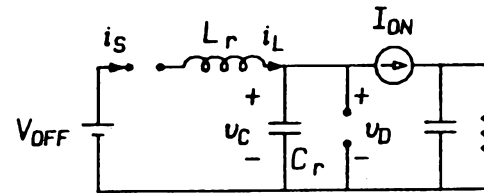
(b)



(c)



(d)



(e)

Figure 3.5: A quasi-resonant buck converter (a) and the sequence of switched-networks (b) through (e) that appear during a switching period.

**Resonant Interval:  $T_1 < t < T_2$** 

During the resonant interval, the switch  $S$  is ON and the diode  $D_2$  is OFF, reducing Eqs.(3.5) through (3.8) to

$$v_D = v_C + V_{dc} \quad (3.20)$$

$$i_S = i_L + I_{dc} \quad (3.21)$$

$$v_L = V_{off} - v_D \quad (3.22)$$

$$i_C = i_S - I_{on} . \quad (3.23)$$

Differentiation of Eqs.(3.20) and (3.21) and substitution with the remaining equations yields

$$\frac{dv_D}{dt} = \frac{1}{C_r} (i_S - I_{on}) \quad (3.24)$$

$$\frac{di_S}{dt} = \frac{1}{L_r} (V_{off} - v_D) . \quad (3.25)$$

This set of second-order equations has the solution

$$v_D(t) = V_{off} [1 - \cos \omega(t - T_1)] \quad (3.26)$$

$$i_S(t) = I_{on} \left[ 1 + \frac{1}{\rho} \sin \omega(t - T_1) \right] . \quad (3.27)$$

It is this interval that earns the converter the name “resonant.” The resonant circuit is clearly visible in Fig. 3.5(d).

The sinusoidal switch current of Eq.(3.27) is a sine wave of amplitude  $I_{on}/\rho$  offset by  $I_{on}$ . Provided that  $\rho < 1$ , the current passes through zero twice during each period of the resonance. This is the advantage of the zero-current resonant switch—the switch  $S$  may be turned OFF when  $i_S = 0$ , drastically reducing switching losses and allowing operation at much higher frequencies. In the half-wave switch of Fig. 3.4(a), the diode  $D_1$  interrupts the current  $i_S$  as it reaches zero from above. From Eq.(3.27), this occurs at a time  $T_2$  given by

$$\omega_0(T_2 - T_1) = \pi + \sin^{-1} \rho \quad (3.28)$$

and the diode voltage at the end of this interval is

$$v_D(T_2) = V_{off} \left( 1 + \sqrt{1 - \rho^2} \right) . \quad (3.29)$$

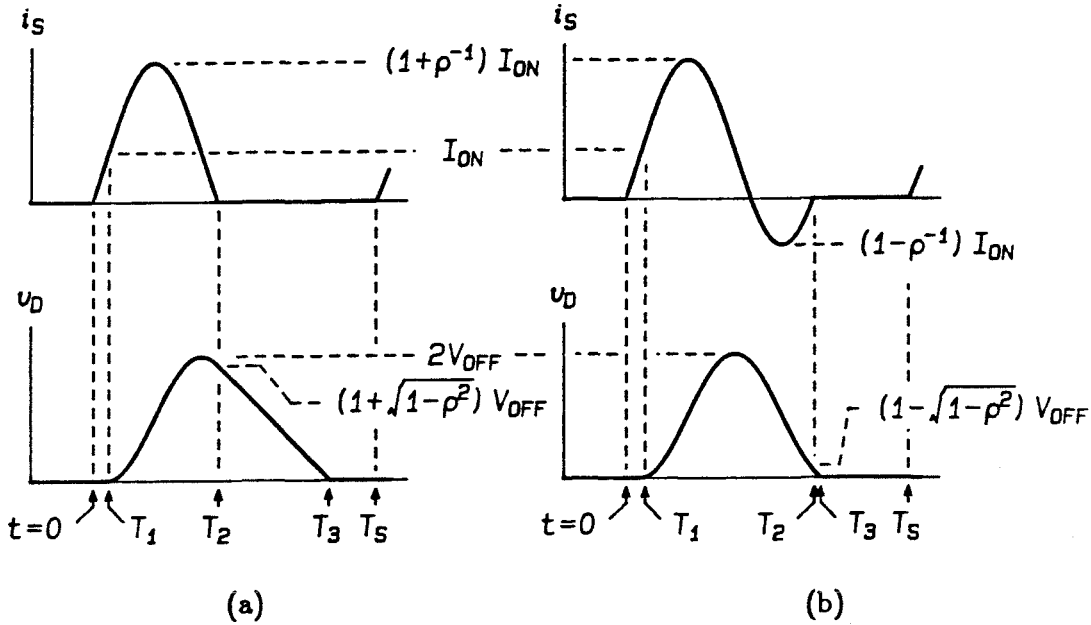


Figure 3.6: Switch waveforms for a zero-current resonant switch: (a) half-wave and (b) full-wave.

The full-wave switch of Fig. 3.4(b) allows the current  $i_S$  to drop below zero, but interrupts the current as it reaches zero from below, as shown in Fig. 3.6(b). In this case,

$$\omega_0(T_2 - T_1) = 2\pi - \sin^{-1} \rho \quad (3.30)$$

and the final diode voltage is

$$v_D(T_2) = V_{\text{off}} \left( 1 - \sqrt{1 - \rho^2} \right) . \quad (3.31)$$

The inverse sine function is understood to yield a result in the first quadrant.

The example of Fig. 3.5 has a half-wave switch. When the current in the switch  $S$  reaches zero, the diode  $D_1$  turns OFF and “disconnects” the resonant circuit. If the switch is full-wave instead (shown in dashed lines in Fig. 3.5), diode  $D_1$  carries negative resonating currents  $i_S$ . When  $i_S$  passes through zero from below, however,  $D_1$  blocks the current and ends the interval, on the assumption that the transistor  $Q$  has been turned OFF by that time.

The transistor  $Q$  may be turned OFF anytime during the “window” between  $T_2$  and the time when the voltage across the switch  $S$  becomes positive. (In the half-wave switch, this window is the time during which  $D_1$  is blocking. In the full-wave switch,  $Q$  must be

turned OFF while  $D_1$  conducts.) Note that while the actual instant at which  $Q$  is turned OFF may be varied, only the turn-OFF of  $D_1$  affects the switch waveforms. Since this turn-OFF is uncontrollable, the converter must be controlled by varying the switching frequency.

### Discharging Interval: $T_2 < t < T_3$

Both the switch  $S$  and the diode  $D_2$  are OFF during this interval, allowing Eqs.(3.6) and (3.8) to be written

$$i_L = -I_{dc} \quad (3.32)$$

$$i_C = -I_{on} . \quad (3.33)$$

The current  $i_L$  has returned to its idle-state value and does not change. From Eqs.(3.5) and (3.33), the diode voltage changes according to

$$\frac{dv_D}{dt} = \frac{dv_C}{dt} = -\frac{1}{C_r} I_{on} . \quad (3.34)$$

Using the initial conditions from Eqs.(3.29) and (3.31), the diode waveform is

$$v_D(t) = V_{off} \left[ 1 + \sqrt{1 - \rho^2} - \rho\omega_0(t - T_2) \right] \quad (3.35)$$

for the half-wave switch, and

$$v_D(t) = V_{off} \left[ 1 - \sqrt{1 - \rho^2} - \rho\omega_0(t - T_2) \right] \quad (3.36)$$

for the full-wave switch.

The interval ends at  $t = T_3$  when the diode voltage reaches zero and  $D_2$  turns ON. This is illustrated in Fig. 3.5(e) where the constant current  $I_{on}$  makes the voltage across  $C_r$  fall linearly. When the voltage reaches zero,  $D_2$  turns ON and takes the current  $I_{on}$  away from  $C_r$ . The interval length is given by

$$\omega_0(T_3 - T_2) = \frac{1}{\rho} \left( 1 + \sqrt{1 - \rho^2} \right) \quad (3.37)$$

for the half-wave switch and by

$$\omega_0(T_3 - T_2) = \frac{1}{\rho} \left( 1 - \sqrt{1 - \rho^2} \right) \quad (3.38)$$

for the full-wave switch.

**Idle Interval:**  $T_3 < t < T_S$

When the previous interval ends at  $T_3$ , both  $i_S$  and  $v_D$  are zero. The resonant switch has returned to its idle state. This state persists until the switch  $S$  is again turned ON, initiating the next cycle. The duration of the idle interval during any switching period is  $T_S - T_3$ , where  $1/T_S$  is the switching frequency,  $F_S$ . Control over the converter is exercised by varying  $T_S$  and hence changing the length of this idle interval.

Table 3.2 summarizes the equations describing  $i_S$  and  $v_D$  during each of the four intervals for the zero-current resonant switch. The corresponding waveforms are shown in Fig. 3.6. The equations of Table 3.2 were derived using *only* Definition 1 concerning the structure of a PWM converter, Definition 2 describing the topology of the resonant switch, and Theorems 1 through 4 derived from those two definitions. No reference was made to sinusoidal-wave or square-wave switch types, and the quantities  $V_{dc}$  and  $I_{dc}$  (related to the topological positions of  $L_r$  and  $C_r$ ) do not appear in any of the equations of Table 3.2. One must therefore conclude that the waveforms  $i_S$  and  $v_D$  are the *same* for *any* converter using a zero-current resonant switch, regardless of underlying PWM topology or location of  $L_r$  and  $C_r$ . Only the type of switch  $S$  has an effect on the waveforms, the half-wave switch cutting off the current  $i_S$  as it passes through zero from above and the full-wave switch interrupting the current as it reaches zero from below.

### 3.4 The Small-Ripple Approximation

The analysis of the switch waveforms in the previous section treated  $I_{on}$  and  $V_{off}$  as dc sources. The small-ripple approximation of Definitions 1 and 2 is what allows such a treatment, reducing the resonant switch to a second-order system and leading to manageable expressions. Because of its importance and leading role in the analysis of quasi-resonant converters, the small-ripple approximation deserves some discussion of its validity and consequences.

It is not *necessary* that a PWM converter operate with extremely small ripple. Neither must quasi-resonant converters have small ripple on their nonresonant reactances. Ripple “inside” these converters—not appearing at the input or output—can be fairly large without impairing the converter operation. For several reasons, however, it is

Interval	Switch Current $i_S(t)/I_{on}$	Diode Voltage $v_D(t)/V_{off}$	Duration of Interval $\omega_0 \Delta t$
$0 < t < T_1$	$\frac{1}{\rho} \omega_0 t$	0	$\rho$
$T_1 < t < T_2$	$1 + \frac{1}{\rho} \sin \omega_0(t - T_1)$	$1 - \cos \omega_0(t - T_1)$	$\left\{ \begin{array}{l} \pi + \sin^{-1} \rho \\ \text{(half-wave)} \\ \\ 2\pi - \sin^{-1} \rho \\ \text{(full-wave)} \end{array} \right.$
$T_2 < t < T_3$			
half-wave:	0	$1 + \sqrt{1 - \rho^2} - \rho \omega_0(t - T_2)$	$\frac{1}{\rho} \left( 1 + \sqrt{1 - \rho^2} \right)$
full-wave:	0	$1 - \sqrt{1 - \rho^2} - \rho \omega_0(t - T_2)$	$\frac{1}{\rho} \left( 1 - \sqrt{1 - \rho^2} \right)$
$T_3 < t < T_S$ (Idle)	0	0	—

Table 3.2: Summary of the equations describing the behavior of the zero-current resonant switch.

unusual to find either kind of converter operating with large ripple.

Large voltage ripple on internal capacitors increases the peak voltage stress, forcing the capacitor to have a higher rating than if the voltage ripple were small. (Capacitors at the input or output have small ripple by nature of the dc input and output voltages.) Inductors with large ripple currents suffer unnecessarily large power loss in their parasitic resistances. And perhaps most important, excessive ripple leads to higher voltage and current stresses on the semiconductor devices.

For these reasons, converters are usually designed with small to moderate ripple waveforms on reactances; values of 5–20% are common. The small-ripple approximation is not grossly violated by ripple of this magnitude, but neither is it well-satisfied.



The fact that the small-ripple approximation is often satisfied is, however, only one of three reasons why it is applied here. Another reason is that the experimental results of Chapter 7 indicate that the ac analysis of Chapter 5 is not particularly sensitive to ripple in  $I_{on}$  and  $V_{off}$ . With ripple as high as 21% in  $I_{on}$ , the small-signal frequency response of a boost converter still agrees very well with the response predicted using the small-ripple approximation. At least in some cases, then, the small-ripple approximation can accurately predict the behavior of a converter even when that converter has appreciable ripple.

The third and most important reason for using the small-ripple approximation has nothing to do with whether the approximation is valid. The approximation is applied here because it paves the way for clear, simple, and *general* dc and ac analyses of quasi-resonant converters. Without the small-ripple approximation,  $I_{on}$  and  $V_{off}$  could not be considered dc or even slowly-varying. This would make the resonant switch a system of fourth or higher order, and the equations describing the resonant waveforms would be unmanageable. Even worse, the resonant switch in each converter would have to be analyzed separately because the resonant waveforms would be functions of the magnitude and shape of the ripple, as well as of the average values of  $I_{on}$  and  $V_{off}$ . The assumption of small ripple may be justified, then, even if the results are not entirely accurate. The approximate information it provides allows simultaneous treatment of all quasi-resonant converters, and this may be more useful—for designing and understanding the converters—than accurate results requiring computer solution.

Small ripple on  $I_{on}$  and  $V_{off}$  is achieved in the same way in PWM and in quasi-resonant converters—by making the inductors and capacitors providing  $I_{on}$  and  $V_{off}$  “stiff.” These reactances are part of the linear network in Figs. 3.1 and 3.4. In a PWM converter, the linear network is driven by rectangular waveforms  $i_S$  and  $v_D$ . These waveforms are quasi-sinusoidal in a quasi-resonant converter, but because they are periodic at the switching frequency they still have no frequency components below the switching frequency. The sizes of the reactances needed to attenuate these driving waveforms to produce small ripple in  $I_{on}$  and  $V_{off}$  are therefore comparable between PWM and quasi-resonant converters operating at the same power level, load, and switching frequency.

The designer should take note, however, that while PWM converters usually operate at constant frequency, quasi-resonant converters are frequency-controlled. The requirements on the filter reactances become more severe as the switching frequency is reduced to regulate against input voltage or load changes.

### 3.5 Averages of the Resonant-Switch Waveforms

The waveforms of a resonant switch are complicated combinations of ramps and sine waves. If these waveforms directly affected the converter input and output properties, the behavior of the converter would be difficult to predict. Fortunately, the small-ripple approximation, which has been invoked repeatedly, is an alternative way of stating that the resonant waveforms do *not* directly affect the small-ripple input and output waveforms. Instead, only the *averages* of the resonant waveforms are important. Expressions for the necessary averages are derived in Section 3.5.1, and some limitations on the values of these expressions are considered in Section 3.5.2.

#### 3.5.1 Averages of $i_S$ and $v_D$

In steady state, the switch is turned ON at constant intervals. The length of these intervals is the switching period  $T_S$ , while the switching frequency  $F_S$  is the reciprocal of  $T_S$ . The average of the current  $i_S$  over a switching period is given by

$$\begin{aligned}\bar{i}_S &= \frac{1}{T_S} \int_0^{T_S} i_S dt \\ &= \frac{F_S}{\omega_0} \int_0^{\omega_0/F_S} i_S(\omega_0 t) d(\omega_0 t) .\end{aligned}\quad (3.39)$$

A similar integration yields  $\bar{v}_D$ , the average of  $v_D$ . Evaluation of the integrals, using the expressions of Table 3.2 for the integrands, yields

$$\bar{i}_S = I_{\text{on}} \frac{F_S}{F_0} G(\rho) \quad (3.40)$$

$$\bar{v}_D = V_{\text{off}} \frac{F_S}{F_0} G(\rho) \quad (3.41)$$

where  $F_0$  is the resonant frequency,  $\omega_0/2\pi$ , and the function  $G$  depends on the type of switch  $S$ . Denoting  $G_{hw}$  and  $G_{fw}$  as the functions appropriate for the half-wave and

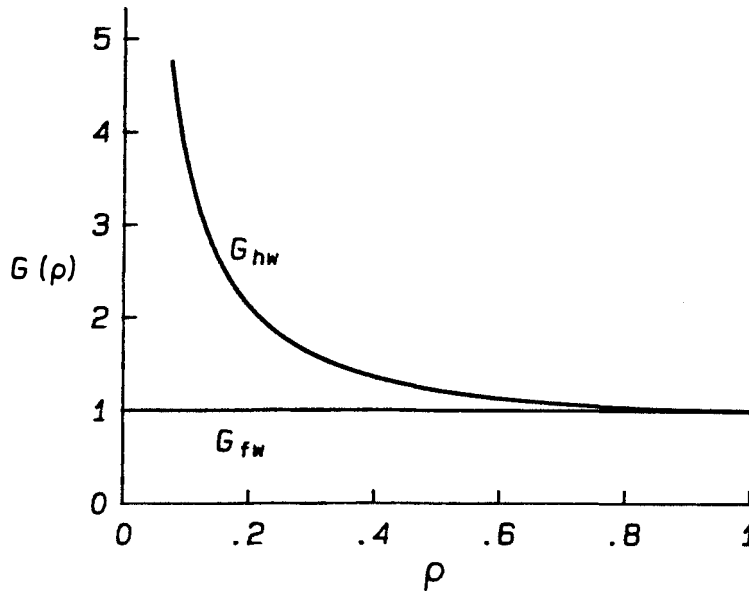


Figure 3.7: Plots of the functions  $G(\rho)$  for the half-wave and full-wave resonant switches, denoted  $G_{hw}$  and  $G_{fw}$ , respectively.

full-wave switches, respectively, the functions are given by

$$G_{hw}(\rho) = \frac{1}{2\pi} \left[ \frac{\rho}{2} + \pi + \sin^{-1} \rho + \frac{1}{\rho} \left( 1 + \sqrt{1 - \rho^2} \right) \right] \quad (3.42)$$

$$G_{fw}(\rho) = \frac{1}{2\pi} \left[ \frac{\rho}{2} + 2\pi - \sin^{-1} \rho + \frac{1}{\rho} \left( 1 - \sqrt{1 - \rho^2} \right) \right] . \quad (3.43)$$

These functions are plotted in Fig. 3.7. Despite the small difference in the waveforms of Fig. 3.6, the functions  $G_{hw}$  and  $G_{fw}$  are quite different.  $G_{hw}$  is strongly dependent on  $\rho$  and in fact grows without limit as  $\rho \rightarrow 0$ . In contrast,  $G_{fw}$  is nearly constant, always being within 1.2% of unity.

### 3.5.2 Restrictions on the Averages

Note that  $\rho$  is always positive and must be less than unity to be a proper argument for the inverse sine function of Eqs.(3.42) and (3.43). The physical meaning of the restriction  $\rho < 1$  is apparent from Fig 3.6. The resonating current is a sinusoid of amplitude  $\rho I_{on}$  with an offset of  $I_{on}$ . If  $\rho > 1$ , the resonating current will not reach zero and the switch cannot turn off into zero current. Since the zero-current turn-OFF is the chief advantage of the resonant switch, only that case is considered here, and  $\rho$  is restricted to  $0 < \rho < 1$ .

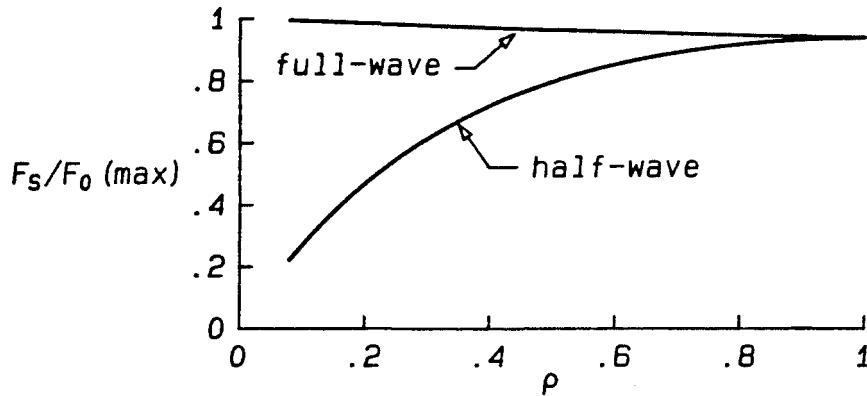


Figure 3.8: Upper limit on the switching frequency in a quasi-resonant converter.

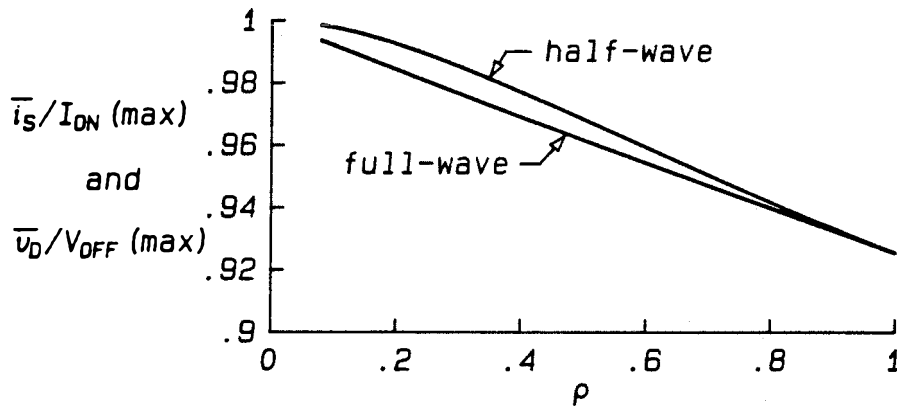


Figure 3.9: Maximum value of the average ratios  $\bar{i}_S/I_{ON}$  and  $\bar{v}_D/V_{OFF}$  for a zero-current resonant switch.

One other physical condition restricts the value of  $\rho$  in Eqs.(3.42) and (3.43). With the discontinuous operation assumed, in which the resonant switch always returns to its idle state before the switch  $S$  is turned on, the time  $T_3$  must be less than the switching period  $T_S$ . Using the equations of Table 3.2, this implies

$$\frac{F_S}{F_0} \leq \frac{1}{G(\rho) + \rho/4\pi} \quad (3.44)$$

This constraint, as a function of  $\rho$ , is plotted in Fig. 3.8. When the limits of Fig. 3.8 are combined with the curves of Fig. 3.7 for  $G(\rho)$ , the result is an upper limit on the average values of Eqs.(3.40) and (3.41). These limits, shown in Fig. 3.9, are achieved when the switching frequency is increased to the point that the switch  $S$  is turned on

just as soon as the diode voltage  $v_D$  reaches zero. If the frequency is increased beyond this point, the switch never reaches its idle state. This represents a different mode of operation of the resonant switch, a “continuous” mode in which the capacitor voltage never reaches its idle value. The initial value of the capacitor voltage for each switching cycle depends upon the conditions during the previous cycle, yielding dynamics in the resonant switch that are missing in the “discontinuous” mode considered so far. The only mode considered here is the one in which the switch *does* have an idle period. In this mode, the curves of Fig. 3.9 show that  $\bar{i}_S$  must always be less than  $I_{on}$  and that  $\bar{v}_D$  cannot exceed  $V_{off}$ .



## Chapter 4

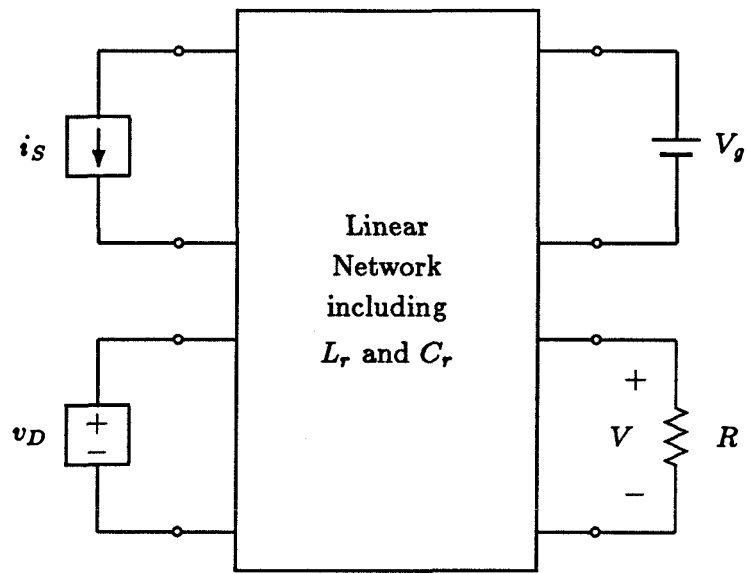
# Dc Analysis of Quasi-Resonant Converters

The average behavior of the resonant switch is used in this chapter to derive expressions for the conversion ratio of quasi-resonant converters. The relation between a quasi-resonant converter and its PWM parent, developed in the preceding chapter, now pays off, allowing the quasi-resonant conversion ratio to be expressed in Section 4.1 in terms of the well-known ratio of the corresponding PWM converter. Following sections explore the implications of the quasi-resonant conversion ratio, showing that some converters behave much like their PWM parents, while others have very different behavior. Some quasi-resonant converters, it will be shown, are particularly well-suited to parallel operation.

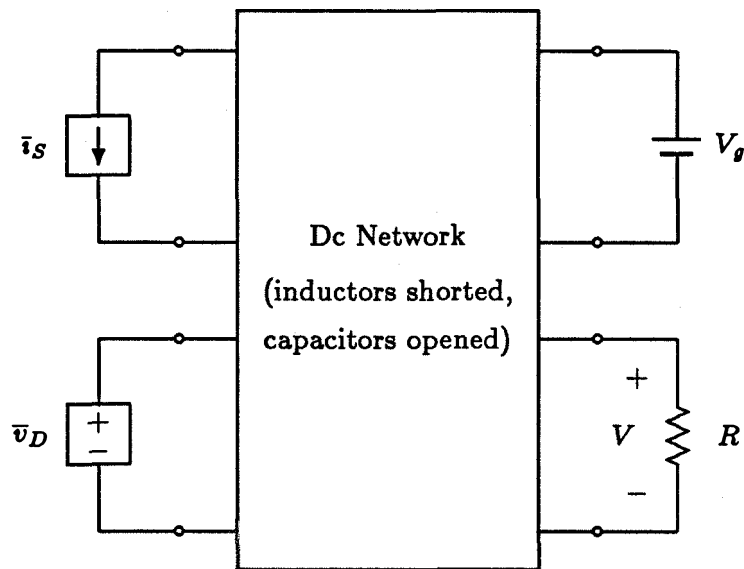
### 4.1 Dc Conversion Ratio

Consider the converter model shown in Fig. 4.1(a). Just as in Figs. 3.1 and 3.4, this model views the converter as a linear network driven by the switch waveforms  $i_S$  and  $v_D$ . The dc behavior of the system, and in particular the dc conversion ratio  $M \equiv V/V_g$ , involves only the dc value of the sources  $i_S$  and  $v_D$ . Hence, for purposes of dc analysis, the model of Fig. 4.1(a) can be replaced by that of Fig. 4.1(b). In this model, the sources  $i_S$  and  $v_D$  are replaced by their average values,  $\bar{i}_S$  and  $\bar{v}_D$ . In addition, all inductors in the linear network become short circuits, since every inductor has zero average voltage in steady-state. Similarly, all capacitors become open circuits. (Note that it is the dc load resistance  $R$ , defined as the ratio of dc load voltage and current, that appears in Fig. 4.1.)

The model of Fig. 4.1(b) applies equally to a PWM converter (in which the transistor current  $i_Q$  is equivalent to the switch current  $i_S$ ) and to any quasi-resonant converter



(a)



(b)

Figure 4.1: (a) A converter viewed as a linear network driven by the switch current and diode voltage waveforms. (b) At dc, the average of the switch waveforms drives the dc network.



derived from the PWM topology. The averaged linear network of a quasi-resonant converter is the *same* as that of its PWM parent, because  $L_r$  (added in series) is shorted and  $C_r$  (added in parallel) is open. Figure 4.1(b) clearly suggests that when a quasi-resonant converter and its PWM parent have the same values of  $\bar{i}_S$  and  $\bar{v}_D$  the conversion ratio  $M$  must be the same.

The averages  $\bar{i}_S$  and  $\bar{v}_D$  are easily found for the PWM converter. Figure 3.2, for example, reveals that

$$\bar{i}_S = DI_{\text{on}} \quad (4.1)$$

$$\bar{v}_D = DV_{\text{off}} . \quad (4.2)$$

For a quasi-resonant converter, the averages are given by Eqs.(3.40) and (3.41) of Chapter 3, repeated here:

$$\bar{i}_S = \frac{F_S}{F_0} G(\rho) I_{\text{on}} \quad (4.3)$$

$$\bar{v}_D = \frac{F_S}{F_0} G(\rho) V_{\text{off}} . \quad (4.4)$$

Comparison of Eqs.(4.1) and (4.2) with Eqs.(4.3) and (4.4) reveals that the conversion ratios of the PWM converter and its quasi-resonant derivative must be equal whenever

$$D = \frac{F_S}{F_0} G(\rho) . \quad (4.5)$$

For a PWM converter, the voltage conversion ratio  $M \equiv V/V_g$  is a function only of  $D$ , that is

$$M \equiv \frac{V}{V_g} = M_P(D) . \quad (4.6)$$

The conversion-ratio function  $M_P(D)$  is well-known for each PWM converter. Table 4.1 lists  $M_P(D)$  for the buck, boost, buck-boost, and Ćuk topologies.

Under the equivalence of Eq.(4.5), the conversion ratio  $M$  for the quasi-resonant converter is given by

$$M = M_P \left[ \frac{F_S}{F_0} G(\rho) \right] . \quad (4.7)$$

This equation is not immediately useful, however, because  $\rho$  involves  $I_{\text{on}}$  and  $V_{\text{off}}$ , quantities that in turn depend on the conversion ratio. A relation between  $\rho$  and  $M$  will

Converter	$M_P(D)$	$D_P(M)$
Buck	$D$	$M$
Boost	$\frac{1}{1-D}$	$\frac{M-1}{M}$
Buck-boost and Ćuk	$\frac{D}{1-D}$	$\frac{M}{1-M}$

Table 4.1: The PWM conversion ratio  $M_P(D)$  and its inverse  $D_P(M)$  for several common PWM converters.

resolve this problem. For every known converter meeting Definition 1 (see, for example, [14] for a catalog of many such converters), the following is true:

$$\frac{V_{\text{off}}}{I_{\text{on}}} = \frac{R}{M}, \quad (4.8)$$

where  $R$  is the dc load resistance, the ratio of dc load voltage and current. This expression, when combined with the definition of  $\rho$  in Eq.(3.11), yields the equivalent relation

$$\rho = R_0 \frac{I_{\text{on}}}{V_{\text{off}}} = M \frac{R_0}{R}. \quad (4.9)$$

That Eq.(4.9) should hold for such a large class of converters is somewhat surprising. Such a general result is usually fairly obvious, but must be given here without proof.

Substitution of Eq.(4.9) in Eq.(4.7) yields

$$M = M_P \left[ \frac{F_S}{F_0} G \left( \frac{M R_0}{R} \right) \right]. \quad (4.10)$$

The function  $G$  is complicated, with combinations of algebraic and trigonometric functions, so that Eq.(4.10) cannot be explicitly solved for  $M$ . It can, however, be solved explicitly for the control variable,  $F_S$ , by inverting the function  $M_P(D)$ .

Since  $M_P(D)$  is always one-to-one for converters meeting Definition 1, the inverse function  $D_P(M)$  always exists. Table 4.1 gives the inverse conversion-ratio functions  $D_P(M)$  for the most common PWM converter topologies.

When Eq.(4.10) is solved for  $F_S/F_0$ , the result is

$$\frac{F_S}{F_0} = \frac{D_P(M)}{G \left( M \frac{R_0}{R} \right)}. \quad (4.11)$$

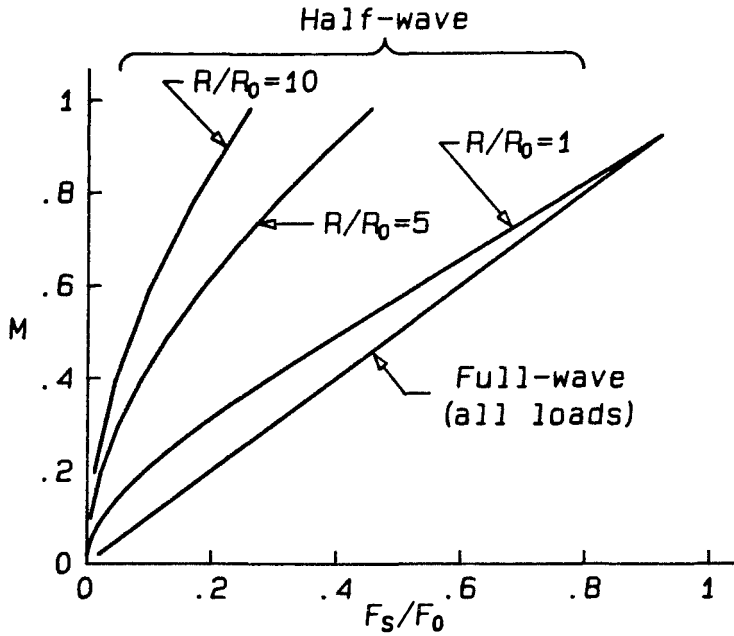


Figure 4.2: Conversion ratio  $M$  for the buck converter with a zero-current resonant switch.

It is unfortunate that no explicit expression for  $M$  can be found, but hardly surprising in light of the complexity of the resonant waveforms. Equation (4.11) is nevertheless very useful. For example, one might step through a range of  $M$  values, plotting the required switching frequency versus  $M$  and thereby generating a plot of  $M$  versus  $F_S/F_0$  without need of a numerical root finder.

The curves of Figs. 4.2 and 4.3 were generated in just this way. These figures give examples of the dependence of the conversion ratio on the load and the switching frequency. The curves end where the switching frequency reaches the upper limit of Eq.(3.44) and Fig. 3.8.

Perhaps the greatest advantage of Eq.(4.11) is that it allows one to express  $F_S/F_0$  as a function of  $M$  and  $R$ . This in turn allows the average ratios  $\bar{i}_S/I_{on}$  and  $\bar{v}_D/V_{off}$  to be expressed as functions of  $M$  alone:

$$\frac{\bar{i}_S}{I_{on}} = \frac{\bar{v}_D}{V_{off}} = \frac{D_P(M)}{G} G = D_P(M) . \quad (4.12)$$

In the ac analysis of the following chapter, this will provide a convenient way of writing the small-signal parameters in terms of the dc quantities  $M$  and  $R$ .

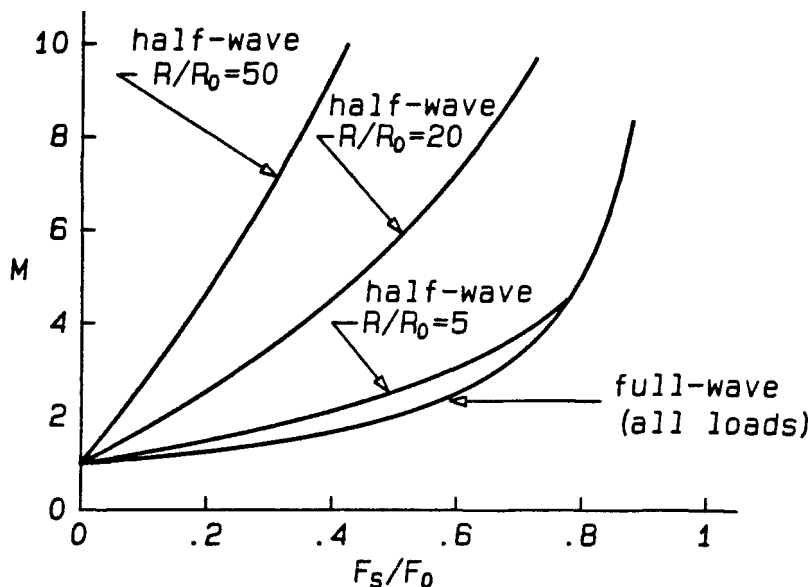


Figure 4.3: Conversion ratio  $M$  for the boost converter with a zero-current resonant switch.

Equation (4.12) states a simple concept worth examining. In a PWM converter, the duty ratio  $D$  gives the ratios  $\bar{i}_Q/I_{on}$  and  $\bar{v}_D/V_{off}$ . The PWM conversion ratio  $M$  is given by the function  $M_P(D)$  of these ratios. In a quasi-resonant converter based on this PWM topology, the conversion ratio  $M$  is the *same* function of the ratios  $\bar{i}_S/I_{on}$  and  $\bar{v}_D/V_{off}$ . In other words, for the same value of  $M$ , a quasi-resonant converter and its PWM parent must have the same ratios  $\bar{i}_S/I_{on}$  and  $\bar{v}_D/V_{off}$ , a ratio given by  $D_P(M)$  for the PWM converter. It is this equivalence that is expressed in Eq.(4.12).

References [4,7,8] contain analyses of the dc behavior of buck, boost, and buck-boost quasi-resonant converters. Since [4,7,8] make assumptions equivalent to the small-ripple approximation, the results are identical to those predicted by Eq.(4.11) for those three converters. The method used here is more powerful than that of [4,7,8] because in one equation, Eq.(4.11), it yields results for *all* zero-current quasi-resonant converters. One needs only the well-known function  $M_P(D)$  of the original PWM converter and the appropriate function  $G_{hw}$  or  $G_{fw}$  for the resonant switch, and Eq.(4.11) immediately gives the relation from which  $M$  can be found. Equation (4.11) is an illustration of how the relation between quasi-resonant converters and the PWM topologies that underlie

them may be exploited to yield general results.

## 4.2 Relation to PWM Conversion Ratio

In [4], a curious effect was noted in the dc conversion ratios of several half-wave quasi-resonant converters. For heavy loads, the ratio was approximately given by

$$\frac{V}{V_g} = M_P(D) \Big|_{D \leftarrow \frac{F_S}{F_0}} \quad (4.13)$$

For example, as  $R/R_0$  becomes small, the conversion ratio plotted in Fig. 4.2 approaches  $F_S/F_0$ , which is  $M_P(F_S/F_0)$  since the buck converter has  $M_P(D) = D$ .

This result is verified and explained by considering Eq.(4.7) and Fig. 3.7. For heavy loads (small  $R$ ),  $\rho \rightarrow 1$ , and

$$G_{hw}(\rho) \rightarrow \frac{3}{4} \left( \frac{1 + \pi}{\pi} \right) \approx 1. \quad (4.14)$$

With  $G_{hw} \approx 1$ , Eq.(4.7) shows that the conversion ratio is obtained by replacing  $D$  with  $F_S/F_0$ , as observed.

If  $G(\rho)$  is constant for all values of  $\rho$ , then  $M$  is a function only of  $F_S/F_0$ , as indicated by Eq.(4.7). This is the case for the full-wave resonant switch, where  $G_{fw}(\rho)$  is unity to within less than 1.2% for  $0 < \rho < 1$ , as seen in Fig. 3.7. According to Eq.(4.7), the conversion ratio is then given by substitution of  $F_S/F_0$  for  $D$  in the conversion ratio of the original PWM converter. This agrees with the results obtained for the buck, boost, and buck-boost converters in [7].

Converters with full-wave switches therefore behave almost exactly like their PWM counterparts. They exhibit the same lack of load dependence, and their conversion ratios have the same dependence on the control variable. Only the control variable itself is different.

## 4.3 Output Resistance

The curves of Fig. 3.7, together with Eq.(4.7), demonstrate that a quasi-resonant converter with a half-wave switch exhibits a strong dependence of the conversion ratio on the load. This means that if the switching frequency is fixed, the output voltage

changes as the load varies. This is in contrast to PWM converters (in the continuous conduction mode) and to full-wave quasi-resonant converters, both of which may be operated open-loop (with constant  $D$  or  $F_S$ ) while showing little sensitivity to load changes. The load-dependence of half-wave converters is very similar to that of PWM converters operating in the discontinuous conduction mode.

The variation in the output voltage as a function of a change in load current, with the control fixed, is an indication of the output resistance of a converter. The incremental output resistance,  $R_{out}$  is defined by

$$R_{out} \equiv -\frac{\partial V}{\partial I_{out}}, \quad (4.15)$$

where the input voltage  $V_g$  and the control variable ( $D$  for a PWM converter,  $F_S$  for a quasi-resonant converter) are held constant. Equation (4.9) and implicit differentiation of Eq.(4.11) can be used to show that

$$R_{out} = -\frac{\partial V}{\partial I_{out}} = -R_0 \frac{G'(\rho) D_P(M)}{G(\rho) D'_P(M)}, \quad (4.16)$$

where the partial derivative is taken with  $F_S$  and  $V_g$  both held constant. The derivative of a function with respect to its argument is indicated by a prime. (Note that  $D'_P(M)$  is *not*  $1 - D_P(M)$ .) The derivative  $G'(\rho)$  is negative while  $D'_P(M)$  is positive, so that  $R_{out}$  is positive as expected.

For example, in the PWM buck converter  $M_P(D)$  is simply  $D$ , so that  $D_P(M) = M$  and  $D'_P(M) = 1$ . The output resistance of a quasi-resonant buck converter may therefore be expressed in the form

$$\frac{R_{out}}{R} = -\rho \frac{G'(\rho)}{G(\rho)}. \quad (4.17)$$

This quantity is plotted in Fig. 4.4 for the half-wave switch. The output resistance of a half-wave quasi-resonant buck converter is an appreciable fraction of the load resistance, particularly for low values of  $MR_0/R$ , or equivalently  $\rho$ .

For full-wave switches,  $G'$  is negligibly small because  $G$  is very nearly constant, as seen in Fig. 3.7. Using  $G' = 0$  in Eq.(4.16) reveals that  $R_{out} = 0$  for all quasi-resonant converters with full-wave switches. Ideally, full-wave converters have no output resistance, just like their PWM counterparts.

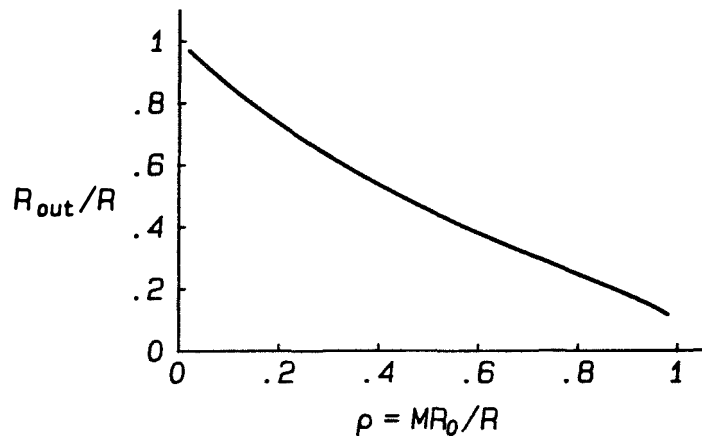


Figure 4.4: Incremental output resistance of the half-wave quasi-resonant buck converter.

The high output resistance of converters with half-wave resonant switches may be considered undesirable, but this feature can be turned to advantage. Unlike PWM and full-wave converters, with their low output resistances, half-wave converters may be connected directly in parallel to the same load. The case of two converters in parallel is shown in Fig. 4.5. All the converters receive the same input voltage and operate at the same switching frequency  $F_S$ , a frequency determined by a single voltage feedback loop regulating the load voltage. Such a scheme has several advantages, including built-in redundancy.

Ideally, each of  $n$  paralleled converters supplies an output current of exactly  $I/n$ , where  $I$  is the total load current, but slight differences in component values inevitably lead to offsets between the various output characteristics of the different converters. For instance, a slightly higher value of resonant inductance in one converter will cause the resonant frequency  $F_0$  to be slightly lower. At the same  $F_S$ , this converter will have a higher ratio  $F_S/F_0$  and will tend to produce a higher output voltage. The converter will have to provide more than its “fair share” of current in order to produce the same output voltage as all the other converters.

The degree of sensitivity of the output current to these inevitable errors is inversely proportional to the output resistance. Consider the case where two converters operate in parallel at the same switching frequency  $F_S$ . Figure 4.6(a) shows a portion of the output

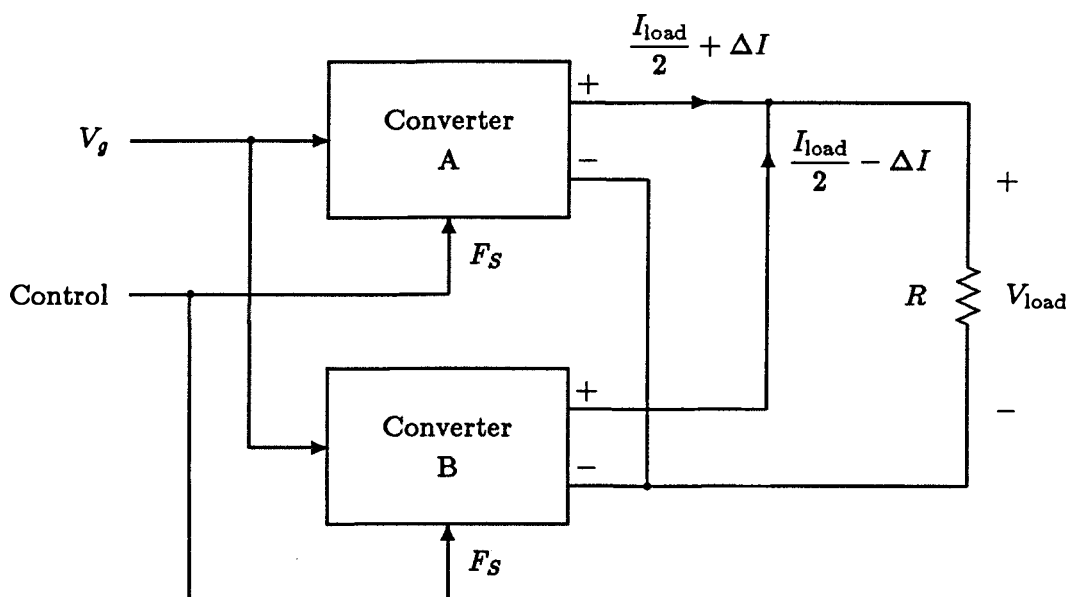


Figure 4.5: Two quasi-resonant converters operating in parallel.

characteristics of the two converters. As a result of component tolerances, converter A has an output voltage curve shifted a small amount  $\Delta V$  relative to converter B. Because their outputs are tied in parallel, both converters must have the same output voltage  $V_{load}$ . The voltage error  $\Delta V$  results in an imbalance  $2\Delta I$  between the two output currents. Converter A supplies a current  $I_{load}/2 + \Delta I$  while converter B supplies  $I_{load}/2 - \Delta I$ , as shown in Fig. 4.5. The current  $\Delta I$  circulates out of converter A and into converter B, never reaching the load. The amount of imbalance is

$$2\Delta I = \frac{\Delta V}{R_{out}}. \quad (4.18)$$

The voltage error  $\Delta V$  will usually be small, so any value of  $R_{out}$  that is a significant fraction of the load resistance keeps the current imbalance tolerably small. Paralleling half-wave converters is therefore practical as long as  $\rho$  is not near unity.

PWM and full-wave converters have very small output resistances, however. The output characteristics of two such converters operating in parallel are indicated in Fig. 4.6(b). The low output resistance means the output curves are nearly flat. Even a small shift  $\Delta V$  results in a large current imbalance  $\Delta I$ . For this reason, elaborate precautions must be taken to provide current-sharing when paralleling PWM or full-wave converters.



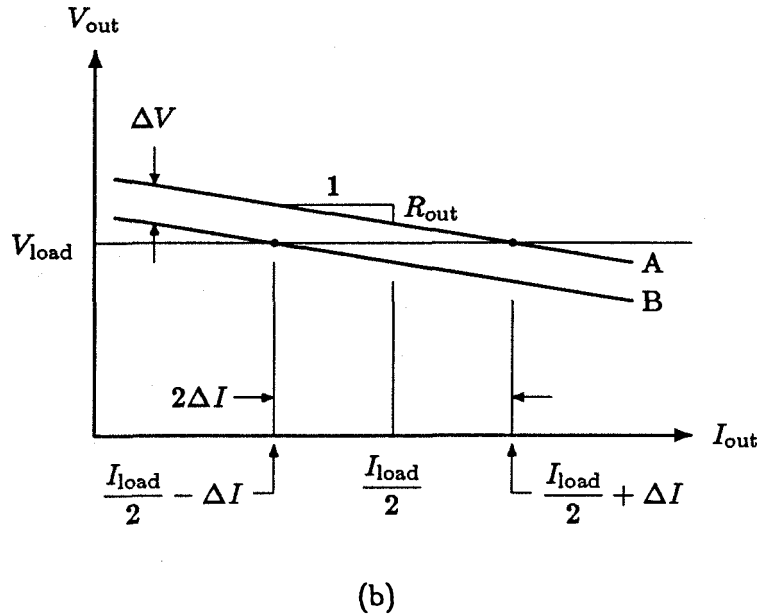
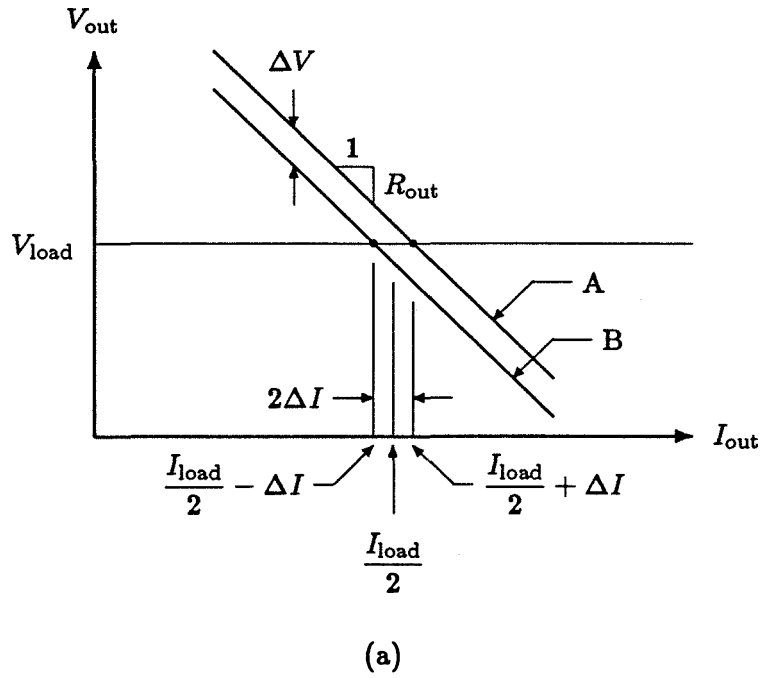


Figure 4.6: (a) Output characteristics of two converters operated in parallel when each converter has an appreciable output resistance. (b) The same characteristics for two converters with small output resistances.

Half-wave topologies in contrast share current naturally, a benefit of their large output resistance.

## Chapter 5

# Small-Signal Analysis of Quasi-Resonant Converters

The dc analysis of the previous section was based on the single assumption that the quantities  $I_{\text{on}}$  and  $V_{\text{off}}$  had small ripple and therefore could be considered constant during each cycle of the resonant switch. This same approximation, along with a restriction to low modulation frequencies, is the basis in this chapter for an ac small-signal model of quasi-resonant converters. In Section 5.1, the goal of an ac model—a low-frequency, time-invariant representation of the resonant switch—is discussed. Section 5.2 then derives a model of the resonant switch which leads to a linear small-signal circuit model in Section 5.3. Section 5.4 discusses the implications of the small-signal circuit model, then, as an illustration of the technique, the small-signal circuit model of a quasi-resonant buck converter is presented in Section 5.5.

### 5.1 Modelling Goal

Of all the characteristics of a switching power converter, it is the time-variance of the system equations that causes the most difficulty. Nonlinearities can be handled in various ways, but if the system is time-dependent, an exact model must consider the behavior of input waveforms over time intervals of less than a switching period. Such precision is usually unnecessary. From an input-output point of view, one is only concerned with the “average” or “low-frequency” behavior of the converter. So long as the system is stable and well-behaved, one requires no knowledge of the switching waveforms, and in fact one would hope to see no evidence at all at the input or output of a converter that the high-frequency switching waveforms were present.

The block diagram of Fig. 5.1 illustrates this concept. The converter, along with its

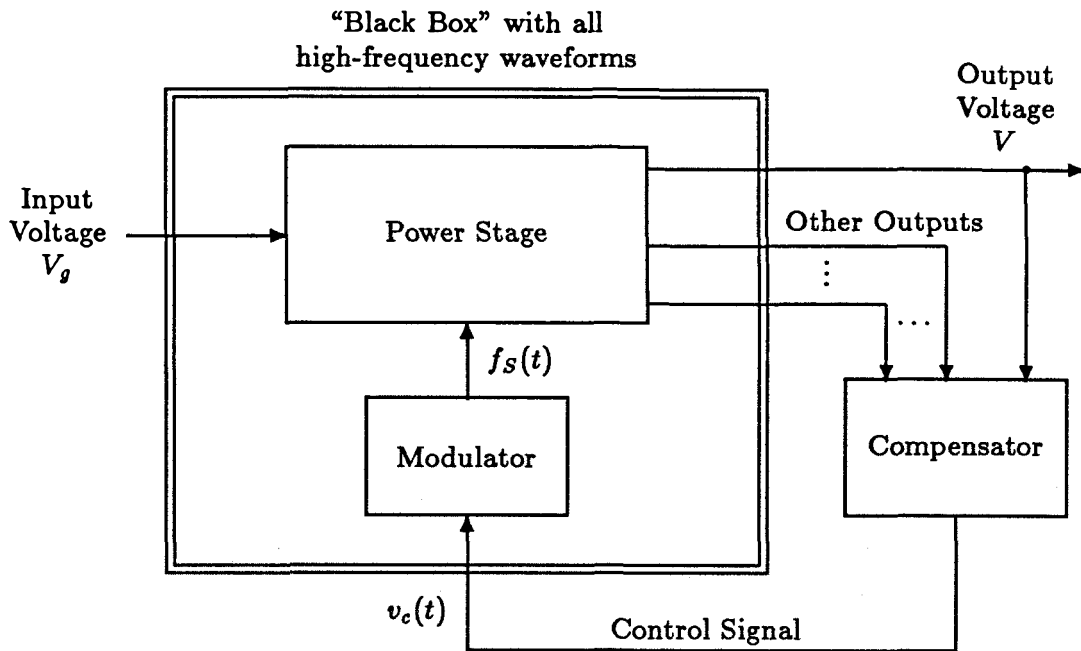


Figure 5.1: Block diagram illustrating control of a quasi-resonant converter.

controller, may be considered a “black box” with the source voltage  $v_g(t)$  and the control voltage  $v_c(t)$  as inputs. The outputs of interest may include the input current  $i_g(t)$ , and the output voltage  $v(t)$  and current  $i(t)$ . The point to be made in Fig. 5.1 is that only the *low-frequency behavior* of all these input and output waveforms is likely to be of interest. The input voltage, output voltage, and output current will by design be low-frequency waveforms, while the input current—if not already low-frequency—will undoubtedly be filtered until it *is* a waveform with small high-frequency content. Since the regulator bandwidth is sure to be well below the switching frequency, the control voltage  $v_c$  may also be considered a low-frequency waveform.

The exact description of a quasi-resonant converter therefore has two problems: first, it is time-varying, and second, it is unnecessarily complicated because it yields nonessential high-frequency information. The goal of this chapter is to remove the time-dependence and simultaneously produce a low-frequency model that is relatively simple.

## 5.2 A Low-Frequency Model for the Resonant Switch

This section derives an approximate time-invariant, low-frequency model for the switch  $S$  and diode  $D_2$ . The time dependence of the  $I$ - $V$  characteristic of the switch  $S$  is responsible for the time-varying system equations and the consequent difficulties discussed in the previous section. The diode  $D_2$ , while not time-varying, nevertheless changes its characteristic (between “OFF” and “ON”) at the switching frequency. Apart from these two elements, every other component of the converter is not only time-invariant but linear.

A low-frequency model that removes the troublesome time-dependent behavior of the semiconductor switches is developed here using two approximations. First, the by now familiar small-ripple approximation, which requires the converter state-variables to have small switching ripple, and second, the *low modulation frequency* (or simply “low-frequency”) approximation, which limits the model to frequencies far below the switching frequency.

Like the small-ripple approximation, the low-frequency approximation is hard to quantify, and its use is justified by a combination of physical and practical considerations. On the physical side, most converters have a closed-loop bandwidth  $\omega_{BW}$  much less than the switching frequency. The open-loop gain falls rapidly above  $\omega_{BW}$ . To the extent that the converter may be treated as a linear system, knowledge of the open-loop small-signal behavior up to  $\omega_{BW}$  is therefore sufficient for design of the closed-loop system. Practically, the low-frequency approximation—like the small-ripple approximation—makes the difference between a manageable analysis problem and a system description that can only be evaluated by a computer. With the low-frequency approximation, small-signal circuit models are easy to obtain. Without it, one must treat the converter as a sampled-data, time-varying system.

The modelling process once again begins by considering the converter as a linear network driven by the switch waveforms  $i_S(t)$  and  $v_D(t)$ , as shown in Fig. 4.1(a). When the converter is dynamically modulated, the waveforms  $i_S(t)$  and  $v_D(t)$  resemble those of Fig. 5.2. The waveforms consist of pulses similar to those of Fig. 3.6, but the amplitude, average, and separation of the pulses vary slowly as the converter is modulated.

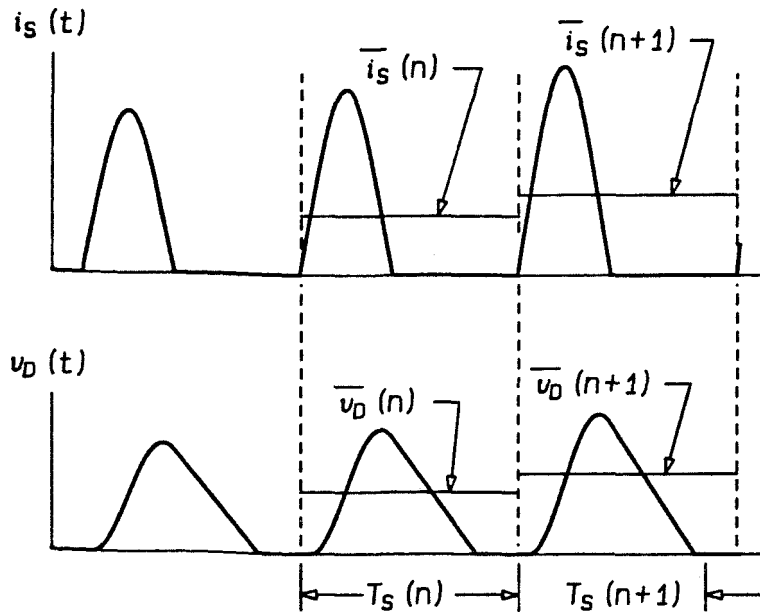


Figure 5.2: Under modulation, the amplitudes and averages of the switch waveforms  $i_s(t)$  and  $v_D(t)$ , as well as the switching period, vary slowly from one cycle to the next.

The spectra of  $i_s(t)$  and  $v_D(t)$  contain components at the switching frequency and its harmonics, at the modulation frequency, and at sidebands generated by both amplitude and frequency modulation of the steady-state waveform. Only the component at the modulation frequency is of interest here, for the following reason. The small-ripple approximation implies that the linear network of Fig. 4.1(a) acts as a low-pass filter, reducing the large-ripple waveforms  $i_s(t)$  and  $v_D(t)$  to small-ripple outputs and state variables. When the small-ripple approximation applies, only the low frequency—that is, modulation frequency—variations of the switch waveforms affect the “external” behavior of the converter. The problem of finding a model for the resonant switch therefore reduces to finding the low-frequency content of the waveforms  $i_s(t)$  and  $v_D(t)$ , or equivalently, finding substitute waveforms that are analytically manageable yet carry the same low-frequency information as the actual switch waveforms.

The technique used here is broadly referred to as *averaging*. Consider the switch waveforms  $i_s(t)$  and  $v_D(t)$ . Over the  $n$ th switching period, these waveforms have some

average values  $\bar{i}_S(n)$  and  $\bar{v}_D(n)$ , as shown in Fig. 5.2. When no modulation is present, the averages are given by Eqs.(3.40) and (3.41), repeated here:

$$\bar{i}_S = I_{\text{on}} \frac{F_S}{F_0} G(\rho) \quad (5.1)$$

$$\bar{v}_D = V_{\text{off}} \frac{F_S}{F_0} G(\rho) . \quad (5.2)$$

Under modulation, the quantities  $I_{\text{on}}$  and  $V_{\text{off}}$  (and hence  $\rho$ ) vary, and  $F_S$  is a discrete variable. The small-ripple and low-frequency approximations together imply that these three quantities change slowly, so that  $F_S$  can be considered a continuous variable  $f_S(t)$ , and the time-varying quantities  $i_{\text{on}}(t)$  and  $v_{\text{off}}(t)$  are nearly constant over a single switching period. (Note the use of lowercase symbols for time-varying quantities.) The averages of Eqs.(5.1) and (5.2) are functions of slowly-varying continuous quantities, so that under the low-frequency approximation the averages themselves can be treated as the continuous functions

$$\bar{i}_S(t) = i_{\text{on}}(t) \frac{f_S(t)}{F_0} G \left[ \frac{R_0 i_{\text{on}}(t)}{v_{\text{off}}(t)} \right] \quad (5.3)$$

$$\bar{v}_D(t) = v_{\text{off}}(t) \frac{f_S(t)}{F_0} G \left[ \frac{R_0 i_{\text{on}}(t)}{v_{\text{off}}(t)} \right] . \quad (5.4)$$

The question is now asked, do these “averaged” waveforms have the same low-frequency information as  $i_S(t)$  and  $v_D(t)$ ? This question is treated (for small-signal deviations) in Appendix B. Unfortunately, it cannot be shown in general that averaging preserves low-frequency information. In fact, as demonstrated in Appendix B, waveforms exist in the quasi-resonant converter itself for which averaging destroys low-frequency information. Averaging is a very useful technique, however, intuitively plausible and applicable to a variety of waveforms. It has long been used in the analysis of modulated waveforms in PWM converters. The discussion of Appendix B emphasizes the fact that averaging will not *always* preserve low-frequency information, and that one should always check by some means—analytical or empirical—whether it does so when applied to a particular situation or set of waveforms. That averaging is valid for the waveforms  $i_S(t)$  and  $v_D(t)$  under small-signal modulation is verified by the experimental results of Chapter 7.

Under the postulate that averaging “works” with the waveforms  $i_S$  and  $v_D$ , the small-signal variations  $\hat{i}_S$  and  $\hat{v}_D$  of the continuous averages of Eqs.(5.3) and (5.4) contain the

same low-frequency information as the variations of the actual waveforms  $i_S(t)$  and  $v_D(t)$ . Replacing the switch  $S$  and diode  $D_2$  with controlled sources generating the variations  $\hat{i}_S$  and  $\hat{v}_D$  therefore yields a low-frequency, time-invariant model of the quasi-resonant converter.

### 5.3 Small-Signal Circuit Model

To obtain a small-signal model, all quantities are considered as the sum of a steady-state component, written with a capital letter, and a small-signal perturbation, denoted by a lowercase symbol and a hat ( $\hat{\cdot}$ ). Perturbations of the continuous averages of Eqs.(5.3) and (5.4) are functions of  $\hat{i}_{on}$ ,  $\hat{v}_{off}$ , and  $\hat{f}_S$ , the last being the small-signal variation of the control variable  $F_S$ . For example,

$$\hat{i}_S = \frac{\partial \bar{i}_S}{\partial i_{on}} \hat{i}_{on} + \frac{\partial \bar{i}_S}{\partial v_{off}} \hat{v}_{off} + \frac{\partial \bar{i}_S}{\partial f_S} \hat{f}_S \quad (5.5)$$

with a similar expansion for  $\hat{v}_D$ . When evaluated and assigned  $h$ -parameter labels, the partial derivatives yield

$$h_{ii} \equiv \frac{\partial \bar{i}_S}{\partial i_{ON}} = \frac{F_S}{F_0} [G(\rho) + \rho G'(\rho)] \quad (5.6)$$

$$h_{iv} \equiv \frac{\partial \bar{i}_S}{\partial v_{OFF}} = -\frac{1}{R_0} \frac{F_S}{F_0} \rho^2 G'(\rho) \quad (5.7)$$

$$h_{if} \equiv \frac{\partial \bar{i}_S}{\partial f_S} = \frac{I_{ON}}{F_0} G(\rho) \quad (5.8)$$

$$h_{vi} \equiv \frac{\partial \bar{v}_D}{\partial i_{ON}} = R_0 \frac{F_S}{F_0} G'(\rho) \quad (5.9)$$

$$h_{vv} \equiv \frac{\partial \bar{v}_D}{\partial v_{OFF}} = \frac{F_S}{F_0} [G(\rho) - \rho G'(\rho)] \quad (5.10)$$

$$h_{vf} \equiv \frac{\partial \bar{v}_D}{\partial f_S} = \frac{V_{OFF}}{F_0} G(\rho) , \quad (5.11)$$

where  $G'(\rho)$  is the derivative of  $G$  with respect to  $\rho$ . For the half-wave switch,

$$G'_{hw}(\rho) = -\frac{1}{4\pi} \left( \frac{1 + \sqrt{1 - \rho^2}}{\rho} \right)^2 . \quad (5.12)$$

Since  $G_{fw}(\rho)$  is very nearly constant for the full-wave switch,  $G'_{fw} \approx 0$ .

The  $h$ -parameters are evaluated using the steady-state values of  $I_{on}$  and  $V_{off}$  in  $\rho$ . Two improvements can be made on the  $h$ -parameter equations above. First, the ratio



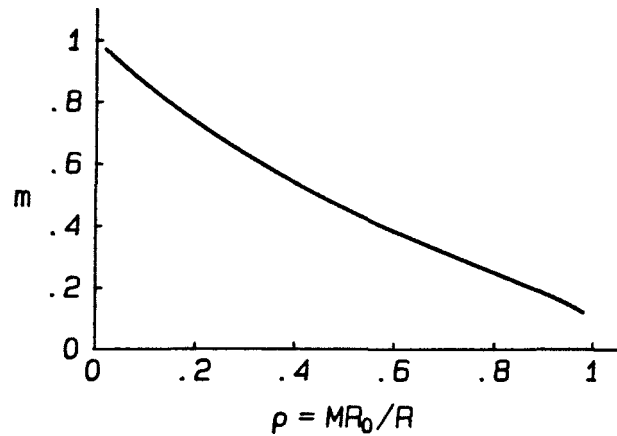


Figure 5.3: Plot of  $m$  versus  $\rho$  for the half-wave resonant switch.

$F_S/F_0$  can be replaced by  $D_P(M)/G(\rho)$  and  $\rho$  itself can be replaced by  $MR_0/R$ , both relations derived in Chapter 4. A second improvement results from defining

$$m \equiv -\rho \frac{G'(\rho)}{G(\rho)}. \quad (5.13)$$

Figure 5.3 shows that  $m$  always lies between 0 and 1 for the half-wave switch.<sup>1</sup> For the full-wave switch,  $m$  is essentially zero for all values of  $\rho$ .

With these substitutions, the  $h$ -parameters become

$$h_{ii} = D_P(M)(1 - m) \quad (5.14)$$

$$h_{iv} = \frac{mMD_P(M)}{R} \quad (5.15)$$

$$h_{if} = \frac{I_{on}D_P(M)}{F_S} \quad (5.16)$$

$$h_{vi} = -\frac{mRD_P(M)}{M} \quad (5.17)$$

$$h_{vv} = (1 + m)D_P(M) \quad (5.18)$$

$$h_{vf} = \frac{V_{off}D_P(M)}{F_S}. \quad (5.19)$$

A useful mnemonic for the units of each  $h$ -parameter is to imagine a fraction bar (/) between the two subscript letters. For instance,  $h_{iv}$  has units of  $i/v = \Omega^{-1}$ , or conductance.

<sup>1</sup>One may note that  $m$ , and the corresponding plot of Fig. 5.3, match exactly Eq.(4.17) and Fig. 4.4 of Chapter 4. The output resistance of a quasi-resonant buck converter is therefore  $m$  times its load resistance.

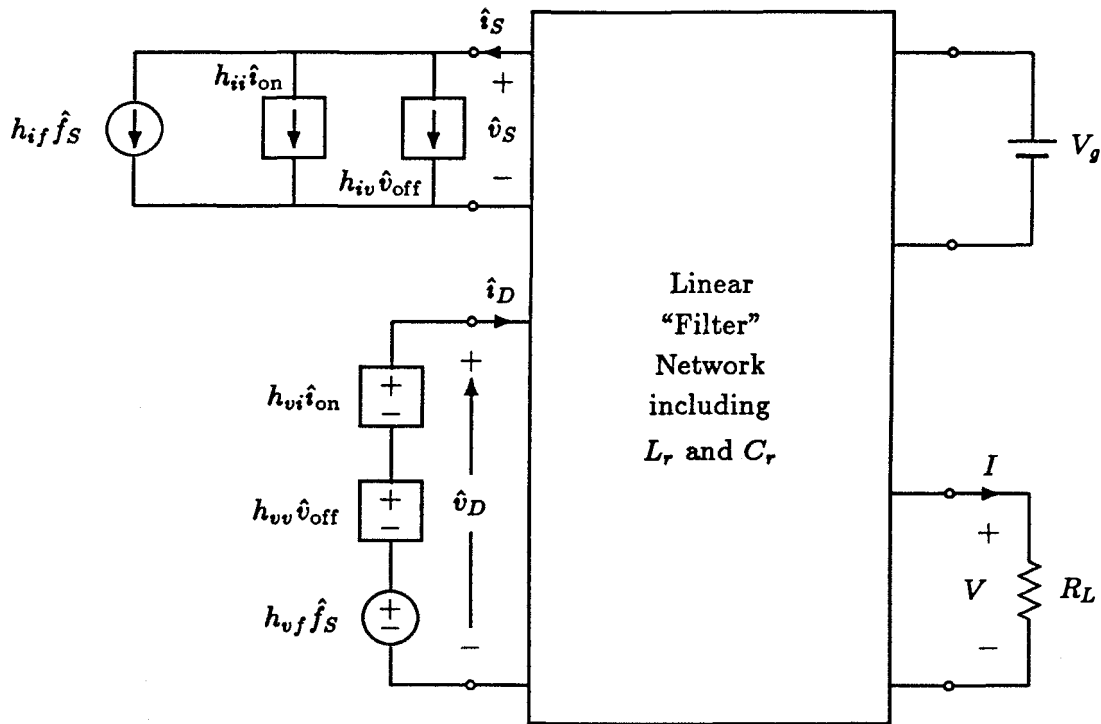


Figure 5.4: Small-signal model for a zero-current quasi-resonant converter.

The small-signal circuit model is shown in Fig. 5.4. Each term in Eq.(5.5) represents a controlled current source of value given by the appropriate  $h$ -parameter, and these separate current generators replace the two-quadrant switch  $S$ . The diode  $D_2$  is replaced by three controlled voltage sources. All quantities in the remaining circuit are replaced by their small-signal variations, including  $I_{on}$  and  $V_{off}$  which are replaced by  $\hat{i}_{on}$  and  $\hat{v}_{off}$ . Frequency variation  $\hat{f}_S$  is considered an independent parameter, and the sources it controls are indicated by circles. Sources dependent upon voltages and currents elsewhere in the circuit are indicated by squares.

It should be noted that the resistance  $R_L$  appearing in the small-signal model of Fig. 5.4 is the *small-signal* resistance of the load, given by the slope of the load's  $V$ - $I$  characteristic. The value  $R$  that appears in the dc equations and in the small-signal parameters is the ratio  $V/I$ , the dc resistance of the load. For a nonlinear load—one that is not a linear resistor—the values of  $R_L$  and  $R$  may be quite different.

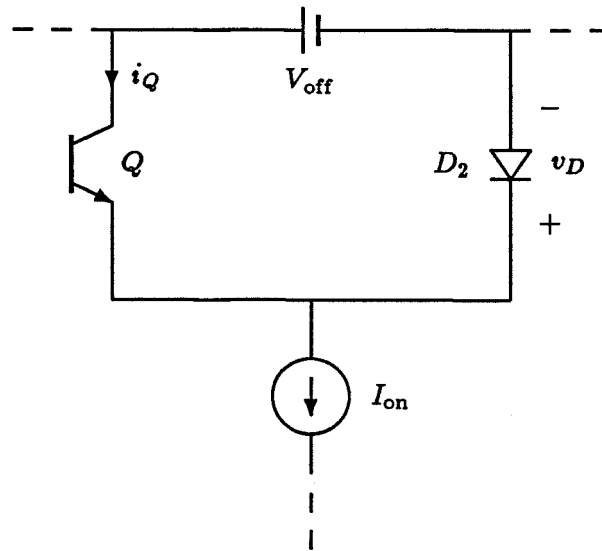
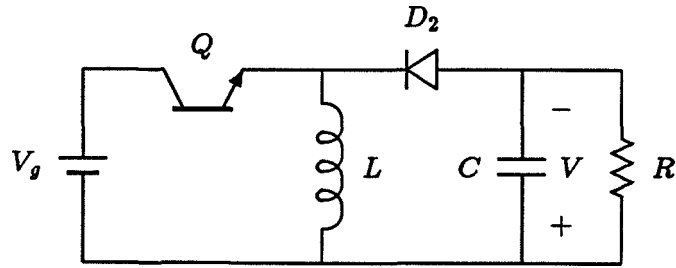


Figure 5.5: The general structure of a PWM switch.

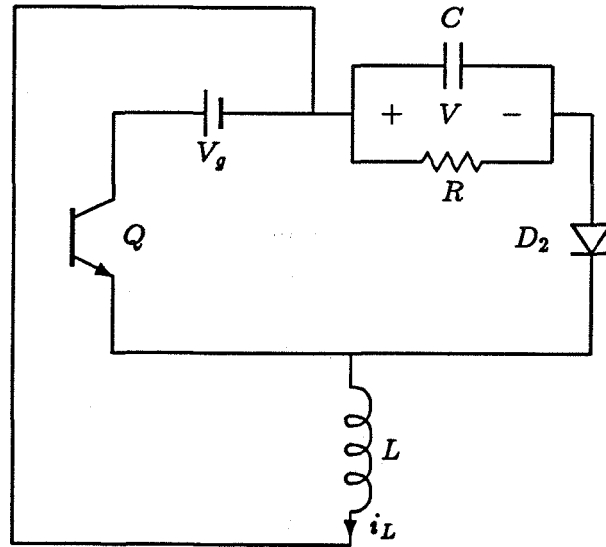
#### 5.4 Interpretation of the Small-Signal Model

The features of the small-signal model are best understood by viewing another version of the circuit of Fig. 5.4. Any PWM converter satisfying the definition of Chapter 3 may be redrawn in the form of Fig. 5.5. That this may always be done is a consequence of the loop and cut-set of Theorems 1 and 2. For example, the buck-boost converter of Fig. 5.6(a) may be redrawn as in Fig. 5.6(b). The fact that the elements producing  $V_{off}$  are “tapped” is of no consequence. Figure 5.5 simply shows that a set of elements generates a voltage  $V_{off}$  across the series connection of  $Q$  and  $D_2$ , as required by Theorem 1.

When a PWM converter in the form of Fig. 5.5 is transformed into a quasi-resonant converter, the transistor  $Q$  is replaced by a two-quadrant switch  $S$ , and a resonant inductor and capacitor are added. In many cases, the resonant elements may be neglected in the dynamic model. If the capacitor  $C_r$  is in parallel with the diode  $D_2$ , for instance, then when  $D_2$  is replaced by a voltage source in the small-signal model,  $C_r$  may be removed. Similarly,  $L_r$  may be removed if it is in series with  $S$ . Even when these elements are not in these positions, the values of  $L_r$  and  $C_r$  are often so much smaller than the other reactances in the circuit that their effect on the dynamics only becomes apparent at frequencies near or above the switching frequency. Since the small-signal model is



(a)



(b)

Figure 5.6: The buck-boost PWM converter (a) can be re-drawn as in (b) to fit the model of Fig. 5.5

valid only for frequencies far below the switching frequency, the resonant elements may often be neglected.

Under the assumption that the resonant inductor and capacitor may be neglected, the small-signal model of a quasi-resonant converter, drawn according to the form of the converter fragment of Fig. 5.5, is shown in Fig. 5.7. In this figure, the quantities  $\hat{v}_{\text{off}}$  and  $\hat{i}_{\text{on}}$  are shown appearing across a single capacitor and in an inductor, respectively. These elements are used for convenience only, and the figure applies equally to cases where more than one element produces  $\hat{v}_{\text{off}}$  or  $\hat{i}_{\text{on}}$ .

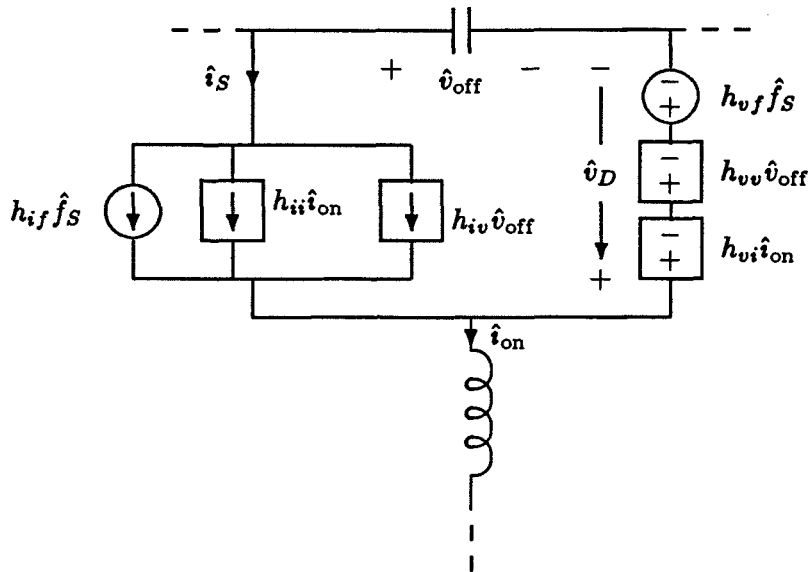


Figure 5.7: The small-signal model of a zero-current quasi-resonant converter, following the structure of Fig. 5.5

Perhaps the most important feature of the small-signal model of a half-wave quasi-resonant converter is the introduction of damping. This damping is indicated in the small-signal model by resistors. Figure 5.8 shows how these resistors arise. In Fig. 5.8(a), the current source  $h_{iv}\hat{v}_{off}$  has been replaced by two current sources, one across the voltage sources of  $D_2$  and one across  $\hat{v}_{off}$ . Figure 5.8(a) is equivalent in every way to Fig. 5.7. In Fig. 5.8(a), however, the current source across the voltage sources of  $D_2$  may be eliminated. The other current source, across  $\hat{v}_{off}$ , is an element that generates a current proportional to the voltage across it. Such an element is a resistor, as shown in Fig. 5.4(b). The value of the resistance across  $\hat{v}_{off}$  is  $h_{iv}^{-1}$ .

By a similar process, the voltage source  $h_{vi}\hat{i}_{on}$  may be replaced by two sources, one in the  $\hat{i}_{on}$  branch and one in series with current sources from the switch  $S$ , as in Fig. 5.8(c). The voltage source in series with ideal current sources may be eliminated, while the source in series with  $\hat{i}_{on}$  becomes a resistor of value  $-h_{vi}$ , as shown in Fig. 5.8(d).

Since  $h_{vi}$  is always negative and  $h_{iv}$  always positive, both resistors in Fig. 5.8(d) are positive. These positive resistors indicate damping in the converter dynamic behavior. The model of Fig. 5.8(d) is not reciprocal, however, and it is not immediately clear

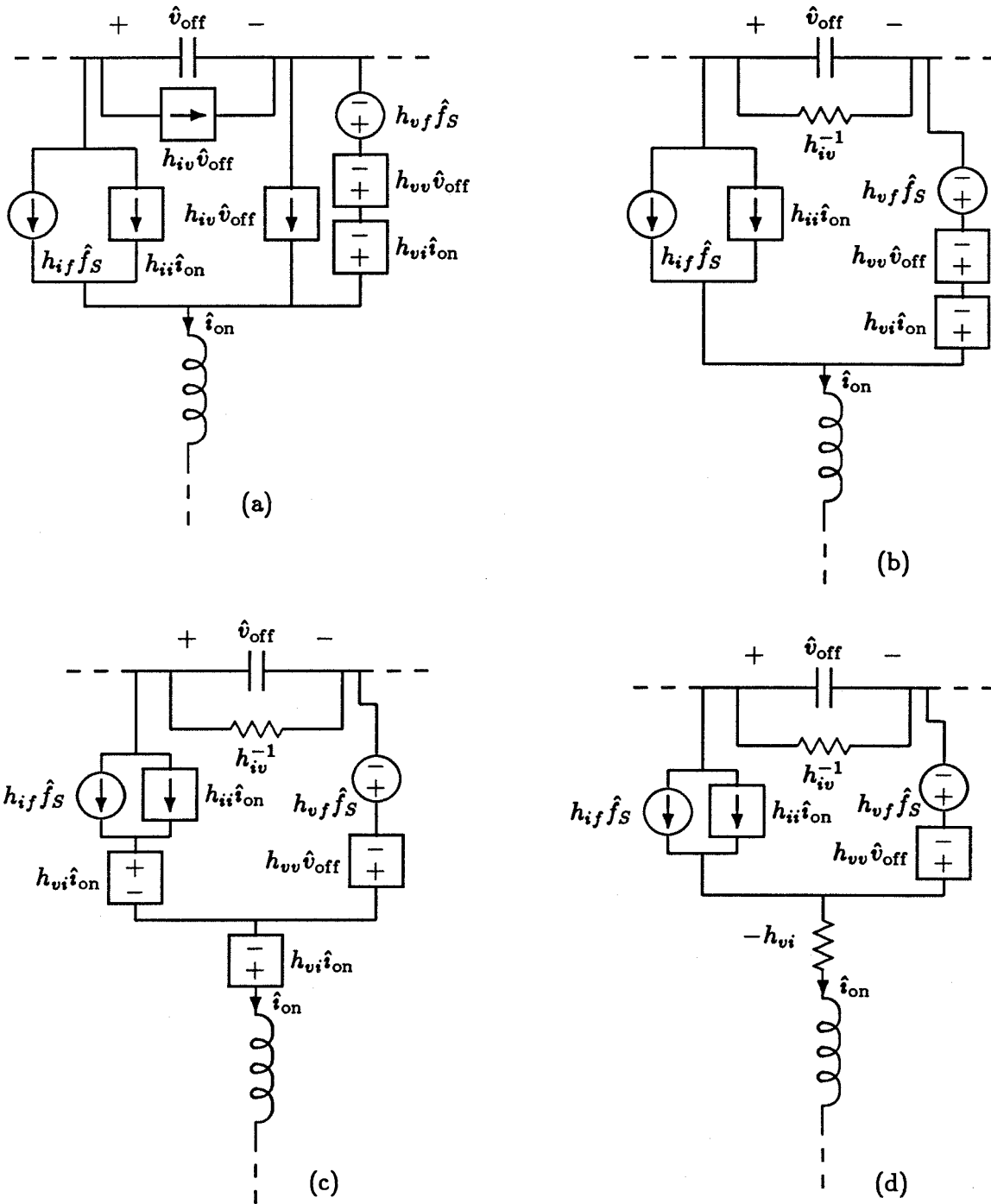


Figure 5.8: The controlled sources in Fig. 5.7 may be moved to new, equivalent positions. The current source  $h_{iv}$ , translated as in (a), becomes a resistor across  $V_{off}$  (b), while the voltage source  $h_{vi}$ , shifted as shown in (c), is equivalent to a resistor in series with  $I_{on}$  (d).

whether the remaining sources generate or absorb power.

To demonstrate that the net effect is indeed damping, let the driving generators (those dependent on  $\hat{f}_S$ ) be set to zero in Fig. 5.7. The power absorbed by the remaining sources is

$$P = \hat{v}_S \hat{i}_S + \hat{v}_D \hat{i}_D \quad (5.20)$$

$$= (\hat{v}_{\text{off}} - \hat{v}_D) \hat{i}_S + \hat{v}_D (\hat{i}_S - \hat{i}_{\text{on}}) \quad (5.21)$$

$$= h_{iv} \hat{v}_{\text{off}}^2 + (h_{ii} - h_{vv}) \hat{v}_{\text{off}} \hat{i}_{\text{on}} - h_{vi} \hat{i}_{\text{on}}^2. \quad (5.22)$$

The first and second terms of Eq.(5.22) represent the power dissipated respectively by the resistors  $h_{iv}^{-1}$  and  $-h_{vi}$  of Fig. 5.8(d). The cross term,  $(h_{ii} - h_{vv}) \hat{v}_{\text{off}} \hat{i}_{\text{on}}$ , may add to or subtract from the power lost in the resistors. However, the quadratic form of Eq.(5.22) can be shown, using the expressions of Eqs.(5.14) through (5.19), to be positive semi-definite. The actual damping may therefore be greater or less than that expected from the resistors  $h_{iv}^{-1}$  and  $-h_{vi}$  alone, but damping is always present.

Note that the switch  $S$  and diode  $D_2$  do not actually dissipate any power. The apparent “damping” is instead a result of modulation of the switching instants which promotes decay of perturbations.

The damping introduced by the half-wave resonant switch is a feature shared with PWM converters operated either under current-mode programming or in the discontinuous conduction mode. In both of these cases, the inductor current is constrained to some fixed value during each switching period. The dependent inductor current is no longer a state variable, and the system order is reduced by one. In current-mode programming, this effect is never fully realized and instead one pole lies between one-sixth and two-thirds of the switching frequency [15]. The damping in current-mode programming is visible in the circuit model of [15] as a resistance in series with the inductor whose current is constrained. Damping in the discontinuous conduction mode of operation is “complete” in the sense that the second pole completely disappears [16].

Control of power converters is difficult because resistive damping of the high- $Q$  resonances internal to the converter must be small for reasons of efficiency. The load represents the only lossless element available for damping. The half-wave resonant switch

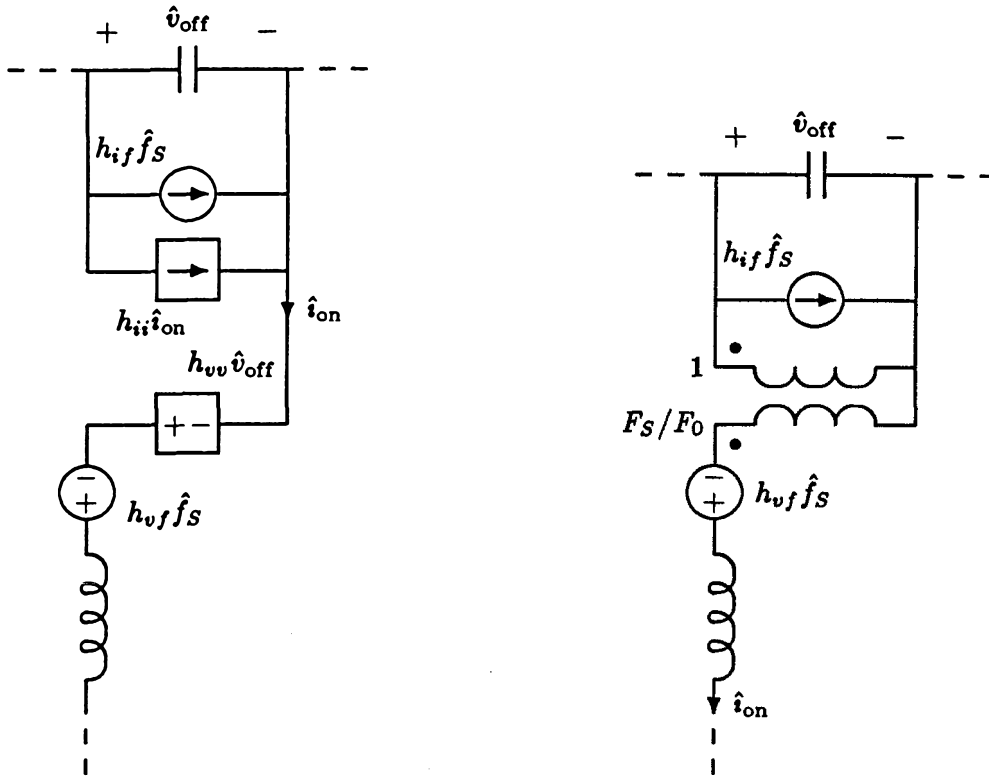


Figure 5.9: In a full-wave quasi-resonant converter, the controlled sources may be shifted to new positions (a), and combined into a transformer (b).

represents a new way to provide lossless damping in a converter. It joins the ranks of current-mode programming [15], discontinuous conduction mode [16], and storage-time modulation [17] as means of introducing the *effects* of damping by appropriate control of the switching process, without actually dissipating any power.

As  $\rho \rightarrow 1$  in a half-wave quasi-resonant converter,  $h_{iv}$  and  $h_{vi}$  both approach zero and the damping disappears.

In converters with a full-wave switch,  $h_{iv}$  and  $h_{vi}$  are zero for all values of  $\rho$  (under the excellent approximation that  $G(\rho) = 1$  for all  $\rho$ ), and  $h_{ii}$  and  $h_{vv}$  both equal  $F_s/F_0$ . For such converters, the small-signal model may be drawn as in Fig. 5.9(a). Both the current sources,  $h_{if} \hat{f}_s$  and  $h_{ii} \hat{i}_{on}$ , have been shifted to positions across  $\hat{v}_{off}$ , and both voltage sources,  $h_{vf} \hat{f}_s$  and  $h_{vv} \hat{v}_{off}$ , have been moved in series with  $\hat{i}_{on}$ . Since both  $h_{ii}$  and  $h_{vv}$  are equal to  $F_s/F_0$ , the two controlled sources constitute a transformer, as



shown in Fig. 5.9(b). The circuit model is therefore reciprocal (with the exception of the independent sources) and lossless.

### 5.5 An Example

Consider as an example the buck converter with a half-wave resonant switch, as in Fig. 5.10(a). The small-signal model, shown in Fig. 5.10(b), is obtained by replacing the resonant switch with its model from Fig. 5.4. The control-to-output and line-to-output transfer functions are easily derived from Fig. 5.10:

$$\frac{\hat{v}}{\hat{f}_s} = h_{vf}H(s) \quad (5.23)$$

$$\frac{\hat{v}}{\hat{v}_g} = h_{vv}H(s) \quad (5.24)$$

where  $H(s)$  is the voltage transfer function of the output filter,

$$H(s) = \frac{H_0}{1 + \frac{1}{Q_f} \frac{s}{\omega_{0f}} + \left(\frac{s}{\omega_{0f}}\right)^2} \quad (5.25)$$

with

$$H_0 = \frac{R}{R + R_l + |h_{vi}|} \quad (5.26)$$

$$\omega_{0f} \approx \frac{1}{\sqrt{L_f C_f}} \sqrt{1 + |h_{vi}|/R} \quad (5.27)$$

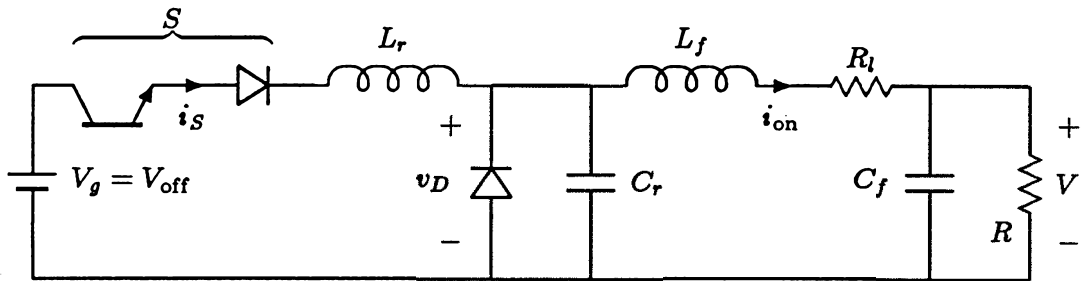
$$\frac{1}{Q_f} \approx \frac{1}{\sqrt{1 + |h_{vi}|/R}} \left[ \frac{R_l + |h_{vi}|}{R_{0f}} + \frac{R_{0f}}{R} \right] \quad (5.28)$$

where

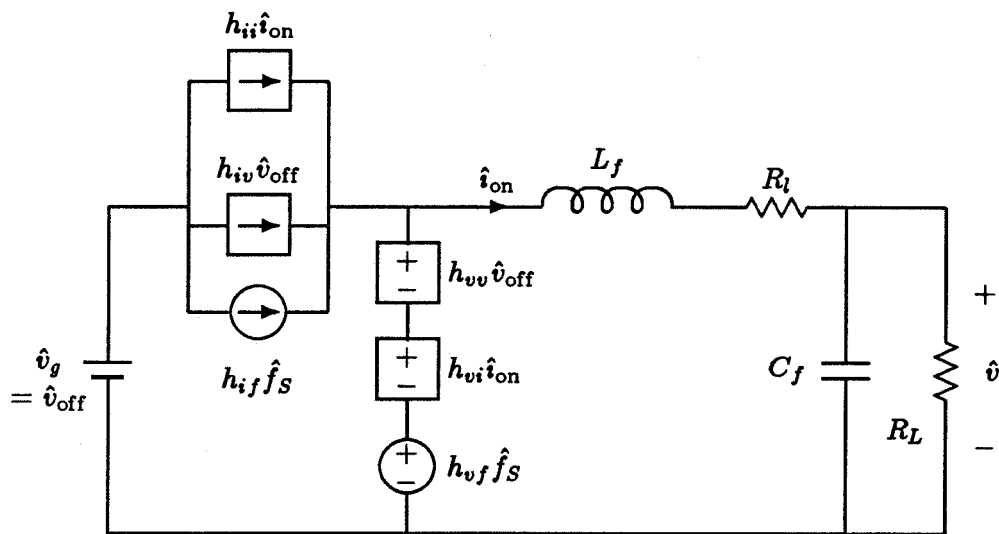
$$R_{0f} \equiv \sqrt{\frac{L_f}{C_f}} \quad (5.29)$$

Equations (5.27) and (5.28) use the approximation  $R_l \ll R$ .

Compared to the PWM buck converter, the introduction of the resistance  $|h_{vi}|$  by the resonant switch reduces the effective  $Q$  factor to  $Q_f$ , and increases the filter corner frequency to  $\omega_{0f}$ . The lossless output resistance noted in the dc performance of the half-wave switch is also present at ac. In fact, the dc output resistance, given in Eq.(4.17) of Chapter 4, is simply  $|h_{vi}|$ , the same resistance introduced by the resonant switch in the ac model.



(a)



(b)

Figure 5.10: A half-wave quasi-resonant buck converter (a) and its small-signal model (b).

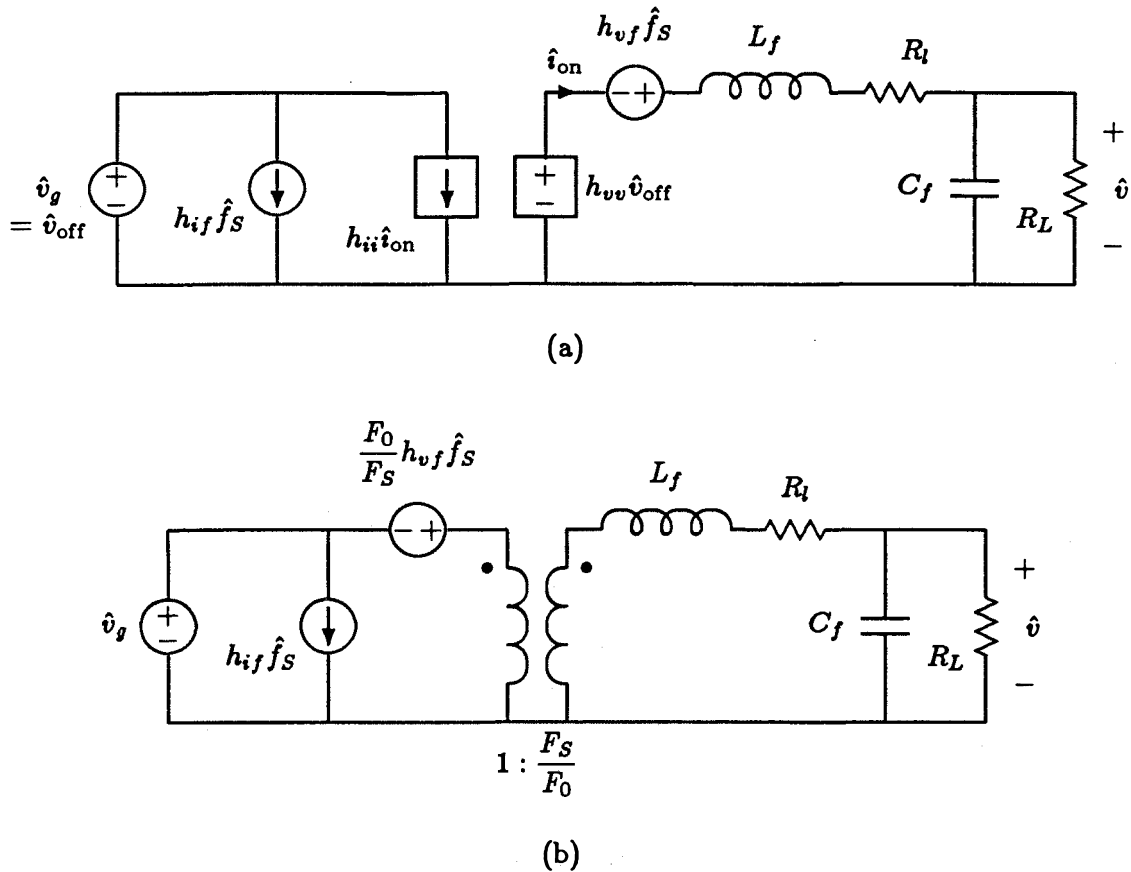


Figure 5.11: Small-signal model for the quasi-resonant buck converter with a full-wave switch.

Chapter 7 presents experimental results for the converter of Fig. 5.10. These results illustrate by means of frequency response curves the damping from  $h_{vi}$  and the consequent reduced  $Q_f$ .

If, instead of a half-wave switch, the buck converter was outfitted with a full-wave resonant switch, then the small-signal model would follow Fig. 5.11(a), because  $h_{iv}$  and  $h_{vi}$  are approximately zero. Since  $h_{ii} = h_{vv} = F_S/F_0$ , the two dependent sources can be combined into a transformer, and the circuit rearranged as in Fig. 5.11(b). This circuit is recognized as the circuit model obtained by state-space averaging [11], with  $D$  replaced by  $F_S/F_0$  and  $\hat{d}$  similarly replaced by  $\hat{f}_S/F_0$ . Note that there is no added damping, and that the network is reciprocal (except for the  $\hat{f}_S$  sources).

## 5.6 Effects of the Resonant Reactances

In the examples of Figs. 5.10 and 5.11, the resonant capacitor  $C_r$  “fell out” of the model since it appeared in parallel with a voltage source. Similarly,  $L_r$  was in series with ideal current sources and was therefore redundant. Not all variations of resonant switches share this feature, but in many cases the resonant reactances may be neglected in the small-signal model even when they are not immediately eliminated from the equivalent circuit.

As a consequence of the small-ripple restriction, the resonant inductor must be a much smaller inductance than any of the inductors present in  $I_{on}$ . Likewise, the resonant capacitor must have a capacitance much less than any capacitors in  $V_{off}$ . Consequently,  $L_r$  and  $C_r$  may frequently be neglected, since their effects only appear in the frequency response at frequencies near or above the switching frequency.

This is not always the case, however, as illustrated by the converter of Fig. 5.12(a) and its corresponding small-signal circuit model, Fig. 5.12(b). This circuit differs from that of Fig. 5.10(a) only in the placement of the resonant capacitor  $C_r$ . The filter inductor  $L_f$  and resonant capacitor  $C_r$  together form an undamped parallel-resonant circuit. Even though  $C_r$  is small,  $L_f$  may be quite large, so that the resulting resonance can occur well below the switching frequency. Measurements described in Chapter 7 indicate that the resonance does indeed appear.

Routinely ignoring the resonant reactances may therefore lead to errors in the small-signal model. A recommended procedure is to retain  $L_r$  in the circuit model *unless* the inductance is in series with the switch  $S$ . The resonant capacitor should also be left in the model unless it appears in parallel with the diode  $D_2$  or in a loop with only  $D_2$  and  $V_g$ .

Despite the possibility that either or both of  $L_r$  and  $C_r$  may be present in the small-signal circuit model, these elements will never increase the order of the system above that of the original PWM converter. Rule 1 of Definition 2 in Chapter 3 reveals that  $C_r$  will always be in a loop of capacitors and voltage sources, once the diode  $D_2$  is replaced by its voltage-source model. Similarly, Rule 2 of Definition 2 indicates that  $L_r$  will always be in a cut-set of inductors in the small-signal model. These topological restraints mean

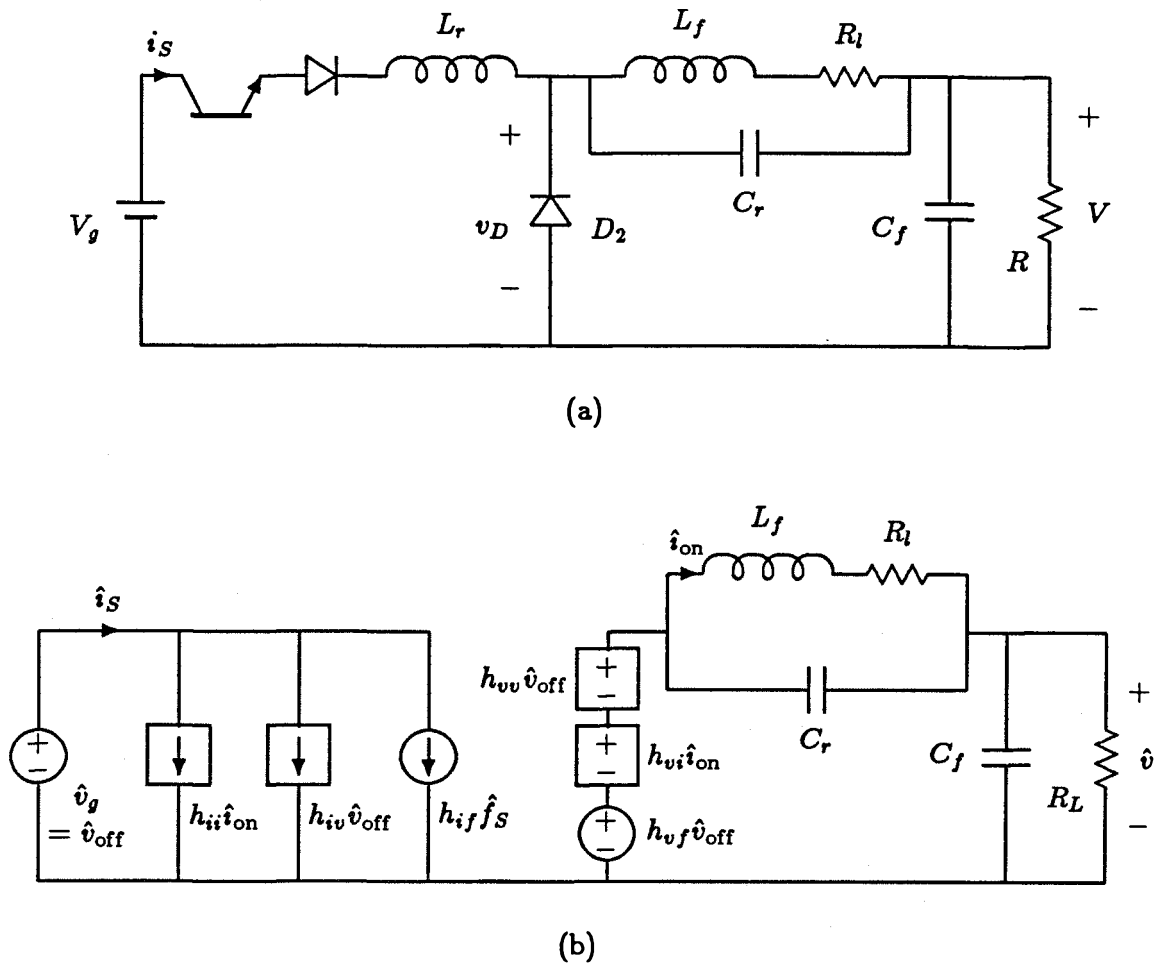


Figure 5.12: (a) A quasi-resonant buck converter with the resonant capacitor across the output filter inductor. (b) The small-signal model for this converter.

that neither  $C_r$  nor  $L_r$  can be state variables. These elements may introduce zeros in the transfer functions and slightly modify the positions of existing poles, but they cannot add any new poles.

The fact that the quasi-resonant converter has the same order as its parent PWM converter indicates that the resonant switch itself has no dynamics. Despite the highly “dynamic” resonant waveforms present during each cycle, the switch waveforms  $i_s$  and  $v_D$  must return to zero at the end of every cycle. The switch cannot carry any information from one cycle over to the next in the form of an initial condition. Having no “memory,” therefore, the resonant switch has no dynamics.



## Chapter 6

# Extensions of Resonant Switches

Chapters 3 through 5 have considered only a limited class of quasi-resonant converters: those based on PWM converters with a single transistor and diode and no transformer. In addition, those chapters have considered only the zero-current resonant switches. Zero-voltage switches may be treated in exactly the same way as zero-current switches, however, and the restrictions of a single switch and no transformers may often be circumvented. In Section 6.1 of this chapter the zero-voltage resonant switch is studied by application of duality principles to the zero-current switch. Section 6.2 next reveals the power of the general analysis method developed in previous chapters. A simple generalization of the functions  $G_{hw}(\rho)$  and  $G_{fw}(\rho)$  is all that is needed to account for another mode of operation of resonant switches—multiple conduction cycles. Finally, Section 6.3 gives an example of modeling a converter with a transformer and more than one transistor switch.

### 6.1 Zero-Voltage Resonant Switches

Resonant switches that turn ON and OFF into zero voltage were introduced in [8]. These switches are duals of the zero-current-switching (ZCS) switches previously analyzed. Rather than consider each zero-voltage-switching (ZVS) quasi-resonant converter as a dual of some other zero-current converter, duality will be applied first to the PWM converter itself, deriving the duals of Definition 1 and Theorems 1 and 2 of Chapter 3. Then, using the dual of Definition 2, the behavior of the zero-voltage resonant switch can be derived in as general a fashion as for the zero-current switch.



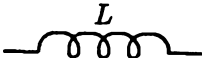
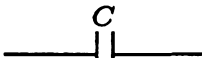



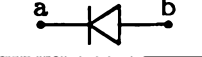


Voltage	$\longleftrightarrow$	Current
Impedance	$\longleftrightarrow$	Admittance
Loop	$\longleftrightarrow$	Cut-set
	$\longleftrightarrow$	
	$\longleftrightarrow$	
	$\longleftrightarrow$	
	$\longleftrightarrow$	
	$\longleftrightarrow$	

Table 6.1: In taking the dual of a network or theorem, the quantities above are interchanged.

### 6.1.1 Duality

Forming the dual of a circuit is both a topological and a quantitative process. “Meshes” and nodes are interchanged to obtain the topology of the new circuit. The voltage and current in each branch are interchanged, so that the circuit elements of each branch are replaced by their duals. Table 6.1 lists elements and quantities that are duals of each other.

Some networks do not have physical duals. For example, a network with coupled inductors would have coupled capacitors in its dual. The equations describing such a network may be written, but the circuit could not be built. Also, a network whose graph is nonplanar has no dual. We assume that all the converters considered have planar graphs and no coupled inductors, so that duals always exist.

### 6.1.2 Dual of a Resonant Switch Converter

As seen in Chapter 3, a quasi-resonant converter can be formed by starting with a PWM converter satisfying Definition 1 and then performing the modifications of Defini-



tion 2. The *dual* of the resulting converter can be developed by applying duality to each step of the transformation from PWM to quasi-resonant converter.

Definition 1, describing PWM converters, is its own dual when one considers that the input current source arising from the dual of item 3 of the definition will always be implemented in practice by a voltage source in series with a “stiff” inductor. The dual of a PWM converter is therefore another PWM converter, a well-known fact. The only change in a PWM converter introduced by duality is the interchanging of the ON and OFF times of the transistor switch as a result of the interchange of the switch current and voltage waveforms. The duty ratio  $D$  of a PWM converter is replaced by its complement,  $1 - D$ , in the dual converter.

Application of duality to the next step in the PWM-to-resonant switch transformation, the rules of Definition 2, yields the following topological rules governing ZVS resonant switches:

**Rule 3:** *The diode  $D_2$ , the resonant inductor  $L_r$ , and a (possibly empty) set of inductors form a cut-set in a ZVS converter.*

**Rule 4:** *The two-quadrant switch  $S$ , the resonant capacitor  $C_r$ , and a (possibly empty) set of capacitors and voltage sources form a loop in a ZVS converter.*

Insertion of the resonant inductor  $L_r$  in series with the diode  $D_2$  and the resonant capacitor  $C_r$  in parallel with the two-quadrant switch  $S$  always forms a ZVS converter. As with the zero-current case, several other locations for  $L_r$  and  $C_r$  are possible for each initial topology.

Theorems 3 and 4 are duals of each other, so the pair is unchanged after application of duality. Continued application of the duality transformation to the waveforms derived in Chapter 3 reveals that only a few changes are necessary to transform the results of Chapters 3, 4, and 5 into ZVS converters. These changes are listed in Table 6.2.

For instance, the ZCS converter has average switch current

$$\bar{i}_S = I_{\text{on}} \frac{F_S}{F_0} G(\rho) . \quad (6.1)$$

Zero-Current		Zero-Voltage
$I_{\text{on}}$	$\longrightarrow$	$V_{\text{off}}$
$V_{\text{off}}$	$\longrightarrow$	$I_{\text{on}}$
$R_0$	$\longrightarrow$	$R_0^{-1}$
$R$	$\longrightarrow$	$R^{-1}$
$\rho$	$\longrightarrow$	$\rho^{-1}$
$i_S$	$\longrightarrow$	$v_S$
$v_D$	$\longrightarrow$	$i_D$
$M$	$\longrightarrow$	$M^{-1}$
$D$	$\longrightarrow$	$1 - D$

Table 6.2: Transformations that change the equations for a ZCS quasi-resonant converter into those for a ZVS converter.

Application of the transformations of Table 6.2 yields the average switch *voltage* in the dual ZVS converter:

$$\bar{v}_S = V_{\text{off}} \frac{F_S}{F_0} G(\rho^{-1}) . \quad (6.2)$$

As a further example, where  $0 < \rho < 1$  for zero-current turn-OFF in the ZCS converter, the requirement for zero-current turn-OFF in the dual ZVS converter is  $0 < \rho^{-1} < 1$ , or  $1 < \rho < \infty$ .

### 6.1.3 Dc and Ac Behavior of ZVS Converters

Performing the substitutions of Table 6.2 on Eq.(4.11), which related the switching frequency and conversion ratio for ZCS converters in Chapter 4, one obtains

$$\frac{F_S}{F_0} = \frac{1 - D_P(M)}{G(\rho^{-1})} . \quad (6.3)$$

This expression, valid for all ZVS quasi-resonant converters, allows plotting of the dc characteristics. Note that the function  $G$  is unchanged by the duality transformation; the argument alone is inverted.

When duality is applied to the small-signal ac model, the subscripts of the  $h$ -parameters must be changed, in addition to the transformations of Table 6.2. The parameter  $h_{i_v}$ , for example, indicates the value of a current source controlled by a voltage

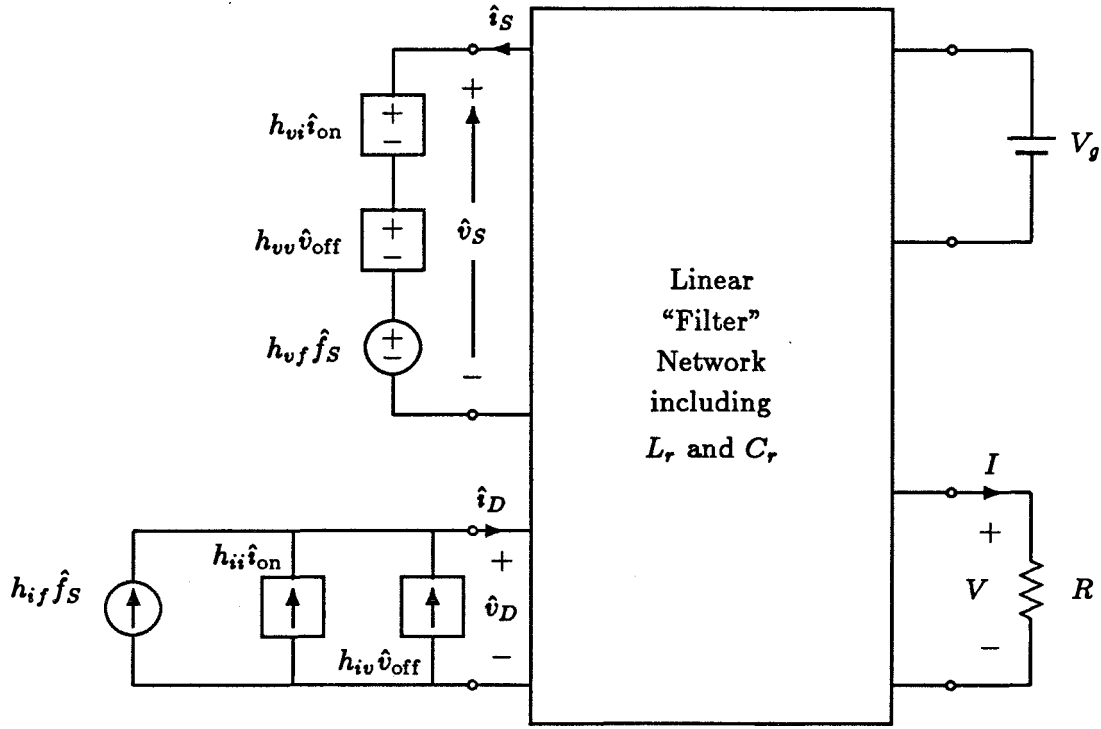


Figure 6.1: The small-signal model of a zero-voltage-switching quasi-resonant converter.

( $v_{\text{off}}$ ). When currents and voltages are interchanged, the source including  $h_{iv}$  is now a voltage source controlled by the current  $i_{\text{on}}$ , so the appropriate parameter of the voltage source is denoted  $h_{vi}$ . The general small-signal model of a ZVS quasi-resonant converter is shown in Fig. 6.1, and the corresponding  $h$ -parameters are given by

$$h_{vv} = [1 - D_P(M)](1 - m) \quad (6.4)$$

$$h_{vi} = \frac{mR[1 - D_P(M)]}{M} \quad (6.5)$$

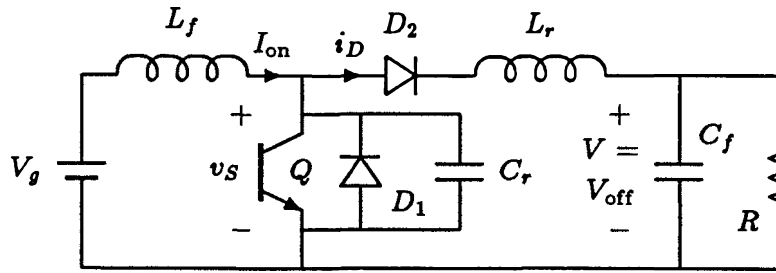
$$h_{vf} = V_{\text{off}} \frac{[1 - D_P(M)]}{F_S} \quad (6.6)$$

$$h_{iv} = -\frac{mM[1 - D_P(M)]}{R} \quad (6.7)$$

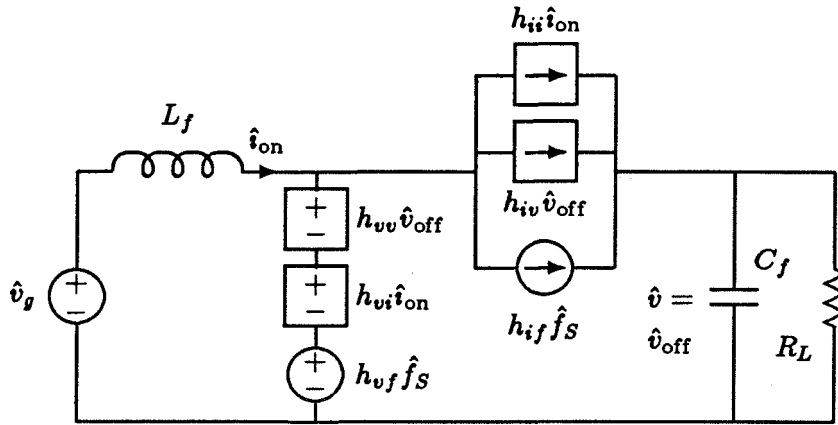
$$h_{ii} = (1 + m)[1 - D_P(M)] \quad (6.8)$$

$$h_{if} = I_{\text{on}} \frac{[1 - D_P(M)]}{F_S} \quad (6.9)$$

Note that  $m$ , actually  $m(\rho)$  for the ZCS converter, is replaced by  $m(\rho^{-1})$  in the ZVS converter.



(a)



(b)

Figure 6.2: A zero-voltage-switching boost converter (a) and its small-signal model (b).

Since  $G_{fw}(\rho)$  is nearly constant with  $\rho$ , so is  $G_{fw}(\rho^{-1})$ . Without any analysis, then, one can surmise that full-wave ZVS resonant converters will behave like their PWM counterparts, both at dc and under low-frequency ac modulation, with duty ratio control  $D$  replaced by the “complementary” switching frequency control  $(1 - F_S/F_0)$ . Alternatively, one can think of the control variable  $F_S/F_0$  replacing the complementary duty ratio  $1 - D$ . The small-signal model for the half-wave ZVS switch, like the model for the ZCS switch, exhibits lossless damping and a lack of reciprocity.

Figure 6.2 shows an example of a ZVS boost converter, along with its small-signal circuit model.

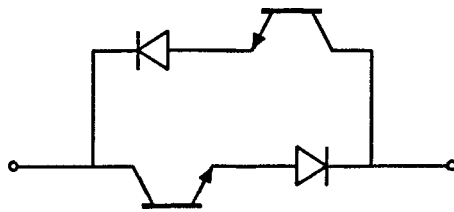


Figure 6.8: A four-quadrant switch that allows all combinations of forward and reverse current and voltage.

## 6.2 Multiple Conduction Cycles

Normally a zero-current resonant switch goes through less than a full cycle of current and voltage during its “resonant” interval. In the half-wave switch, the current is interrupted when it first reaches zero from above, while the full-wave switch interrupts the current when it first passes through zero from below. If a full-wave switch is used, or if a four-quadrant switch, shown in Fig. 6.3, replaces the PWM converter’s transistor, then the switch current may go through one or more complete resonances, crossing zero in both directions, before it is interrupted [7]. Figure 6.4 shows two examples of such behavior. With the notation of [7], a multiple conduction-cycle mode of the resonant switch is referred to as a  $k/2$ -cycle mode, where  $k$  is an integer. Odd values of  $k$  indicate that the current is interrupted when crossing zero from above, as in the half-wave resonant switch. Even values of  $k$  indicate behavior as in the full-wave switch. The half-wave and full-wave modes studied in previous sections correspond to  $k = 1$  and  $k = 2$ , respectively.

The only change needed to include these modes in the dc and ac analyses of previous sections is to modify the function  $G$ . In general, the function  $G(\rho)$  corresponding to the  $k$ th mode is denoted by  $G_k(\rho)$  and is given by

$$G_k(\rho) = \frac{1}{2\pi} \left[ \frac{\rho}{2} + k\pi - (-1)^k \sin^{-1} \rho + \frac{1}{\rho} \left( 1 - (-1)^k \sqrt{1 - \rho^2} \right) \right]. \quad (6.10)$$

For  $k = 1$  and  $k = 2$ ,  $G_1$  and  $G_2$  agree with  $G_{hw}$  and  $G_{fw}$  as expected. Even values of  $k$  lead to behavior very similar to the normal full-wave resonant switch. The function  $G_k(\rho)$  is approximately constant and equal to  $k/2$  when  $k$  is even. This leads to a load-independent conversion ratio and a lack of lossless damping. For even values of  $k$ , the converter always behaves like its PWM counterpart, with the substitution of  $kF_S/2F_0$

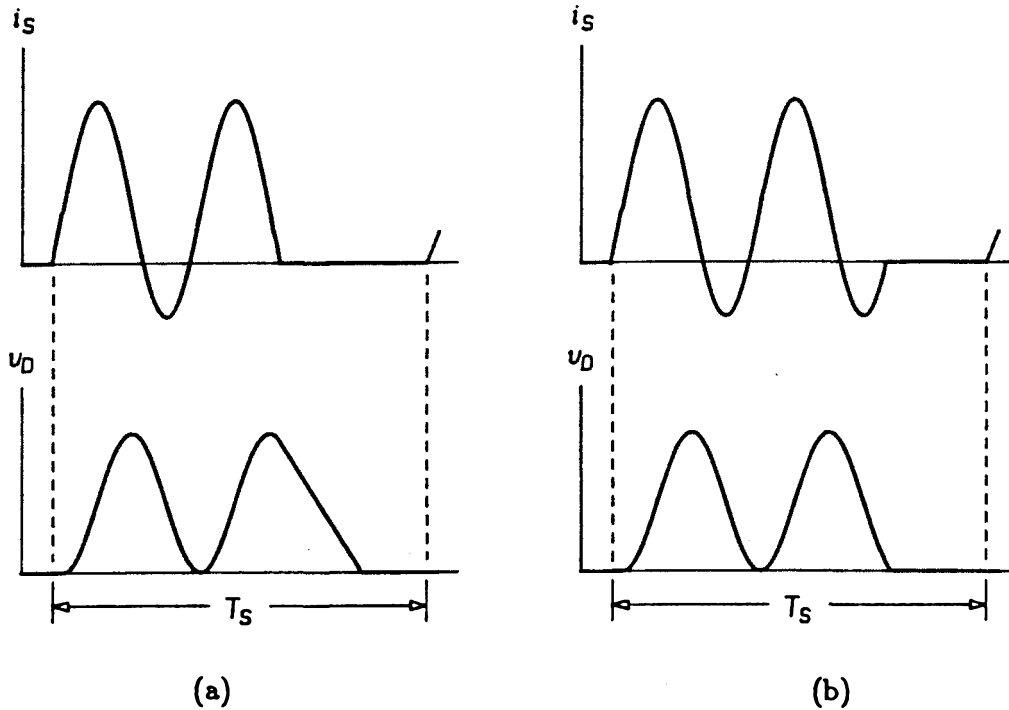


Figure 6.4: Multiple conduction cycle switch waveforms: (a)  $k = 3$ , (b)  $k = 4$ .

for the control variable  $D$ . For odd  $k$  values,  $G$  is sensitive to the operating point. Load-dependent conversion ratio and lossless damping are observed, as with the half-wave switch.

Zero-voltage resonant switches may also operate with multiple conduction cycles. In this case, the behavior is again found simply by modifying the  $G$  functions of Section 6.1.3.

### 6.3 Converters with Transformers

The previous analysis may be adapted to many quasi-resonant converters containing transformers. Converters based on isolated PWM converters with a single transistor and diode, for example the flyback, SEPIC, and isolated Čuk converters, may be analyzed in this way. Some converters with multiple switches may also be treated, as demonstrated in the following section. This section assumes that the transformer has a magnetizing current that is either small-ripple (as in the flyback converter) or is negligibly small (as in the isolated Čuk topology).

The presence of a transformer in a quasi-resonant converter may be handled in several ways. One approach might be to shift the transformer completely through the circuit to the source or load. The remaining circuit, with elements scaled by reflection through the moving transformer, would then be analyzed as usual. Another approach is given here, one that gives particularly simple relations when the resonant inductor and capacitor are on opposite sides of the transformer.

Define  $I_{\text{on}}$  as the ON current seen by the transistor, and  $V_{\text{off}}$  as the OFF voltage seen by the diode. The transistor will always be on the source side, and the diode on the load side of the isolation transformer. This is a consequence of the fact that a transistor generates ac power, the only kind of power that can cross a transformer. The diode in turn converts the ac power from the transformer back into dc power suitable for the load.

Let the transformer have a turns ratio of  $1:N$ , so that the load-side (secondary) voltage is  $N$  times higher than the source-side (primary) voltage. If the resonant inductor  $L_r$  and capacitor  $C_r$  are on opposite sides of the transformer, then  $R_0$  may be defined as before,  $R_0 = \sqrt{L_r/C_r}$ . If both  $L_r$  and  $C_r$  happen to be on the same side of the transformer, one of these elements must be reflected across the transformer and the resulting value used in the definition of  $R_0$ . With  $R_0$  defined this way, the relations  $\rho = R_0 I_{\text{on}}/V_{\text{off}}$  and  $\rho = MR_0/R$  still hold.

The only change needed in both the dc analysis of Chapter 4 and the ac analysis of Chapter 5 is in  $D_P$ , the inverted PWM conversion ratio function. With no transformer, or a 1:1 transformer, a PWM converter has a conversion ratio  $M \equiv V/V_g = M_P(D)$ . With a transformer turns ratio of  $1:N$ , the conversion ratio is  $M = NM_P(D)$ . The inverted gain function  $D_P$  becomes  $D_P(M/N)$ . For example, in a buck-boost converter,  $M_P(D) = D/(1 - D)$ . The transformer-isolated version of this converter, the flyback converter, has a conversion ratio  $M = ND/(1 - D)$ , so that in the flyback converter the duty ratio is found from  $D = D_P(M/N)$ .

An example in the following section will demonstrate the dc and ac analysis of a quasi-resonant converter with a transformer.

## 6.4 Converters with Multiple Switches

Many converters with more than one transistor or diode may be converted into quasi-resonant converters. As long as the multiple switches operate with some symmetry, these resonant converters may be analyzed by simple modifications to the process already put forth. In lieu of a general treatment, the principles involved will be demonstrated by an example.

Figure 6.5(a) shows a half-bridge PWM converter. The two large capacitors labeled  $C_\infty$  have small ripple; they are not resonant capacitors. Balanced operation is assumed so that these two capacitors always divide the source voltage  $V_g$  exactly between them. The switching waveforms for this converter are shown in Fig. 6.5(b). The transistors  $Q_1$  and  $Q_2$  are driven out of phase, alternately applying  $+V_g/2$  and  $-V_g/2$  to the transformer primary. The voltage pulses are rectified by the diode bridge and filtered by  $L_f$  and  $C_f$  to produce a dc load voltage  $V$ .

The ON current in each transistor, defined as  $I_{on}$ , is the reflected inductor current. The inductor current is therefore  $I_{on}/N$ . The OFF voltage across the diode bridge is defined as  $V_{off}$  and in this case is the voltage  $V_g/2$  across one of the  $C_\infty$  capacitors, reflected to the secondary of the transformer. Hence  $V_g/2 = V_{off}/N$ . The conversion ratio  $M = V/V_g$  for this converter is  $D/2N$ , so that  $D_P(M/N) = M/2N$ . The factor of  $N$  of course comes from the transformer, while the factor of two is a result of the voltage divider formed by the two large input-side capacitors.

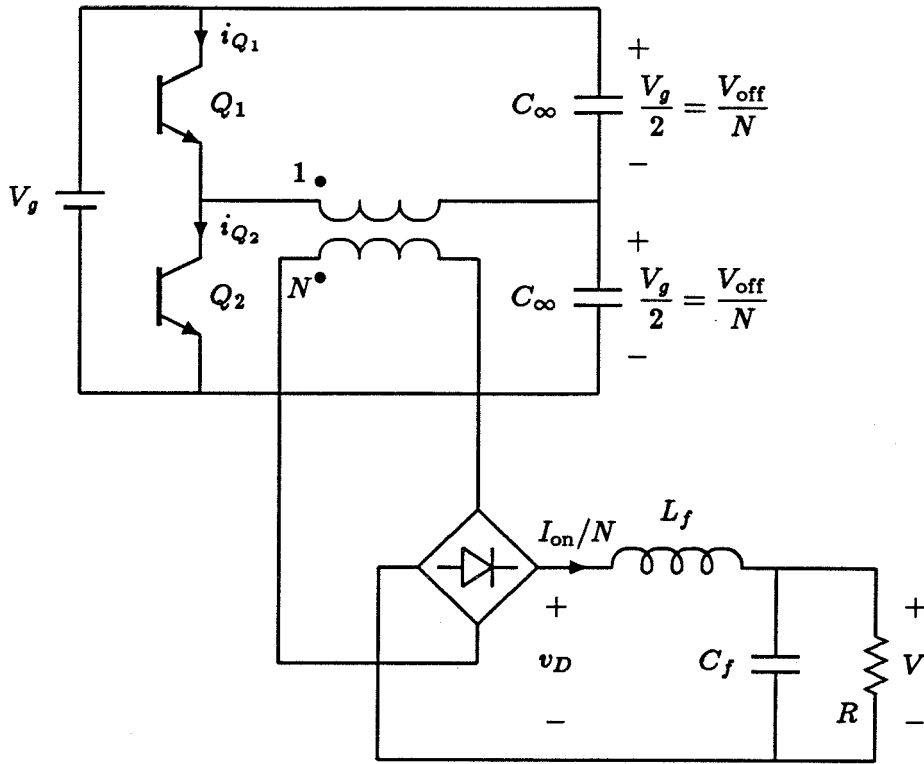
Figure 6.6(a) shows one of several ways to make a half-bridge quasi-resonant converter. The corresponding switch waveforms are shown in Fig. 6.6(b). The switching frequency is defined according to the waveforms following the rectifier bridge. Thus  $S_1$  and  $S_2$  are each operated at  $F_S/2$ , but 180 degrees out of phase so that the effective frequency at the output side of the transformer is  $F_S$ .

Since  $L_r$  and  $C_r$  are on opposite sides of the transformer,  $R_0$  and  $\rho$  are defined as usual. The dc gain is found from

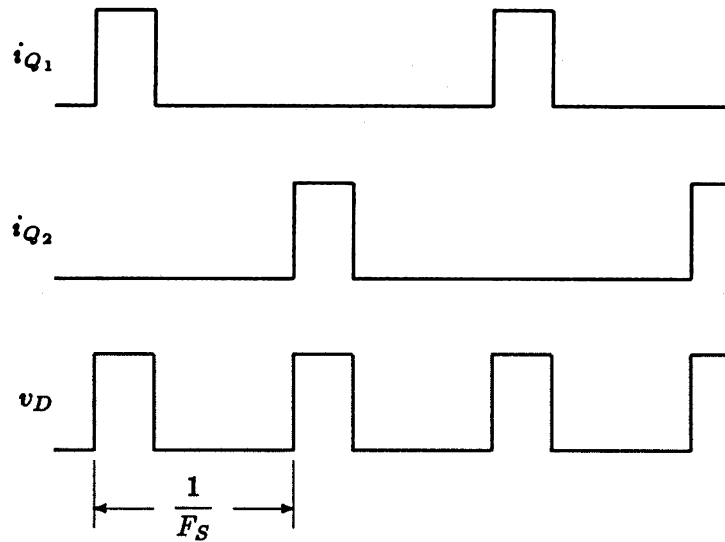
$$\frac{F_S}{F_0} = \frac{D_P(M/N)}{G(MR_0/R)} = \frac{M}{2N} \frac{1}{G_{hw}(MR_0/R)} \quad (6.11)$$

where  $G_{hw}$  is used because the two-quadrant switches in Fig. 6.6(a) form half-wave





(a)

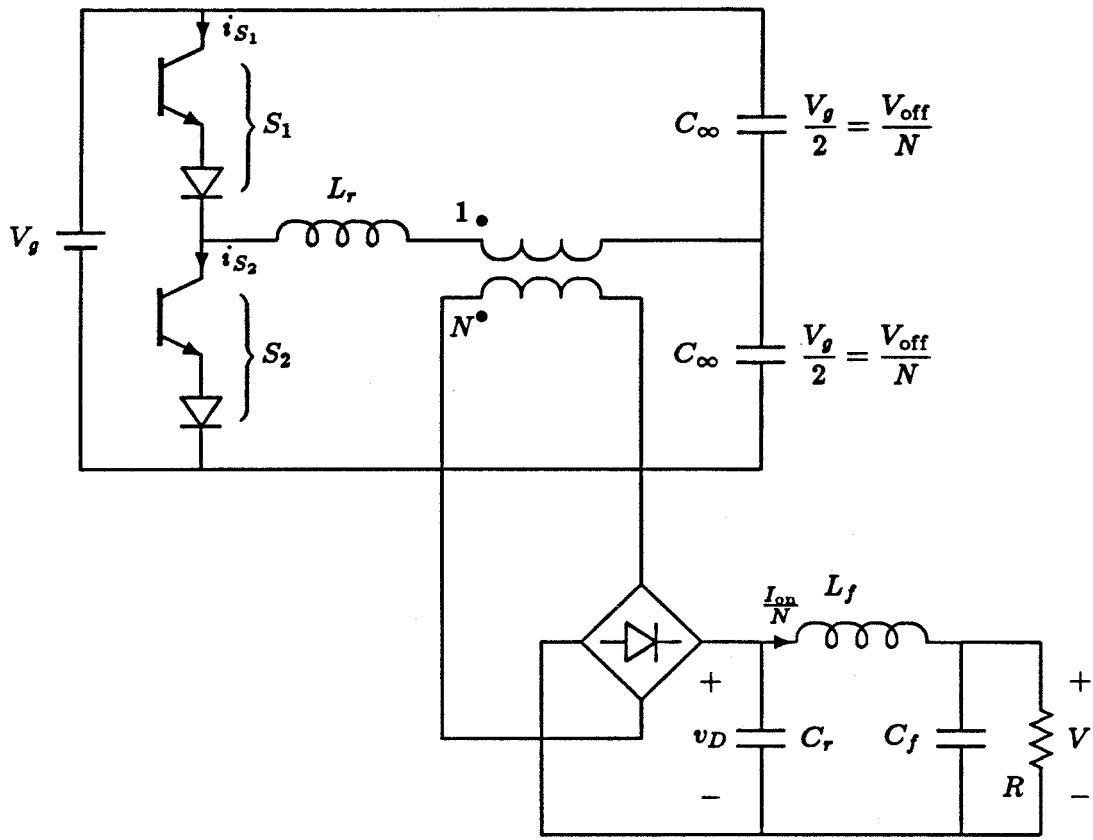


(b)

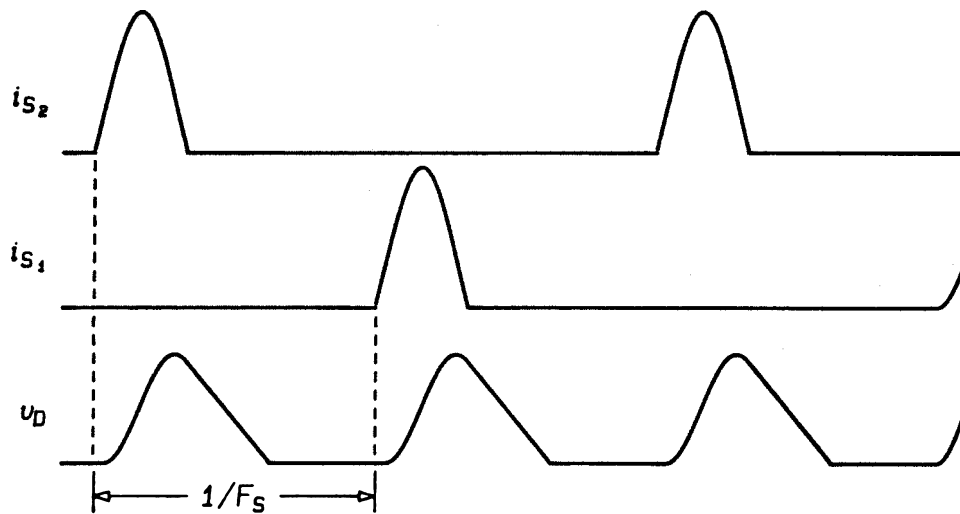
Figure 6.5: A half-bridge PWM converter (a) and its waveforms (b).

switches.

The small-signal dynamic model is best presented as separate circuits for the input and output sides of the converter, coupled by dependent sources as shown in Fig. 6.7. The presence of the resistors indicates the ever-present damping effect of the half-wave switch.

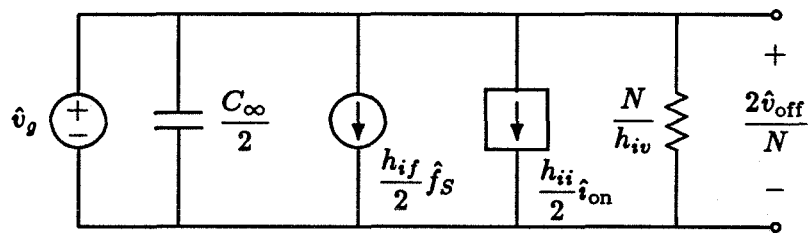


(a)

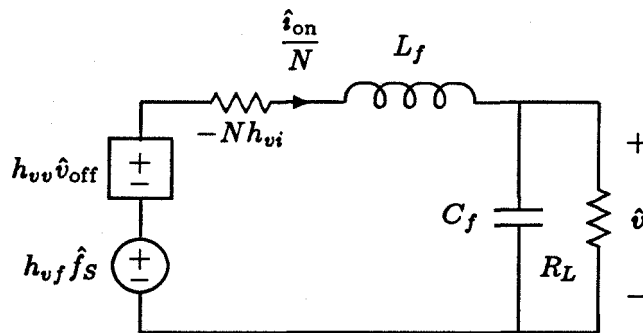


(b)

Figure 6.6: A half-bridge quasi-resonant converter (a) and its switching waveforms (b).



(a)



(b)

Figure 6.7: Small-signal model of the half-bridge quasi-resonant converter: (a) input-side portion, (b) secondary-side portion.

## Chapter 7

# Experimental Verification

Both the dc and ac analyses of previous chapters relied on assumptions that have not been quantified. The small-ripple and low-frequency approximations are necessary for a clear and simple analysis, but it was noted that these approximations may not always be well-satisfied, and just how “small” or how “low” is needed for good agreement is not clear. The results of experimental work given in this chapter demonstrate that the analyses are valid when the approximations are met, and, surprisingly, often give good results even when the approximations are poorly satisfied. The good agreement between the measurements and the predictions is encouraging, and demonstrates that the models developed here can be useful design tools.

### 7.1 Dc Measurements

The general dc analysis method of Chapter 3 yields results identical to those found in [4,7,8] for the buck, boost, and buck-boost converters with “sine-wave type” switches. Adequate agreement between dc analysis and measurements has been demonstrated for these converters in [4,7,8]. The purpose of this section is to demonstrate that the conversion ratio is independent of the placement of the resonant elements.

Chapter 3 showed that, as long as the resonant inductor and capacitor satisfy Rules 1 and 2 of Definition 2, the waveforms  $i_S$  and  $v_D$  are always the same. Consequently, the dc conversion ratio is independent of the placement of the resonant elements. This is reflected in Eq.(4.11). One equation is sufficient to yield the conversion ratio for all variations of a given topology; one does not need separate expressions for sine-wave, square-wave, L1, L2, and M types of circuits.

To verify this result, a resonant-switch buck converter was constructed according to

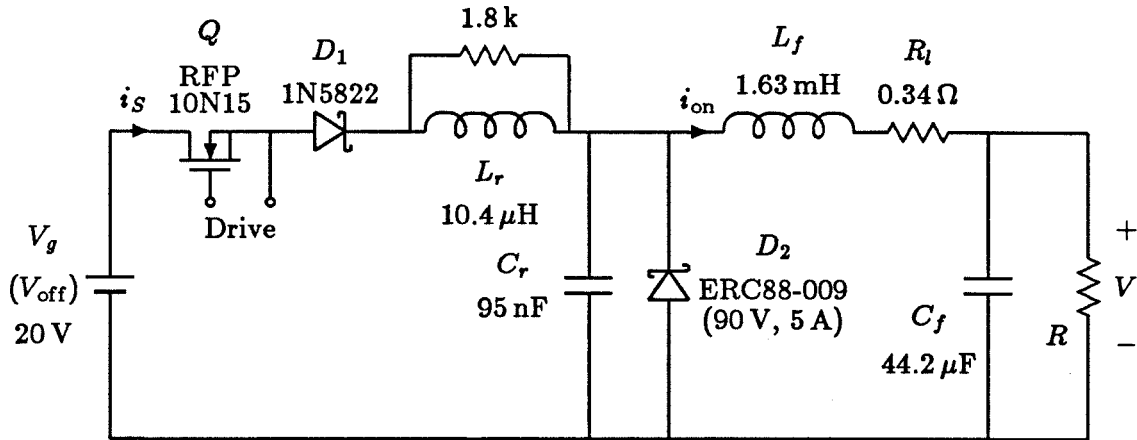
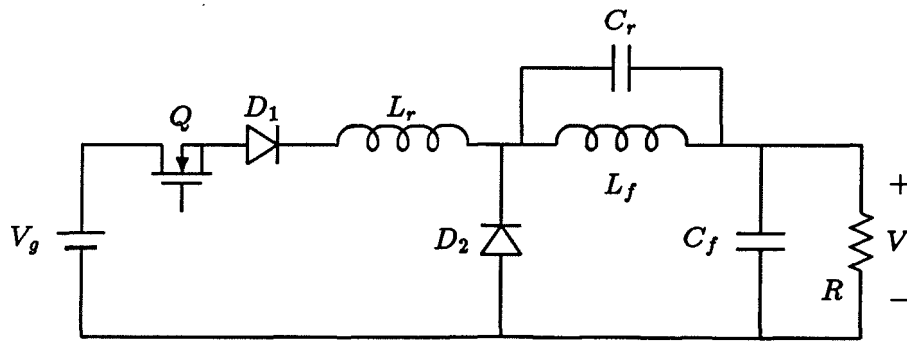


Figure 7.1: An experimental quasi-resonant buck converter with a half-wave switch. The resonant capacitor and inductor are in the “L1-sine” position.

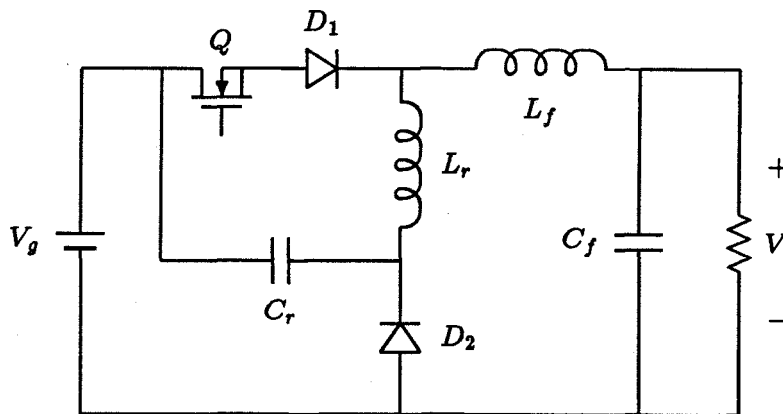
Fig. 7.1. (The 1.8 k resistor across  $L_r$  was added to reduce ringing of  $L_r$  with its parasitic capacitance during the time when the switch  $S$  is OFF.) The resonant elements were then moved to two other positions, as shown in Fig. 7.2. The names “L1, sine-wave type,” etc., follow [9]. Figure 7.3 compares the measured conversion ratio  $M$  of the L1-sine converter with the values predicted by Eq.(4.11). The frequency and load dependence are both in good agreement. As might be expected, the conversion ratio is always slightly less than the predicted value as a result of losses in  $R_l$ , the resonant tank, and ON losses of the transistor and diodes. All losses were neglected in Eq.(4.11).

Measurements of the conversion ratio of the other two variations of the converter yielded values nearly identical at every operating point. With fixed input voltage, the output voltage differed by no more than 2 mV between any of the three variations, a margin of less than 3 percent. This result supports the claim in Chapter 4 of a common conversion ratio among all the variations of a quasi-resonant converter topology.

Although, as has been emphasized, all the variations of a given quasi-resonant converter have the same conversion ratio, these topological variations are not necessarily equivalent in other respects. Ripple voltages and currents and peak stresses in some components may vary widely between different variations. Some of these effects are catalogued in [9]. When losses are considered, the conversion ratio may be sensitive to these



(a)



(b)

Figure 7.2: Two variations of the quasi-resonant buck converter: (a) “L2-sine” type and (b) “M-square” type.

differences, leading to slightly different conversion ratios between topological variations. In the limit of high efficiency and small ripple, however, the conversion ratio is the same for all variations of a given topology, as demonstrated by the measurements made here.

## 7.2 Small-signal Measurements

Under small-signal conditions and at low modulation frequencies, a power converter may be treated as a linear, time-invariant system. This approximation allows one to verify its small-signal behavior by measuring the frequency response—the relation of the magnitude and phase of the fundamental component of the system output relative to

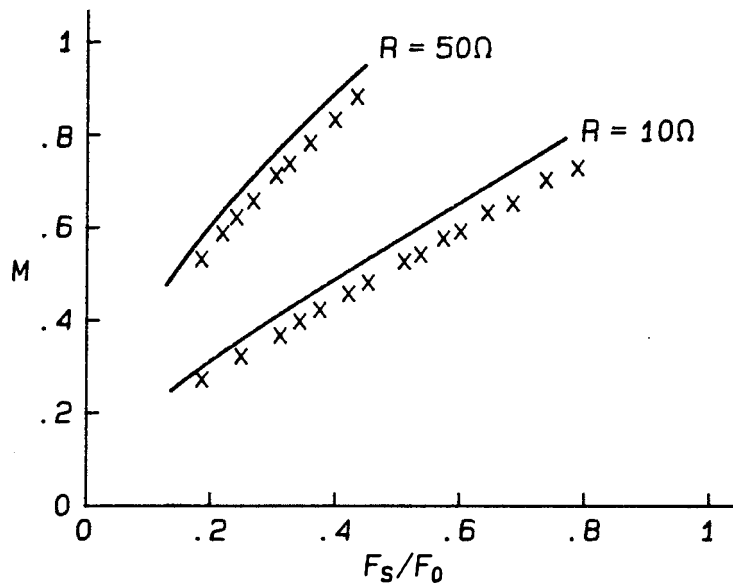


Figure 7.3: Measured values of the conversion ratio  $M$  of the buck converter of Fig. 7.1. The theoretical conversion ratio is given by the solid curves.

an exciting sinusoid. Automated frequency-response measurement systems simplify this task and allow the results to be stored and presented in graphical form.

Since a power converter output by nature contains “noise” in the form of switching ripple, the output waveforms under modulation contain not only the modulation frequency but also the switching frequency, its harmonics, and “cross-modulation” components. The frequency response, however, is concerned only with the component of the output waveform at the modulation frequency. The solution to the measurement problem is to use a network analyzer in conjunction with a sine-wave generator, or synthesizer, as shown in Fig. 7.4.

The synthesizer generates a pure sinusoid  $\hat{v}_c$  at the desired modulation frequency,  $f_m$ . This sinusoid is applied to the modulator which varies the converter control variable, the switching frequency, at  $f_m$ . The waveform  $\hat{v}_c$  is also applied to channel A of the analyzer. Channel B measures the converter output. The analyzer filters these waveforms, saving only the components at  $f_m$ . Comparison of the magnitude and phase of the  $f_m$  components of the channel A and channel B waveforms yields the frequency response at  $f_m$ . The synthesizer is stepped through all desired values of the modulation frequency to obtain a frequency-response curve.



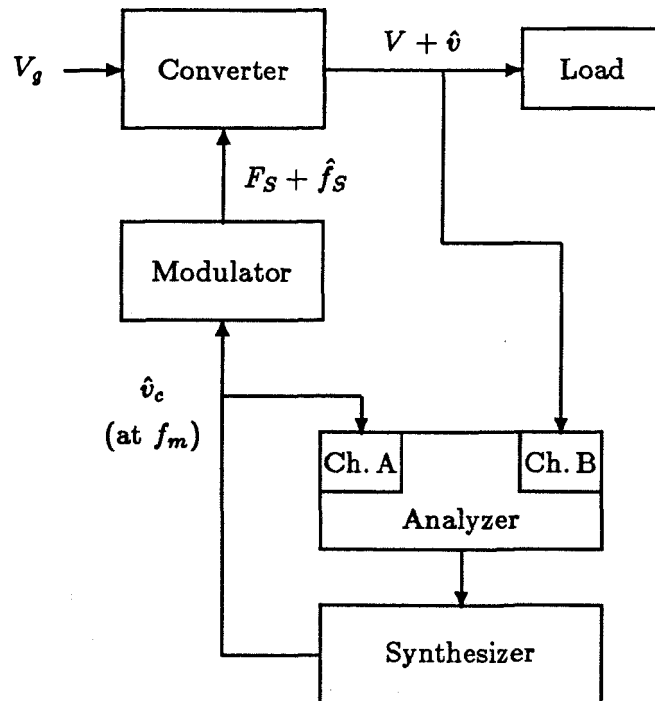
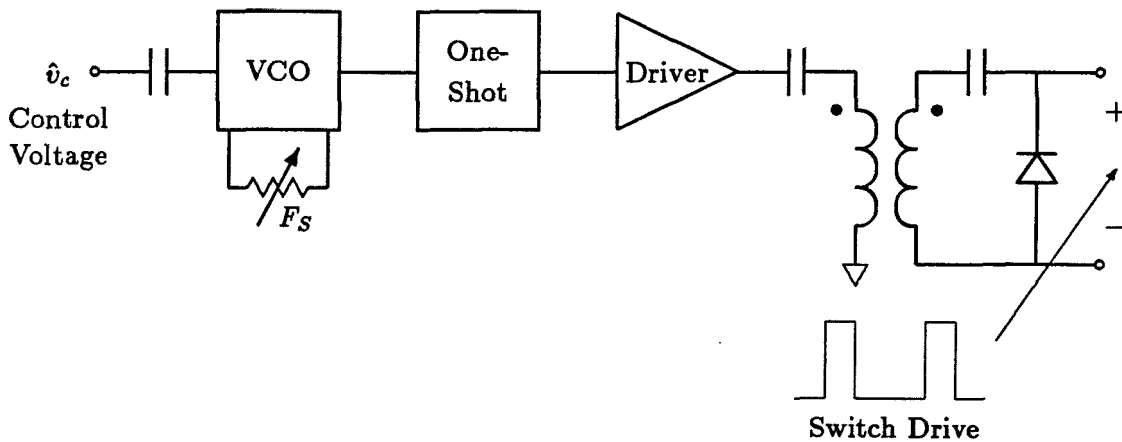


Figure 7.4: A network analyzer coupled with a synthesizer measures the frequency response of a quasi-resonant converter and its modulator.

The modulator used to control the switching frequency of the resonant-switch converters appears in Fig. 7.5. The dc switching frequency is set manually, while modulation of the switching frequency is determined by the voltage  $\hat{v}_c$  ac-coupled to the voltage-controlled oscillator (VCO) input. The one-shot delivers a pulse of fixed width at the beginning of each switching period. The pulse, amplified by the driver, is applied to the transistor gate through an isolation transformer and level-shifting circuit. For a zero-current-switching (ZCS) converter, the pulse width is manually adjusted so that the pulse ends during the time that diode  $D_1$  is blocking, when the transistor  $Q$  is carrying no current. For a ZVS converter, the pulse is set to end when  $D_1$  is ON and  $Q$  is under zero voltage.

To obtain the predicted frequency response curves that follow, the VCO was modelled as a constant ratio between  $\hat{v}_c$  and  $\hat{f}_S$ , with no dynamics. This assumption is justified in Section 7.3, where the internal circuits of different VCO's and their accompanying dynamics are discussed.



*Figure 7.5: Block diagram of the method used to drive the transistor of a quasi-resonant converter. The voltage-controlled oscillator (VCO) modulates the switching frequency under the control of the signal  $\hat{v}_c$ .*

It should be noted that, while all the frequency-response measurements made here are of the control ( $\hat{f}_S$ ) to output ( $\hat{v}$ ) transfer function, any transfer function of interest can be measured in a similar fashion. For example, the input voltage  $v_g$  may be modulated and the input current  $i_g$  measured. The ratio  $\hat{v}_g/\hat{i}_g$  is the small-signal input impedance. One of the advantages of a small-signal model such as that developed in Chapter 5 is that it gives a circuit from which all transfer functions may be found.

### 7.2.1 Half-wave Buck Converters

The control-to-output transfer function of a half-wave quasi-resonant buck converter was derived in Chapter 5, resulting in the model of Fig. 5.10 and Eqs.(5.23) through (5.28). To verify the model, a converter was constructed according to Fig 7.1. (Since a linear resistance was used as the load in the experimental circuits, the dc load  $R$  and small-signal resistance  $R_L$  are equal.) When the converter is operated with a load of  $10.4\Omega$  (nearly equal to  $R_0$ ), and a conversion ratio of 0.72, the measured frequency response is as shown in Fig. 7.6. The response predicted by Eqs.(5.23) through (5.28) is shown as a dashed line in the figure. The agreement is very good. Note that the maximum modulation frequency in Fig. 7.6 is only 1/12 of the switching frequency, so that

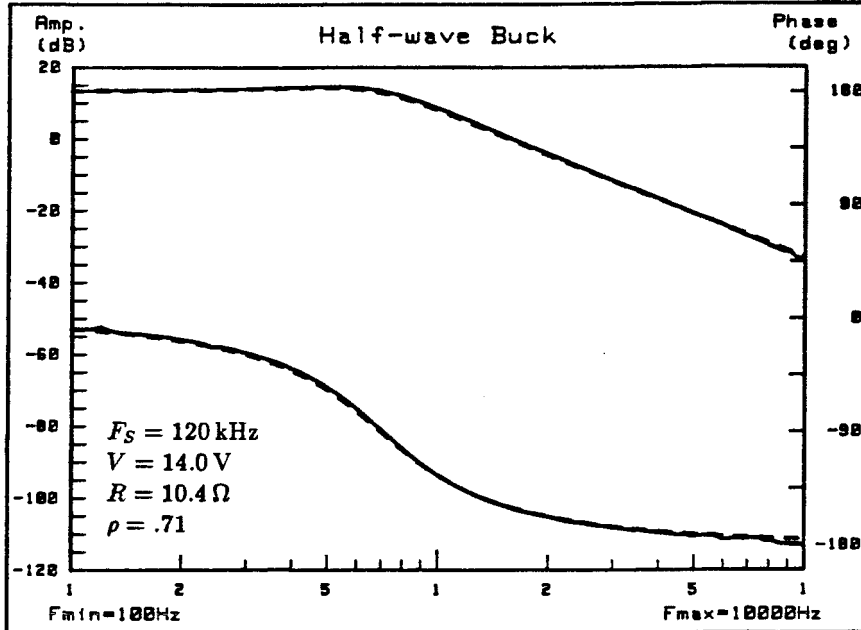


Figure 7.6: Magnitude (upper curves) and phase (lower curves) of the control-to-output response of the half-wave buck converter of Fig. 7.1 operating with a relatively large value of  $\rho$ . The solid curve is the measured response and the dashed lines show the response predicted by the small-signal model.

the low-frequency approximation is well-satisfied. The ratio  $\rho = MR_0/R$  is 0.71 at this operating point, a fairly high value. The second-order response has a  $Q$  of approximately unity. The output filter alone has a  $Q$  of 1.6, and it is this  $Q$  that would appear if the resonant elements were removed and the circuit operated as a PWM buck converter.

When operated at the lower value  $MR_0/R = 0.15$ , achieved by increasing the load to  $49.7 \Omega$  while keeping the conversion ratio nearly the same, the frequency response changes considerably. In a PWM buck converter, increasing the load resistance would increase the loaded  $Q$  of the output filter, leading to an underdamped frequency response. The response of the quasi-resonant buck converter, shown in Fig. 7.7, exhibits the opposite effect. The lower value of  $\rho$  has increased the damping (represented by  $-h_{oi}$  in the circuit model of Fig. 5.10) to such an extent that the poles have separated to positions at roughly 100 Hz and 5 kHz. A PWM buck converter with the same element values in the output filter would exhibit an underdamped response with a  $Q$  of about 5.6.

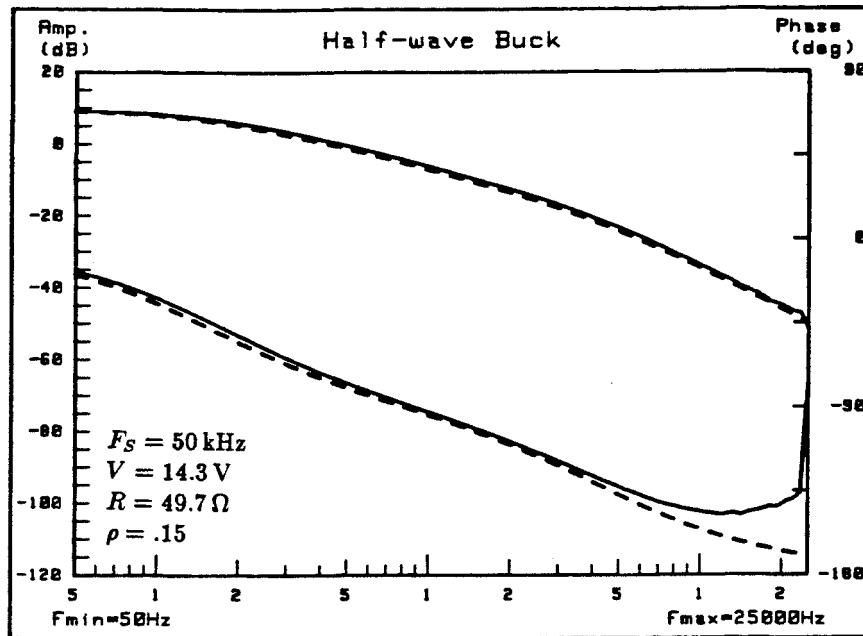


Figure 7.7: Frequency response of the half-wave buck converter of Fig. 7.1 operating with a low value of  $\rho$ . The solid curves are the measured response and the dashed curves show the predicted response.

### 7.2.2 Full-wave Buck Converter

The full-wave resonant-switch contributes no damping to a power converter. To confirm this result, the half-wave resonant switch of Fig. 7.1 was changed to a full-wave switch by moving the diode  $D_1$  to a position across the transistor. The resulting frequency response is shown in Fig. 7.8. Except for the phase deviations near half the switching frequency, the agreement between the measurement and the response predicted using the small-signal model of Chapter 5 is quite good. (Phase discrepancies near half the switching frequency are commonly observed in PWM converters. These deviations are to be expected as the low-frequency approximation breaks down, and neglect of the modulator sampling process becomes invalid.)

A third curve appears in Fig. 7.8, showing the measured response obtained by shorting  $L_r$ , removing  $C_r$ , and operating the converter as a PWM converter with a duty ratio  $D$  equal to the ratio  $F_S/F_0$  of the resonant converter. (The third curve was in fact obtained by perturbing the frequency with the modulator of Fig. 7.5, the same as for the

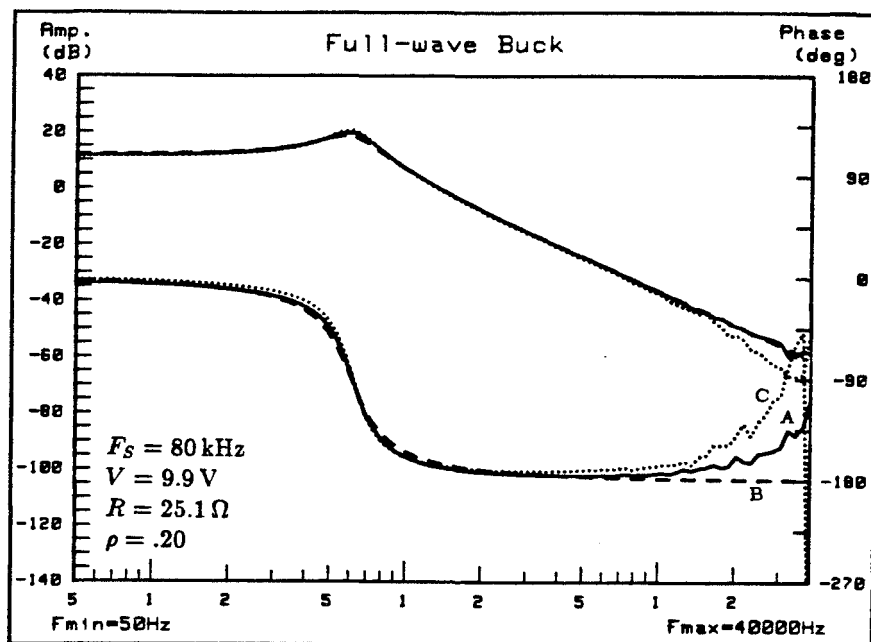


Figure 7.8: Measured frequency response (A) of a full-wave buck converter (solid line). Shown by dashed lines is the predicted response for the full-wave converter (B) and the measured response of a PWM converter at the same operating point (C).

resonant-switch version of the converter. However, it can be shown that

$$\frac{\hat{d}}{D} = \frac{\hat{f}_s}{F_s}, \quad (7.1)$$

and hence modulating the frequency is equivalent to modulating the duty ratio.) Again except for the phase deviations at high frequencies, the response of the full-wave switch converter, the PWM converter, and the model from Chapter 5 are all nearly identical. This demonstrates the claim made in Chapter 5 that full-wave converters behave just like their PWM parents, with the control variable  $d$  replaced by  $f_s/F_0$ .

### 7.2.3 Effects of $C_r$ and $L_r$

Section 5.6 of Chapter 5 pointed out that the resonant elements  $L_r$  and  $C_r$  were often negligible, but warned that in some cases they might have important effects. Figure 7.9 illustrates such a case, showing the measured response of a buck converter with the topology of Fig. 5.12(a) and the element values of Fig. 7.1. The resonant capacitor  $C_r$  appears across  $L_f$  in this example (a topology referred to as the “L2” configuration

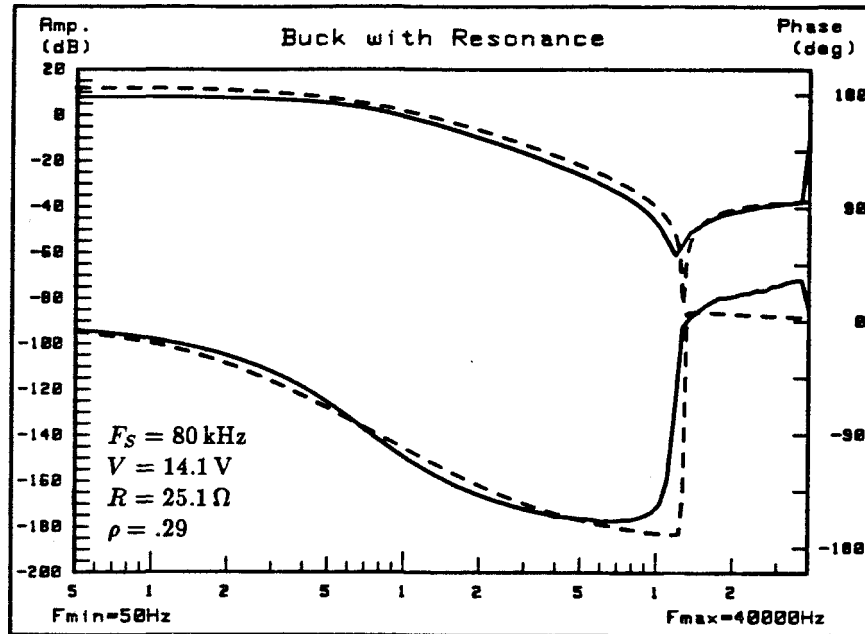


Figure 7.9: Frequency response of a quasi-resonant buck converter showing a resonant peak from the interaction of  $L_f$  and  $C_r$ . The solid curves show the measured response while the dashed curves indicate the prediction from the small-signal model.

in [9]) and the load is  $25.1 \Omega$ . The frequency-response curves of Fig. 7.9 contain a high- $Q$  resonance from the parallel-resonant circuit formed by  $L_f$  and  $C_r$ . With this configuration,  $C_r$  can be “small” relative to other capacitors in the circuit, but if  $L_f$  is large, the resonant notch can easily appear within the frequency range of interest, with attendant difficulties in controlling the converter. Thus, while the positions of  $C_r$  and  $L_r$  make no difference in the dc conversion ratio, they can make a large qualitative difference in the frequency response.

#### 7.2.4 Zero-voltage-switching Boost Converter

Figure 7.10 shows the circuit of an experimental ZVS boost converter with a half-wave switch. The frequency response predicted by the model of Chapter 5 is compared with the measured response in Fig. 7.11, and the agreement is seen to be excellent. The presence of a right half-plane zero is evident from the 270 degree phase lag seen in Fig. 7.11. Right half-plane zeros make it extremely difficult to design a high-bandwidth regulator, and one may wonder whether the half-wave switch can ever provide enough

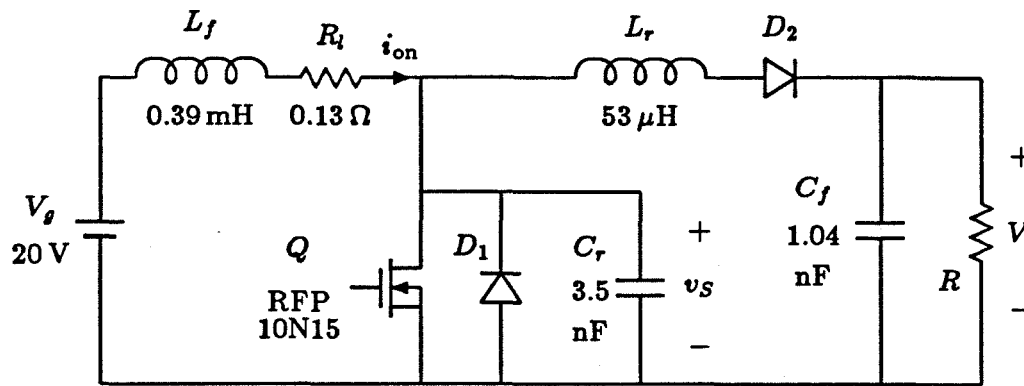


Figure 7.10: Circuit of an experimental zero-voltage-switching boost converter.

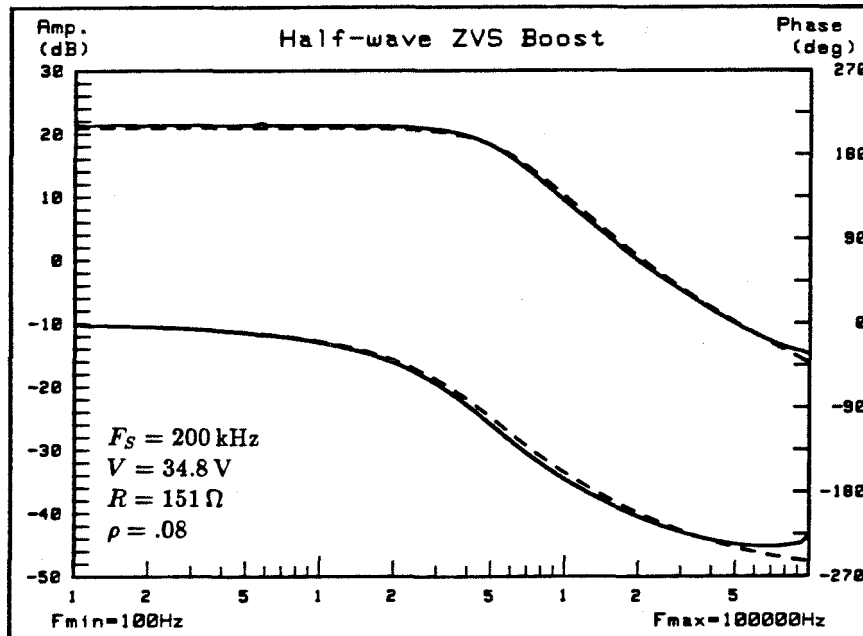


Figure 7.11: Measured (solid curves) and predicted (dashed curves) frequency response of the ZVS boost converter of Fig. 7.10.

damping to move the RHP zero out to high frequencies or even into the left half-plane. From the analytic form of the transfer function, derived using the method of Chapter 5, the (radian) zero frequency is

$$\omega_z = -\frac{h_{ii}R/M - R_l - h_{vi}}{L_f} . \quad (7.2)$$

With the use of the parameter expressions from Chapter 6,

$$\omega_z = -\frac{1}{L_f} \left( \frac{R}{M^2} - R_l \right) . \quad (7.3)$$

The zero frequency is largest when  $R_l$  is negligibly small. The percentage ripple current in the input inductor can be shown to be proportional to the ratio of  $R/M^2 L_f$  to  $F_S$ , so the frequency  $\omega_z/2\pi$  will always be much less than the switching frequency.

If  $R_l$  is larger than  $R/M^2$ , the zero can be pushed into the left half-plane. Attempting to stabilize the converter with this approach suffers from two drawbacks, though. First, the power loss in  $R_l$  is  $R_l M^2/R$  times the output power. The zero crosses into the left half-plane only when the efficiency is less than 50%. Second, this method creates a left half-plane zero by moving the RHP zero through zero frequency. The resulting zero will therefore occur at low frequencies and, most important, will move back and forth as the load changes. If the load becomes too large, the zero will cross into the right half-plane at very low frequencies, with disastrous results on the feedback loop.

In conclusion, the damping of the half-wave switch is of no use in removing the right half-plane zero in the ZVS boost converter. The same conclusion holds for zero current-switching boost converters.

### 7.2.5 Small-ripple Approximation

It is worthwhile to check how well the small-ripple approximation is justified in each of the preceding measurements. Table 7.1 gives the percent ripple in  $V_{off}$  and  $I_{on}$  for each of the frequency response curves of this chapter. The percent ripple is defined by

$$\text{percent ripple} = \frac{1}{2} \frac{\text{pk-pk excursion}}{\text{average value}} . \quad (7.4)$$

A triangular waveform just touching zero therefore has 100% ripple.



Figure	% Ripple	
	$V_{off}$	$I_{on}$
7.6	.5	1
7.7	.5	12
7.8 (Resonant)	.3	6
7.8 (PWM)	.1	5
7.9	.5	4
7.11	.7	21

*Table 7.1: Percent ripple in  $I_{on}$  and  $V_{off}$  for each of the measurements presented in this chapter.*

While the ripple on  $V_{off}$  is small in every case,  $I_{on}$  has a significant ripple, especially in the ZVS boost converter of Fig. 7.10. Although the ripple in  $I_{on}$  was highest for the measurement of Fig. 7.11, the agreement with the small-signal model, based on the small-ripple approximation, is best for this measurement! At least in this case, the parameters of the small-signal model are not extremely sensitive to the amount of ripple, and the small-signal approximation is justified.

### 7.3 Modulators for Frequency-Controlled Converters

The voltage-controlled oscillator (VCO) used to control quasi-resonant converters is not understood as well as are PWM (duty-ratio) modulators. Duty-ratio modulators are usually either of the naturally-sampled or uniformly-sampled types. The naturally-sampled kind is most common, not only because it is simpler and cheaper, but also because it contributes no phase lag. The uniformly-sampled modulator introduces a phase lag proportional to the modulation frequency [18].

A similar situation exists with VCO's. The most common kind provides a linear frequency-voltage characteristic but produces phase lag. Another kind has an undesirable nonlinear characteristic, but has the advantage of zero phase lag.

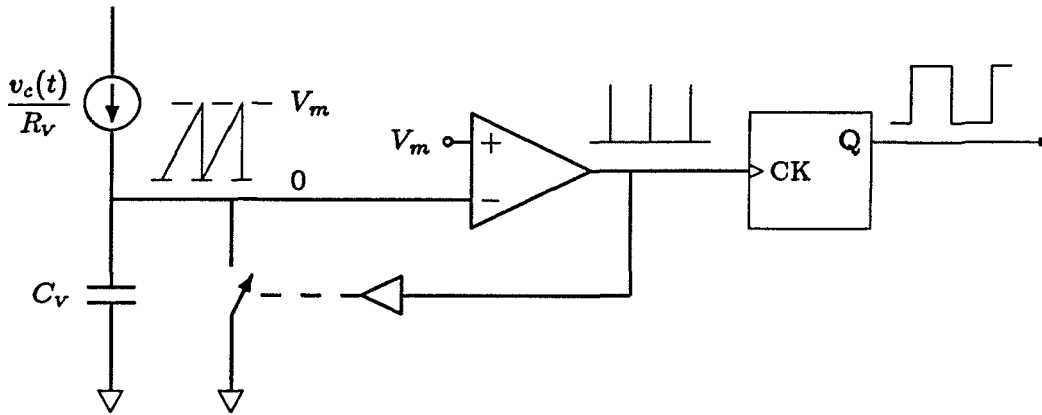


Figure 7.12: Diagram of a VCO with frequency a linear function of input voltage  $v_c$ .

### 7.3.1 VCO Linear in Frequency

Commercially available VCO's use an internal structure similar to that of Fig. 7.12. A voltage-controlled current source generates a current  $v_c/R_v$  proportional to the control (input) voltage  $v_c$ . The current is integrated by the capacitor  $C_v$  until the rising capacitor voltage reaches the value  $V_m$ . In this circuit,  $V_m$  may be changed to set the range of the VCO output, but during modulation,  $V_m$  is fixed. When the capacitor voltage reaches  $V_m$ , it triggers the comparator which closes a switch to dump the capacitor and initiate a new cycle. The short pulses from the output of the comparator clock a flip-flop to produce a square-wave output. Under dc conditions, the frequency is given by

$$F_S = \frac{1}{R_v C_v} \frac{V_c}{V_m} = \frac{1}{\tau_v} \frac{V_c}{V_m}, \quad (7.5)$$

where  $V_c$  is the dc value of the control voltage and  $\tau_v$  is defined as the time constant  $R_v C_v$ .

A small-signal model of this VCO is shown in Fig. 7.13. The control voltage is integrated, scaled, and sampled. The reset of the integrator is modeled by applying an "infinite hold",  $e^{-\epsilon s}/s$ , to each output sample and continuously subtracting this value from the integrator output. The small delay,  $e^{-\epsilon s}$ , with  $\epsilon \rightarrow 0$ , prevents the output of the sampler from reaching its input instantaneously.

The sampled-data model assumes constant-frequency sampling, which of course is not true. The output samples give the correct *value* of the frequency in each interval; constant sampling only neglects the fact that these frequency points actually occur at

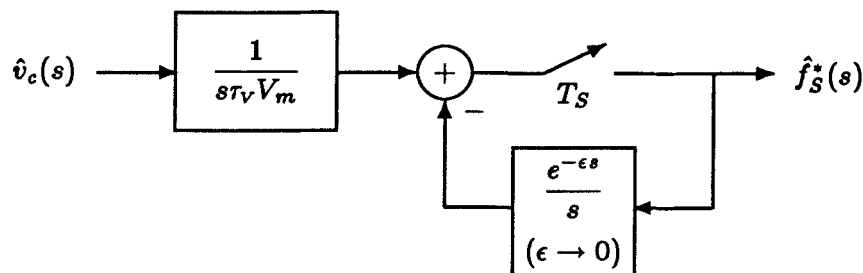


Figure 7.19: Small-signal model of the linear-in-frequency VCO.

varying times.

The sampled frequency waveform  $\hat{f}_S^*(s)$ , is given by

$$\hat{f}_S^*(s) = \frac{1}{\tau_v V_m} \frac{[\hat{v}_c(s)/s]^*}{1 + [e^{-\epsilon s}/s]^*}, \quad (7.6)$$

where an asterisk (\*) indicates sampling. For general waveforms  $v_c(t)$ , a transfer function relating  $\hat{f}_S^*(s)$  to either  $\hat{v}_c(s)$  or  $\hat{v}_c^*(s)$  cannot be found. When  $\hat{v}_c(t)$  is a pure sinusoid, however, its transform consists only of delta functions at the modulation frequency  $f_m$ . Sampling generates delta functions at other frequencies, but does not affect the transform value at  $f_m$  [19, pp 118–121]. Thus, when  $\hat{v}_c(t)$  is a single sinusoid at  $f_m$ ,

$$\hat{v}_c^*(s)|_{s=j\omega_m} = \frac{1}{T_S} \hat{v}_c(s)|_{s=j\omega_m}. \quad (7.7)$$

In addition, the integrated version of  $\hat{v}_c$  may also be pulled out from under the sampling operation, with the result that

$$\hat{f}_S^*(s)|_{s=j\omega_m} = \hat{v}_c(j\omega_m) \frac{1}{\tau_v V_m} e^{-j\omega_m T_S/2} \left( \frac{\sin(\omega_m T_S/2)}{\omega_m T_S/2} \right). \quad (7.8)$$

The magnitude and phase of this transfer function are plotted in Fig. 7.14 over a frequency range up to half the switching frequency. While the magnitude is nearly unity over this range, the modulator contributes a significant phase lag.

### 7.3.2 VCO Linear in Period

The phase lag of a commercial VCO can be avoided at the expense of linearity by using a VCO whose dc characteristic is linear in period instead of in frequency. Such a circuit is shown in Fig. 7.15. The circuit is very similar to that of Fig. 7.12. The only

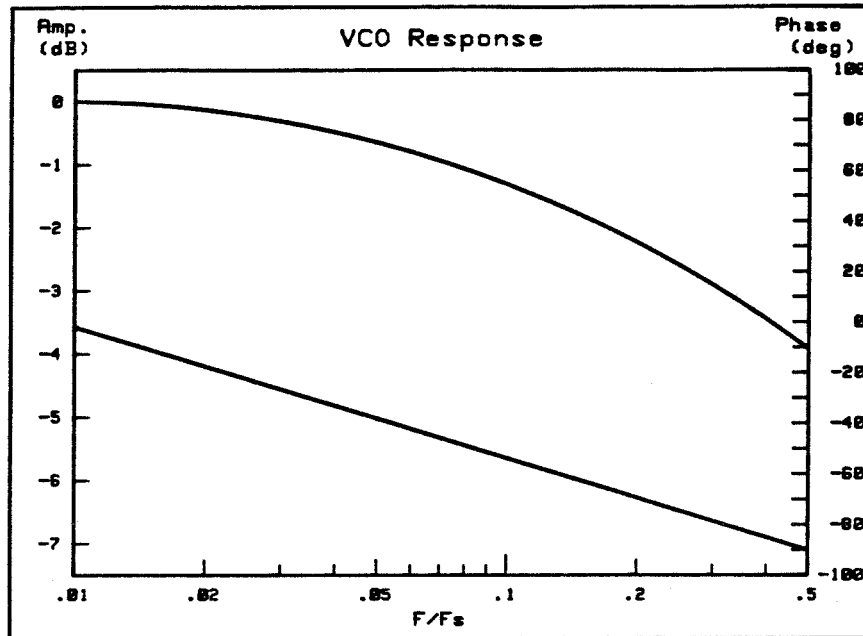


Figure 7.14: Frequency response of the linear-in-frequency VCO.

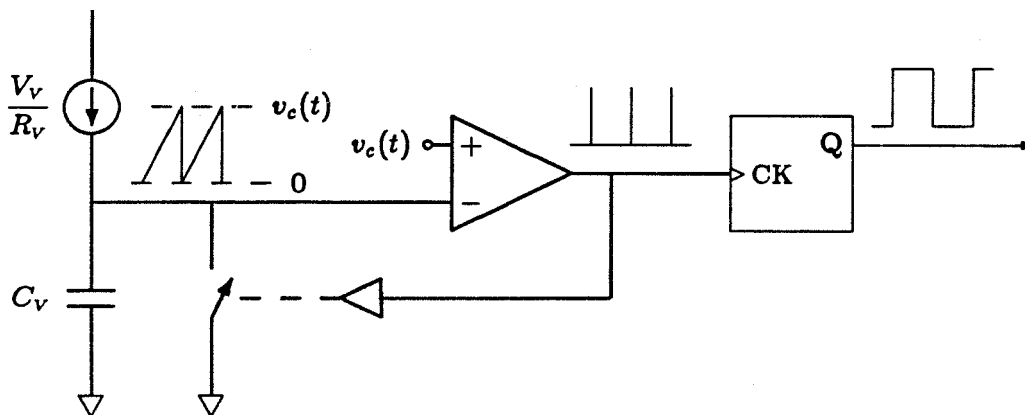


Figure 7.15: Diagram of a VCO with the period a linear function of input voltage.

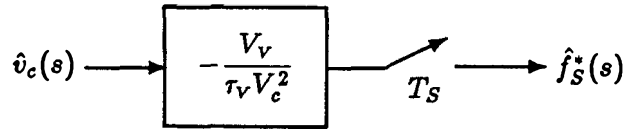


Figure 7.16: Small-signal model of the linear-in-period VCO.

difference is that the current  $V_V/R_V$  is held constant and the frequency is modulated by varying the triggering voltage of the comparator,  $v_c$ . At dc,

$$F_S = \frac{1}{\tau_V} \frac{V_V}{V_c}, \quad (7.9)$$

with  $\tau_V = R_V C_V$  as before. The frequency varies inversely with the control voltage.

A small-signal model for this circuit appears in Fig. 7.16. The model contains no dynamics; only the sampler affects the frequency response. For sinusoidal  $v_c(t)$ , the input-to-output transfer function is simply a constant, with no phase lag.

### 7.3.3 VCO Measurements

All the frequency-response curves previously shown were taken using a VCO linear in period. The purpose was to verify the small-signal model of the converter itself, so a VCO that contributed no phase lag was appropriate. Practical regulator systems will most likely use a VCO linear in frequency to avoid changes in the feedback gain as the load changes. In this case the designer must be aware of the additional phase lag.

Figure 7.17 shows four frequency-response curves. Curves (A) and (B) are the same as those in Fig. 7.11, the measured and predicted frequency response of a ZVS boost converter using a linear-in-period VCO. The response of the same converter modulated with a commercial linear-in-frequency VCO (74LS629), is added to this plot as curve (C) (accounting for the different dc gain of the two VCO's). Curve (D) shows the predicted response for this case, including the gain and phase contribution of the modulator from Fig. 7.14. The model of Section 7.3.1 accounts fairly well for the observed additional phase lag near half the switching frequency.

Since all the frequency-response curves included here rely on the small-signal model of the converter, a model which is only valid well below the switching frequency, deviations

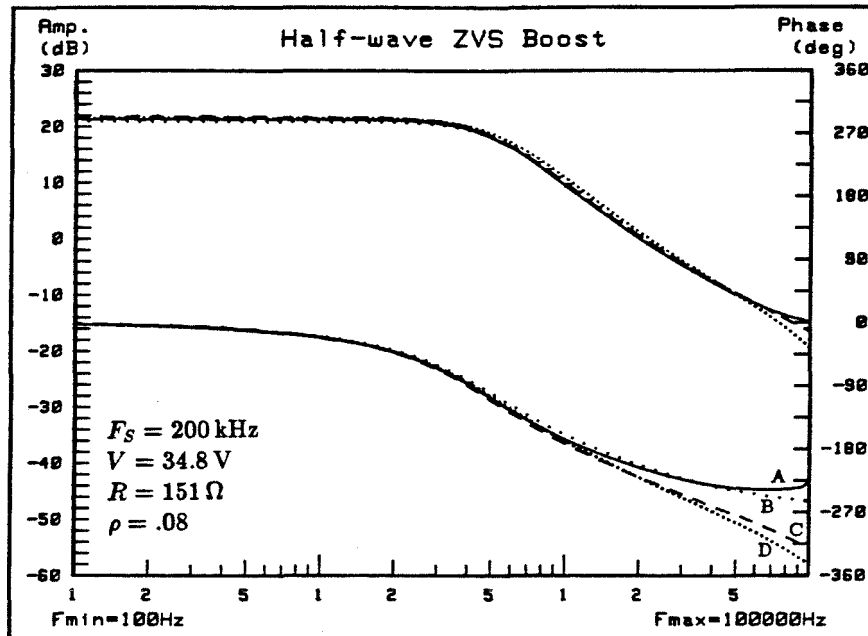


Figure 7.17: Frequency response of a ZVS boost converter with two different VCO's. VCO of Fig. 7.15: measured (A), predicted (B). VCO of Fig. 7.12: measured (C), predicted (D).

of the magnitude and phase from the values predicted by the small-signal model near  $F_S/2$  must be expected. The curves of Fig. 7.17 are a convincing argument, however, that the commercial VCO introduces phase lag, while the linear-in-period VCO does not.

## Chapter 8

# Conclusion

Quasi-resonant converters possess a unique combination of features. With their quasi-sinusoidal waveforms, they have the desirable features of zero-current or zero-voltage switching and insensitivity to parasitics. The presence of an idle interval in the sequence of switched networks makes these converters easy to analyze, however, when compared to most other resonant converters.

Converters with resonant switches come in an astounding variety of topologies. The quasi-resonant converter is first of all based upon any one of many PWM topologies. To the basic PWM converter is added either a zero-voltage or a zero-current resonant switch. The switch can be either half-wave or full-wave, and the resonant reactances may appear in many different positions within the topology without changing the dc behavior.

By limiting consideration to a certain class of converters—those with single switches and no coupling—the analysis of this part was able to apply the topology and behavior of a PWM converter to its quasi-resonant offspring, yielding general expressions for the dc conversion ratio and small-signal coefficients. The dc behavior of any converter with a resonant switch was shown to be governed by Eq.(4.11) or Eq.(6.3) for zero-current or zero-voltage converters, respectively. These equations use the known conversion ratio of the underlying PWM converters. The parameters of the small-signal dynamic model use this same ratio, giving visible evidence of the role the underlying PWM converter plays in the behavior of the resonant converter.

The general analysis performed here revealed that the qualitative behavior of a quasi-resonant converter is determined mainly by the type of resonant switch used, full- or half-wave. A converter with a full-wave switch is similar to its PWM parent in every respect. The dc conversion ratio and ac small-signal behavior (to the extent that the resonant

reactances may be neglected in the small-signal model) are both obtained by substitution of the resonant control variable  $f_S/F_0$  for the duty ratio  $d$  which controls the PWM converter. Full-wave converters have load-independent conversion ratios and undamped dynamic responses. Half-wave converters, in contrast, demonstrate behavior remarkably similar to PWM converters in the discontinuous conduction mode. The conversion ratio is load-dependent, producing a lossless output resistance that fosters current-sharing among paralleled converters. The half-wave switch also introduces lossless damping in the small-signal dynamic response.

The dc analysis of quasi-resonant converters relies on the assumptions of losslessness and of small ripple in the converter's non-resonant reactances, while the small-signal analysis makes the additional approximation that modulation occurs far below the switching frequency. The loss in accuracy caused by these approximations is rewarded by the benefits of generality and simplicity in the resulting models. The approximate analysis provides a means of understanding how quasi-resonant converters behave and how the many variations relate to one another and to their PWM parents.

The most remarkable aspect of the analytic results is their generality. One needs to know only the underlying PWM topology and the type of resonant switch used in order to evaluate both the dc and ac behavior of a quasi-resonant converter. All other variations of the circuit have no effect on the "external" performance of the converter. For circuits of such apparent complexity as resonant power converters, it is astonishing that a fairly simple analysis should be so all-encompassing. That such an analysis is possible is both a result of and unmistakable evidence for the PWM heritage of quasi-resonant converters.



**Part II**

**Input-Current Shaping for  
Single-Phase Ac-Dc Power Converters**



## Chapter 9

# Introduction

Electrical power comes in many forms. Some power sources, such as solar cells and batteries, provide dc voltages. Others—for instance the utility power grid and portable or emergency generators—generate ac voltages. The voltage of a power source, whether dc or ac, may range from very low, as in a 1.5 V dry cell, to extremely high, as in the transmission of utility power.

Electrical loads are equally varied. Their requirements cover the spectrum from low to high voltage, and include both dc and ac waveforms. Some loads, for example a variable-speed induction motor, even require a power source whose voltage and frequency change during operation.

In very few applications is the available power source ideally suited for the load at hand. Instead, the power delivered by the source must be *converted* in voltage and/or frequency before it will meet the requirements of the load. This conversion is the job of a *power converter*.

One of the most common power converters is the *ac-dc converter*, which supplies a dc load with power drawn from an ac source. The popularity of ac-dc converters results from the fact that ac power sources and dc loads are so common. The most widely available source of electrical power is the utility grid, which supplies power in the form of a low-frequency, sinusoidal voltage. Virtually all electronic systems, however—including equipment for instrumentation, communication, and computing—ultimately require dc voltages.

Ac-dc converters range from extremely simple circuits to complicated, microprocessor-controlled systems. For applications where the quality of the dc output voltage is not critical, a few rectifiers and a filter capacitor suffice to convert ac voltage to dc. At low to medium power levels, such a simple rectifier circuit is often followed by a dc-dc con-

verter to smooth and regulate the output voltage. At high power levels, phase-controlled rectification provides a regulated dc output voltage using rugged semiconductor devices.

All these methods of generating a dc voltage from an ac power line share certain drawbacks, each the result of a poor input-current waveform:

- distortion of the line voltage, affecting both the offending equipment and any other equipment on the same power line
- conducted and radiated electromagnetic interference as a result of harmonic currents drawn from the power source
- poor utilization of the capacity of the power source.

Until fairly recently, these drawbacks were of little concern. Electronic equipment was not very common and consumed relatively small amounts of power. The bulk of the load on the utility grid—motors, lighting, and heating—was fairly insensitive to line-voltage quality. The situation has changed over the past decades, however, and now electronic loads are so common that they represent a significant portion of the total load at many installations.

At the same time, electronic systems have become more demanding. Each new generation of electronic equipment performs more functions with ever greater speed and precision. Complicated systems can draw large amounts of power, making it important to fully utilize the capacity of the power line. The complexity of modern systems also makes them more sensitive to the quality of the line voltage.

Yet even as the quality of utility power is becoming increasingly important to electronic systems, the ac-dc converters present in those systems are threatening that quality. This is why the power community is placing new emphasis on the input-side behavior of “off-line” ac-dc converters. The designer of a utility-powered ac-dc converter must now consider the effects of the converter not only on the dc load, but also on the ac power source and any other equipment supplied by that source. In short, the designer must now consider the quality of the input current as well as of the output voltage.

*Input-current shaping* is the process of improving the input-current waveform of an ac-dc converter, with the goal of alleviating problems of noise, line-voltage distortion, and

poor utilization. Both single-phase and three-phase ac-dc converters may need current shaping, but the present discussion is limited to power converters supplying a dc load from a *single-phase* source of sinusoidal (ac) voltage. Although many of the techniques to be discussed are applicable to three-phase power converters, the limitations imposed on the converter by the current-shaping process are very different in the single-phase and three-phase cases.

The purpose of this part is to examine the problem of single-phase current shaping from a system viewpoint. It will be determined that, although countless circuits exist for improving input-current waveforms, all the circuits can be best understood as variations of only a few basic shaping methods. The system viewpoint also reveals that single-phase ac-dc conversion forces certain requirements and limitations on *any* power converter. In particular, a single-phase ac-dc converter faces severe limitations in the areas of energy storage, isolation, and regulation. Methods are derived for determining whether a particular converter is suitable for current-shaping, and a new shaping topology is suggested with the desirable features of isolation, high-quality input current, and fast, independent output-voltage regulation.

Chapter 10 introduces a general single-phase ac-dc conversion system. Various parameters of the system are defined and some conventions introduced. As a further introduction, measured waveforms will demonstrate the poor input-current waveshape of a common ac-dc conversion method.

Quantitative measures of input-current quality are considered in Chapter 11. The most common measure of input-side performance is *power factor*, and the definition and implications of this quantity are studied in detail. Depending on the specific application, other details of the current waveform may be important. Some of these—harmonic content and peak value—and the reasons for their importance are also considered. The chapter concludes with an argument showing that an ac-dc converter should draw a distorted line current if the line voltage is distorted.

The next question to be considered is how to actually impose a desirable waveshape on the input current. The simplest solutions use passive circuits. These circuits do not produce ideal waveforms, but because of their simplicity they are favored in some

applications. Chapter 12 presents and analyzes several passive current-shaping methods.

Active current-shaping methods offer a variety of ways to achieve high-quality current waveforms. Almost all the active shaping methods are based on either buck or boost dc-dc converter topologies. Either topology can be operated in several modes, some of which are analyzed in Chapter 13. A unique and little-known “automatic” shaping method, using the discontinuous conduction mode of operation, is presented and analyzed.

The more general problem of determining whether or not a specific dc-dc converter is suitable as a current shaper is treated in Chapter 14. This chapter considers the requirements a dc-dc converter must meet if it is to perform either “automatic” or the more usual controlled current shaping. In addition to several conventional topologies, the performance of *resonant* converter topologies as current shapers is considered. Resonant dc-dc converters offer some advantages at very high switching frequencies, and it is of interest to see whether these same advantages can be incorporated in ac-dc converters with current-shaping.

The problems of supplying a dc load from an ac power source include several difficulties in addition to that of obtaining a desirable current waveform. One of these, the need for significant stored energy, is studied in Chapter 15, which derives the theoretical limitations and compares the performances of several schemes proposed to mitigate the problem. The ac-dc power conversion process also constrains the way in which a current-shaping power converter can be isolated and regulated. The difficulties in achieving these two very necessary features are discussed in Chapter 16.

Chapter 17 summarizes the features of the ac-dc power conversion process, the methods of achieving high-quality input-current waveforms, and the impact of current shaping on the design and control of a power converter. The strengths and weaknesses of the various techniques must be understood, so that designers of electronic systems can intelligently choose ways of solving the problems of poor input-current waveforms.

The importance of clean, well-regulated dc power for sensitive loads is still paramount, but designers can no longer ignore the effects of their equipment on the ac power line. This work provides an understanding of the constraints forced on any single-phase ac-dc conversion system and of the impact of these constraints on system performance.

In addition, the following chapters introduce a framework for classifying current-shaping converters and for determining what converter topologies are suitable for current-shaping. In the fight against polluted power lines, a designer needs tools for understanding the problem and the various solutions. These are the tools found in the following chapters.





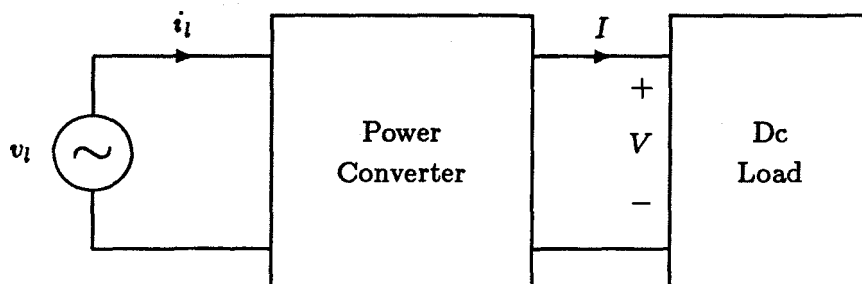
## Chapter 10

# The Input-Current Problem

This chapter serves two purposes. First, it introduces in Section 10.1 the elements of a single-phase ac-dc power conversion system and sets forth conventions and definitions for later use. Second, the most common method of ac-dc conversion is reviewed in Section 10.2. The problems associated with this method are the motivation for the discussions and circuits of later chapters.

### 10.1 Definitions and Conventions

Figure 10.1 illustrates the general case of a dc load supplied by a single-phase ac line. The line voltage  $v_l$  is the waveform  $V_l \sin \omega_l t$ , a sine wave with peak value  $V_l$  and radian frequency  $\omega_l$ . The line period is the time interval  $T_l = 2\pi/\omega_l$ . Often it will be more convenient to consider waveforms as functions of the angle  $\theta = \omega_l t$ . For example, the line voltage may be written  $V_l \sin \theta$ . The line current, or input current, is denoted  $i_l$ , and  $V$  and  $I$  are the dc voltage and current at the dc load. The conversion ratio of the



*Figure 10.1: An ac-dc conversion system. The power converter transforms the ac line voltage  $v_l$  into a dc voltage  $V$  and current  $I$  suitable for the dc load.*

ac-dc converter is defined by

$$M \equiv \frac{V}{V_l}, \quad (10.1)$$

and is the ratio of the dc load voltage to the *peak* of the sinusoidal line voltage.

The system of Fig. 10.1 draws average input power

$$P_{in} = \frac{1}{2\pi} \int_0^{2\pi} v_l i_l d\theta, \quad (10.2)$$

while the dc load receives average power

$$P_{out} = VI. \quad (10.3)$$

When the losses within the power converter are negligible,  $P_{in}$  and  $P_{out}$  can be equated.

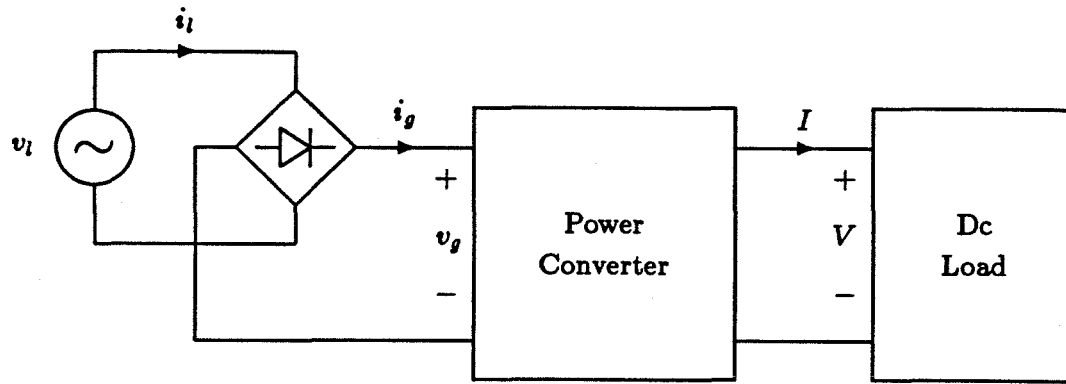
In this case, the average power processed by the converter is denoted  $P$ .

The dc load resistance is defined by

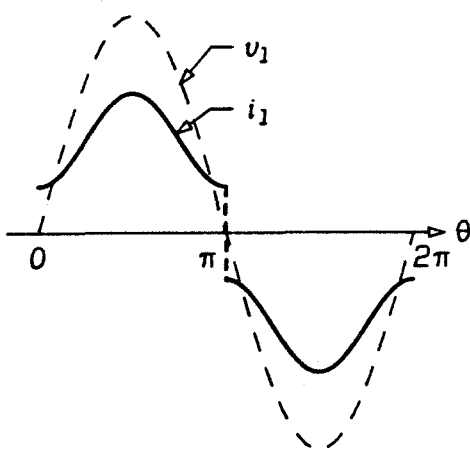
$$R \equiv \frac{V}{I}, \quad (10.4)$$

regardless of whether or not the actual dc load is resistive. The dc load may be nonlinear, or it may actually be a switching or linear post-regulator. In any case, the dc load at a given operating point has some average voltage and current, and the ratio of these quantities defines  $R$ .

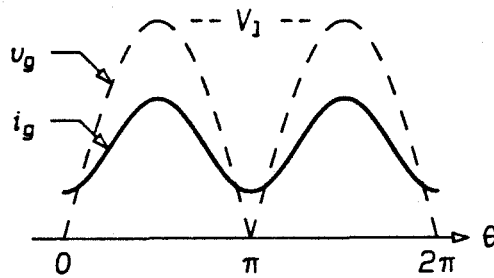
Frequently, the line voltage is rectified by a bridge rectifier, as shown in Fig. 10.2(a). The waveforms on the line side of the rectifier are periodic with period  $T_l$ , as shown in the sample waveforms of Fig. 10.2(b). These waveforms have odd symmetry and contain only odd harmonics. On the load side of the rectifier bridge, as illustrated in Fig. 10.2(c), the waveforms have even symmetry, contain only even harmonics, and are periodic with period  $T_l/2$ . The waveforms on the load side of the rectifier will be used frequently, and it would be inconvenient to refer to the rectified voltage  $v_g$  as  $V_l |\sin \theta|$  or to describe the current  $i_g$  with different expressions over the two intervals  $0 < \theta < \pi$  and  $\pi < \theta < 2\pi$ . In the following chapters, therefore, the expressions for currents, voltages, and control parameters will be given with the understanding that, unless otherwise specified, these expressions are valid over the interval  $0 < \theta < \pi$ . The appropriate rectification or unfolding needed to extend a given waveform into the interval  $\pi < \theta < 2\pi$  will be understood from the context.



(a)



(b)



(c)

Figure 10.2: An ac-dc conversion system in which the line voltage is first rectified (a). Illustrative waveforms from the line (b) and load (c) sides of the rectifier bridge.

The power converter that performs the ac-dc conversion is responsible for the current waveform drawn from the line. When the shape and quality of the line current is a specific and principal goal of the power converter, the converter is called a “current-shaping power converter,” “input-current shaper,” or simply “shaper.”

Ideally, the ac-dc power converter of Fig. 10.1 draws a sinusoidal current  $i_l = I_l \sin \theta$  from the line; this is the “best” current waveform that can be drawn from the sinusoidal line voltage, according to the criteria of Chapter 11. When the line current closely approximates this ideal waveform, the line current and voltage are related by a constant, defined by

$$R_{em} = \frac{V_l}{I_l} \quad (10.5)$$

and called the *emulated resistance*. The name reflects the fact that a power converter drawing a line current proportional to the line voltage appears as a resistance to the power line. Such a power converter may be known as a “unity power factor” or “harmonic free” power converter, or it may be called a “resistor emulator.” All three names imply the same ideal line-current waveshape.

The system of Fig. 10.1 consists of three elements: the ac source, a power converter, and the dc load. In a given application, the ac source and dc load are specified, and the power engineer’s task is the design of a suitable power converter. The converter serves several purposes.

1. It must convert the ac input voltage into a dc output voltage. Equivalently, the power converter converts ac power to dc power.
2. It must provide a clean, well-regulated dc output voltage. This includes removing any line-frequency ripple from the output voltage, as well as maintaining the dc output voltage against line and load variations. (Not every application may require a tightly-regulated output voltage).
3. The power converter must provide isolation, if the system requires it.
4. The power converter must draw an acceptable input-current waveform from the line.

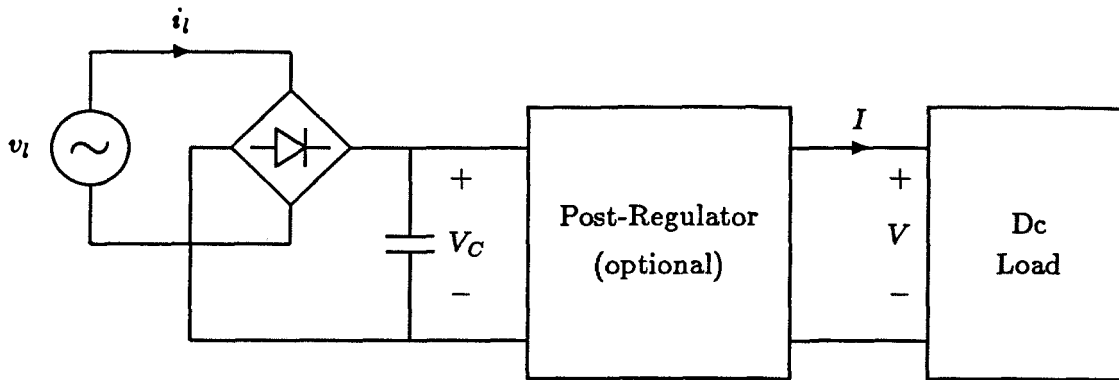


Figure 10.3: A capacitor-input filter ac-dc conversion system.

Item 4 is, of course, the problem of main interest here, but it will be seen in Chapters 15 and 16 that the other functions are intimately connected with the input-current problem.

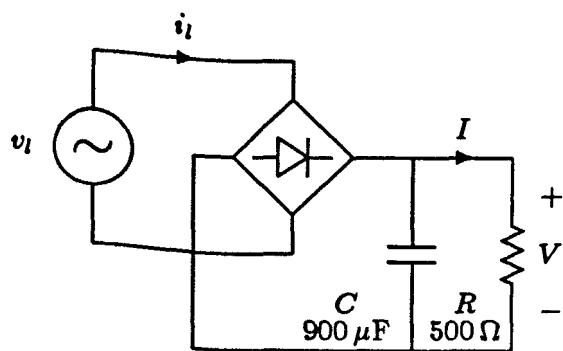
## 10.2 The Capacitor-Input Filter

At low to medium power levels, the most common method of producing clean dc power from the ac line uses a *capacitor-input filter*, followed by a post-regulator. Figure 10.3 shows such a system. The capacitor-input filter is simply a bridge rectifier followed by a filter capacitor. The bridge converts ac voltage to dc while the capacitor forces the dc output voltage  $V_C$  to have small ripple. The (optional) post-regulator processes the “raw” voltage  $V_C$  and provides a regulated dc voltage to the load.

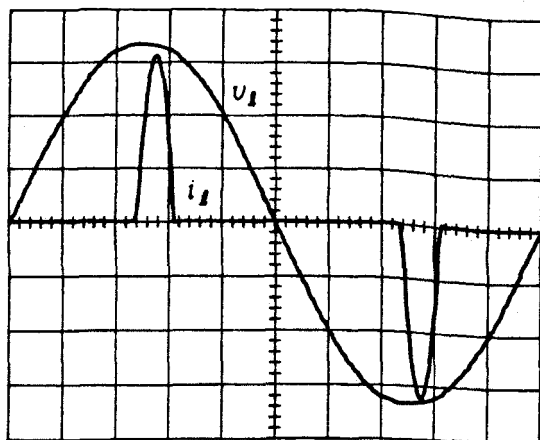
The system of Fig. 10.3 has several advantages. The capacitor-input filter is cheap, simple, and rugged, while the post-regulator generates a tightly-regulated dc voltage. Switching post-regulators, often used, offer a convenient place to introduce isolation, and also permit multiple dc outputs.

Unfortunately, the capacitor-input filter suffers from a poor input-current waveshape. Since the output capacitor is large and maintains a nearly constant voltage, the diode bridge turns ON only for a short time during each cycle, when the line voltage is near its peak. The line current therefore consists of short pulses with relatively high peak values.

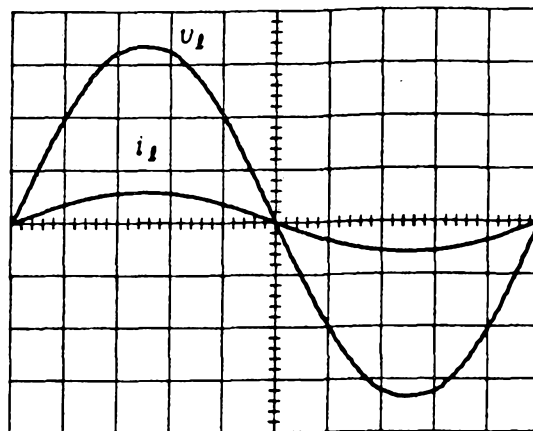
Figure 10.4(a) shows a capacitor-input filter feeding a resistive load. The line voltage



(a)



(b)



(c)

Figure 10.4: Experimental capacitor-input filter (a), with its line voltage and current waveforms (b). A resistor connected directly across the line has the waveforms shown in (c). Scale factors: 50 V/div, 1 A/div, and 1.67 mS/div.

and resulting current are shown in Fig. 10.4(b). The traces shown were captured with a digital oscilloscope.

With a line voltage of 120 V rms, the circuit of Fig. 10.4(b) delivers 50 W to the load resistor. The peak and rms line currents are 3.1 A and 0.88 A, respectively. For comparison, Fig. 10.4(c) shows the line-current waveform for a resistor that draws the same 50 W when connected directly across the 120 V power line. Although both circuits consume the same average power, the peak and rms input current of the resistive load are only 0.58 A and 0.42 A, respectively.

The peak and rms input currents of the capacitor-input filter are much higher than those of the purely resistive load, a fact which impacts the entire power distribution system. Compared to the resistive load, the higher current of the capacitor-input filter demands that the generators, transformers, connectors, wires, and circuit breakers—in short, the entire distribution system—all have higher ratings and hence greater size, weight, and cost.

The “peaky” input current of the capacitor-input filter also leads to harmonic currents in the line. The line voltage of Figs. 10.4(b) and 10.4(c) is a relatively pure sine wave, with no harmonics larger than 1% of the fundamental. The current waveform of Fig. 10.4(c) has this same purity since the resistive load is linear. The capacitor-input filter, however, drawing the distorted current waveform of Fig. 10.4(b), has the harmonic content shown in Fig. 10.5. The large harmonic currents are a source of noise and interference to other devices on the same power line. In addition, the harmonic currents are drawn through the finite source impedance of the line, distorting the line voltage at the load.

Chapter 11 contains a more general discussion of input-current quality, but in this example it is obvious that the resistor of Fig. 10.4(c) draws the “better” current waveform from the ac power line. That resistor sees ac voltage, however, while the capacitor-input filter supplies its load with dc voltage. What is needed is a method of ac-dc conversion that supports a dc load, as does the capacitor-input filter, while drawing a benign line current like that of the resistive load. The circuits that perform this function, both active and passive, are the subject of the following chapters.

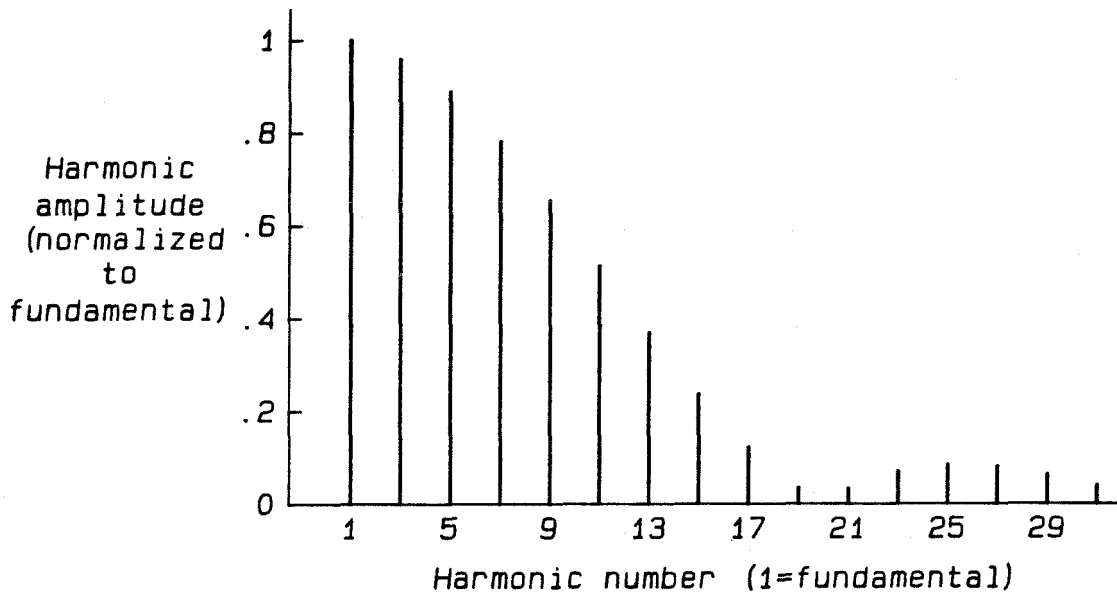


Figure 10.5: Harmonic content of the line-current waveform of Fig. 10.4(b).



## Chapter 11

# Input-Current Quality and Power Factor

When discussing the shaping of input-current waveforms, one needs some measure of input-current quality. Power factor is probably not only the most common measure, but also the most commonly misunderstood. The definition of power factor and its implications, both in general and in a system with sinusoidal voltage, are considered in detail in Section 11.1. Other important features of the input current, such as distortion and peak current, are considered in Section 11.2. The chapter concludes with arguments showing that input current ideally should be proportional to the input voltage rather than to some internal, ideal sinusoidal reference.

### 11.1 Power Factor

Power factor is probably the most common parameter describing the way a load utilizes the utility line. Power factor considers both the line voltage and current waveforms, conveniently compressing these two quantities into a scalar, dimensionless quantity. Despite its simplicity, the power factor provides useful information concerning the input-side performance of an ac-dc converter.

#### 11.1.1 Definition

Consider a load drawing a current  $i_l$  from the utility power line with voltage  $v_l$ . Both  $i_l$  and  $v_l$  are periodic waveforms with period  $T_l$ . The load draws average power

$$P = \frac{1}{T_l} \int_{T_l} v_l i_l dt, \quad (11.1)$$

where  $\int_{T_l}$  represents the integral over any continuous interval of length  $T_l$  (a single period

of the line voltage). The power factor is defined by

$$\text{PF} \equiv \frac{P}{V_{l,\text{rms}} I_{l,\text{rms}}}, \quad (11.2)$$

where the rms line voltage and current are given by

$$V_{l,\text{rms}} \equiv \sqrt{\frac{1}{T_l} \int v_l^2 dt} \quad (11.3)$$

$$I_{l,\text{rms}} \equiv \sqrt{\frac{1}{T_l} \int i_l^2 dt}. \quad (11.4)$$

In words, power factor is the ratio of average power (also called real, true, or active power) to volt-amperes (VA).

### 11.1.2 Power Factor and Rms Current

The line voltage is usually delivered through a relatively small impedance, so that the voltage  $v_l$ , along with its rms value  $V_{l,\text{rms}}$ , may be considered given and fixed. For a given application, a certain amount of average power  $P$  is required to perform useful work. The only “variable” left in the power factor definition is the rms current  $I_{l,\text{rms}}$ . For given values of  $V_{l,\text{rms}}$  and  $P$ , the more rms current a device draws from the power line, the lower the power factor.

As an illustration, consider the example of the previous chapter. The capacitor-input filter of Fig. 10.4 supplies its load with 50 W from the 120 V line while drawing 0.88 A of rms current. A resistive load, also drawing 50 W at the same line voltage, requires only 0.42 A rms. The capacitor-input filter operates with a power factor of 0.48, while the resistor has a power factor of unity.

As another example of the effect of low power factor and high rms current, consider the usual 120 V, 15 A distribution circuits available in homes and offices. With 120 V rms input voltage and 12 A rms input current, a device with unity power factor draws 1440 W from the ac line. If the same 1440 W load was to be supplied through a capacitor-input filter with, for instance, a power factor of only 0.7, then the rms input current would be 17.1 A, too much for the 15 A rating of the distribution circuit. To accommodate such a load, one would have to install a larger distribution circuit (20 A for example), install a

240 V line, or somehow increase the power factor of the 1440 W unit so that the capacity of the 15 A line would be better utilized.

Power factor is therefore a measure of how efficiently a device uses its rms input-current rating. High power factor means the device draws no more rms current than is “necessary,” while low power factor means that the rms current is higher than it need be to perform the same amount of electrical work.

### 11.1.3 Power Factor and Proportional Waveforms

One way of interpreting power factor comes from recognizing that the integral

$$\frac{1}{T_l} \int_{T_l} v_l i_l dt \quad (11.5)$$

is an inner product  $\langle v_l, i_l \rangle$  on the space of periodic functions that have a Fourier series expansion. In terms of inner products, power factor can be written

$$\text{PF} = \frac{\langle v_l, i_l \rangle}{\|v_l\| \|i_l\|}, \quad (11.6)$$

where  $\|v_l\|$  indicates the induced norm  $\langle v_l, v_l \rangle^{1/2}$ , the rms value of  $v_l$ . Similarly,  $\|i_l\|$  is just another way of denoting  $i_{l,\text{rms}}$ . The Cauchy-Schwartz inequality asserts that

$$\langle v_l, i_l \rangle \leq \|v_l\| \|i_l\| \quad (11.7)$$

with equality if and only if  $v_l$  and  $i_l$  are proportional.

The power factor, therefore, is never greater than unity, and reaches that limiting value *only* when the input current  $i_l$  is proportional to the line voltage  $v_l$ . Unity power factor, and hence minimum rms current for a given voltage and power level, is achieved only when the load appears to be a linear resistor, since the resistor has proportional voltage and current waveforms. This explains why some power converters with near-unity power factor are referred to as “resistor emulators.”

The relation between power factor and proportional waveforms is not always fully appreciated. The Cauchy-Schwartz inequality implies that maximum power factor results when the line current  $i_l$  is proportional to the line voltage  $v_l$ . It also implies that the current waveform producing unity power factor is *unique*. Only one waveform is

proportional to  $v_l$  with a constant of proportionality giving the correct average power. Finally, the requirement of proportionality means that if the line voltage is distorted (not a true sinusoid), then the input current should also be distorted! This result may come as a surprise, but sine-wave currents, known to be the ideal waveform for ac line voltages, are ideal not because they are sinusoids but because they are proportional to the ideal line voltage. If the line voltage is distorted, then the line current should and must be distorted to obtain unity power factor.

#### 11.1.4 Frequency-domain Interpretation

Power factor has been seen from two viewpoints so far, the time-domain definition of Eq.(11.2) and the vector-space equivalent of Eq.(11.6). A third interpretation, this time in the frequency domain, is possible using the Parseval equality. Let the periodic functions  $v_l$  and  $i_l$  be represented by Fourier series in the phase-angle sinusoid form:

$$\text{FS}[v_l] = V_0 + \sum_{k=1}^{\infty} \sqrt{2}V_k \sin(k\omega_l + \gamma_k) \quad (11.8)$$

$$\text{FS}[i_l] = I_0 + \sum_{k=1}^{\infty} \sqrt{2}I_k \sin(k\omega_l + \phi_k) . \quad (11.9)$$

With this form of Fourier expansion, the coefficients are found by first calculating

$$a_k = \frac{2}{T_l} \int_{T_l} v_l \cos(k\omega_l t) dt \quad (11.10)$$

$$b_k = \frac{2}{T_l} \int_{T_l} v_l \sin(k\omega_l t) dt \quad (11.11)$$

$$c_k = \frac{2}{T_l} \int_{T_l} i_l \cos(k\omega_l t) dt \quad (11.12)$$

$$d_k = \frac{2}{T_l} \int_{T_l} i_l \sin(k\omega_l t) dt . \quad (11.13)$$

The magnitudes  $V_k$  and  $I_k$  and phase angles  $\gamma_k$  and  $\phi_k$  are then given by

$$\left. \begin{aligned} V_k &= \sqrt{\frac{a_k^2 + b_k^2}{2}} \\ I_k &= \sqrt{\frac{c_k^2 + d_k^2}{2}} \\ \gamma_k &= \tan^{-1} \frac{a_k}{b_k} \\ \phi_k &= \tan^{-1} \frac{c_k}{d_k} \end{aligned} \right\} k = 1, 2, \dots \quad (11.14)$$

The values  $V_0$  and  $I_0$  are defined as the dc values (averages) of  $v_l$  and  $i_l$ , respectively. The rest of the  $V_k$  and  $I_k$  are the *rms values* of the  $k$ th voltage and current harmonics. If any  $V_k$  or  $I_k$  is zero, then the corresponding phase angle is also defined as zero.

The Parseval equality for this form of the series states that

$$v_{l,rms} = \|v_l\| = \left( V_0^2 + \sum_{k=1}^{\infty} V_k^2 \right)^{1/2} \quad (11.15)$$

$$i_{l,rms} = \|i_l\| = \left( I_0^2 + \sum_{k=1}^{\infty} I_k^2 \right)^{1/2} \quad (11.16)$$

$$P = \langle v_l, i_l \rangle = V_0 I_0 + \sum_{k=1}^{\infty} V_k I_k \cos(\phi_k - \gamma_k) . \quad (11.17)$$

According to Eq.(11.16), every harmonic component of the input current  $i_l$  contributes to the rms input current, and therefore to the needed line capacity and to the losses in the input wiring. Equation (11.17), however, shows that a current component only performs work if it is matched by a voltage component at the same frequency and of the same phase. Current harmonics without corresponding voltage components do no work. The presence of any such unmatched components reduces the power factor below unity. Similarly, voltage harmonics without matching current components lower the power factor.

The time-domain interpretation of power factor concluded that voltage and current must be proportional for unity power factor. It is therefore necessary not only that the frequency components of voltage and current match each other one for one, but that they match in the same proportion throughout the entire spectrum. Unity power factor occurs only when the spectral components of current and voltage are proportional and

in phase:

$$\text{PF} = 1 \iff \left\{ I_k = \frac{V_k}{R_{em}} \text{ and } \phi_k = \gamma_k, \quad k = 0, 1, \dots \right\}, \quad (11.18)$$

where  $R_{em}$ , the constant of proportionality, is the emulated resistance.

### 11.1.5 Power Factor for Sinusoidal Voltage

Line voltage is ideally sinusoidal, but in practice it often contains distortion. (Removal of the sources of this distortion is one reason for shaping input-current waveforms.) Since the distortion is usually small and unpredictable, however, the input voltage is almost always assumed to be a pure sinusoid when analyzing line-supplied power converters. For convenience, the input-voltage waveform is assumed to be a sine wave with no phase shift, that is

$$v_l = V_l \sin \omega_l t. \quad (11.19)$$

In the Fourier expansion of the line voltage, Eq.(11.8),  $V_1 = V_l/\sqrt{2}$  and  $V_k = 0$  for  $k \neq 1$ . The phase shifts,  $\gamma_k$ , are all zero. With this input voltage, the power factor can be rewritten in terms of Fourier components as

$$\text{PF} = \frac{V_1 I_1 \cos \phi_1}{V_1 \left( I_0^2 + \sum_{k=1}^{\infty} I_k^2 \right)^{1/2}} \quad (11.20)$$

$$= \frac{I_1}{I_{l,\text{rms}}} \cos \phi_1. \quad (11.21)$$

The power factor consists of two terms. The first,  $I_1/I_{l,\text{rms}}$ , is called the *distortion factor*. The distortion factor is simply the ratio of the rms value of the fundamental of the current to the rms value of the entire current waveform. In the usual case that  $i_l$  has no dc component, the distortion factor can be rewritten

$$\frac{I_1}{I_{l,\text{rms}}} = \frac{1}{\sqrt{1 + (\text{THD})^2}}, \quad (11.22)$$

where THD is the total harmonic distortion. The distortion factor demonstrates the effect on power factor when the current waveform deviates from the ideal, sinusoidal shape. This term considers no phase information; it is concerned only with the harmonic content or power spectrum of the line current. When  $i_l$  contains harmonics other than the fundamental—harmonics that cannot contribute any average power—the distortion

factor is less than unity and the power factor is correspondingly reduced. When  $i_l$  contains only the fundamental component  $I_1$ , the current is a pure sinusoid and the distortion factor is unity.

The second term,  $\cos \phi_1$ , is called the *displacement factor*, and is the cosine of the angle between the fundamental components of the line current and voltage. This term reduces the power factor whenever the two fundamental components are out of phase. In the case of a linear load, the line current contains only a fundamental component and power factor is given solely by the displacement factor, a familiar result for motors and other reactive loads.

Electronic loads are nonlinear, and the input current can be both distorted and phase shifted. Breaking down the power factor into factors representing displacement and distortion is helpful because these two problems require very different solutions. Displacement of the fundamental current can be removed by adding reactances in series or in parallel with the load. Parallel capacitor banks, for instance, are commonly used to compensate for large inductive loads. Distortion may be more difficult to fix, depending on the frequency of the offending harmonic components. Distortion can be reduced by filtering, but the multiple tuned filters sometimes required are expensive and sensitive to line frequency.

It should be emphasized that the breaking of power factor into displacement and distortion factors is valid only when the line voltage is sinusoidal. When the line voltage is itself distorted, the volt-amperes may be divided into several reactive and distortive terms [22], but this process does not seem to aid in the interpretation of power factor. The main conclusion, that the current and voltage must be proportional for unity power factor, remains true regardless of any distortion in the line voltage.

## 11.2 Other Measures of Current Quality

Power factor is a useful quantity, but it does not convey all the information about an input-current waveform that may be needed. For example, power factor is a scalar number that does not distinguish between distortion and displacement, yet these two problems require very different solutions. Even when power factor is presented as two

numbers, the displacement and distortion factors, the nature of the distortion is not revealed. Some other figures of merit for input-current waveforms are now considered.

In the case of distorted (non-sinusoidal) line currents, the frequency and relative magnitudes of the unwanted harmonics are important factors. If the distortion lies near the line frequency, for example in the third and fifth harmonics, then any filter used to reduce the distortion is tuned to these low frequencies and consequently must be large and heavy. If, on the other hand, the distortion is a result of high-frequency switching effects, then small, high-frequency filters suffice to remove the noise.

Susceptibility of certain equipment to various frequencies may also be of concern in determining the relative importance of harmonics in the input current. For example, one common weighting of harmonic content is the *telephone influence factor* (TIF) [23], which considers the effect of harmonic currents in the utility line coupling into the phone system. At each frequency in the voice band, the TIF provides a weighting factor to aid in determining allowable harmonic currents.

High-frequency components of the input current may be important in the time domain as well. If the input current passes through a rectifier bridge, as is commonly the case, then discontinuities or steep edges in the current waveform cause the rectifiers to turn OFF very fast. Rapid reverse recovery of the rectifiers can generate additional noise, compounding the problems of harmonic currents.

In active current-shaping schemes, the peak value of the input current may be of greater concern than the rms value because of the stress the peak current places on semiconductor switches. If current stress is an issue, then rectangular, trapezoidal or truncated sine waveforms may be preferred over a sinusoidal input current [35]. The power factor in this case is of course less than with the ideal sine-wave current waveform, but the peak current with a nonsinusoidal waveform can be as much as 21% less than in a sine wave delivering the same average power.

### 11.3 Sine Wave or Proportional Current?

As seen in Section 11.1.3, power factor reaches its optimal value only when the input current is proportional to the input voltage. The conclusion was reached that if the



line voltage was a distorted waveform, then the line current should be distorted as well, containing harmonic currents proportional to the harmonics of the distorted voltage. But what is the effect on the utility line of these harmonic currents? Might it not be better from a system-wide point of view to force each device on the line to draw a sine-wave current in phase with the fundamental of the line voltage? Such a scheme would require an internal sine reference locked to the fundamental of the voltage, and would be much more complicated than a circuit generating proportional input current.

Fortunately, it is easy to show that the simpler solution—proportional input current—is better for both the individual power converter and for the power line as a system. It is true that a distorted line voltage leads to harmonic currents in converters emulating resistive loads. However, these harmonic currents tend to *cancel* the very harmonic currents that cause the voltage distortion in the first place.

Consider the power system of Fig. 11.1(a). The utility line is represented by an ideal voltage source  $v_g$  producing a sine-wave voltage, in series with an impedance  $Z_g$ . The line, with voltage  $v_l$ , supports two loads. The first load draws a distorted current  $i_{dist}$ , producing distortion in the line voltage. The second load is an ac-dc power converter, drawing a current  $i_{pc}$  which is either a fixed sine wave or proportional to the line voltage. In the latter case the power converter appears to the line as a resistor of value  $R_{em}$ . At each harmonic frequency, the power source and its impedance can be replaced with a Norton equivalent circuit. The equivalent circuits for the  $k$ th harmonic ( $k > 1$ ) are shown in Figs. 11.1(b) and (c). A tilde ( $\sim$ ) denotes a phasor quantity and the  $k$  subscript emphasizes that these phasors are at  $k$  times the fundamental frequency.

At each harmonic frequency, the source impedance  $\tilde{Z}_{g,k}$  is assumed non-zero. Since  $\tilde{V}_{g,k}$  is zero for every  $k > 1$  (the voltage  $v_g$  is undistorted), the current source labeled  $\tilde{V}_{g,k}/\tilde{Z}_{g,k}$  is an open circuit. For the case where the power converter draws a pure sinusoid, shown in Fig. 11.1(b),  $\tilde{I}_{pc,k} = 0$  for  $k > 1$  and this current source is also an open circuit. The entire harmonic current of the distorting load,  $\tilde{I}_{dist,k}$  must pass through the impedance  $\tilde{Z}_{g,k}$  generating a harmonic voltage  $-\tilde{I}_{dist,k}\tilde{Z}_{g,k}$  in the line voltage.

If instead the power converter draws a current proportional to the line voltage, the equivalent circuit of Fig. 11.1(c) applies. Here the current source  $\tilde{V}_{g,k}/\tilde{Z}_{g,k}$  is still an open

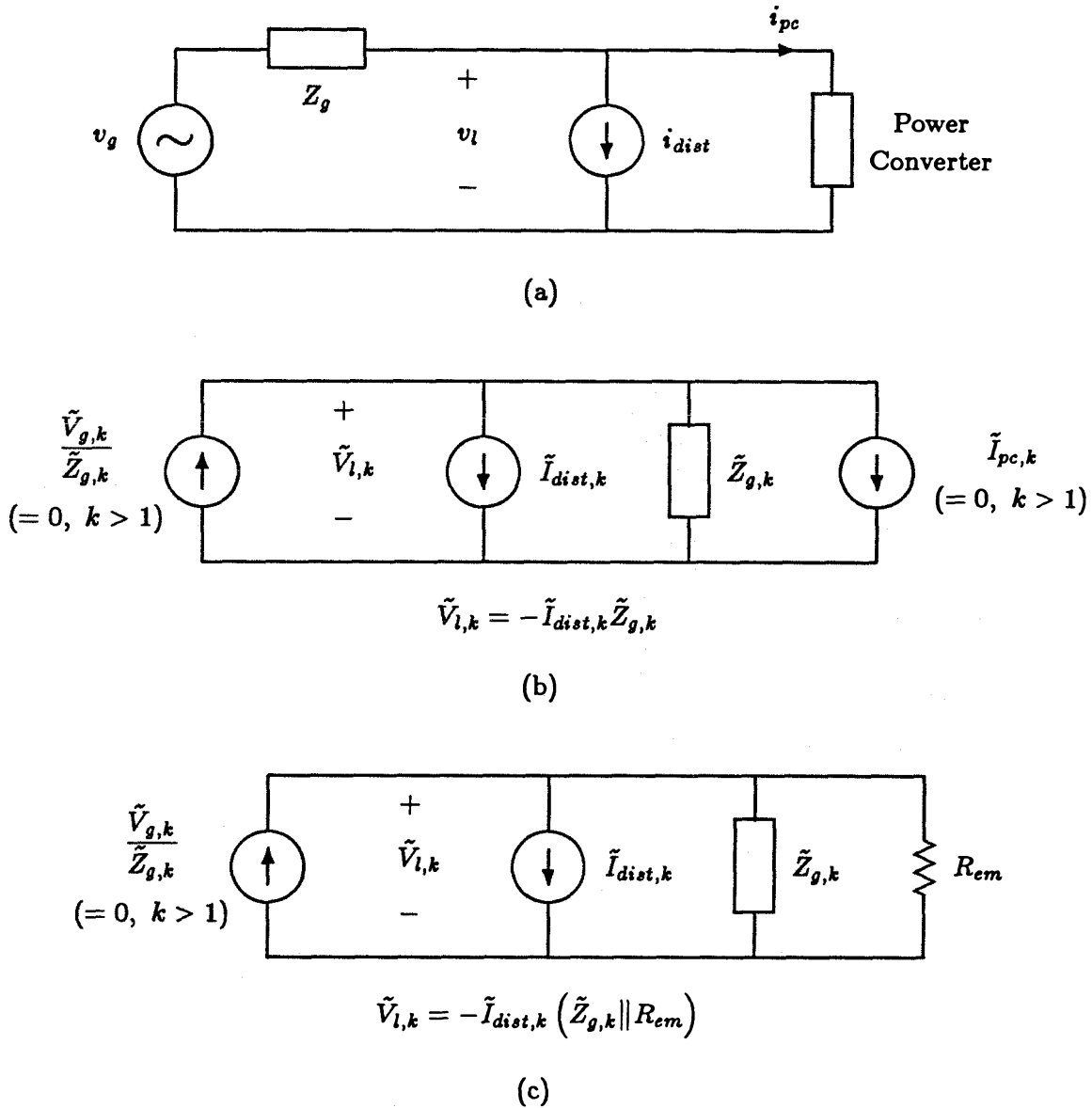


Figure 11.1: A power system including a source of distorted current and a power converter (a). Model of the system at the  $k$ th harmonic frequency when the power converter draws a sinusoidal current (b) and when the power converter emulates a resistor (c).

circuit, but the power converter now appears in the equivalent circuit as a resistor  $R_{em}$ . The harmonic current  $\tilde{I}_{dist,k}$  now flows in the parallel combination of  $R_{em}$  and  $\tilde{Z}_g$ . The magnitude of the impedance of this parallel combination is always less than that of  $\tilde{Z}_{g,k}$  alone (since  $R_{em}$  and the real part of  $\tilde{Z}_{g,k}$  are both positive). Hence the magnitude of the harmonic voltage produced by the distorted load is *less* when the power converter draws a proportional current.

Note that when the resistor-emulating power converter draws harmonic currents from the power line, it still achieves unity power factor, because the harmonic currents are directly proportional to harmonics of the distorted line voltage.

Usually the line impedance  $\tilde{Z}_{g,k}$  is small at frequencies of interest, dominating the parallel combination of  $\tilde{Z}_{g,k}$  and  $R_{em}$ . The effect of any single power converter in attenuating voltage distortion is therefore small. However, if many devices on the power line have proportional currents, their combined effect is that of a small  $R_{em}$  and the effect on the line may be significant. In effect, the distorted load draws its harmonic currents from the power converters instead of through the line impedance  $Z_g$ . The result is a reduction of harmonic voltage relative to the case where the power converters draw only fundamental current.

The important point is that drawing a proportional current from the power line is beneficial not only to the load, which achieves unity power factor, but also to the power line. Every device that emulates a resistor makes some contribution to removing distortion from the line voltage.



## Chapter 12

# Passive Current-Shaping Methods

Some circuits for improving input-current waveforms of ac-dc converters use only passive components—reactances and semiconductor rectifiers. These passive circuits—essentially filters—are valued for their simplicity and ruggedness. They avoid the relatively fragile semiconductor switches and complicated control circuits found in active current-shaping circuits.

Passive schemes have the drawback of excessive size and weight compared to equally effective active circuits. The passive circuits are incapable of providing regulation against load variations and are also sensitive to variations in the line frequency. Finally, most passive circuits provide only an approximation to a sine-wave input current, and the maximum achievable power factor is something less than unity.

In many applications, however, the attractions of simplicity and robustness outweigh these drawbacks. At very high power levels, for example, fast-switching with active devices is impractical. Thus when electric utilities transmit large amounts of power over dc links, passive filters are used to improve the waveforms on the ac side of dc-ac converters [24, Sec. 8.8]. Another application where passive filters have an advantage is in the rare instance of a high-frequency ac supply. In passive schemes, the reactances are sized in inverse proportion to the line frequency, while in active schemes the switching frequency must be some factor above the line frequency. For fixed performance, passive filters shrink as the line frequency increases, but active circuits have to switch much faster. At some point the passive filters will be favored. In the 20 kHz power distribution proposed for the space shuttle [25, pp. 300–303], for instance, any current-shaping for ac-dc power converters would likely be passive.

The inductor-input filter studied in Section 12.1 is probably the most common passive filter used. The filter is simple and relatively cheap. Its main drawbacks are a 0.90

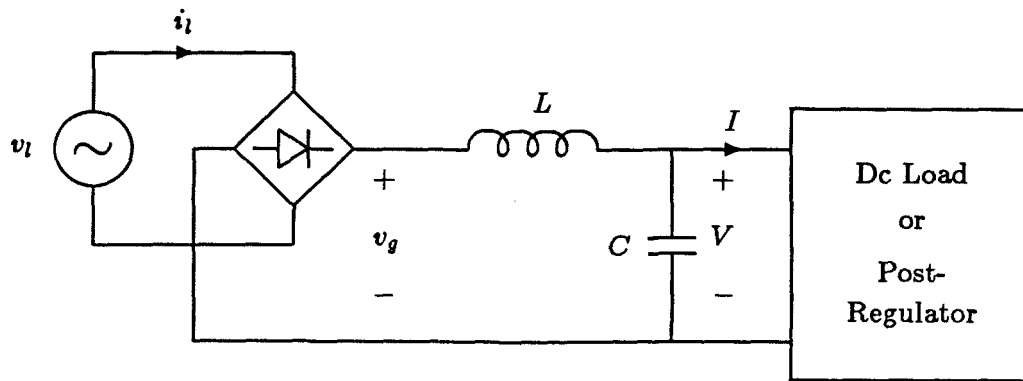


Figure 12.1: The inductor-input filter.

upper limit on power factor, and discontinuity of the input current for reasonably large power factor. The resonant-input filter of Section 12.2, which uses a single series-resonant circuit, is an alternative way to passively shape input current. Although heavy and expensive, it shows that unity power factor is possible using just a few passive components and no active devices. More often used as a voltage regulator, the ferroresonant transformer can also be considered as a passive current shaper. It too has a resonant circuit that encourages sinusoidal input current, as seen in Section 12.3. Finally, power factor can be improved by removing harmonic currents using tuned filters, a method considered in Section 12.4. A comparison shows that a set of tuned filters offers considerable size and weight savings over a resonant-input filter.

### 12.1 Inductor-Input Filter

A simple way to improve the input-current performance of a capacitor-input filter is to place an inductor in series with the output of the bridge rectifier, as shown in Fig. 12.1. This configuration is called the *inductor-input filter*. The inductor promotes continuity of the input current, broadening the short pulses drawn by the capacitor-input filter and increasing the power factor.

Several analyses of the inductor-input filter appear in the literature [26],[27]. The analysis presented here emphasizes simultaneous exposure of the effects of inductance  $L$ , line (radian) frequency  $\omega_l$  or line period  $T_l$ , and load  $R \equiv V/I$ . The dimensionless

parameter  $K_l$ , defined by

$$K_l \equiv \frac{\omega_l L}{\pi R} = \frac{2L}{RT_l} \quad (12.1)$$

serves this purpose well and supplants the normalized units of [26] and [27]. The “ $l$ ” subscript on  $K_l$  means that  $K_l$  involves the *line* frequency. The output voltage  $V$  of the inductor-input filter is assumed constant for purposes of analysis.

The filter operates in either the continuous conduction mode (CCM), in which the rectifier bridge always conducts, or in the discontinuous conduction mode (DCM) when the bridge is OFF during some portion of the line period. This is analogous to PWM dc-dc converters which have both continuous and discontinuous conduction modes. In fact, the parameter  $K_l$  of Eq.(12.1) is defined in exactly the same way as the parameter  $K_S \equiv 2L/RT_S$  found in dc-dc converter analysis. Where  $K_l$  is defined using the line period  $T_l$ ,  $K_S$  uses the switching period  $T_S$ . Both parameters are measures of the position of the operating points of their respective circuits relative to the CCM/DCM boundary.

### 12.1.1 Continuous Conduction Mode

In the continuous conduction mode, the bridge rectifier is always conducting, and the voltage  $v_g$  is a rectified sine wave with peak value  $V_l$ . Since the average voltage across the inductor must be zero, the output voltage is

$$V = \frac{2}{\pi} V_l, \quad (12.2)$$

where  $V_l$  is the *peak* value of the line voltage. Integration of the voltage across the inductor gives the shape of the inductor current  $i_g$ . The constant of integration is chosen to produce average current  $I$ , yielding

$$i_g(\theta) = \frac{V_l}{\omega_l L} \left[ 1 + 2K_l - \cos \theta - \frac{2\theta}{\pi} \right]. \quad (12.3)$$

The rms value of the line current is the same as the rms value of  $i_g$ ,

$$i_{g,rms} = \frac{2V_l}{\pi R} \sqrt{1 + \left( \frac{5}{24} - \frac{2}{\pi^2} \right) / K_l^2}, \quad (12.4)$$

found by integrating the square of Eq.(12.3). The power factor follows directly from Eqs.(12.2) through (12.4), and is a function *only* of  $K_l$ :

$$\text{PF} = \frac{2\sqrt{2}}{\pi} \frac{1}{\sqrt{1 + \left(\frac{5}{24} - \frac{2}{\pi^2}\right) / K_l^2}} \approx \frac{0.90}{\sqrt{1 + (0.075/K_l)^2}} . \quad (12.5)$$

The displacement factor,  $\cos \phi_1$ , is found by calculating the Fourier sine and cosine coefficients of the input current, the odd extension of Eq.(12.3) into the full line period, and is given by

$$\cos \phi_1 = \frac{1}{\sqrt{1 + \left(\frac{\pi}{8} - \frac{1}{\pi}\right)^2 / K_l^2}} \approx \frac{1}{\sqrt{1 + \left(\frac{0.074}{K_l}\right)^2}} . \quad (12.6)$$

The boundary of CCM, referred to as critical conduction, occurs when the current of Eq.(12.3) just reaches zero at some point during a cycle. Equation (12.3) can be differentiated to find that the minimum current occurs when

$$\theta = \sin^{-1} \left( \frac{2}{\pi} \right) \approx 40^\circ . \quad (12.7)$$

The value of  $K_l$  that makes the current exactly zero at this point is found to be

$$K_{l,\text{crit}} = \frac{1}{2} \left\{ \frac{2}{\pi} \sin^{-1} \left( \frac{2}{\pi} \right) + \cos \left[ \sin^{-1} \left( \frac{2}{\pi} \right) \right] - 1 \right\} \approx 0.1053 . \quad (12.8)$$

### 12.1.2 Discontinuous Conduction Mode

In the discontinuous conduction mode (DCM), the rectifier bridge is OFF during some fraction of each cycle. Analysis of this mode of operation is more difficult than for CCM. The power factor and its displacement-factor component cannot be written explicitly in terms of the parameter  $K_l$ , but they are nevertheless functions *only* of this parameter. Here, an implicit equation for the turn-ON and turn-OFF angles of the rectifier bridge is derived. The power factor, output voltage, and the parameter  $K_l$  are then expressed as explicit functions of these angles.

The analysis is divided into two cases, corresponding to the two inductor current waveforms of Fig. 12.2. In both cases, conduction of the bridge rectifiers begins when the input voltage rises to meet the output voltage. The angle  $\theta_1$  is defined as the value of  $\theta$  at this instant, giving the relation

$$\frac{V}{V_l} = \sin \theta_1 . \quad (12.9)$$



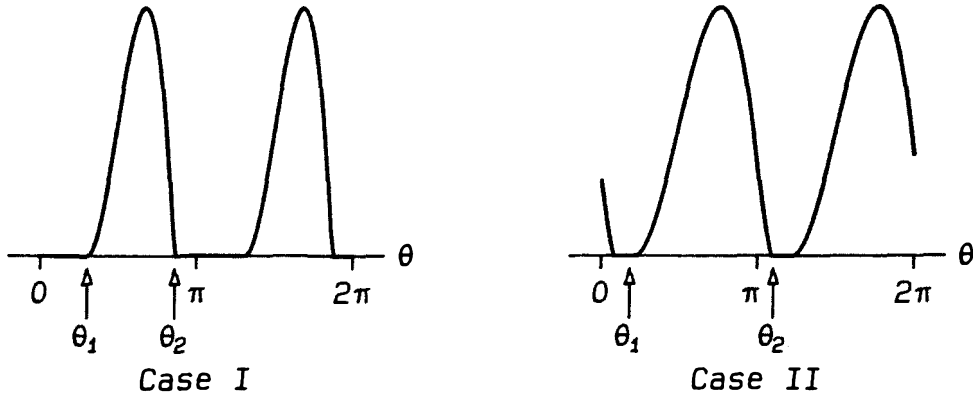


Figure 12.2: Inductor-current waveforms for the discontinuous mode of operation of the inductor-input filter.

The angle  $\theta_2$  is defined as the value of  $\theta$  at the instant the inductor current reaches zero. For case I of Fig. 12.2,  $\theta_2$  lies in the same half cycle of the line voltage as  $\theta_1$ , that is,  $\theta_2 < \pi$ . Case II occurs when the inductor current extends into the next half cycle, and  $\theta_2 > \pi$ .

The inductor current for case I is given over the interval  $\theta_1 < \theta < \theta_2$  by

$$i_g(\theta) = \frac{V_l}{\omega_l L} [\cos \theta_1 - \cos \theta - (\theta - \theta_1) \sin \theta_1] . \quad (12.10)$$

The cut-off angle  $\theta_2$  is found by solving

$$\cos \theta_1 - \cos \theta_2 - (\theta_2 - \theta_1) \sin \theta_1 = 0 . \quad (12.11)$$

This transcendental equation must be solved before  $K_l$  or the power factor can be found. Once  $\theta_2$  is known, however, the average and rms inductor currents can be calculated, along with the output voltage and  $K_l$ :

$$K_l = \frac{1}{\pi^2 \sin \theta_1} \left\{ \sin \theta_1 \left[ 1 - \frac{1}{2} (\theta_2 - \theta_1)^2 \right] - \sin \theta_2 + (\theta_2 - \theta_1) \cos \theta_1 \right\} \quad (12.12)$$

$$i_{g, \text{avg}} = \frac{V_l}{\omega_l L} \pi K_l \sin \theta_1 \quad (12.13)$$

$$i_{g, \text{rms}}^2 = \left( \frac{V_l}{\omega_l L} \right)^2 \frac{1}{\pi} \left\{ \frac{1}{3 \sin \theta_1} \left( [(\theta_2 - \theta_1) \sin \theta_1 - \cos \theta_1]^3 + \cos^3 \theta_1 \right) \right. \\ \left. + \frac{1}{2} (\theta_2 - \theta_1) + \frac{1}{4} \sin 2\theta_2 + 2(\theta_2 - \theta_1) \sin \theta_1 \sin \theta_2 \right. \\ \left. - \frac{1}{2} \sin \theta_1 \cos \theta_2 - 2 \sin(\theta_2 - \theta_1) \right\} \quad (12.14)$$

$$\frac{V}{V_l} = \frac{\cos \theta_1 - \cos \theta_2}{(\theta_2 - \theta_1)} . \quad (12.15)$$

The power factor is given by

$$\text{PF} = \frac{\sqrt{2} i_{g,\text{avg}} \sin \theta_1}{i_{g,\text{rms}}} \quad (12.16)$$

and the displacement factor by

$$\cos \phi_1 = \frac{b_1}{\sqrt{a_1^2 + b_1^2}} , \quad (12.17)$$

where the Fourier coefficients of the fundamental,  $a_1$  and  $b_1$  are given by

$$a_1 = \frac{2}{\pi} \left[ \sin(\theta_2 - \theta_1) - (\theta_2 - \theta_1) \left( \frac{1}{2} + \sin \theta_1 \sin \theta_2 \right) - \frac{1}{4} (\sin 2\theta_2 - \sin 2\theta_1) \right] \quad (12.18)$$

$$b_1 = \frac{2}{\pi} \left[ (\theta_2 - \theta_1) \sin \theta_1 \cos \theta_2 - \cos(\theta_2 - \theta_1) + 1 + \frac{1}{2} (\cos^2 \theta_2 - \cos^2 \theta_1) \right] . \quad (12.19)$$

The boundary between cases I and II occurs when  $\theta_2 = \pi$ . The value of  $\theta_1$  corresponding to this from Eq.(12.11) is approximately 0.8105 radians, about 46 degrees. The conduction parameter  $K_l$  is approximately 0.051 at this boundary. The boundary between cases I and II also marks the change between continuous and discontinuous line current. For  $K_l > 0.051$ , the line current is discontinuous.

For case II, analysis proceeds just as in case I except that for  $\theta > \pi$  the voltage from the bridge is  $-V_l \sin \theta$ , to account for the rectification of the line voltage. The inductor current now follows Eq.(12.10) for  $\theta_1 < \theta < \pi$ , but for  $\pi < \theta < \theta_2$ ,

$$i_g(\theta) = \frac{V_l}{\omega_l L} \left[ (2 + \cos \theta_1 + \theta_1 \sin \theta_1) + \cos \theta - \theta \sin \theta_1 \right] . \quad (12.20)$$

The cut-off angle  $\theta_2$  solves

$$\cos \theta_1 + \theta_1 \sin \theta_1 + \cos \theta_2 - \theta_2 \sin \theta_1 + 2 = 0 . \quad (12.21)$$

The average inductor current is still given by Eq.(12.13), but the conduction parameter, rms inductor current, and conversion ratio for case II are given by

$$K_l = \frac{1}{\pi^2 \sin \theta_1} \left\{ \sin \theta_1 \left[ 1 - \frac{1}{2} (\theta_2 - \theta_1)^2 \right] + 2(\theta_2 - \pi) + (\theta_2 - \theta_1) \cos \theta_1 + \sin \theta_2 \right\} \quad (12.22)$$

$$\begin{aligned}
i_{g,rms}^2 = & \left( \frac{V_l}{\omega_l L} \right)^2 \frac{1}{\pi} \left\{ \frac{1}{3 \sin \theta_1} \left( [(\theta_2 - \theta_1) \sin \theta_1 - \cos \theta_1]^3 + \cos^3 \theta_1 \right) \right. \\
& + (\theta_2 - \theta_1) \left( \frac{1}{2} - 2 \sin \theta_1 \sin \theta_2 \right) + 2 \sin(\theta_2 - \theta_1) \\
& + 4(\sin \theta_2 - \sin \theta_1) + \frac{1}{4}(\sin 2\theta_1 - \sin \theta_1) \\
& \left. + 4(\theta_2 - \pi) \left( 1 + \cos \theta_1 + \theta_1 \sin \theta_1 - \frac{1}{2}(\theta_2 + \pi) \sin \theta_1 \right) \right\} \quad (12.23)
\end{aligned}$$

$$\frac{V}{V_l} = \frac{1}{(\theta_2 - \theta_1)} (2 + \cos \theta_1 + \cos \theta_2) . \quad (12.24)$$

The power factor for case II is evaluated with Eqs.(12.16) and (12.13), using the expressions Eqs.(12.22) and (12.23) for  $K_l$  and  $i_{g,rms}$ , respectively. The displacement factor for case II is found from Eq.(12.17) with the following expressions for the Fourier coefficients:

$$\begin{aligned}
a_1 = & \frac{2}{\pi} \left\{ -\sin(\theta_2 - \theta_1) - \frac{1}{4}(\sin 2\theta_2 - \sin 2\theta_1) + \frac{1}{2}(\theta_1 - \theta_2) \right. \\
& \left. + (\theta_2 - \theta_1) \sin \theta_1 \sin \theta_2 - 2 \sin \theta_2 + 2 \sin \theta_1 \right\} \quad (12.25)
\end{aligned}$$

$$\begin{aligned}
b_1 = & \frac{2}{\pi} \left\{ -(\theta_2 - \theta_1) \sin \theta_1 \cos \theta_2 + 2 \cos \theta_1 + 2 \cos \theta_2 \right. \\
& \left. + \cos(\theta_2 - \theta_1) + \frac{1}{4}(\cos 2\theta_2 - \cos 2\theta_1) + 3 - 2(\pi - \theta_1) \sin \theta_1 \right\} . \quad (12.26)
\end{aligned}$$

The above expressions are unwieldy, and a plot of the results in the following section will convey much more information. One point to note in the expressions for conversion ratio and power factor is that these quantities may be considered functions *only* of the conduction parameter  $K_l$ . From Eqs.(12.11) and (12.21), the angle  $\theta_2$  is a function only of  $\theta_1$ . Since Eqs.(12.12) and (12.22) are one-to-one,  $\theta_1$  and  $\theta_2$  may be considered functions of  $K_l$  alone. The conversion ratio, the power factor, and the displacement factor, all expressed here as functions of  $\theta_1$  and  $\theta_2$ , are therefore functions of  $K_l$  alone.

### 12.1.3 Interpretation

Because power factor and its displacement factor component are functions of  $K_l$  alone in both CCM and DCM, a single plot is sufficient to show the effect of all operating conditions. In Fig. 12.3, the power factor and displacement factor are plotted versus  $K_l$  on a log scale. The conduction parameter  $K_l$ , it will be recalled, is the ratio  $\omega_l L / \pi R$ .

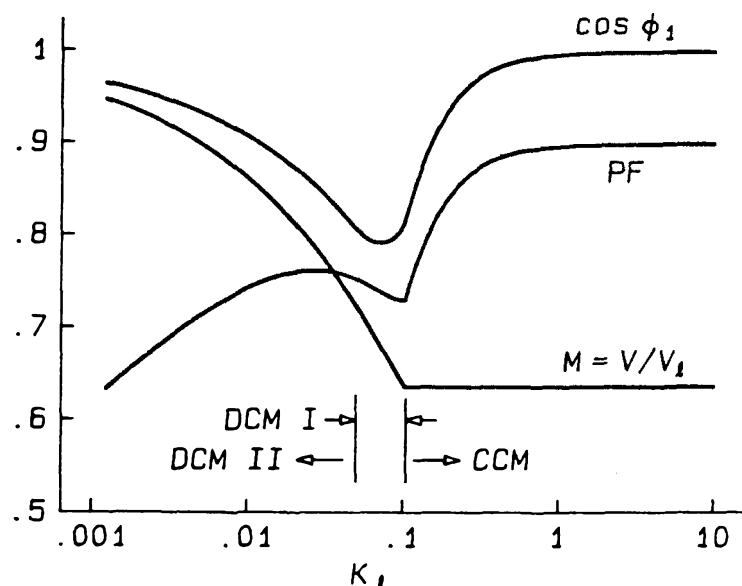


Figure 12.3: Power factor, displacement factor  $\cos \phi_1$ , and conversion ratio  $M \equiv V/V_l$  for the inductor-input filter.

The plot of Fig. 12.3 therefore includes the effects of line frequency, filter inductance, and effective load resistance.

The conversion ratio  $V/V_l$  is also included in the plot of Fig. 12.3. In CCM the conversion ratio is constant at the value  $2/\pi$ . As  $K_l$  is reduced and the filter enters DCM, the conversion ratio rises. In the limit  $K_l \rightarrow 0$ , the output voltage equals the peak value of the input sine wave and the conversion ratio is unity.

Maximum power factor with the inductor-input filter is 0.90, achieved as  $K_l \rightarrow \infty$ . As  $K_l$  is reduced, the power factor falls to a value of only 0.732 at the critical point. As  $K_l$  falls below  $K_{l,crit}$ , the power factor initially increases, a somewhat surprising result. If  $K_l$  declines still further, the power factor decreases monotonically.

The curious behavior of the power factor is explained by the waveforms of Fig. 12.4 and the displacement factor curve of Fig. 12.3. Figure 12.4 shows the waveshape of the line current (“unfolded” inductor current) as  $K_l$  varies. For large  $K_l$ , as in Fig. 12.4(a), the line current is nearly a square wave. The fundamental component is in phase with the line voltage; distortion alone limits the power factor to 0.90. As  $K_l$  falls, some ripple appears across the previously flat tops of the square wave, as shown in Fig. 12.4(b), and the fundamental lags slightly.

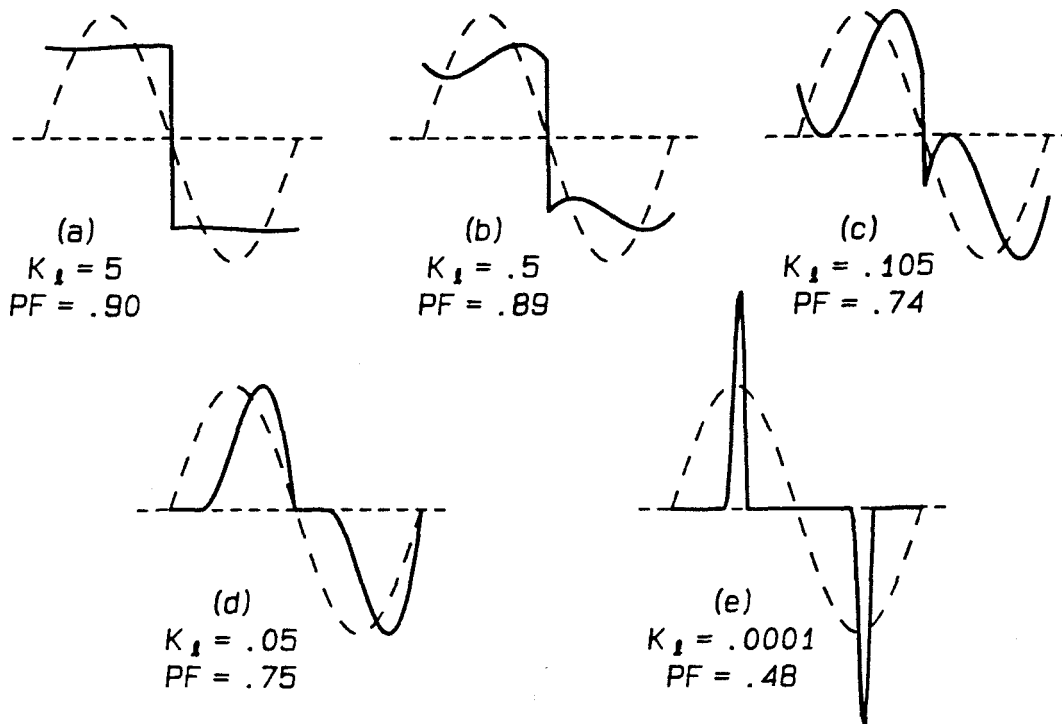


Figure 12.4: Line-current waveforms (solid curves) for the inductor-input filter as  $K_L$  changes. The dashed curves represent the line voltage.

Note the discontinuities in the line current in Fig. 12.4(a) through Fig. 12.4(c). “Continuous conduction” of the inductor-input filter means only that the bridge rectifier is always conducting. The line current is actually discontinuous (in the sense that it has vertical jumps) all through CCM and into part of DCM. Only when the circuit enters case II of DCM does the line current become continuous.

Critical conduction is illustrated in Fig. 12.4(c). From Eq.(12.7), the input current touches zero when  $\theta \approx 40^\circ$ . Since the current is *not* zero when the rectifier bridge switches, at  $\theta = 0$  and  $\theta = \pi$ , the line current is discontinuous. The distortion is small, but phase displacement of the fundamental keeps the power factor relatively low. As  $K_L$  falls to its critical value, shown in Fig. 12.4(d), the distortion of the current increases, but at the same time the displacement factor decreases. The combined effect is an increase in power factor.

Eventually, for very small  $K_L$ , the line current becomes a narrow, nearly centered spike, as in Fig. 12.4(e). The fundamental is almost in phase in this case, and the low

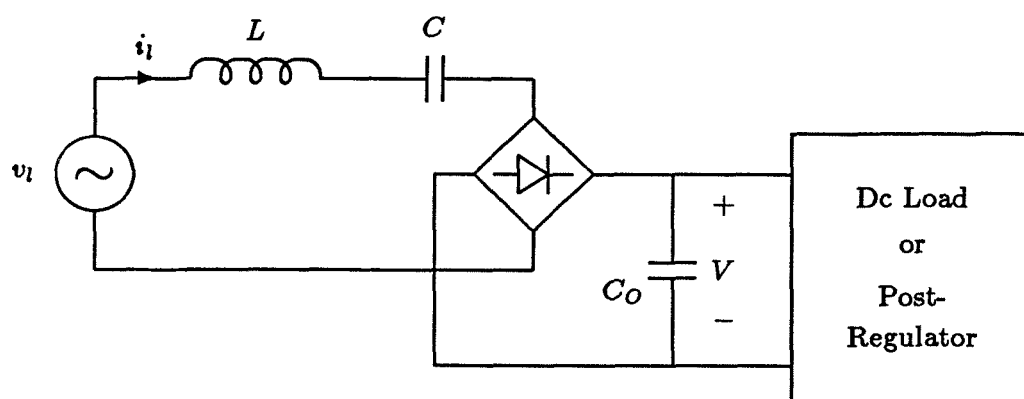


Figure 12.5: The resonant-input filter.

power factor is a result of distortion alone.

The inductor-input filter offers the advantages of passivity, simplicity, and ruggedness. Undesirable aspects of the filter as an input-current shaping method are the large, heavy inductor, the lack of output-voltage regulation, the fact that power factor varies with the load, the discontinuity of the input current, and the 0.90 upper limit on power factor.

## 12.2 Resonant-Input Filter

In the inductor-input filter, an inductance is added to the circuit of the capacitor-input filter with the intent of extending the narrow current pulses and thereby improving power factor. In a similar manner, one can add a series-resonant circuit to a capacitor-input filter with the idea of allowing only line-frequency sinusoidal currents to flow. The resulting circuit, called the resonant-input filter (by analogy with the inductor-input filter), is shown in Fig. 12.5. The qualitative operation of this filter is easy to understand when one considers that if the  $Q$  and characteristic resistance  $R_0$  of the series-resonant circuit are both high enough, then only currents at the “notch” frequency can get through to the line, and the power factor will be near unity.

The following analysis of the resonant-input filter uses the same assumptions as in the previous section, namely that the output voltage is pure dc and that all the components are ideal. It is also assumed that the series-resonant filter is tuned to the line frequency.

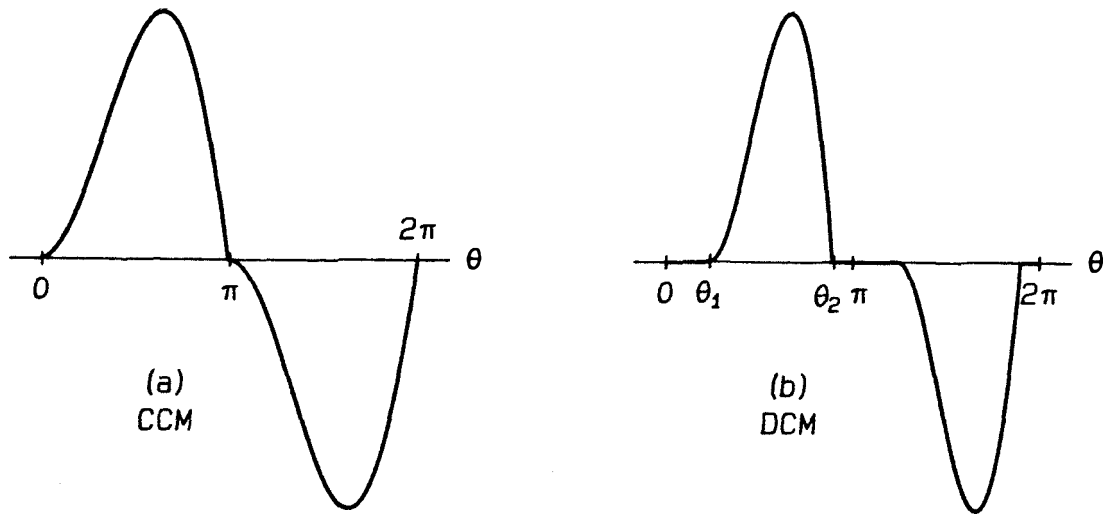


Figure 12.6: Typical line-current waveforms of the resonant-input filter in continuous conduction mode (a) and discontinuous conduction mode (b).

As with the inductor-input filter, the power factor and conversion ratio are functions of the single parameter

$$K_l \equiv \frac{\omega_l L}{\pi R}. \quad (12.27)$$

The inductance  $L$  is the resonant inductance in this case, and  $R$  is the ratio  $V/I$ , the effective dc load seen by the filter. Since the resonant frequency and line frequency are the same, the conduction parameter  $K_l$  is also given by

$$K_l = \frac{R_0}{\pi R}, \quad (12.28)$$

where

$$R_0 \equiv \sqrt{\frac{L}{C}}. \quad (12.29)$$

The resonant-input filter has both continuous and discontinuous conduction modes, the latter occurring when the rectifier bridge is open for some fraction of a cycle. In contrast to the inductor-input filter, however, the series inductance of the series-resonant filter ensures that the line current is *always* continuous. Fig. 12.6 shows typical line-current waveforms for CCM and for DCM.

### 12.2.1 Continuous Conduction Mode

When the diode bridge conducts continuously, it applies a square-wave voltage of magnitude  $V$  to one side of the series-resonant circuit. The other end of the resonant circuit is subject to the line voltage,  $V_l \sin \theta$ . Since the resonant circuit is assumed to have no losses, it cannot be driven at its resonant frequency. The fundamental components of the line voltage and the square wave from the bridge must cancel in magnitude and phase to ensure finite currents in the resonant circuit.

With this restriction, the output voltage must be

$$V = \frac{\pi}{4} V_l . \quad (12.30)$$

The input current and its average and rms values are given by

$$i_g(\theta) = \frac{V_l}{2R_0} \left[ \theta \sin \theta + \frac{\pi}{2} \left( \frac{\pi^2}{2} K_l - 1 \right) \sin \theta \right] \quad (12.31)$$

$$I = i_{g,\text{avg}} = \left( \frac{V_l}{2R_0} \right) \frac{\pi^2}{2} K_l \quad (12.32)$$

$$i_{g,\text{rms}} = \left( \frac{V_l}{2R_0} \right) \frac{\pi^3}{4\sqrt{2}} \sqrt{K_l^2 + \frac{4}{3\pi^4} - \frac{8}{\pi^6}} . \quad (12.33)$$

The power factor in CCM is found from the simple expression

$$\text{PF} = \frac{K_l}{\sqrt{K_l^2 + \frac{4}{3\pi^4} - \frac{8}{\pi^6}}} \approx \frac{1}{\sqrt{1 + (0.073/K_l)^2}} . \quad (12.34)$$

The boundary between CCM and DCM occurs when  $K_l$  reaches the critical value  $K_{l,\text{crit}} = 2/\pi^2 \approx 0.20$ .

### 12.2.2 Discontinuous Conduction Mode

In DCM,  $\theta_1$  is defined as the angle at which the rectifier bridge turns ON and current begins to flow, as shown in Fig. 12.6. The time at which the bridge turns OFF again defines  $\theta_2$ . Between  $\theta_1$  and  $\theta_2$ , the line current obeys

$$i_g(\theta) = \frac{V_l}{2R_0} \left[ (\theta - \theta_1) \sin \theta - \sin \theta_1 \sin(\theta - \theta_1) \right] . \quad (12.35)$$

The cut-out angle  $\theta_2$  must be found by solving the expression

$$(\theta_2 - \theta_1) \sin \theta_2 - \sin \theta_1 \sin(\theta_2 - \theta_1) = 0 . \quad (12.36)$$



Once  $\theta_1$  and  $\theta_2$  are known, the rest of the circuit waveforms can be calculated.

To simplify the following expressions, define the three functions

$$f(\theta_1, \theta_2) \equiv [\cos(\theta_2 - \theta_1) + 2] \sin \theta_1 + \sin \theta_2 - (\theta_2 - \theta_1) \cos \theta_2 \quad (12.37)$$

$$g(\theta_1, \theta_2) \equiv [\cos(\theta_2 - \theta_1) - 2] \sin \theta_1 + \sin \theta_2 - (\theta_2 - \theta_1) \cos \theta_2 \quad (12.38)$$

$$\begin{aligned} h(\theta_1, \theta_2) \equiv & \frac{2}{3}(\theta_2 - \theta_1)^3 - (\theta_2 - \theta_1)^2 [\sin 2\theta_1 + \sin 2\theta_2] \\ & + (\theta_2 - \theta_1) [1 + \cos 2(\theta_2 - \theta_1) - \cos 2\theta_1 - 2 \cos 2\theta_2] \\ & - (\theta_2 - \theta_1)^2 \sin 2\theta_2 - \sin 2\theta_1 - \left[1 - \frac{1}{2} \cos 2\theta_1\right] \sin 2(\theta_2 - \theta_1). \end{aligned} \quad (12.39)$$

In terms of these functions, the average and rms line currents and the conversion ratio are given by

$$I = \frac{V_l}{2R_0} \frac{g(\theta_1, \theta_2)}{\pi} \quad (12.40)$$

$$i_{l,\text{rms}}^2 = \left(\frac{V_l}{2R_0}\right)^2 \frac{1}{4\pi} h(\theta_1, \theta_2) \quad (12.41)$$

$$\frac{V}{V_l} = \frac{1}{4} f(\theta_1, \theta_2). \quad (12.42)$$

The conduction parameter is given by

$$K_l = \frac{2}{\pi^2} \frac{g(\theta_1, \theta_2)}{f(\theta_1, \theta_2)} \quad (12.43)$$

and the power factor is

$$\text{PF} = \frac{f(\theta_1, \theta_2)g(\theta_1, \theta_2)}{\sqrt{2\pi h(\theta_1, \theta_2)}}. \quad (12.44)$$

### 12.2.3 Interpretation

As with the inductor-input filter, the conduction parameter is a one-to-one function of  $\theta_1$ , so that the conversion ratio and power factor may be considered functions only of  $K_l$ . Figure 12.7 plots these quantities versus the log of  $K_l$ . The curve is similar to that of Fig. 12.3 for the inductor-input filter, but in this case the power factor is higher, 0.94 at critical conduction and approaching unity for large  $K_l$ . The power factor also increases monotonically with  $K_l$ .

Figure 12.8 shows the line-current waveforms for several values of  $K_l$ . When  $K_l$  is large, as in Fig. 12.8(a), the line current is nearly sinusoidal and the power factor is near

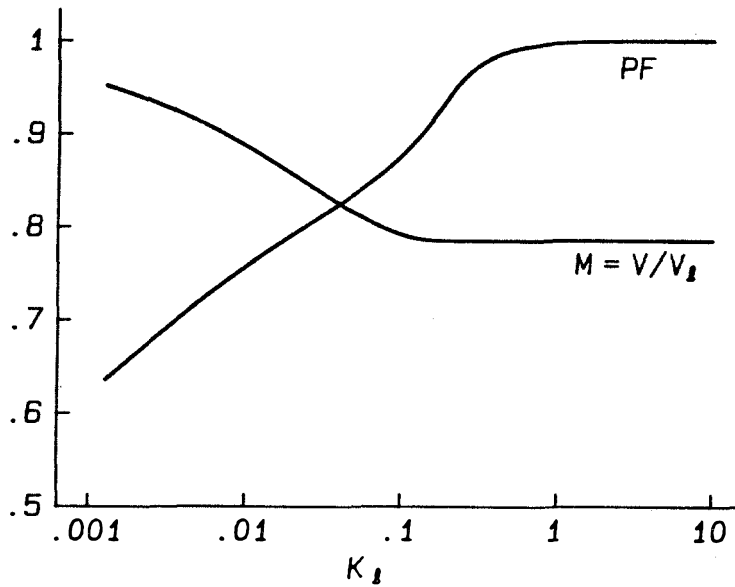


Figure 12.7: Power factor and conversion ratio of the resonant-input filter.

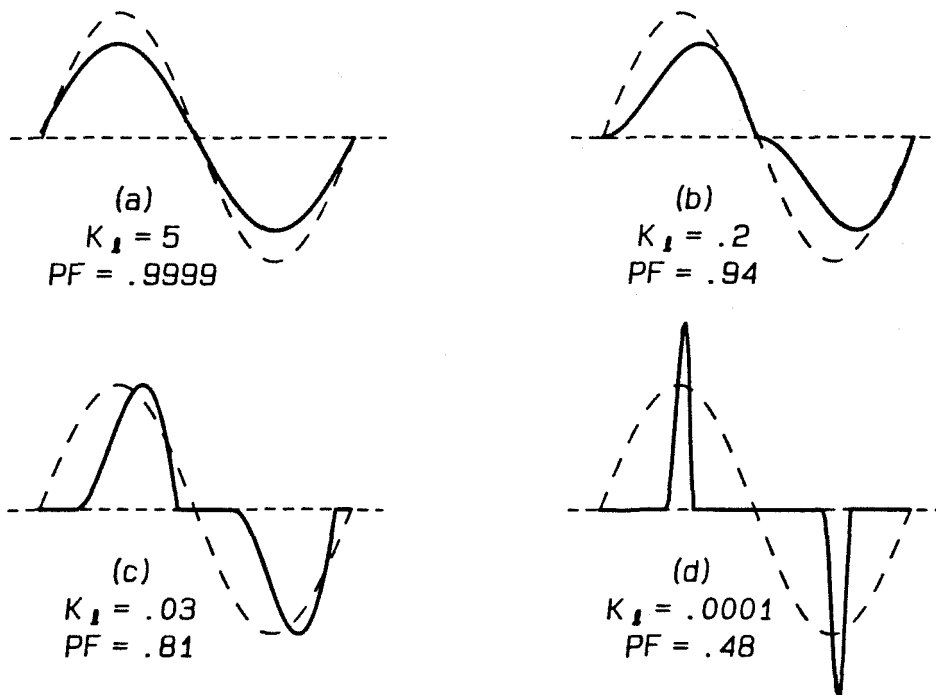


Figure 12.8: Line-current waveforms (solid curves) for the resonant-input filter as  $K_s$  changes. The dashed curves represent the line voltage.

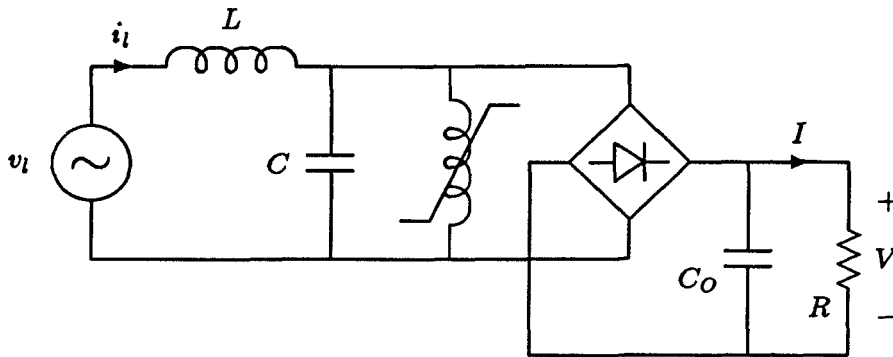


Figure 12.9: Equivalent circuit of a ferroresonant transformer.

unity. For instance, if  $K_l > 1$  then the power factor is greater than 0.997. Figure 12.8(b) illustrates the critical value of  $K_l$ , the boundary between CCM and DCM. Even at this boundary, the power factor is still a high 0.94. As  $K_l$  is further reduced, as in Fig. 12.8(c), the power factor falls. At very low values of  $K_l$ , as in Fig. 12.8(d), the filter draws the narrow pulses characteristic of the capacitor-input filter or of the inductor-input filter with low  $K_l$ .

The major disadvantages of the resonant-input filter are the large size of the reactive elements and the large rms current in both the capacitors. The circuit is useful mainly as a demonstration that passive circuits with very few components can achieve essentially unity power factor.

### 12.3 Ferroresonant Transformer

The ferroresonant transformer, or “ferro,” is a device usually regarded as a line-voltage regulator, rather than as a means of shaping input current. Because the ferro uses a high- $Q$  resonant circuit, much like the resonant-input filter, it draws a line current that closely approximates a sine wave under proper conditions.

An equivalent circuit of a simple ferroresonant transformer, supplying a dc load, is shown in Fig. 12.9 [28, pp. 319–322]. The circuit contains a series L-C resonant circuit, parallel-loaded with a saturating transformer, a rectifier bridge and the dc load. The transformer core saturates when the volt-seconds exceeds a certain fixed value.

With  $\int v dt$  thus fixed over each half cycle and the operating period fixed by the line frequency, the average rectified voltage at the transformer secondary is also fixed. The ferro therefore regulates the output voltage against changes in the line-voltage amplitude and waveshape.

The resonant L-C circuit gives the ferro a second-order forward voltage gain with a large resonant peak, on the assumption that the saturating transformer and load present an impedance much larger than the characteristic resistance of the resonant circuit. This low-pass characteristic lets the ferro reject noise and spikes from the power line. The *reverse-current* transfer function, the gain with which currents generated by the saturating transformer and the load reach the line, is the same as the *forward-voltage* transfer function. Harmonic currents generated by the saturating core and load are therefore attenuated at a rate of -40 dB per decade of frequency before reaching the line.

The advantages of the ferroresonant transformer as a current-shaping method include:

- simplicity and exceptional ruggedness
- rejection of line-generated noise and spikes, and good regulation against line-voltage fluctuations
- built-in isolation.

The drawbacks of the ferro are:

- sensitivity of the dc output voltage to frequency and load variations
- losses and interference generated by the saturating transformer
- large size and weight, as one would expect of any line-frequency transformer.

It is unlikely that the ferro would be used specifically as a means of shaping input current. When chosen as a means of regulating against line-voltage spikes and variations, however, the ferro provides significant improvement in current waveshape and power factor over a capacitor-input filter.

## 12.4 Tuned Filters

When the input-current waveform drawn by an ac-dc power converter suffers from distortion, the line current can be “cleaned up” and the power factor improved by removing the harmonic currents with tuned resonant filters. These filters can be parallel-resonant filters in series with the line, or series-resonant traps shunting the line. Shunt traps are preferred for the reason that they carry only the harmonic current, whereas a series filter must carry the entire fundamental current.

On the other hand, shunt traps add some risk to a system. If these traps are placed across the power line, they will absorb currents not only from the intended source of harmonic current, but also from any other device generating distortion on the line. Moreover, if the line voltage itself is distorted, it will drive these filters at resonance. Both effects are dangerous to shunt filters, which may fail as a result of excessive currents. In addition, tuned filters—whether series or shunt—can lead to stability problems in a power system. The undamped resonances of the filters are easily excited, and the resulting ringing decays slowly as a result of the high  $Q$ .

Shunt harmonic traps are an economical way of removing harmonic currents, however, especially at high power levels. In fact, such filters are used in the ac-dc conversion process for transmission of hundreds of megawatts at very high dc voltages [24, Sec. 8.8].

### 12.4.1 Size of Tuned Filters

Although shunt filters are more common, the size of series filters is considered here to provide a direct comparison with the resonant-input filter. A line with shunt filters is simply the dual of the series case, but the load is considered as a source of harmonic current instead of voltage, as in the resonant-input filter.

Consider the situation shown in Fig. 12.10. A series of tuned filters have been added to a capacitor-input filter. The  $k$ th filter, with inductance  $L_k$ , capacitance  $C_k$ , and quality factor  $Q_k$ , is tuned to the  $k$ th harmonic, that is,  $k\omega_l$  (radian frequency). On the assumption that the filters yield a near-unity power factor, the input current is a line-frequency sine wave and the bridge rectifier conducts continuously. The voltage

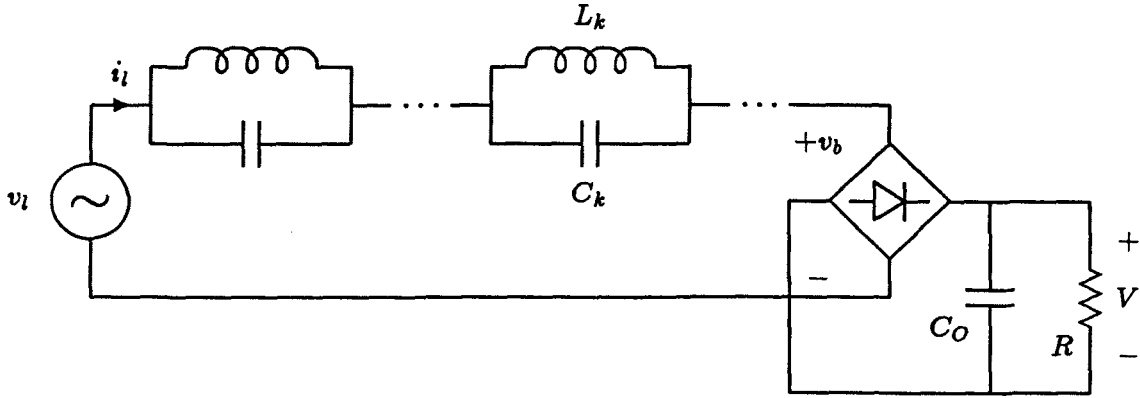


Figure 12.10: Tuned filters added to a capacitor-input filter to prevent current harmonics in the line.

waveform  $v_b$  at the rectifier input is therefore a square wave, with Fourier expansion

$$v_b = \frac{4V}{\pi} \sum_{k=1,3,\dots}^{\infty} \sin k\theta. \quad (12.45)$$

The line voltage is the fundamental sine wave  $V_l \sin \theta$ . Under the assumption that the line-frequency impedance of the series filters is negligible, the line-frequency voltage across the filters must be zero and the fundamental component of  $v_b$  must cancel the line voltage. This yields the conversion ratio

$$\frac{V}{V_l} = \frac{4}{\pi}. \quad (12.46)$$

The magnitude of the impedance  $Z_k$  of the  $k$ th tuned filter at the  $k$ th harmonic frequency,  $k\omega_l$ , is approximately

$$\|Z_k(jk\omega_l)\| = \frac{Q_k R_{0k}}{\sqrt{1 + 4\delta_k^2 Q_k^2}}, \quad (12.47)$$

where  $R_{0k}$  is the characteristic resistance of the filter,  $R_{0k} \equiv \sqrt{L_k/C_k}$ , and  $\delta_k$  is the *detuning* [24, pp. 355–356]. The detuning is an equivalent relative frequency variation accounting for deviations of the element values and line frequency from the required resonant frequency. Obtained by linearization of the filter's impedance curve near the resonant peak, the detuning is related to the variation in line (radian) frequency  $\Delta\omega_l$ , and the tolerances of the inductance and capacitance,  $\Delta L_k$  and  $\Delta C_k$ , by

$$\delta_k = \frac{\Delta\omega_l}{\omega_l} + \frac{\Delta L_k}{2L_k} + \frac{\Delta C_k}{2C_k}. \quad (12.48)$$

The magnitude  $I_k$  of the  $k$ th harmonic of the line current is found by dividing the harmonic voltage of  $v_b$  by the impedance of the  $k$ th filter at resonance, accounting for detuning. It is assumed that all filters except the  $k$ th have negligible impedance at the  $k$ th harmonic. Define the ripple ratio  $\mathcal{R}_k$  as

$$\mathcal{R}_k \equiv \frac{I_k}{I_1}, \quad (12.49)$$

the ratio of the  $k$ th harmonic current to the fundamental line current.

The size of the filter elements, in terms of their stored energy, can now be determined. Since every filter has a resonant frequency above the line frequency, a useful approximation is that all the fundamental current flows in the inductor of each filter, while the capacitor supports the harmonic voltage. With this approximation, the peak energy stored in each element is

$$U_{Lk} = \frac{P}{k^2\omega_l} \left(\frac{4}{\pi}\right)^2 \frac{1}{\mathcal{X}_k} \quad (12.50)$$

$$U_{Ck} = \frac{P}{k^2\omega_l} \left(\frac{4}{\pi}\right)^2 \mathcal{X}_k, \quad (12.51)$$

with the factor  $\mathcal{X}_k$  defined by

$$\mathcal{X}_k \equiv \frac{Q_k \mathcal{R}_k}{\sqrt{1 + 4\delta_k^2 Q_k^2}}. \quad (12.52)$$

The stored energy is directly proportional to the power  $P$ , and is inversely proportional to the line frequency  $\omega_l$ . The factor  $\mathcal{X}_k$  appears in the denominator of  $U_{Lk}$  and in the numerator of  $U_{Ck}$ . If the sum of the stored energies can be considered a measure of the overall size of the filter, then setting  $\mathcal{X}_k$  to unity yields the minimum size, corresponding to an energy sum of about 3.2 times  $P/\omega_l$ .

Equation (12.52) contains useful information about the factors constraining filter design. Ideally, the filter will have small ripple ratio  $\mathcal{R}_k$ , for good filtering. The filter  $Q$  should not be extremely large, because high  $Q$ 's are difficult and expensive to obtain. The factor  $\mathcal{X}_k$  contains the product of  $Q_k$  and  $\mathcal{R}_k$ , however. If  $\mathcal{X}_k$  should be near unity, then  $Q_k$  and  $\mathcal{R}_k$  cannot both be small. In other words, if a low  $\mathcal{R}_k$  is needed, then  $Q_k$  must be large. High values of  $Q_k$  aggravate the effects of detuning, however. If  $Q_k$  is large, then  $\delta_k$  must be very small to prevent the factor  $\sqrt{1 + 4\delta_k^2 Q_k^2}$  from reducing  $\mathcal{X}_k$ .

To maintain a small ripple ratio  $\mathcal{R}$  with reasonable stored energy therefore requires a high-Q filter with small detuning.

#### 12.4.2 Size Comparison with Resonant-Input Filter

For comparison, consider the stored energy of the elements in the resonant-input filter of Section 12.2. On the assumption that the filter is achieving near-unity power factor, the stored energies in the resonant inductor and capacitor are

$$U_L = U_C = \frac{P}{\omega_l} \frac{\pi^3}{8} K_l . \quad (12.53)$$

With the resonant-input filter, power factor and stored energy are both functions of  $K_l$ . Obtaining a higher power factor requires a larger filter, according to Eqs.(12.34) and (12.53). With the series filters discussed in Section 12.4.1, power factor is a function of how many filters are used, and hence how many harmonic currents are removed. Table 12.1 compares the sum of the peak energies for the resonant-input filter and a set of tuned filters under the following assumptions:

- each tuned filter completely removes its appropriate harmonic current
- each tuned filter has the same quality factor  $Q_k$  and ripple ratio  $\mathcal{R}_k$
- each tuned filter has  $\lambda_k = 1$
- the resonant-input filter line current is nearly sinusoidal

For each value of power factor at the left of Table 12.1, the highest harmonic that must be removed by tuned filters is shown, along with the total stored energy in the filters. For comparison, the value of  $K_l$  needed to obtain the same power factor with a resonant-input filter appears along with the resulting stored energy.

Although the resonant-input filter is much simpler than the tuned filters and requires only two resonant components, these two components must support far more stored energy than a set of tuned filters. A set of tuned filters providing the same power factor as a resonant-input filter is much smaller and less massive than the resonant-input filter. Another advantage of the tuned filters is that the resonant capacitors see only



Power Factor	Tuned Filters		Resonant-Input Filter	
	Highest Harmonic Removed	Stored Energy ( $P/\omega_l$ )	$K_l$	Stored Energy ( $P/\omega_l$ )
.944	3	.22	.21	1.6
.970	7	.34	.29	2.2
.980	11	.38	.36	2.8
.985	15	.41	.42	3.3

*Table 12.1: Comparison of the size (in terms of peak stored energy) of a set of tuned filters and a resonant-input filter.*

the harmonic currents, which are very small. In the resonant-input filter, however, the resonant capacitor carries the entire line current and must therefore be a very low-loss capacitor.



## Chapter 13

# Active Shaping Methods

Shaping circuits with active devices have several advantages over passive circuits, each a result of the extra control afforded by an active switch. For instance, active circuits usually achieve a better power factor than a passive circuit of equal size and weight. Furthermore, the active current-shaper is better able to maintain its high power factor despite variations in the line and load. Finally, even a single active device allows a current-shaping circuit to not only provide unity power factor, but to regulate the dc output voltage at the same time.

The active devices that provide these benefits go by the generic name of “switches.” In practice a switch may be a power FET, a bipolar transistor, a thyristor, or a GTO. The important characteristic of all these devices is that the turn-ON (and usually turn-OFF as well) of the device is determined by an “intelligent” control circuit. This is in contrast to the diode rectifiers of passive circuits which are turned ON and OFF by the circuit waveforms, without any possibility of intervention or control.

Ingenious engineers have proposed an astounding variety of active circuits for improving input-current waveshapes. Despite their variety, active shaping circuits use one of just a few basic methods to shape the input current and obtain a dc output voltage. This chapter introduces three categories of shaping circuits, examining both the basic features and the nonidealities.

Most active current-shaping circuits are built around either a buck or a boost dc-dc converter topology. The buck-based circuits are studied in Section 13.1, while Section 13.2 examines boost-based current shapers. Circuits built around either topology can be *slow switching*, in which the switches turn ON and OFF only a few times within each line period, or *fast switching*, with a switching frequency far above the line frequency. The emphasis here is on analysis of the fast-switching methods, but schemes using slow

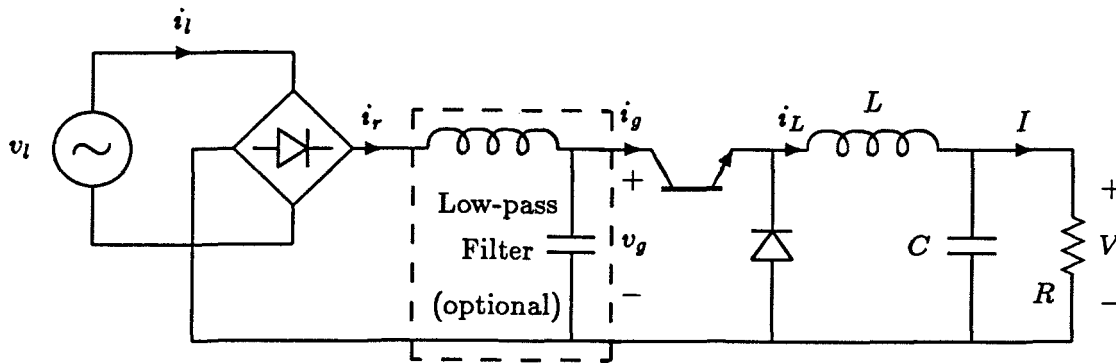


Figure 13.1: A buck-based input-current shaping circuit.

switching are included for completeness. Slow-switching methods are important at high power levels where active switches are slow.

A unique mode of operation of certain shaping converters results in “automatic” current shaping, in which the converter draws an input current proportional to the input voltage while the control variable is held constant. This remarkable behavior, examined in Section 13.3, is found in both buck-based and boost-based converters. A converter topology which achieves the same “automatic” shaping feature while drawing resonant pulses of input current is also presented.

### 13.1 Buck-Based Topologies

The buck converter is one of the simplest dc-dc switching converters. When used as a current-shaper, the buck topology requires a rectifier bridge, as shown in Fig. 13.1. Neglecting the low-pass filter for the moment, the bridge rectifier applies a rectified sinusoidal voltage to the converter input and simultaneously unfolds the buck converter’s input current to produce a bipolar line current. Assuming that the inductor current  $I_L$  is nearly constant, the operation of the circuit of Fig. 13.1 as a current shaper is easy to understand. The transistor and diode chop the inductor current into a pulse-width modulated (PWM) input-current waveform controlled by the switching of the transistor. The switch is controlled so that the PWM waveform  $i_g$ , after unfolding by the rectifier

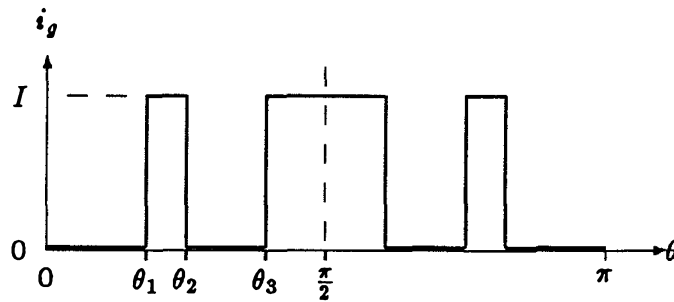


Figure 13.2: Representative input current  $i_g$ , for a buck current shaper.

bridge, approximates a desirable line current. The optional low-pass filter is often used to remove the high-frequency components of the PWM waveform, producing a smooth, continuous line-current.

Several variants of the system shown in Fig. 13.1 can be found in practice. In some cases, particularly at higher power levels, an active bridge circuit performs both rectification and PWM. Such a bridge replaces the bridge rectifier and the active switch of Fig. 13.1. At low switching frequencies, the filter is usually on the line side of the bridge rectifier. At higher frequencies, however, placing the filter on the load side allows the rectifier bridge to switch at the line frequency, instead of at the switching frequency.

Current-shaping circuits based on the buck-converter can be recognized by this feature: a source of nearly dc current is chopped to create the input current. Without any filtering, then, the input current is a rectangular waveform alternating between zero and some fixed value.

### 13.1.1 Slow-switching Buck-based Methods

Active switches are slow at high power levels, and current-shaping must be performed with only a few switching transitions during each cycle of the line voltage. While such slow switching rules out unity power factor, even very slow switching offers great improvements over “unshaped” methods such as phase-controlled rectification.

The input current of a buck shaping circuit, illustrated in Fig. 13.2, is a set of current pulses with amplitude equal to the inductor current. The current in the inductor is approximately constant and equal to the load current  $I$ . Two parameters determine the

circuit's behavior as a current shaper: the number of current pulses in a half cycle of the line, and the location of the pulse edges. These values are constrained by the minimum ON or OFF time of the semiconductor switches, *i.e.*, how fast the devices can switch. The actual transition times, or switching angles  $\theta_k$ , determine the relative amplitude and phase of the harmonics in the input-current waveform.

If the switching angles have even symmetry within each half cycle of the line voltage, and odd symmetry within a full cycle, the input current has unity displacement factor and no second-order harmonics. With such symmetry, only  $p$  switching angles need be determined when  $p$  pulses of current are present in a half cycle of the line. The rest of the transitions follow from the symmetry. For example, the pulse number  $p$  is 3 in Fig. 13.2, and the first three switching angles,  $\theta_1$  through  $\theta_3$ , completely determine the input-current waveform.

### Single Pulse

The slowest switching possible allows only one pulse of current within each half cycle of the line voltage. In this case,  $p = 1$  and only one switching angle,  $\theta_1$ , can be chosen. The power factor in this case is given by

$$\text{PF} = \frac{2\sqrt{2}}{\pi} \frac{\cos \theta_1}{\sqrt{1 - 2\theta_1/\pi}}, \quad (13.1)$$

and is plotted in Fig. 13.3. As  $\theta_1 \rightarrow 0$ , the current waveform becomes a square wave and the power factor approaches 0.90, just as in the inductor-input filter with  $K_l \rightarrow \infty$ . The peak power factor is 0.96, occurring at an angle  $\theta_1 \approx 21^\circ$ .

If this current-shaping circuit is required to provide a regulated output voltage, then the freedom to choose  $\theta_1$  is lost. The width of the current pulse also determines the conversion ratio  $M$ , according to

$$M \equiv \frac{V}{V_l} = \frac{2}{\pi} \cos \theta_1, \quad (13.2)$$

a relation included in Fig. 13.3. The shaping circuit is able to enforce unity displacement factor by means of symmetrical switching, but the power factor becomes a function of the conversion ratio.

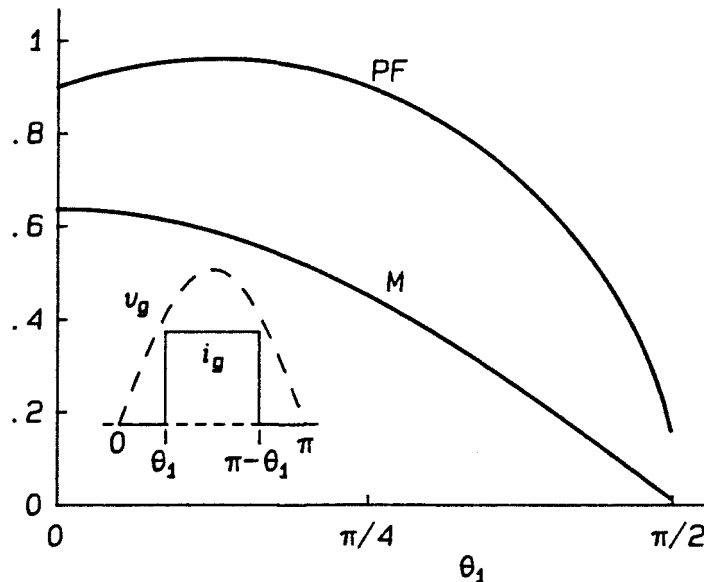


Figure 13.9: Power factor and conversion ratio  $M$  of a buck shaper with  $p = 1$ . The independent variable  $\theta_1$  marks the beginning of the current pulse.

The flyback converter discussed in Reference [29] uses the single-pulse technique. (A flyback converter is a buck-based current shaper since it has the feature of chopping a dc inductor current to create the input-current waveform.) In this circuit, the active switch turns ON when the line voltage reaches one-half its peak value. The angle  $\theta_1$  is then  $30^\circ$ , yielding a power factor of about 0.95.

### Optimal PWM

When the speed of the semiconductor switches allows pulse numbers  $p$  greater than one, some criteria must be chosen for determining the  $p$  independent switching angles  $\theta_1, \dots, \theta_p$ . In *optimal* control schemes [30], these angles are selected to optimize some measure of the harmonic content of the input current  $i_g$ . A common criterion is the selective elimination of individual harmonics. With  $p$  pulses in a half cycle, the first  $p - 1$  odd harmonics of the input-current waveform can be removed by properly choosing the  $p$  switching angles.

The optimal switching angles are also functions of the dc output voltage. An interesting result is that, at fixed output voltage, increasing the pulse number  $p$  actually

*decreases* the power factor of the unfiltered input current. In other words, the distortion factor of the input current is not improved by faster switching.

The advantages of PWM, with or without an optimal control method, are realized only when the input filter is considered. If low-order harmonics are removed by PWM, then the input filter must remove only higher-order harmonics. Consequently, the size and weight of the input filter is smaller than without PWM. As the switching speed increases, that is as  $p$  becomes larger, the distortion of the current  $i_g$ , while just as large or larger than for lower  $p$ 's, shifts to higher frequencies and is more easily removed by filtering.

The switching angles needed to eliminate a certain set of harmonics are a complicated function of the number of angles  $p$  and the conversion ratio (although the angles are independent of the load). Power processors using such a scheme must be microprocessor controlled. The switching angles are stored in memory and retrieved based on the operating point of the converter.

### Sawtooth Modulation

Sawtooth modulation is a PWM control method that trades "optimality" of the switching angles for a simpler control scheme. The switching angles, instead of being numerically determined and provided by a microprocessor, are determined by an analog control circuit.

The control method behind sawtooth modulation is illustrated in Fig. 13.4 [31,32]. A sawtooth carrier wave is compared to a reference voltage, usually the rectified line voltage. The switching angles are generated by the intersection of the two waveforms. The transistor switch is turned OFF when the sawtooth overtakes the reference voltage. The switch is turned ON when the sawtooth voltage falls below the reference signal. As the reference voltage rises, it exceeds the sawtooth for a greater portion of time, increasing the ON time of the transistor and consequently increasing the input current. In this way, the average input current roughly follows the reference voltage.

As the switching frequency is raised higher and higher, the switching angles generated by sawtooth modulation approach the optimal angles. At lower frequencies, however,



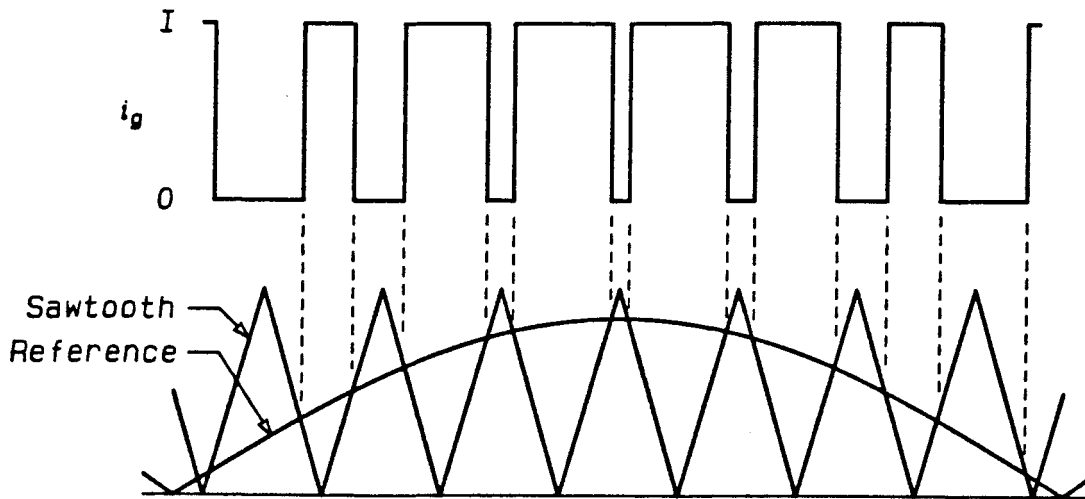


Figure 13.4: The sawtooth control scheme for buck current shapers.

where both optimal PWM and sawtooth modulation are most practical, the sawtooth angles are not optimal. Sawtooth modulation nevertheless generates unity displacement factor and is a big improvement over phase-controlled rectifier input-current waveforms.

### 13.1.2 Fast-Switching Buck Shaper

When the transistor of a buck topology is switched at a rate much higher than the line frequency, it is possible to obtain a very good approximation to the desired sinusoidal input current with a small input filter. Examples of fast-switching buck-based current shapers are found in [33] and [34]. As noted previously, the flyback topology used in [34] is not considered a buck-derived topology in dc-dc conversion, but for current-shaping applications it contains the defining feature of buck-based topologies: a stiff current pulse-width modulated to produce the input-current waveform.

When analyzing fast-switching topologies, it is helpful to introduce the concept of a *switching-frequency average*. This average is taken over a single period of the transistor switch, and is denoted by an overbar, e.g.,  $\bar{i}_l$ . If the switching frequency is fast enough, the sequence of switching-frequency averages of a waveform can be considered a continuous waveform itself, greatly simplifying analysis of the converter. To contrast with switching-frequency averages, averages over a cycle or half cycle of the line period will be denoted with triangular brackets, e.g.,  $\langle i_l \rangle$ .

The concept of switching-frequency averaging is also used in Chapter 5 of Part I and considered in detail in Appendix B, where it is concluded that the averaging operation may yield false results in some cases. Averaging has been found to be valid in the situations where it is applied in this and later chapters, but the reader is once again warned of the possibility that averaging may fail when applied to an arbitrary waveform.

As an example of the utility of the switching-frequency average, consider the buck topology of Fig. 13.1 when fast switching is used. The inductor  $L$  has essentially constant current  $I$  and the load has dc voltage  $V$ . The line current  $i_l$  is an unfolded version of the filtered PWM current  $i_g$ . The transistor switch should be operated so that, at low frequencies, the waveform  $i_g$  approximates a rectified sine wave. The filter, actually performing the switching-frequency average, removes the high-frequency harmonics of the PWM waveform, leaving a rectified sine wave to be unfolded into the line.

Suppose the transistor is operated at fixed switching frequency. During each switching period, of duration  $T_S$ , the transistor is ON for a fraction of time called the duty ratio,  $d$ . Since switching occurs many times during each cycle of the line, the duty ratio may be considered a continuous function  $d(\theta)$  over a line cycle. The average, or low-frequency current in the filter is then  $\bar{i}_g = d(\theta)I$ . For this current to be the desired rectified sine wave,  $d(\theta)$  must be a rectified sine wave,  $d(\theta) = D_m |\sin \theta|$ , with peak value  $D_m$ .

The averaged current is precisely the filtered current presented to the line by the filter, provided the switching frequency is far above the line frequency and the filter corner is properly chosen.

The operating conditions of the converter are easily found from the switching-frequency averaged waveforms. If the line current is  $i_l(\theta) = I_l \sin \theta$ , with peak value  $I_l = D_m I$ , then the processed power is

$$P = \langle V_l I_l \sin^2 \theta \rangle = \frac{V_l I D_m}{2} . \quad (13.3)$$

The dc output voltage is

$$V = \langle D_m V_l \sin^2 \theta \rangle = \frac{D_m}{2} V_l , \quad (13.4)$$

and the emulated resistance is

$$R_{em} = \frac{V_l}{I_l} = \frac{2R}{D_m^2} . \quad (13.5)$$

These values are all ideal, neglecting the effect of the input filter as well as any disturbances in the line voltage. In practice, fast-switching buck current shapers are usually operated with a feedback loop closed around the input current. Such closed-loop control of the input-current waveshape ensures near-unity power factor despite noise and disturbances in the system.

The control circuit in [33] uses hysteretic control. The filtered input current is compared to a sinusoidal reference signal (generated from the input voltage). When the input current deviates from this reference by more than a fixed amount (the hysteresis), the active switch changes state to bring the current back within bounds. The switching frequency is not constant in this scheme.

The control circuit for the flyback topology of [34] uses constant-frequency switching with duty-ratio control. The filtered input current is fed back, as one would expect, but a “minor loop” is also closed around the voltage across the input-filter inductor. The output voltage is fed back through a low-pass filter, closing a low-bandwidth feedback loop that provides regulation of the output voltage.

### The Input Filter

The filter for a fast-switching buck topology must be carefully chosen. If the corner frequency is too high, the high-frequency harmonics will not be sufficiently attenuated and the line current will have high-frequency distortion. On the other hand, if the corner frequency is too low the converter cannot produce the desired sine wave near crossover.

To understand the crossover distortion problem, consider the current waveform  $i_r$  at the load side of the input bridge rectifier in Fig. 13.1. If the line current  $i_l$  is sinusoidal, the current  $i_r$  is a rectified sine wave. Such a waveform has cusps, and these discontinuities of slope lead to a relatively slow ( $1/n$ ) roll-off of the magnitude of the coefficients in the Fourier expansion of the waveform. To accurately produce a rectified sine wave current  $i_r$ , particularly near the cusps, these high-frequency harmonics must be present in the current  $i_g$  and must be admitted by the filter. The purpose of the filter, however, is to remove the high-frequency current components resulting from the switching process. In removing the switching ripple from the input-current waveform, the filter must cause

distortion of the rectified sine wave. This distortion is most noticeable near the cusps, where the high frequency components are most important. The only way to alleviate this conflict is to raise the switching frequency and the filter cut-off frequency relative to the line frequency so that only the very high-order harmonics of the rectified sine wave are affected.

Another interpretation of this problem, in the time domain, comes from considering the fact that the input filter is a second-order, low-pass filter. This low-pass characteristic applies both to the voltage transfer function from the line side to the load side, and by reciprocity to the load-to-line current transfer function. The PWM action of the active switch applies current steps to the filter. The filter's response to a step function has an initial slope of zero, and a finite rise time. Since the cusp of the desired sine-wave current has finite slope, it is never possible to reproduce the cusp exactly. However, as the rise time of the filter decreases (that is, as the filter corner frequency is placed higher), the amount of time it takes for the filter to "catch up" to the reference sine wave diminishes, and the effect of the filter on the cusp of the rectified sine wave becomes small.

To meet a specification on switching ripple in the line current, the filter corner must be placed some fixed "distance" below the switching frequency. For example, a two-pole filter provides 80 dB of attenuation if placed 2 decades below the switching frequency.

Simultaneously satisfying both the distortion and the ripple constraints implies a minimum separation between the switching frequency and the line frequency. Tighter specifications require more separation and hence higher switching frequencies.

Although a rectified sine-wave current waveform may be missing upper harmonics, it can still yield high power factor. The reason is that a large portion of the power is delivered by the dc and low-frequency components of a rectified sine wave:

<u>Component</u>	<u>Power</u>
dc	81%
2nd harmonic	18%
4th harmonic	1%
6th harmonic	.1%

For instance, if the current waveform on the load side of the rectifier bridge is low-pass

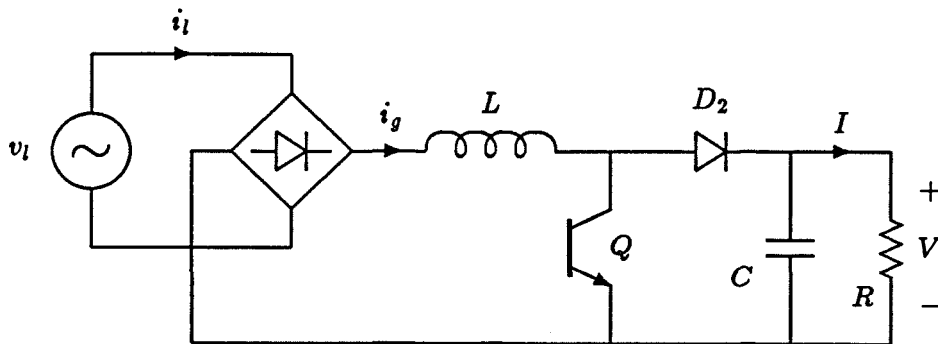


Figure 13.5: The boost current shaper.

filtered so that only the dc and the second-harmonic components remain, the power factor is 0.995, assuming no phase shift in the second harmonic. It therefore appears that the filter in a fast-switching, active current shaper has little effect on the power factor.

Closer examination reveals that the situation is not so benign. Figure 10.2 of Chapter 10 illustrates one potential problem. If a rectified sine wave is low-pass filtered, it does not reach zero at the cusps, as indicated in Fig. 10.2(c). When such a waveform is unfolded into the line by the bridge rectifier, the line current is discontinuous at  $\theta = 0$  and  $\theta = \pi$ , as in Fig. 10.2(b). Although the load-side current waveform contains only low-frequency components, the switching of the rectifier bridge modulates this waveform, creating high-frequency sidebands in the line current. The effect of these high-frequency components is seen in the time domain as a discontinuity of the line current. Although the power factor is the same on either side of the rectifier bridge, the harmonic content is quite different.

## 13.2 Boost-Based Topologies

The basic boost current-shaping topology, shown in Fig. 13.5, consists of a bridge rectifier followed by a boost dc-dc converter. When the switch  $Q$  is ON, it connects the inductor  $L$  to ground, so that the current  $i_g$  in the inductor increases. When the switch is OFF, the rectifier  $D_2$  comes ON and the inductor is connected to a stiff voltage  $V$ , provided by the large capacitor  $C$ . As long as the voltage  $V$  is greater than the input

voltage, the current  $i_g$  decreases. Controlling the active switch therefore shapes the input current  $i_g$ . The bridge rectifier unfolds this current to produce the line current  $i_l$ .

The buck topologies of the previous section were characterized by an input current consisting of “chops” of a dc current from a stiff inductance. In contrast, the boost current-shapers are defined by the chopping of a stiff voltage to produce a PWM voltage waveform across a relatively small inductance. Whereas the input current (before filtering) in a buck shaper is a PWM, rectangular waveform, the input current of a boost circuit is an integrated version of a PWM voltage waveform. The boost topology therefore has some “built-in” filtering, and the input current is continuous even without an input filter.

The switch in the boost topology can be operated slowly while maintaining reasonably good power factor. Some examples of this kind of operation are presented first. When the switching frequency is much higher than the line frequency (fast switching), true sine-wave current is possible. Guidelines for design of fast-switching boost shapers are given, and some variations of the basic boost shaping scheme are examined.

### 13.2.1 Slow-switching Boost

With a switching frequency a scant 8 or 10 times the line frequency, the boost topology of Fig. 13.5 can deliver a power factor of better than 90 percent. Figure 13.6 shows some examples of the line-current waveform. Two parameters determine the power factor for a given switching frequency: the conduction parameter

$$K_l \equiv \frac{\omega_l L}{\pi R} \quad (13.6)$$

and the conversion ratio  $M \equiv V/V_l$ . The waveforms of Fig. 13.6 have five constant-frequency switching intervals in each half cycle of the line, and the conversion ratio is  $V/V_l = 1.5$ .

For large  $K_l$ , as in Fig. 13.6(a), the dc inductor current is large and the line current is nearly a square wave. The power factor in this case approaches 0.90, just as in the inductor-input filter with large  $K_l$ . (It is interesting to note that the boost topology is an inductor-input filter if the transistor is kept OFF indefinitely.) With decreasing  $K_l$ ,

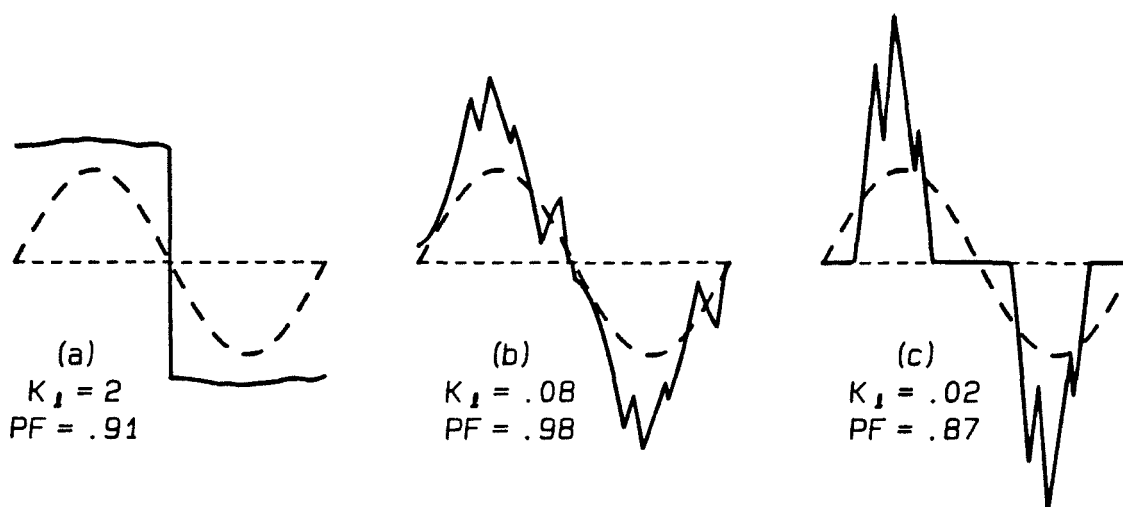


Figure 13.6: Waveforms of the boost current shaper with slow switching.

the inductor current becomes more “peaky”, as in Fig. 13.6(b). For still lower  $K_L$ , the inductor current becomes discontinuous, as shown in Fig. 13.6(c).

The input current is shaped by controlling the switching times. Power factor, or other criteria, can be optimized over these variables. A numerical multivariable optimization routine can find the best switching scheme to meet power factor or harmonic distortion constraints. The switching instants shown in Fig. 13.6, for example, were calculated to yield optimal power factor for the case of constant switching frequency and no minimum ON or OFF time. In practice, the maximum and minimum ON and OFF times will likely be limited.

Optimal values for the switching times change as the load and output voltage change. An optimal control scheme would therefore be complicated, probably requiring micro-processor control and switching times stored in memory.

Problems with the boost topology at low frequency include high peak currents and the intelligent control needed. Line current is discontinuous at the crossover of the input-voltage sine wave unless  $K_L$  is low. The fundamental of the input current tends to lag because of the difficulty in increasing the inductor current early in the cycle when the input voltage is low. Proper choice of the inductance can correct this effect at the expense of higher peak current. The most important drawback, however, is the drastic change

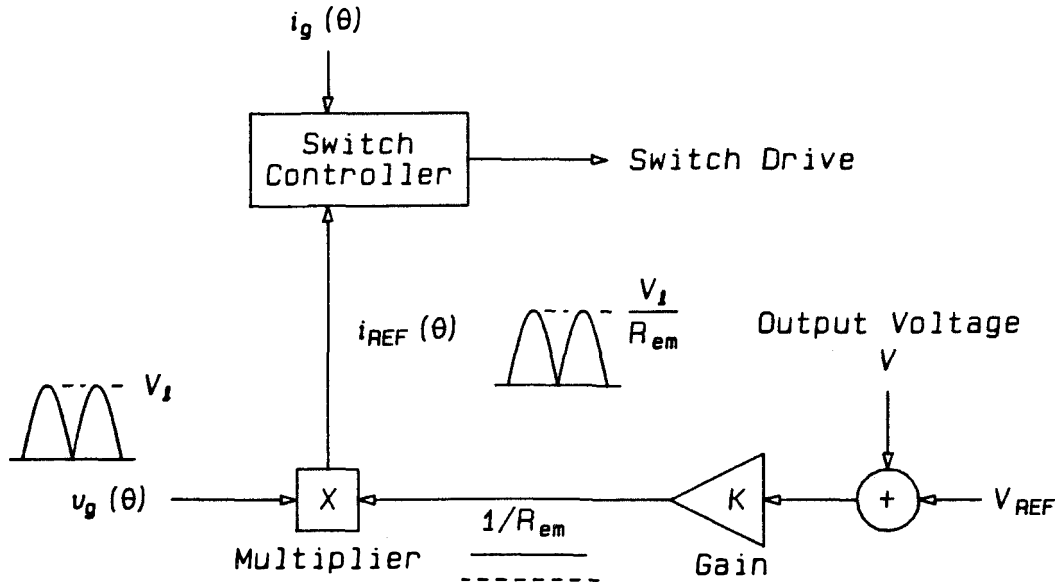


Figure 13.7: Control circuit for a boost current shaper.

in the form of the line current as the load varies, demonstrated in Fig. 13.6. This is one reason why buck-based current shapers are preferred over boost-based circuits at high power levels and low switching frequencies.

### 13.2.2 Fast-Switching Boost Current Shapers

When the boost topology operates with a switching frequency well above the line frequency, the inductor current can be made to closely follow the rectified input voltage [35,36,37,38,39]. The input current is then a sinusoid proportional to the line voltage, with some added high-frequency switching ripple. Fast-switching boost current shapers are sometimes called “resistor emulators,” although any converter with unity power factor emulates a resistor.

Figure 13.7 illustrates the common features of most boost controller circuits. The (rectified) line voltage  $v_g$  serves as a (rectified) sinusoidal reference waveform. To set the amplitude of the current reference signal  $i_{ref}$ , the output voltage is compared to a reference and the resulting error signal, following amplification, is multiplied with  $v_g$ . The reference signal  $i_{ref}$  is therefore a rectified sine wave whose amplitude is determined by the desired output voltage. The boost converter’s active switch is operated so that



the input current closely follows this reference. As noted in Chapter 16, the output-voltage error signal must be severely bandlimited (to less than the line frequency) in order to prevent distortion of the input-current waveform. Although the control circuit of Fig. 13.7 provides both current shaping and output-voltage regulation, the bandwidth of the voltage control loop is very low.

The block diagram of Fig. 13.7 contains the features found in most boost-shaper control circuits [36,37,38,39]. However, the way in which the input current  $i_g$  is made to follow the reference signal  $i_{ref}$  is different in each of these references. In [36] and [37], the signal  $i_{ref}$  feeds a linear duty-ratio modulator. In [38], a synchronized hysteretic (bang-bang) control is used. When the input current exceeds the hysteresis band surrounding the reference signal  $i_{ref}$ , the active switch turns ON or OFF at the next clock pulse. Reference [39] uses a simple hysteretic (bang-bang) control scheme in which the switch changes state as soon as the input current leaves the hysteresis band around  $i_{ref}$ .

A somewhat different control method is used in [35]. There an integrated-circuit current-mode-programming controller programs the input current using the dc output voltage as a reference. Ideally, the circuit should draw constant input current, yielding a square-wave line current. However, the duty-ratio limit imposed by the compensating ramp of the current-mode control varies with the line voltage, resulting in a serendipitous improvement in power factor. This circuit yields very good power factor with surprisingly few components.

The following steady-state analysis applies to all fast-switching boost current shapers, regardless of the control method used. The switching frequency is assumed to be much higher than the line frequency so that the switching-frequency-averaged waveforms can be used.

When the duty ratio of the transistor switch is  $d(\theta)$ , the average voltage across the inductor is

$$\bar{v}_L(\theta) = v_g(\theta) - d'(\theta)V, \quad (13.7)$$

where  $d'(\theta)$  is  $1 - d(\theta)$ , the complement of the switch duty ratio. For unity power factor, the current must be related to the rectified line voltage by

$$i_g(\theta) = \frac{V_l}{R_{em}} |\sin \theta|, \quad (13.8)$$

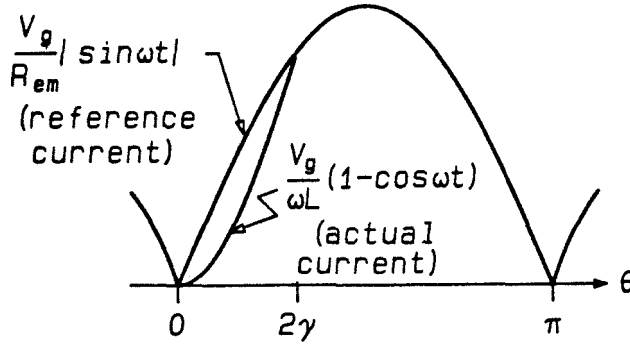


Figure 13.8: Distortion of the boost input-current waveform near the cusp of the reference waveform.

where  $R_{em}$  is a constant, called the emulated resistance. The duty ratio required to generate this current waveform is found by differentiating Eq.(13.8), multiplying by  $L$ , and equating the result to Eq.(13.7), which yields

$$d'(\theta) = \frac{1}{M} \frac{1}{\cos\gamma} \sin(\theta - \gamma), \quad (13.9)$$

where

$$\tan \gamma \equiv \pi K_e, \quad (13.10)$$

$$K_e \equiv \frac{\omega_l L}{\pi R_{em}}, \quad (13.11)$$

and  $M$  is the conversion ratio  $V/V_i$ . The conduction parameter  $K_e$  is analogous to the conduction parameter  $K_l$  defined earlier for passive shaping circuits and for the slow-switching boost topology. The difference is that  $K_e$  involves the *emulated* resistance  $R_{em}$ , while  $K_l$  contains the effective *dc load* resistance  $R$ .

The duty ratio  $d'(\theta)$  of Eq.(13.9) must lie between 0 and 1. The latter constraint is satisfied when

$$M > \frac{1}{\cos\gamma} \quad (13.12)$$

but the constraint that  $d'(\theta)$  be positive cannot be satisfied for  $\theta$  near zero. The physical explanation of this effect is illustrated in Fig. 13.8. For small  $\theta$ , the input voltage is near zero. The inductor current, trying to follow the commanded current  $v_g(\theta)/R_{em}$ , rises fastest with the switch on, i.e.,  $d' = 0$ . With the switch held continuously ON, the

current  $i_g$  is

$$i_g(\theta) = \frac{1}{L} \int_0^\theta V_l \sin \theta' d\theta' = \frac{V_l}{\omega_l L} (1 - \cos \theta) . \quad (13.13)$$

Equation (13.8) represents the desired current while Eq.(13.13) is the highest current possible for small  $\theta$ . The two waveforms converge when  $\theta = 2\gamma$ ; after this time the desired current waveform can be followed exactly. If the inductor current is programmed to follow Eq.(13.8), the actual effect is

$$i_g(\theta) = \begin{cases} \frac{V_l}{\omega_l L} (1 - \cos \theta) & 0 < \theta < 2\gamma \\ \frac{V_l}{R_{em}} \sin \theta & 2\gamma < \theta < \pi \end{cases} \quad (13.14)$$

and

$$d'(\theta) = \begin{cases} 0 & 0 < \theta < 2\gamma \\ \frac{1}{M \cos \gamma} \sin(\theta - \gamma) & 2\gamma < \theta < \pi . \end{cases} \quad (13.15)$$

This assumes the switch duty ratio can reach zero. In practice the minimum ON time may be restricted and the time when the inductor current finally reaches the reference current may be somewhat later than  $\theta = 2\gamma$ .

This "lag" effect in the initial inductor current affects the output voltage and power factor. To find the output voltage, the average output current  $I$ ,

$$I = \frac{1}{\pi} \int_0^\pi i_g(\theta) d'(\theta) d\theta , \quad (13.16)$$

is evaluated using Eqs.(13.14) and (13.15), and the result multiplied by  $R$  to obtain

$$M = \left[ \frac{R}{2R_{em}} \left( 1 - \frac{2\gamma}{\pi} + \frac{1}{\pi} \sin 2\gamma \right) \right]^{1/2} . \quad (13.17)$$

The mean-square current can be found from Eq.(13.14) and the power factor follows:

$$\text{PF} = \frac{1 - \frac{2\gamma}{\pi} + \frac{1}{\pi} \sin 2\gamma}{\left\{ 1 - \frac{2\gamma}{\pi} + \frac{1}{2\pi} \sin 4\gamma + \frac{2}{\pi} \cot^2 \gamma \left[ 3\gamma - 3 \sin \gamma \cos \gamma - 2 \sin^3 \gamma \cos \gamma \right] \right\}^{1/2}} . \quad (13.18)$$

The Fourier coefficients of the odd extension of Eq.(13.14) into the complete line period yield the displacement factor,

$$\cos \phi_1 = \frac{\frac{\pi}{2} - \gamma + \frac{1}{2} \sin 2\gamma}{\left\{ \left( \frac{\pi}{2} - \gamma + \frac{1}{2} \sin 2\gamma \right)^2 + \left[ \cos \gamma \left( \cos \gamma - \frac{\gamma}{\sin \gamma} \right) \right]^2 \right\}^{1/2}} . \quad (13.19)$$

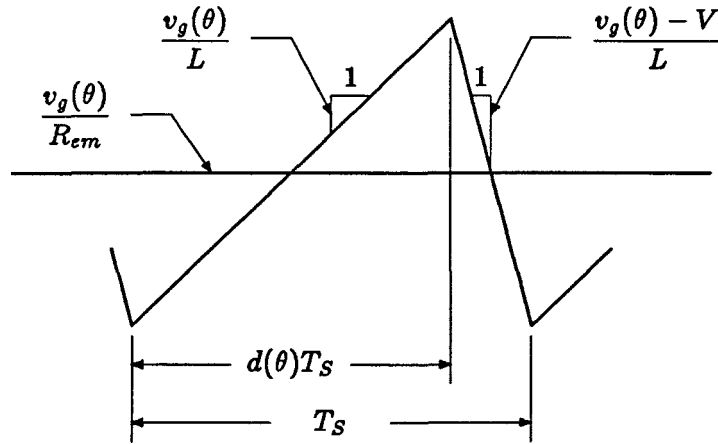


Figure 13.9: Switching ripple superimposed on the input current of a boost current shaper.

Equations (13.18) and (13.19) consider only the effect of the initial “lag” in the current waveform, and are independent of the switching frequency. The effect on power factor of the high frequency ripple current has been studied by Rippel [36], who neglected any error at the cusp, essentially assuming  $\gamma = 0$ . If the two nonidealities, nonzero  $\gamma$  and finite switching ripple, each cause small deviations from the ideal current waveform, one may treat the two effects separately and find the power factor as the product of the power factors derived by the separate calculations.

To evaluate the effect on power factor of switching ripple alone, consider Fig. 13.9, where the inductor current is shown over a single switching period. Again, with the assumption that the switching frequency is much greater than the line frequency, the reference current can be considered constant during any one switching cycle. The rms current contains both line-frequency and switching-frequency components. Since the ripple component has zero average, the total mean-square current is the sum of the mean squares of the line component (smooth waveform with initial “lag”) and the switching-ripple component (zero-average triangular waveform). The peak-to-peak value of the ripple current is

$$\Delta i_r(\theta) = \frac{d(\theta)T_s v_g(\theta)}{L}. \quad (13.20)$$

For negligible “lag” effect near the cusp, the duty ratio  $d(\theta)$  is found from Eq.(13.9)

with  $\gamma = 0$ ,

$$d(\theta) = 1 - d'(\theta) = 1 - \frac{1}{M} \sin \theta . \quad (13.21)$$

The mean-square ripple current during any single switching cycle is just the peak-to-peak value squared and divided by 12, or

$$\overline{i_{r,\text{rms}}^2}(\theta) = \left(1 - \frac{1}{M} \sin \theta\right)^2 \frac{T_S^2 V_l^2 \sin^2 \theta}{12L^2} \quad (13.22)$$

$$= \frac{V_l^2}{2R_{em}^2} \left(1 - \frac{1}{M} \sin \theta\right)^2 \frac{2 \sin^2 \theta}{3K_{es}^2} , \quad (13.23)$$

where  $K_{es}$  is defined by

$$K_{es} \equiv \frac{\omega_S L}{\pi R_{em}} . \quad (13.24)$$

The  $e$  subscript refers to the dependence of  $K_{es}$  on the *emulated* resistance, while the  $s$  subscript indicates that it is the *switching* frequency  $F_S = \omega_S/2\pi$  that appears in  $K_{es}$ .

Under the assumption of high switching frequency, the mean-square ripple current can be considered a continuous function of  $\theta$ , and the total mean-square ripple current is found by averaging Eq.(13.23) over a half cycle of the line, to find

$$I_{r,\text{rms}}^2 = \frac{V_l^2}{2R_{em}^2} \frac{1}{3K_{es}^2} \left[ 1 - \frac{16}{3\pi} \left(\frac{1}{M}\right) + \frac{3}{4} \left(\frac{1}{M}\right)^2 \right] . \quad (13.25)$$

The total mean-square current is the mean square of the ideal current,  $V_l^2/2R_{em}$ , plus the mean square of the ripple from Eq.(13.25). The resulting power factor is

$$\text{PF} = \frac{1}{\left\{ 1 + \frac{1}{3K_{es}^2} \left[ 1 - \frac{16}{3\pi} \left(\frac{1}{M}\right) + \frac{3}{4} \left(\frac{1}{M}\right)^2 \right] \right\}^{1/2}} . \quad (13.26)$$

Since the ripple has zero average during each switching cycle, it adds no phase displacement to the power factor. Equation (13.26) represents distortion alone.

In Fig. 13.10, Eqs.(13.18), (13.19), and (13.26) are plotted against  $K_e$  and  $K_{es}$  on a log scale. Since  $K_{es} = (\omega_S/\omega_l)K_e$ , the curves showing the ripple effect are shifted relative to the lag-effect curves as the switching frequency changes. Figure 13.10 shows the relationship of the two power factor components for  $\omega_S = 1000\omega_l$ . For lower switching frequency, the ripple curves move to the right, defining a more narrow region where the power factor is near unity. For higher switching frequency, the ripple curves move left and a broader range of  $K_e$  values give acceptable power factor. When the power factor is

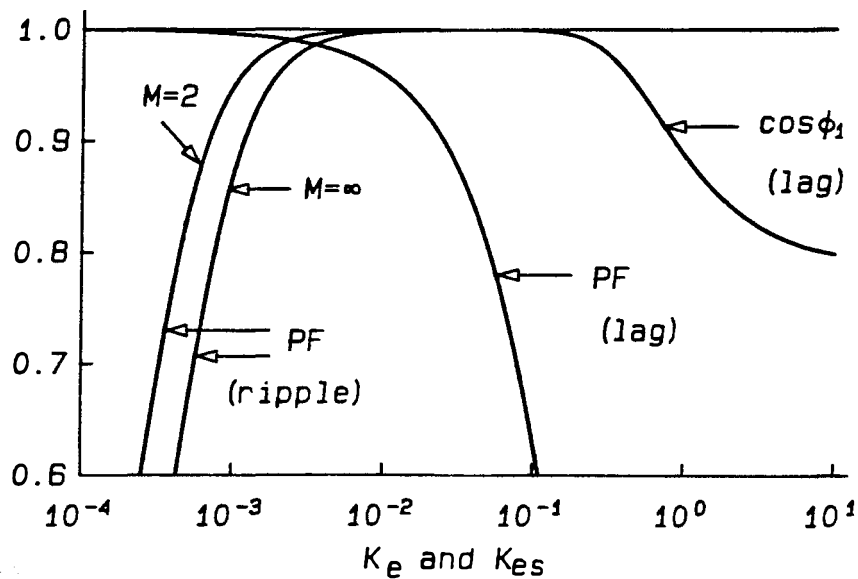


Figure 13.10: Power factor of the fast-switching boost shaper, with separate consideration of distortion near the cusp and switching-frequency ripple.

near 1, it may be found by multiplying the two power factors obtained by considering the ripple and lag effects separately. When either individual effect is large, the approximation breaks down.

Fig. 13.10 shows how the inductance  $L$  must be chosen in terms of the load and switching frequency if near-unity power factor is needed. Alternatively, if the acceptable switching ripple (and hence  $K_{es}$ ) is specified, Fig. 13.10 shows the necessary separation of the line and switching frequencies to obtain a specified power factor.

Both [36] and [37] show that the inductor current goes discontinuous near the cusp if  $K_{es} < 1$ . This is frequently taken as a lower bound for acceptable current ripple.

### 13.2.3 Variants of the Boost Shaper

The boost topology offers a surprising number of possibilities for current-shaping. In addition to the slow- and fast-switching modes described above, and the “automatic” shaping mode to be discussed in Section 13.3, two other variations of interest are described below.

### Boost with Constant Current

In Section 13.2.1 it was noted that with the active switch always OFF, the boost topology was equivalent to the inductor-input filter. A boost shaper can actually be used to emulate an inductive-input filter, using the fast-switching action to simulate a much larger inductance than is actually present in the circuit.

Instead of following a rectified sinusoidal reference, the input current  $i_i$  is maintained constant through control of the active switch. The effect is that of an inductor-input filter with  $L \rightarrow \infty$ , so that the power factor approaches 0.90. This approach has an important difference, however. In the inductor-input filter with power factor near 0.90, a large inductor is required and the filter capacitor can be small. With constant input current in the boost topology, the inductance can be small if the switching frequency is high, and the filter capacitor is large instead. Since capacitors are volumetrically more energy efficient than inductors, the boost topology with constant input current might have a weight or volume advantage. In addition, the boost converter provides active current limiting and output-voltage regulation, features missing in the inductor-input filter.

The most important benefit of this constant-current scheme, however, and the only reason one would choose it over a method generating unity power factor, is that the peak input current, and hence the peak transistor current, is lower by a factor of  $\pi/4$ , or 21%, compared to a boost topology generating sinusoidal line current.

### Boost with Tapped Transformer

Reference [40] presents an interesting slow-switching boost current shaper. The boost converters examined so far all have a PWM voltage waveform, alternating between zero and the output voltage, applied to one end of the inductor. The transitions of this PWM voltage waveform are varied to control the shape and magnitude of the input current. Instead of such a PWM voltage waveform, [40] uses a staircase waveform. An autotransformer with several taps is inserted between the boost inductor and the output filter capacitor. Active switches connect the autotransformer to the boost inductor in a push-pull fashion, opening and closing the appropriate taps to obtain the desired staircase

voltage. The switches operate slowly, but the circuit requires many more active switches than a simple boost current shaper. Furthermore, the autotransformer is large, operating at the line frequency, yet the ac input and dc output are *not* isolated.

This circuit generates very clean line-current waveforms with surprisingly few steps in the voltage staircase. With its high parts count and large autotransformer, however, it is best suited for high-power operation where fast switching is impractical.

### 13.3 “Automatic” DCM Shapers

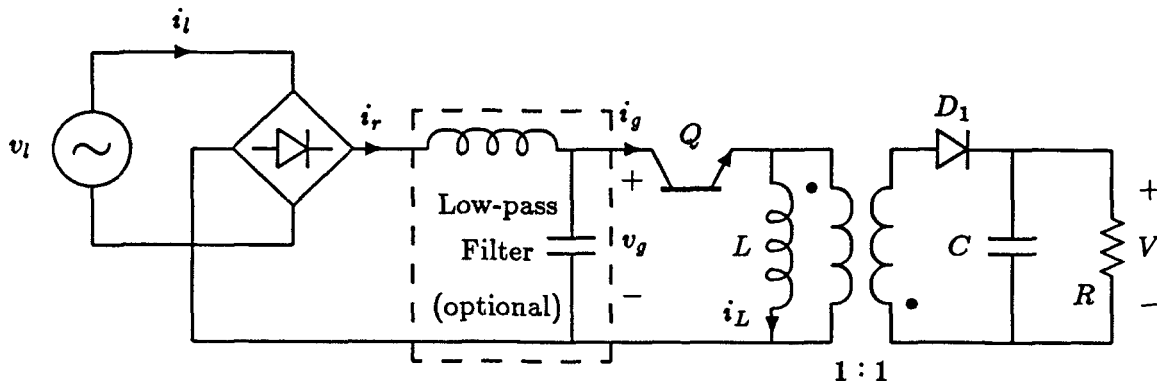
In 1979, a paper was presented at the sixth Powercon conference by two engineers from Sorensen Company, D. Chambers and D. Wang [41]. The paper described a boost converter used as a current shaper, and also suggested a flyback converter providing isolation as well as current shaping. Both circuits used the discontinuous conduction mode (DCM) of operation. The unusual feature of both these converters was that they achieved nearly unity power factor, yet the active switch operated at constant switching frequency and duty ratio! The input current was not sensed and no feedback loop was closed around the input current. Instead, the current shaping took place “automatically.” Although many papers have since been written on current shaping, using both buck and boost topologies, the unique method proposed by Chambers and Wang seems to have been neglected.

This section explains the behavior of “automatic” current shapers and presents the equations needed for design of these converters. The flyback, boost, and buck topologies are considered, and an interesting circuit is introduced that uses resonant switching to obtain automatic current shaping.

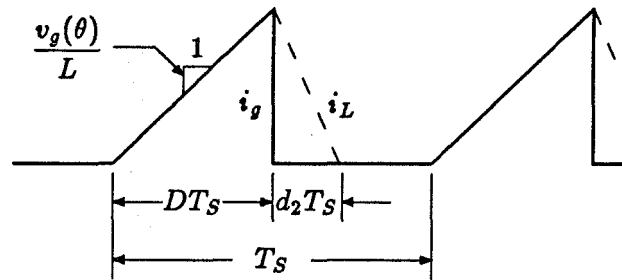
#### 13.3.1 DCM Flyback Shaper

To understand the unusual shaping method in [41], consider the flyback current shaper of Fig. 13.11(a), shown with a 1:1 transformer turns ratio for convenience. The transformer in this converter not only transfers power across the isolation boundary, but stores a significant amount of energy as well. The magnetizing inductance of the transformer,  $L$ , is therefore explicitly shown in Fig. 13.11. The output capacitor  $C_O$  is





(a)



(b)

Figure 13.11: Flyback current-shaping circuit (a), and its input-current pulse (solid line) and magnetizing current  $i_L$  (dashed line) (b) during a single switching period in DCM.

assumed large enough that the output voltage  $V$  has negligible ripple.

Suppose the transistor is operated at constant frequency  $F_S$  and duty ratio  $D$ , and that the magnetizing current  $i_L$  is zero at the start of each switching cycle. When the transistor switch is turned ON, the input voltage  $v_g$  appears across  $L$ , and the current  $i_L$  ramps up from zero, as shown in Fig. 13.11(b). After a time interval  $DT_S$ , the switch is turned OFF. The magnetizing current commutates to the diode  $D_1$  and the output voltage  $V$  appears across the magnetizing inductance. The magnetizing current ramps down over an interval  $d_2 T_S$ , until it reaches zero and is interrupted as the diode  $D_1$  turns OFF. For the rest of the switching period the magnetizing current remains at zero and the dc load is supplied only by the output capacitor. It is the turn-OFF of diode  $D_1$

before the start of the next cycle that defines DCM operation.

The input current  $i_g$  is equal to the magnetizing current  $i_L$  during the interval  $DT_S$  and is zero thereafter. The current  $i_g$  therefore consists of triangles. The area under these triangles is

$$\begin{aligned} \text{Area} &= \frac{1}{2}(\text{base})(\text{height}) \\ &= \frac{1}{2}(DT_S) \left( \frac{DT_S v_g}{L} \right) \\ &= \frac{D^2 T_S^2}{2L} v_g, \end{aligned} \quad (13.27)$$

a quantity directly proportional to  $v_g$  when duty ratio and switching frequency are fixed. The average current over each switching cycle,

$$\bar{i}_g(\theta) = \frac{D^2 T_S}{2L} v_g(\theta), \quad (13.28)$$

is therefore proportional to  $v_g$  as well. Note that the switching-frequency-averaged current,  $\bar{i}_g$ , can be considered a continuous function  $\bar{i}_g(\theta)$  when the switching frequency is far enough above the line frequency that the average of  $i_g$  over a switching period changes very little from one switching cycle to the next.

When a high-frequency filter is added to perform this averaging, as shown in Fig. 13.11(a), the filtered (averaged) current drawn from the line is proportional to the line voltage. But this is exactly the condition for unity power factor! This remarkable circuit performs current shaping while the active switch operates at constant duty ratio and switching frequency. In other words, even though an active switch is required, no intelligent control is needed. Line current “automatically” follows input voltage. The only restriction is that the switching frequency be far enough above the line frequency that a small filter can perform the required averaging without distorting the line-current waveform. Another advantage to this mode of operation is that the transistor ON-time is constant. The duty ratio does not have to reach zero (as in a buck shaper) or unity (as required in a boost shaper).

The conversion ratio  $M \equiv V/V_i$  is related to the circuit parameters by

$$M = \frac{D}{\sqrt{2K_S}}, \quad (13.29)$$

where the conduction parameter  $K_S$  is defined by

$$K_S \equiv \frac{2L}{RT_S}, \quad (13.30)$$

a quantity similar to  $K_I$  and  $K_{eS}$  defined earlier for boost topologies. The parameter  $K_S$ , however, involves the dc load,  $R$ , (rather than the emulated resistance) and the switching frequency. Discontinuous conduction mode requires that the inductor current reach zero before the start of the next switching period. In terms of  $K_S$  and the conversion ratio  $M$ , this constraint requires that

$$K_S \leq \frac{1}{2(M+1)^2} \quad (13.31)$$

for the converter to remain in DCM throughout each cycle of the line.

At a given conversion ratio  $M$ , the peak stored energy in the inductor,  $Li_{pk}^2/2$ , can be made arbitrarily small by reducing  $L$  and increasing the switching frequency,  $F_S$ , so that the conduction parameter  $K_S$  remains constant.

The peak switch and inductor current is given by

$$i_{pk} = I \sqrt{\frac{8}{K_S}}. \quad (13.32)$$

With the constraint of Eq.(13.31), the current stress in the switch must be at least

$$i_{pk} \geq 4(M+1)I. \quad (13.33)$$

The peak current stress in this circuit is much higher than in a fast-switching boost or buck shaper with the same dc output current. This is the price of “automatic” current shaping: the transistor must handle large peak currents.

The technique of “automatic” current shaping by a converter in discontinuous conduction mode (DCM) is not limited to flyback converters. The triangular current pulses drawn by buck and boost topologies in DCM can also lead to high power factor without direct control, although neither converter is as ideal as the flyback.

### 13.3.2 DCM Buck Shaper

An input-current pulse of the buck topology is illustrated in Fig. 13.12. For this

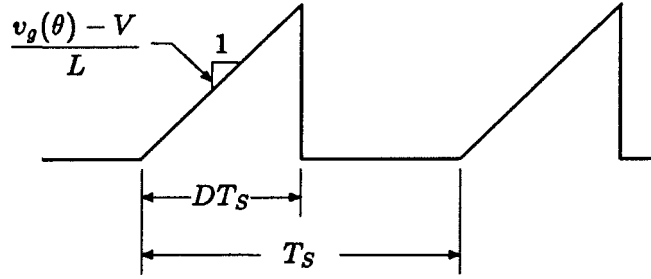


Figure 13.12: Input-current pulse of the buck topology in DCM.

converter, the averaged input current is

$$\bar{i}_g(\theta) = \frac{D^2 T_S^2}{2L} (v_g(\theta) - V) . \quad (13.34)$$

The buck topology, however, cannot draw any input-current pulses when the input voltage  $v_g(\theta)$  is less than the output voltage  $V$ . The buck circuit only draws current for  $\alpha < \theta < \pi - \alpha$ , where

$$\alpha \equiv \sin^{-1}(M) . \quad (13.35)$$

This limited operating interval implies that the DCM buck shaper gives poor power factor for large values of  $M$ . With large  $M$ ,  $\alpha$  is large and the converter conducts input current over short intervals centered around  $\theta = \pi/2$ .

The quantities needed for design of this circuit can now be calculated, taking into account the limited operating interval of the converter. For convenience, define the following two functions:

$$g(M) \equiv 1 - \frac{2\alpha}{\pi} - \frac{2}{\pi} M \cos \alpha \quad (13.36)$$

$$h(M) \equiv 1 - \frac{2\alpha}{\pi} - \frac{6}{\pi} M \cos \alpha + 2 \left(1 - \frac{2\alpha}{\pi}\right) M^2 . \quad (13.37)$$

Since  $\alpha = \sin^{-1}(M)$ , the functions  $g(M)$  and  $h(M)$  are functions only of  $M$ . Note also that both  $g(M)$  and  $h(M)$  approach unity as  $M \rightarrow 0$ .

The duty ratio  $D$  is given in terms of  $M$  and  $K_S$  by

$$D^2 = \frac{2K_S M^2}{g(M)} , \quad (13.38)$$

and the rms average input current and peak input current are

$$\bar{i}_{g,rms} = \frac{M\sqrt{2h(M)}}{g(M)} I \quad (13.39)$$

$$i_{g,pk} = \frac{2\sqrt{2}}{\sqrt{g(M)K_S}} I, \quad (13.40)$$

where  $I$  is the dc output current. The power factor,

$$\text{PF} = \frac{g(M)}{\sqrt{h(M)}}, \quad (13.41)$$

is a function only of  $M$ . Because of the symmetry of the current pulses within a half cycle of the line voltage, the input current suffers no phase displacement. Equation (13.41) represents distortion alone.

The first step in designing a DCM buck shaper is to choose the conversion ratio  $M$ . Usually this is determined by the system and load requirements, but if the designer has some freedom, he should choose  $M$  as small as possible to obtain the best power factor. With  $M$  chosen,  $D$  and  $K_S$  should be picked to reduce the peak input current as much as possible, since this current appears in the transistor switch. The duty ratio cannot be chosen arbitrarily large, however. For the converter to remain in DCM at all times, the constraint  $M > D$  must be satisfied. The best choice for low current stress is therefore  $D = M$ , which implies that  $K_S = g(M)/2$ . With these values, the peak current stress is  $4I/g(M)$ .

The power factor and optimal (for  $K_S = g(M)/2$ ) peak switch current stress are plotted in Fig. 13.13. Both quantities are most ideal as  $M$  approaches zero, but practical constraints (such as efficiency and minimum transistor ON time) limit the lowest duty ratio available. The peak stored energy in the inductor can be made arbitrarily small at a given operating point by reducing  $L$  and increasing the switching frequency, so that  $K_S$  remains at the desired value.

### 13.3.3 DCM Boost Shaper

The efficacy of the boost converter as an “automatic” current shaper lies somewhere between that of the flyback and buck topologies. In contrast to the buck converter, the boost topology in DCM conducts input-current pulses over the entire line cycle. A

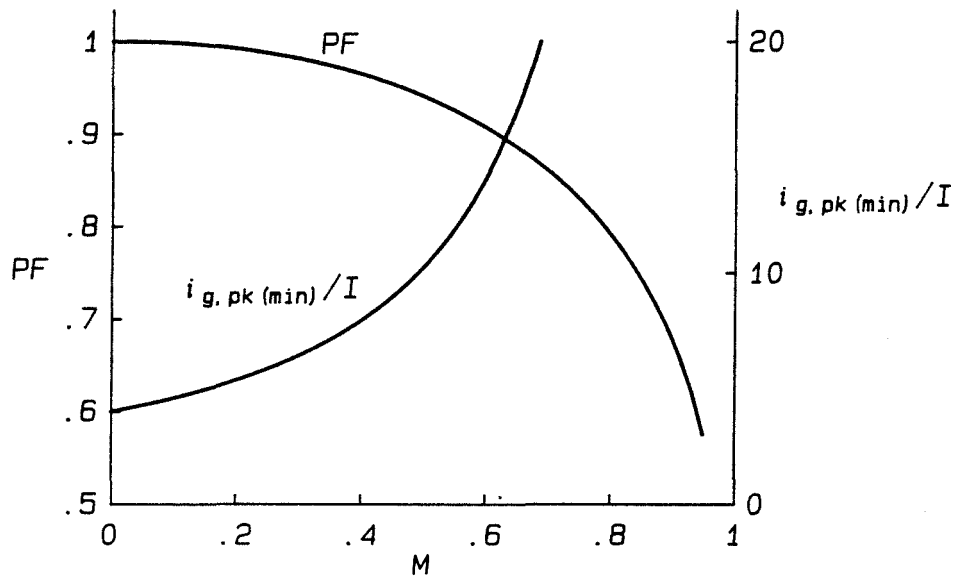


Figure 13.13: Power factor and minimum switch current stress in the DCM buck current shaper.

representative current pulse is shown in Fig. 13.14. In the boost converter, the input current contains both halves of the inductor-current pulse, instead of just the rising half as in the buck and flyback converters. The analysis is complicated somewhat by this fact.

Once again for convenience, define two functions:

$$f(M) \equiv \frac{2}{\pi} \int_0^{\pi} \frac{M \sin^2 \theta}{M - \sin \theta} d\theta \quad (13.42)$$

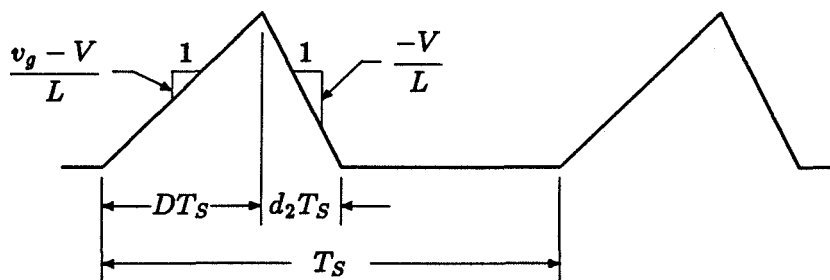


Figure 13.14: Input-current pulse of the boost topology in DCM

$$p(M) \equiv \left[ \frac{2}{\pi} \int_0^\pi \left( \frac{M \sin \theta}{M - \sin \theta} \right)^2 d\theta \right]^{1/2}. \quad (13.43)$$

The integrals are not available in closed form, but  $f(M)$  and  $p(M)$  are functions only of  $M$ . Furthermore, as  $M \rightarrow \infty$ , both  $f(M)$  and  $p(M)$  approach unity.

The interval  $d_2$  of Fig. 13.14 is related to the (controlled) interval  $D$  by

$$d_2(\theta) = \frac{v_g(\theta)}{V - v_g(\theta)} D, \quad (13.44)$$

while the averaged input current is

$$\bar{i}_L(\theta) = \frac{2M}{f(M)} \frac{M \sin \theta}{M - \sin \theta} I. \quad (13.45)$$

The rms averaged input current and the power factor are

$$\bar{i}_{L,rms} = \sqrt{2} M \frac{p(M)}{f(M)} I \quad (13.46)$$

$$\text{PF} = \frac{f(M)}{p(M)}. \quad (13.47)$$

The duty ratio is related to the conversion ratio  $M$  and conduction parameter  $K_S$  according to

$$D^2 = \frac{2K_S M^2}{f(M)}. \quad (13.48)$$

The transistor experiences its highest peak current,

$$i_{L,pk} = \frac{2\sqrt{2}}{\sqrt{K_S f(M)}} I, \quad (13.49)$$

at the peak of the line voltage.

Just as in the DCM buck converter of the previous section, the choice of  $K_S$  for lowest current stress is constrained by the condition that the converter remain in DCM at all times. For the boost,  $K_S$  is maximized for a given  $M$  when  $D$  is minimized. From Eq.(13.44), the minimum duty ratio is  $(M - 1)/M$ , and the minimum current stress is

$$i_{L,pk(\min)} = \frac{4M^2}{(M - 1) f(M)} I. \quad (13.50)$$

This minimum current stress is plotted along with the power factor in Fig. 13.15. Once again, the peak stored energy in the inductor can be made arbitrarily small by increasing the switching frequency.

The boost topology achieves its maximum power factor at high conversion ratios, but the power factor is high over a larger range of conversion ratios than in the buck topology.

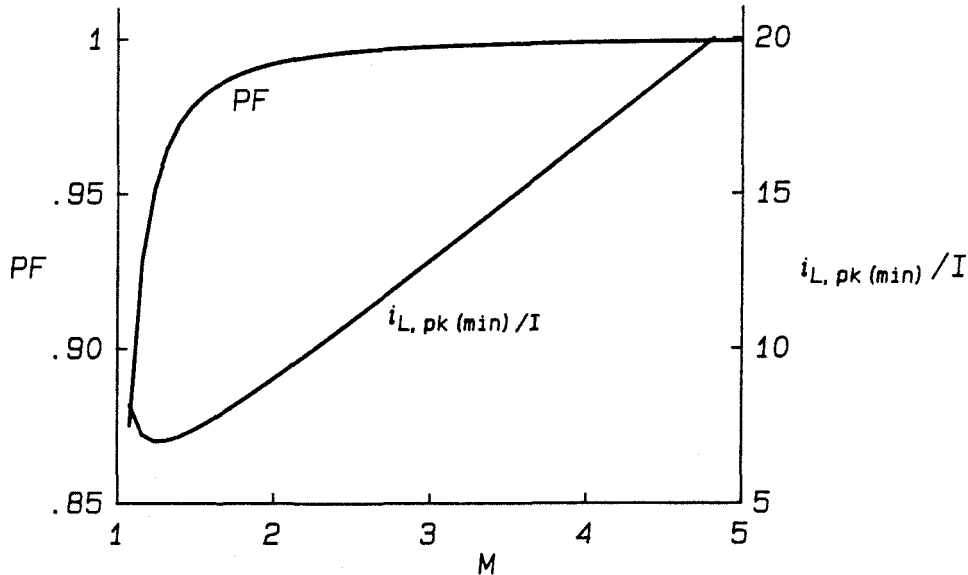


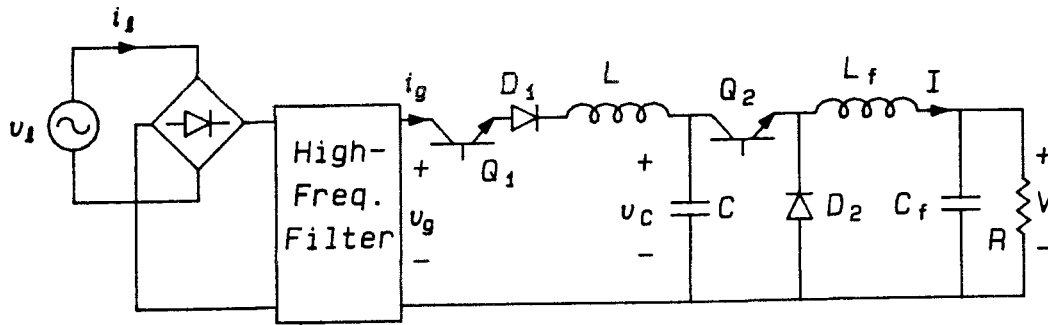
Figure 13.15: Power factor and minimum current stress in the DCM boost current shaper.

#### 13.3.4 A Resonant Pulse “Automatic” Shaper

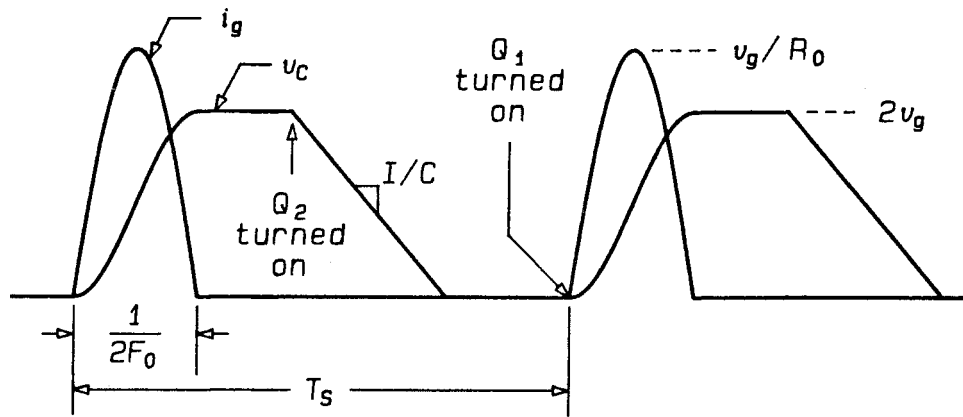
Shaping takes place automatically in the flyback converter of Section 13.3.1 because the area under the triangular input-current pulses is proportional to the pulse height, which in turn is proportional to the input voltage. Another waveshape with pulse area proportional to peak height is the half-sine pulse. If the amplitude of such a current pulse could be made proportional to the input voltage of a shaping circuit, the average input current would follow the input voltage, resulting in automatic current shaping.

The circuit of Fig. 13.16(a) implements such a scheme. Assume that the initial current and voltage of the resonant elements  $L$  and  $C$  are zero. Diode  $D_2$  is ON and carries the dc current  $I$  of the large inductor  $L_f$ . Switch  $Q_2$  is held OFF. The switch  $Q_1$  is turned ON to begin a cycle, applying the rectified line voltage  $v_g$  across the series-resonant circuit formed by  $L$  and  $C$ . The input current  $i_g$  is a half-sine pulse, as shown in Fig. 13.16(b). When the resonating current in  $L$  reaches zero, diode  $D_1$  is back-biased, interrupting the resonance. Capacitor  $C$  is charged to  $2v_g$  at the moment the resonance is interrupted. After  $D_1$  blocks, switch  $Q_1$  may be turned OFF. Note that both the turn-ON and turn-OFF of  $Q_1$  take place at zero current, so that the switch suffers very





(a)



(b)

Figure 13.16: An automatic current shaper (a) and its resonant waveforms (b).

little switching loss.

Some time after the end of the resonant pulse,  $Q_2$  is turned ON, forcing diode  $D_2$  to turn OFF. The current  $I$  in the large inductor  $L_f$  is then drawn from  $C$ . The capacitor, holding the entire energy drawn from the line during the input-current pulse, transfers that energy to the filter inductor. When  $C$  discharges to zero volts, the diode  $D_2$  again turns ON,  $Q_2$  may be turned OFF, and the circuit is in the same condition as initially.

The conversion ratio for this circuit is

$$M^2 = \frac{1}{2\pi} \frac{F_S}{F_0} \frac{R}{R_0}, \quad (13.51)$$

where the resonant frequency  $F_0$  and characteristic impedance  $R_0$  are defined by

$$F_0 \equiv \frac{1}{\sqrt{LC}} \quad (13.52)$$

$$R_0 \equiv \sqrt{\frac{L}{C}}. \quad (13.53)$$

Because the capacitor takes some time to discharge, the maximum switching frequency is limited to

$$\frac{F_S}{F_0} < 2 - 4M, \quad (13.54)$$

and the conversion ratio is therefore restricted to  $0 < M < \frac{1}{2}$ .

The peak input current is  $V_i/R_0$ , and is related to the output current by

$$i_{g,pk} = \frac{2\pi M}{(F_S/F_0)} I. \quad (13.55)$$

If the switching frequency approaches the maximum value given in Eq.(13.54), the current stress in the transistor  $Q_1$  can be as low as  $\pi M/(1 - 2M)$ . The resonant-pulse shaper therefore holds the possibility of far lower current stress than the buck, boost, or flyback DCM automatic shaping converters.

The advantages of this circuit are the automatic current shaping, the zero-current switching of  $Q_1$ , the potential for low current stress, and the probable lower EMI associated with the resonant pulse compared to a triangular pulse. Despite the resonant input waveform, the circuit is not a "resonant converter" because switch  $Q_2$  must turn ON subject to full voltage and current, as in a PWM converter. The drawbacks of the circuit include the fact that, although it requires two active switches, only one degree of freedom is available for control. Consequently, the switching frequency must vary to regulate the amount of power reaching the load.

## Chapter 14

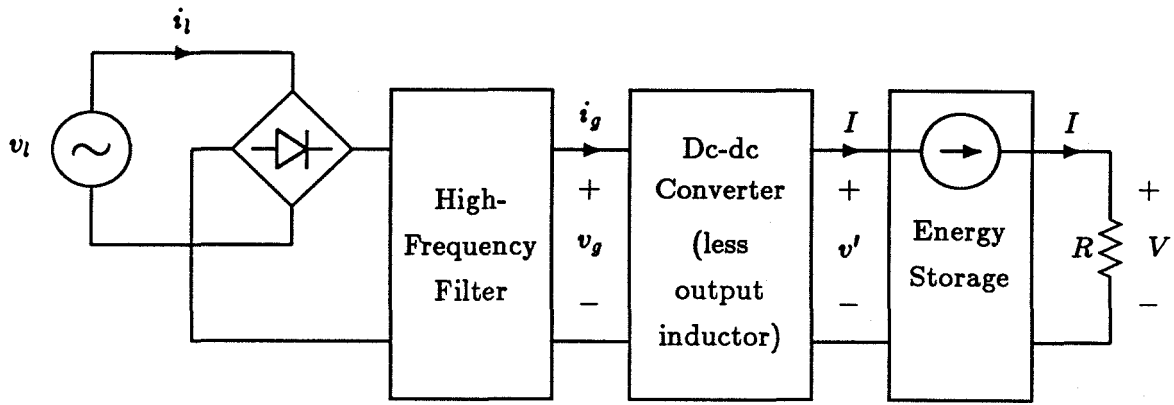
# Using Dc-Dc Converters in Shaping Applications

Three kinds of active current-shaping circuits were studied in the previous chapter. The buck-based circuits modulate the current from a stiff inductor to create a PWM waveform approximating the desired input-current waveform. Circuits based on a boost converter control the input current by applying a PWM voltage to the input inductor. Finally, circuits using buck, boost, or buck-boost (flyback) converters in the discontinuous conduction mode (DCM) shape the input current “automatically.”

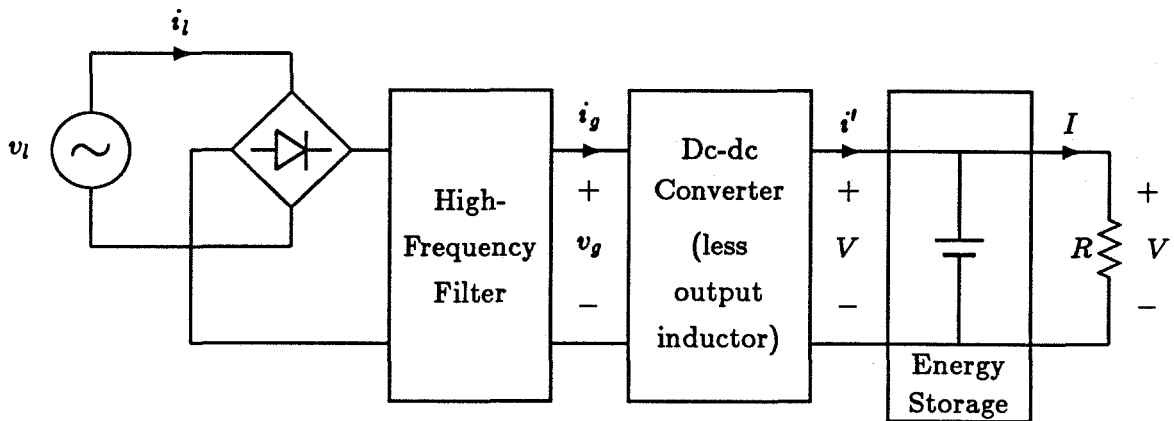
The question now arises, what other dc-dc converters might be suitable as current shapers? In addition to the buck and boost, several other PWM converter topologies are used in dc-dc conversion. Beyond the more common PWM topologies are many resonant topologies, currently a topic of much interest for high-frequency power conversion. This chapter develops criteria for determining how dc-dc converters behave in shaping applications, and whether a given topology is suitable for shaping, “automatic” or otherwise.

### 14.1 Environment of a Shaping Converter

The block diagrams of Fig. 14.1 illustrate the role played by a dc-dc converter topology when used as a current shaper. A rectifier bridge and (sometimes optional) high-frequency filter connect the power line to the converter. The box labeled “dc-dc converter” is a dc-dc power-converter topology with the output filter element removed. For converters in which the load and its parallel capacitor are fed by an inductor, this filter element is the output inductor. Such converters are said to have current-fed loads. The buck converter is an example, but not all buck-like shapers have current-fed loads. In a



(a)



(b)

Figure 14.1: Block diagrams illustrating the function of a dc-dc converter acting as a current shaper. A converter with a current-fed load (a) supplies a constant current to the dc load. If the converter has a voltage-fed output (b), the converter output voltage is dc.

converter with a voltage-fed load, the load and its capacitor are fed by pulsating currents and the output filter element is the load capacitor. The boost and flyback converters both have voltage-fed loads.

With the output filter element removed, the dc-dc converter stores insignificant energy, meaning that its element values are functions only of the *switching* frequency, not of the *line* frequency. To provide energy storage and maintain dc waveforms at the load, the output filter element of the converter is made very large, or is made to *appear* very large. The necessity for energy storage and the methods of making large apparent filter elements are discussed in Chapter 15.

### Current-Fed Output

Figure 14.1(a) shows the situation found in shapers with current-fed loads. The energy storage takes place at the converter output either in a large inductor or in a set of elements mimicking a large inductor. The effect in any case is to draw a nearly constant load current  $I$  from the converter. A converter with a voltage-fed load, illustrated in Fig. 14.1(b), instead has a large capacitor or other circuit maintaining a constant voltage  $V$  at the converter output. For the present, only these two cases in which the energy storage occurs directly at the converter output are considered. It is possible for current-shaping converters to store energy “internally,” in elements that do not have constant voltage or current and are not connected directly to the load. However, such circuits require extra switches and control and are not “basic” dc-dc converter topologies. Some examples, from [47], are mentioned in Section 15.2.4.

Consider first the case of a current-fed output, shown in Fig. 14.1(a). When the dc-dc converter topology performs *dc-dc* conversion, the average of the voltage  $v'$  over *each* switching cycle is equal to the dc output voltage  $V$ . The output inductor is in steady-state and is “volt-second balanced.” This fact is often used for calculating the conversion ratio and operating point of the converter.

When used in a current-shaping *ac-dc* application, however, the output inductor is no longer in steady-state. Over a *line* period the average of  $v'$  is  $V$ , but the switching-frequency-averaged voltage  $\bar{v}'$  is not constant. A significant line-frequency voltage ap-

appears across the inductor (or other energy-storage circuit), and this is why the inductor must be large to maintain a constant current  $I$ .

The dc-dc converter operates with *apparent* conversion ratio  $M' \equiv \bar{v}'/v_g$ , where the symbol  $M'$  is used to distinguish the apparent (or operating-point) conversion ratio of the converter topology from the conversion ratio of the entire shaping circuit,  $M \equiv V/V_l$ . While  $M$  is a fixed, dc quantity, the ratio  $M'$  varies throughout the line cycle. By assumption, the converter (excluding the energy-storage circuitry) stores insignificant energy, so that the current conversion ratio  $\bar{i}_g/I$  is also equal to  $M'$ .

The *apparent load* of the dc-dc converter is designated  $R'$ , determined by  $R' = \bar{v}'/I$ . Since  $\bar{v}'/\bar{v}_g$  and  $\bar{i}_g/I$  both equal  $M'$ , the apparent load is

$$R' = M'^2 \frac{v_g}{\bar{i}_g}. \quad (14.1)$$

The meaning of the apparent conversion ratio  $M'$  and apparent load  $R'$  is this: when operating in a current shaper with instantaneous apparent load  $R'$  and apparent conversion ratio  $M'$ , the state variables and control inputs—that is, the operating point of the converter—are the *same* as when the converter operates as a dc-dc converter with steady-state dc load  $R'$  and conversion ratio  $M'$ . Given the variations of  $M'$  and  $R'$  in a shaping application, one can determine the necessary range of control inputs from the well-known dependence of  $M'$  on load and control when performing dc-dc conversion.

### Voltage-Fed Output

In a shaper with a voltage-fed output, the case shown in Fig. 14.1(b), energy storage takes place in a constant-voltage circuit, such as a large capacitor. The dc-dc converter delivers a switching-frequency-averaged current  $\bar{i}'$  to the energy-storage circuit. In this case, the apparent conversion ratio of the dc-dc converter is  $M' = V/v_g$  which is also equal to  $\bar{i}_g/\bar{i}'$  as a result of the converter's insignificant energy storage. The apparent load  $R'$  is  $V/\bar{i}'$ . An important result is that the apparent load, when expressed in terms of the input quantities and apparent conversion ratio  $M'$ , is the *same* as for the case of a current-fed output, given in Eq.(14.1) above.

## Operating-Point Variations of Shaping Converters

For converters with unity power factor, the line voltage and line current are in-phase sine waves. The time-varying input power is therefore

$$P_{in}(\theta) = 2P \sin^2 \theta , \quad (14.2)$$

where  $P$  is the power in the dc load (neglecting losses in the shaping circuitry). This must be the same power delivered to the energy-storage circuit since the high-frequency filter and dc-dc converter store insignificant energy.

In converters with current-fed loads, corresponding to Fig. 14.1(a), the voltage  $\bar{v}'$  varies as

$$\bar{v}'(\theta) = \frac{P_{in}(\theta)}{I} \quad (14.3)$$

so that the apparent resistance  $R'$  is

$$R'(\theta) = \frac{\bar{v}'}{I} = 2R \sin^2 \theta . \quad (14.4)$$

The apparent resistance of a converter with current-fed output varies at twice the line frequency between zero and a value equal to twice the dc load resistance.

In a converter with voltage-fed output, as in Fig. 14.1(b), the current  $\bar{i}'$  varies as

$$\bar{i}'(\theta) = \frac{P_{in}(\theta)}{V} \quad (14.5)$$

and the apparent resistance is

$$R'(\theta) = \frac{R}{2 \sin^2 \theta} . \quad (14.6)$$

The apparent resistance of a converter with voltage-fed output varies between infinity and one-half the dc load resistance.

## 14.2 Necessary Conditions for Shaping

The goal of current shaping is to maintain the ratio  $v_g/\bar{i}_g$  at a constant value, called the emulated resistance,  $R_{em}$ . With the ratio  $v_g/\bar{i}_g$  held constant at the value  $R_{em}$ , Eq.(14.1) implies that

$$\frac{R'}{M^2} = R_{em} . \quad (14.7)$$

This equation yields a surprising amount of information about the requirements on a dc-dc converter used as a shaper.

Equation (14.7) is a *necessary* condition for dc-dc converters operating as current shapers. Any converter that fits one of the block diagrams of Fig. 14.1 must operate according to Eq.(14.7). However, not every dc-dc converter can be used as a shaper in the manner of Fig. 14.1. In some converters, the requirements of a constant dc load and proportional input voltage and current force the converter to have line-frequency energy storage. This means that one or more elements in the converter, *in addition to* the energy-storage elements at the dc load, must be sized according to the line frequency instead of the switching frequency. Converters with this requirement for large internal elements suffer from extra size and weight without any added benefits, except possibly isolation.

Consider, for example, the flyback topology of Fig. 13.11, but now operating in the continuous conduction mode (CCM). The current  $I_L$  in the inductor  $L$  is now assumed to be nearly constant. The average input current is

$$\bar{i}_g(\theta) = d(\theta)I_L . \quad (14.8)$$

The duty ratio  $d(\theta)$  must therefore be sinusoidal,  $D_m \sin \theta$ . The switching-frequency-averaged voltage across the inductor is

$$\overline{v}_L(\theta) = D_m V_l \sin^2 \theta - (1 - D_m \sin \theta) V . \quad (14.9)$$

The average of  $v_L$  over a cycle of the line must of course be zero, but Eq.(14.9) has components at the line frequency ( $\sin \theta$ ) and components at twice the line frequency (from the  $\sin^2 \theta$  term). The inductor is subject to line-frequency voltages and must be correspondingly large.

The flyback topology in CCM provides isolation, a very useful feature, but the flyback inductor (or transformer magnetizing inductance) must store large amounts of energy, regardless of how high the switching frequency is raised. Because the stored energy is significant, Eq.(14.7) cannot be used to find the operating point of this converter when it is used as a shaper.



A second necessary condition for dc-dc converters acting as shapers with small energy storage takes into account the problem found in the flyback topology. The following procedure determines whether a converter has, like the flyback converter, limitations that prevent low-energy shaping. Starting with a dc-dc converter topology,

1. Remove any input or output filters, so that only the basic topology remains.
2. Remove the output filtering element, either an inductor (in the case of a current-fed output) or a capacitor (in converters with voltage-fed outputs).
3. If the topology has an inductor in series with the input, this inductor may be removed. On the assumption that shaping is possible, high-frequency modulation controls the voltage on this inductor, and the element can be made small by raising the switching frequency.

Now look at each remaining reactance. If the element is an inductor, find what determines its average voltage. If it is a capacitor, find what determines the average current. When converting a dc input to a dc output, these averages are always zero, but it must be determined whether this “resetting” of reactive state variables will occur when the converter is used as a shaper.

If the current in an inductor returns to a fixed value at the end of every cycle (equivalent to the inductor having zero average voltage), *regardless of operating point*, then this effect will remain when shaping is performed. For example, in the flyback converter in DCM, the inductor current is clamped to zero at the end of every switching cycle by the conduction of a rectifier, regardless of the value of other voltages and currents in the circuit. Similarly, in the quasi-resonant topologies to be examined in Section 14.4.4, the resonant inductor current is clamped to a fixed value by a diode turning OFF. The size of these inductances in the DCM flyback and quasi-resonant converters can be independent of the line frequency when the converters are used as shapers.

When the flyback converter is CCM, however, the average voltage across the inductor (or magnetizing inductance) is determined by the input voltage, the output voltage, and the duty ratio of the switch. In the dc-dc application, the inductor has zero average voltage during each switching cycle only because the converter is in steady-state,

drawing dc power from the source and supplying the same dc power to the load. In a shaping application, in which the converter topology is not in steady-state, the switching-frequency-averaged inductor voltage is not zero. The inductor, seeing a line-frequency voltage, must be sized according to the line frequency and is therefore large.

In any converter in which the resetting of an inductor depends on the input voltage or current, or on the other states—in other words, on the operating point of the converter—one can expect that the inductor will be large. The converter cannot provide shaping while storing energy only in the output filter.

Likewise, if after carrying out the steps above a capacitor is found to have a switching-frequency-averaged current which depends on the operating point of the converter, then that capacitor will be large when the converter is used as a shaper.

### 14.3 Automatic Current Shaping

Section 13.3 of Chapter 13 analyzed the operation of three converter topologies which, when operated in DCM, yield unity or near-unity power factor without intelligent control. That is, the average input current is proportional to the input voltage even when the control (switching frequency and duty ratio) is held constant. Equation (14.7) now provides a tool for determining *without any analysis* whether or not a dc-dc converter can provide automatic current-shaping.

To provide constant  $v_g/\bar{i}_g$ , *i.e.*, unity power factor, the ratio  $R'/M'^2$  must be constant. For this ratio to be constant without benefit of control, the converter must have

$$M' \propto \sqrt{R'} \quad (14.10)$$

over its entire operating range when the control is fixed. Any converter satisfying this relation will automatically provide unity power factor, in the limit of high switching frequency.

For example, in Section 13.3.1 the flyback topology in DCM was found to have unity power factor with fixed control. The conversion ratio of this topology in DCM, when used as a dc-dc converter, is [16]

$$M' = \frac{D\sqrt{T_s}}{\sqrt{2L}} \sqrt{R'} . \quad (14.11)$$

When switching frequency ( $1/T_S$ ) and duty ratio  $D$  are held constant, the conversion ratio is proportional to the square root of the load resistance.

When operated as a dc-dc converter, the resonant-pulse shaping circuit of Section 13.3.4 has a conversion ratio

$$M' = \sqrt{\frac{1}{\pi} \frac{F_S}{F_0} \frac{R'}{R_0}}, \quad (14.12)$$

as given in Eq.(13.50). With constant switching frequency, the conversion ratio satisfies Eq.(14.10) and current shaping is automatic.

Another converter satisfying Eq.(14.10) is the Ćuk converter operated in the discontinuous capacitor-voltage mode (DCVM) [42]. The conversion ratio of this converter is

$$M' = \frac{1}{D'} \sqrt{\frac{2C}{T_S}} \sqrt{R'}, \quad (14.13)$$

where  $D'$  is the fractional OFF-time of the transistor switch. When operated in this mode with high enough switching frequency, the converter provides unity power factor with constant switching frequency and  $D'$ .

The procedure of Section 14.2 can be used to show that the Ćuk topology in DCVM can operate as a shaper with little stored energy. The input and output inductors are removed according to the procedure, and the current in the capacitor over a single switching period is observed. By definition of DCVM, the capacitor voltage is returned to zero at the end of the ON ( $DT_S$ ) interval, so that its average current is always zero. Since the capacitor voltage is reset regardless of the input and output voltages and regardless of the current in the two inductors, the topology operates as a shaper without line-frequency energy storage.

If the same topology is operated in the discontinuous inductor-current mode (DICM), it still has a conversion ratio  $M'$  proportional to the square root of the apparent load  $R'$  [43]. However, following the procedure of Section 14.2 shows that the resetting of the capacitor depends on the duty ratio and the relative currents in the two inductors. As these quantities vary during a period of the line, the average current in the capacitor varies as well. The capacitor must store significant energy, and must be sized according to the line frequency.

## 14.4 Resonant Converters as Shapers

Resonant dc-dc converters offer the advantages of low switching loss and insensitivity to certain parasitic reactances, characteristics that permit high-frequency switching. In the constant effort to reduce the size and weight of switching converters, such high-frequency operation is very attractive. This section examines the possibility of using resonant dc-dc converters as input-current shapers with small internal energy storage. Two features are of particular interest: the possibility of an “automatic” shaping mode as in the previous section, and limitations of the converters that would restrict or prevent their use in ac-dc conversion.

The resonant converters considered here are the series- and parallel-resonant converters and the quasi-resonant buck and boost converters discussed in Part I.

### 14.4.1 The Output Plane

If one assumes that a resonant dc-dc converter used as a shaper has no line-frequency energy storage, then the ac-dc converter system fits one of the block diagrams of Fig. 14.1. The concepts of apparent load  $R'$  and apparent conversion ratio  $M'$  can be used to determine the necessary operating-point excursions of a current-shaping resonant converter.

The *output plane* is a plot of normalized output current versus normalized output voltage. For a dc-dc converter, the output voltage is divided by the input voltage to obtain the normalized output voltage. In a shaping converter, this quantity is simply  $M'$ , the apparent conversion ratio. The normalized output current is defined by

$$J' \equiv R_0 \frac{(\text{output current})}{(\text{input voltage})}, \quad (14.14)$$

where  $R_0$  is some normalizing resistance, usually the characteristic resistance of a resonant tank. The normalized output current can be related to the apparent load  $R'$  by

$$J' = \frac{R_0 M'}{R'}. \quad (14.15)$$

Combination of Eq.(14.15) with Eq.(14.7) reveals that

$$M' J' = \frac{R_0}{R_{em}} \quad (14.16)$$

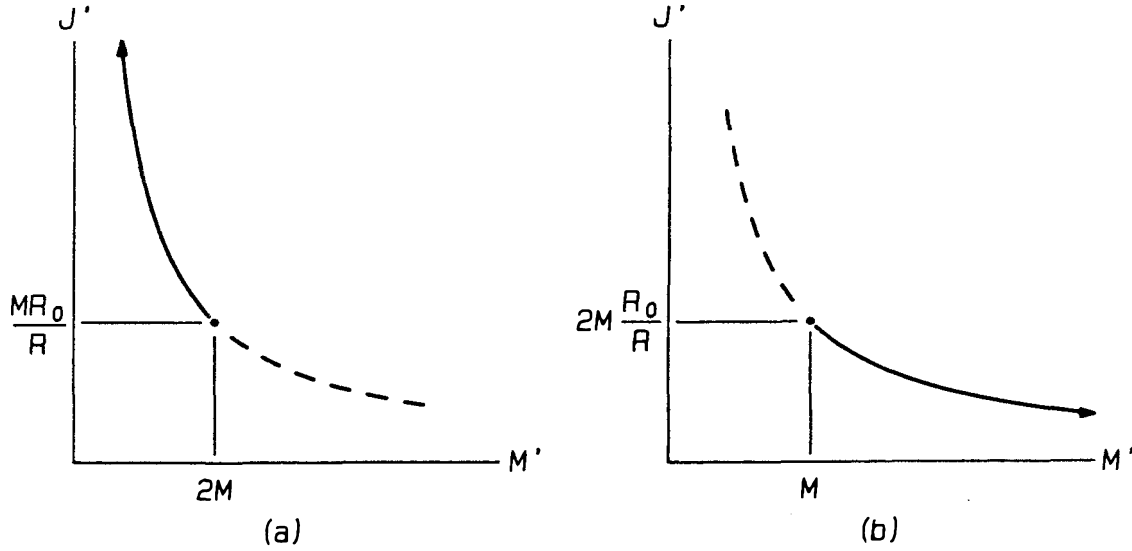


Figure 14.2: Locus of points in the output plane traversed by current-shaping dc-dc converters with (a) current-fed and (b) voltage-fed outputs.

for a current-shaping converter. In the output plane, with  $J'$  plotted versus  $M'$ , Eq.(14.16) defines a hyperbola.

For a converter with current-fed output, as illustrated in Fig. 14.1(a),

$$J' = \frac{R_0 I}{v_g}, \quad (14.17)$$

so that  $J'$  varies as  $1/\sin \theta$ . The apparent conversion ratio  $M'$  varies as  $\sin \theta$ , as seen in Section 14.1. Throughout a cycle of the line voltage, the operating point of a current shaper with current-fed output follows the curve shown in Fig. 14.2(a). As the input voltage approaches its cusp, the converter must have  $J' \rightarrow \infty$  and  $M' \rightarrow 0$  to maintain shaping.

For converters with voltage-fed outputs, shown in Fig. 14.1(a),

$$J' = \frac{R_0 \bar{i}'}{v_g} \quad (14.18)$$

which varies as  $\sin \theta$ , while the apparent conversion ratio is proportional to  $1/\sin \theta$ . The variation of the operating point of voltage-fed-output shapers is shown in Fig. 14.2(b). In such converters, shaping requires that  $J' \rightarrow 0$  and  $M' \rightarrow \infty$  at the cusp.

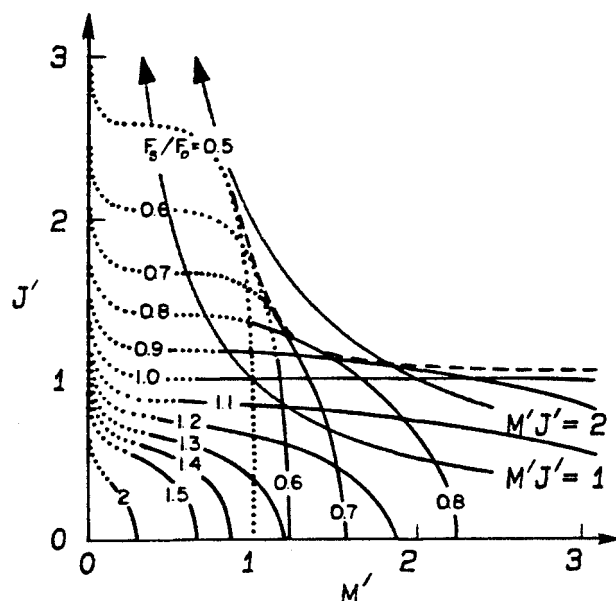


Figure 14.3: Output-plane curves for the parallel-resonant converter [44], overlaid with curves of constant  $M'J'$  necessary for current shaping.

#### 14.4.2 Parallel-Resonant Converter

The parallel-resonant converter [2] has a current-fed output. For good shaping, its operating point must follow a curve like that of Fig. 14.2(a).

In [44], the operation of the parallel-resonant converter is described by curves of constant control (switching frequency) in the output plane. These curves (taken from Fig. 4 of [44]) are shown in Fig. 14.3, overlaid by the hyperbolic operating-point curves needed for good shaping.

Two conclusions can be drawn from this figure. First, the parallel-resonant converter does not provide automatic current shaping. With the control (switching frequency) fixed, none of the operating-point curves approximates a hyperbola. To achieve an undistorted input current, the switching frequency must be changed throughout a cycle of the line. A second conclusion is that the switching-frequency excursion must be large, and even so it is not possible to follow the cusp of the input voltage, where shaping requires  $M' \rightarrow 0$  and  $J' \rightarrow \infty$ . Since the converter is incapable of reaching this operating point, some distortion must occur near the cusp.

Note that the failure to follow the cusp is a different effect than that found in fast-

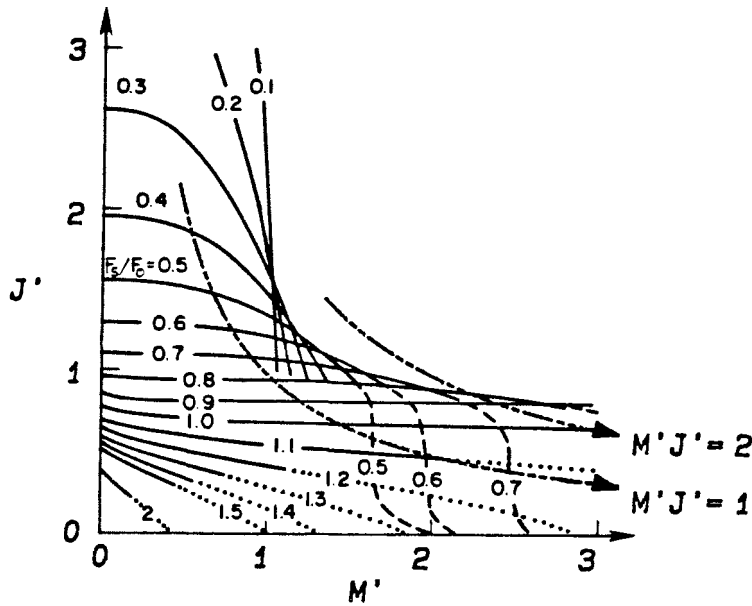


Figure 14.4: Output-plane curves for the parallel-resonant converter with no output inductor [44], overlaid with curves of constant  $M'J'$  necessary for current shaping.

switching buck or boost PWM shapers. In the PWM converters, low-pass filters at the input prevented reproduction of the high-frequency components of the cusp. In the parallel-resonant converter, however, the dc-dc topology itself is unable *in steady-state* to provide low output voltages at high (normalized) output currents. In both PWM and resonant converters, inability to follow the cusp does not mean that good shaping is impossible. The bottom of the cusp represents a small portion of the total energy delivered to a converter. If the deviation from proportional input current can be confined to a small fraction of the input waveform, high power factor can still be achieved. From Fig. 14.2(a), one can surmise that operating the converter at high output voltage (large  $M$ ) shifts the operating curve further into the allowed region, lessening the fraction of time in which shaping is lost.

In [44], the behavior of the parallel-resonant converter with the output inductor removed is also studied. In this case, the converter has a voltage-fed output. Figure 14.4 curves from Fig. 12 of [44]. Without an output inductor, the parallel-resonant converter still does not shape current automatically, but it is able to follow the cusp of the input

voltage. A relatively small switching-frequency excursion is sufficient for good regulation and control.

#### 14.4.3 Series-Resonant Converter

The series-resonant converter [1] has a voltage-fed output, with pulsating currents feeding the load and its capacitor. Hence the apparent conversion ratio  $M'$  varies as  $1/\sin \theta$  and the apparent load as  $1/\sin^2 \theta$ . Current shaping therefore requires that  $M'$  approach infinity. The series-resonant converter, however, is unable to provide conversion ratios greater than unity. It is not possible for the series-resonant converter to operate as a current shaper with small internal energy storage.

#### 14.4.4 Quasi-Resonant Converters as Shapers

The approximate analysis of quasi-resonant converters in Part I provides an excellent tool for determining the behavior of these converters in shaping applications. Only the buck and boost topologies are considered here, since these circuits can operate as shapers according to Fig. 14.1. In contrast, a quasi-resonant flyback current shaper, just like its PWM parent (in CCM), must store large amounts of energy in both the transformer and the output capacitor.

The operating point of a quasi-resonant converter is described by the parameter  $\rho$ ,

$$\rho = \frac{R_0 I_{\text{on}}}{V_{\text{off}}} = \frac{M' R_0}{R'} , \quad (14.19)$$

which is exactly the normalized output current  $J'$  from Eq.(14.15). The behavior of quasi-resonant converters as shapers will be studied by plotting the conversion characteristics in the output plane. First, a fixed value of control variable  $F_S/F_0$  is chosen, then for every permissible value of  $\rho$  or  $J'$  the conversion ratio  $M'$  is calculated. The resulting curves of constant control in the  $M'$ - $J'$  plane can then be compared to the hyperbolas of constant  $M'J'$  that must be followed during current shaping.

Every quasi-resonant converter has a limited operating range. For zero-current switching converters, the converter must satisfy  $0 < J' < 1$ . With zero-voltage switching, the requirement becomes  $1 < J' < \infty$ . The consequence of violating these limits on  $J'$  is a failure of the resonant switch to turn ON or OFF with zero stress. For example,



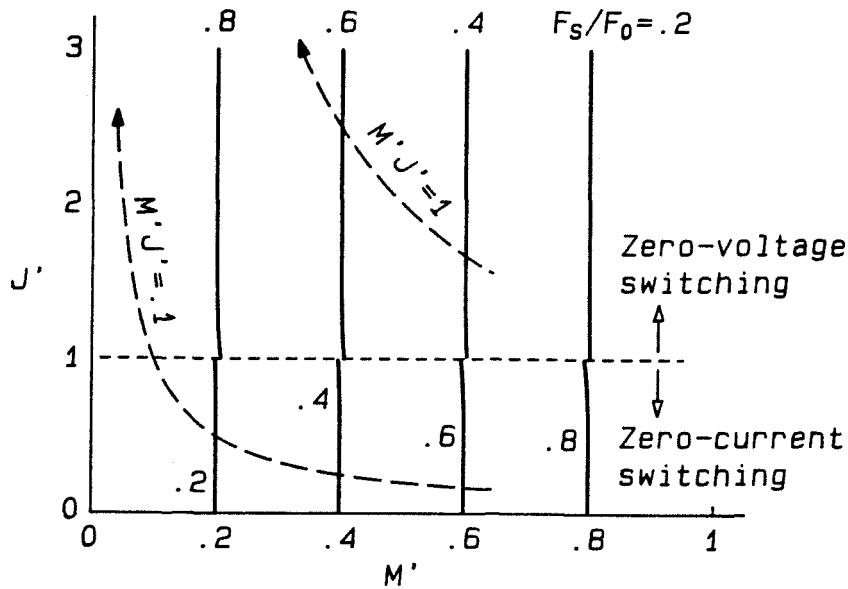


Figure 14.5: Operating curves for the full-wave quasi-resonant buck converter, overlaid with curves of constant  $M'J'$  necessary for current shaping.

if  $J'$  exceeds unity in a zero-current resonant switch, the resonant circuit cannot bring the switch current back to zero. Such a turn-OFF is actually *worse* than in a PWM converter because some inductance is intentionally put in series with the switch in the quasi-resonant converter. When attempting to interrupt the current in this inductor, the active switch will experience a voltage spike.

### Buck Topology

Figures 14.5 through 14.7 show operating curves for quasi-resonant buck converters, overlaid with the constant  $M'J'$  curves that a current shaper must follow. The figures cover the four permutations generated by the options of zero-current or zero-voltage switching, and half-wave or full-wave resonant switches.

With a full-wave resonant switch, a quasi-resonant buck converter has virtually the same control characteristics as a PWM buck converter, except that the ratio of switching to resonant frequency,  $F_S/F_0$ , replaces the duty ratio as the control variable. The operating curves, shown in Fig. 14.5, are nearly vertical lines. For zero-current operation, the converter must operate below  $J' = 1$ , and with a zero-voltage switch operation is

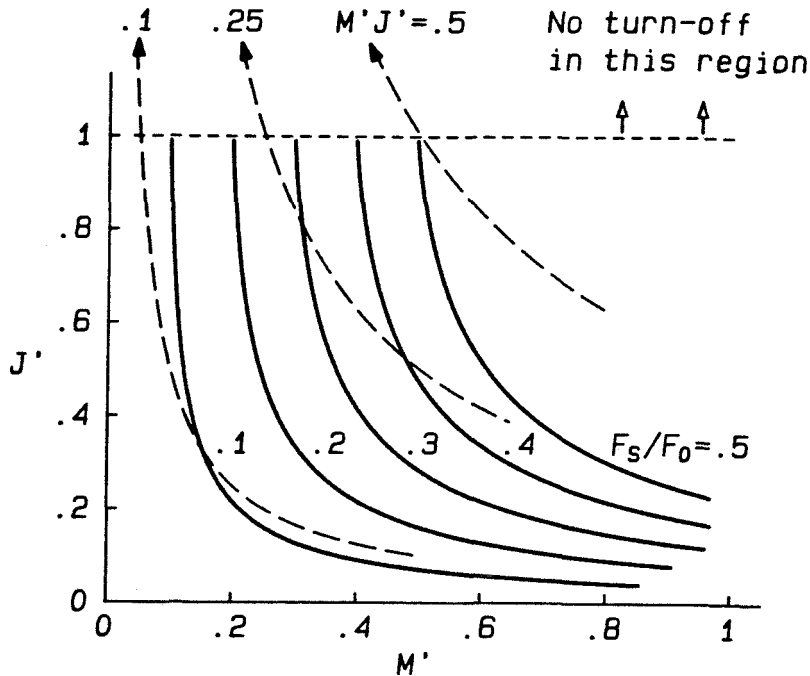


Figure 14.6: Operating curves for the zero-current switching, half-wave buck converter, overlaid with curves of constant  $M'J'$  necessary for current shaping.

confined to  $J' > 1$ . The conversion ratio  $M'$  is always less than unity.

Since a quasi-resonant buck converter has a current-fed output,  $J'$  varies as  $1/\sin \theta$  during shaping, and therefore becomes arbitrarily large. Zero-current switching requires  $J' < 1$  for zero-current turn-OFF, however, so that a buck converter with a zero-current resonant switch will fail to turn OFF near the cusp of the input voltage. The zero-voltage version is better suited to shaping, and is capable of providing the required range of  $J'$  while maintaining zero-voltage turn-OFF. The switching frequency in the zero-voltage converter must range from some minimum value up to the resonant frequency.

Figure 14.6 shows the operating curves for a zero-current switching, half-wave buck converter. The half-wave resonant switch “bends” the curves in the output plane in a way that aids shaping. The zero-current converter still suffers from an inability to follow the constant  $M'J'$  shaping curve above  $J' = 1$ . If the turn-OFF failure can be tolerated and confined to a small portion of the cusp, however, the half-wave converter requires a much smaller variation of switching frequency to achieve proportional input current.

The output curves for the zero-voltage switching, half-wave buck converter are shown

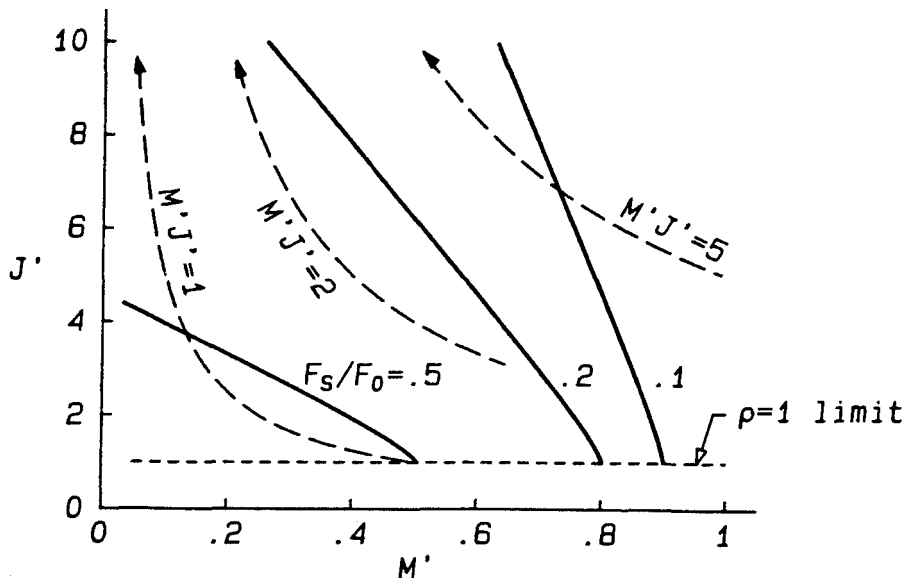


Figure 14.7: Operating curves for the zero-voltage switching, half-wave buck converter, overlaid with curves of constant  $M'J'$  necessary for current shaping.

in Fig. 14.7. The converter can follow a curve of constant  $M'J'$  up to arbitrarily large  $J'$ . Here again, the half-wave switch introduces an output resistance that allows shaping with a relatively small variation in switching frequency.

With the switching frequency fixed, none of the quasi-resonant buck converter variations provide automatic current shaping. The half-wave resonant switch does lend some help in this direction, however, allowing a smaller range of control variation than in PWM or full-wave buck converters.

### Boost Topology

A quasi-resonant boost converter has a voltage-fed output, so that at the cusp of the input voltage  $M' \rightarrow \infty$  and  $J' \rightarrow 0$ . A zero-current-switching boost topology is therefore able to follow  $J'$  down to zero, but the switch in a zero-voltage-switching converter will fail to turn OFF as  $J'$  falls below unity.

Operating curves for full-wave quasi-resonant boost converters are shown in Fig. 14.8, overlaid with constant  $M'J'$  shaping curves. Only the zero-current-switching converter can follow the cusp as  $J' \rightarrow 0$ . Just as in the PWM boost converter, a large range of the

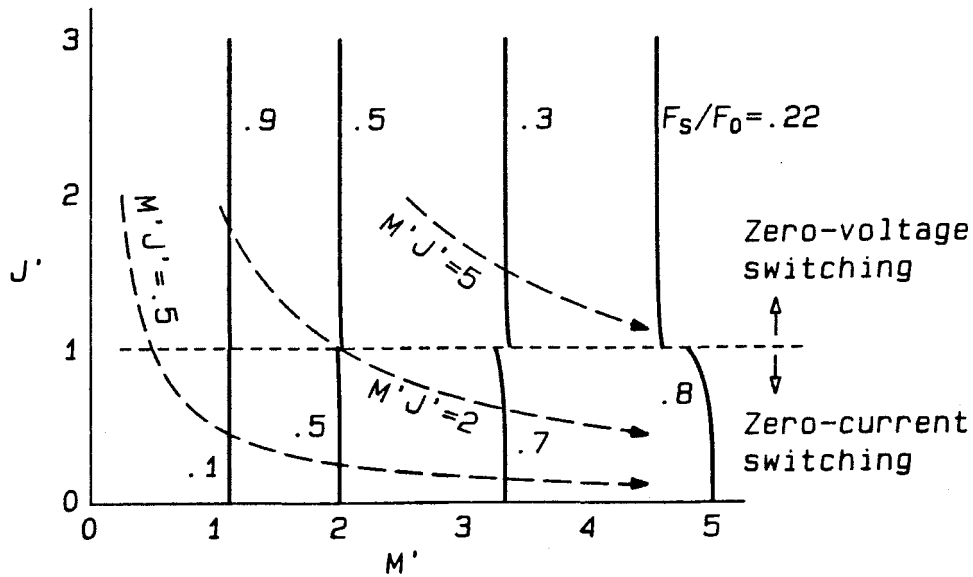


Figure 14.8: Operating curves for full-wave quasi-resonant boost converters, overlaid with curves of constant  $M'J'$  necessary for current shaping.

control variable is required to provide shaping.

In Fig. 14.9, the output curves of the zero-current, half-wave boost converter are overlaid with the constant  $M'J'$  shaping curves. The half-wave switch helps the shaping considerably, bending the operating curves in the output plane so that a small variation of switching frequency can provide shaping. The curves for the zero-voltage, half-wave boost converter, shown in Fig. 14.10, are also a fair approximation to the shaping curves, but this converter cannot turn OFF below  $J' = 1$ .

In summary, half-wave quasi-resonant converters are good candidates for current shaping. The half-wave resonant switch changes the vertical output curves of the parent PWM converter into closer approximations to the constant  $M'J'$  shaping curves. The zero-voltage-switching buck converter and zero-current-switching boost converters are the best candidates because they are able to follow the cusp of the input voltage without losing the valuable property of zero-current or zero-voltage turn-OFF.

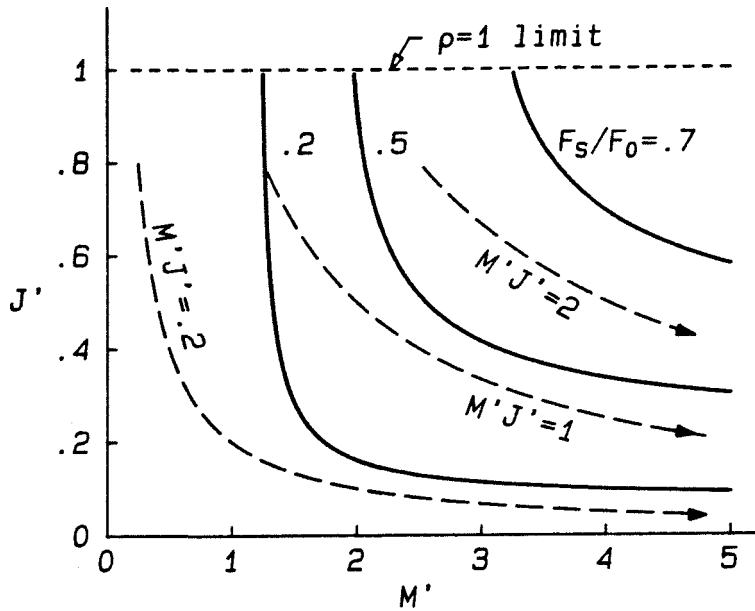


Figure 14.9: Operating curves for the zero-current switching, half-wave boost converter, overlaid with curves of constant  $M'J'$  necessary for current shaping.

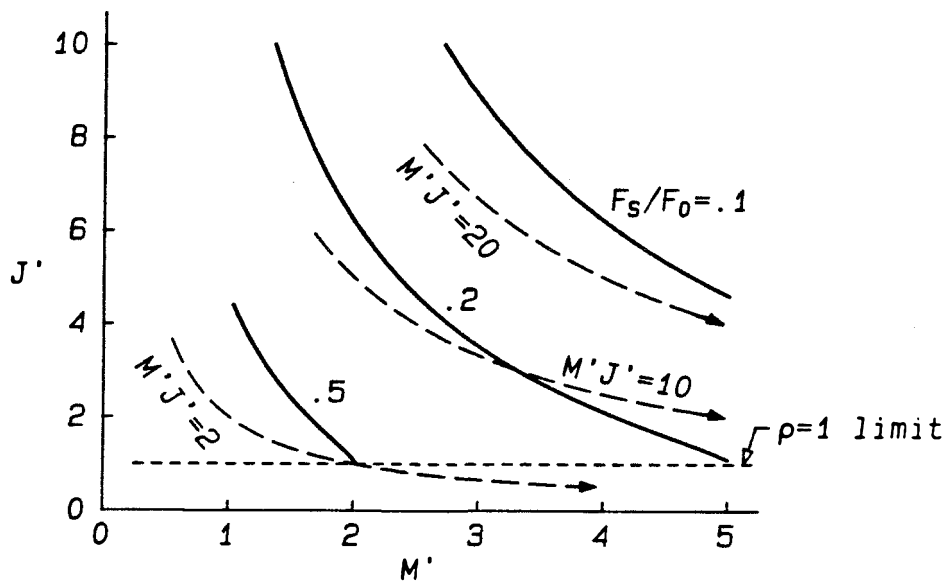


Figure 14.10: Operating curves for the zero-voltage switching, half-wave boost converter, overlaid with curves of constant  $M'J'$  necessary for current shaping.



## Chapter 15

# Energy Storage

All single-phase ac-dc converters with good power factor must store a significant amount of energy. This unfortunate fact is at the heart of many of the problems of single-phase ac-dc conversion. Large amounts of stored energy increase the volume, weight, and cost of a power converter. Moreover, the large reactive elements needed to store the energy force the converter to behave sluggishly and to respond slowly to commands and disturbances.

The necessity for stored energy and the theoretical limit on minimum stored energy is first derived, then several energy-storage methods are examined. The chapter concludes with a discussion of the implications of energy storage.

### 15.1 Minimum Stored Energy

The amount of energy a current-shaping power processor must store to balance the difference between input and output power depends on the input-current waveform. The stored-energy requirement is found here for the ideal case of sinusoidal, in-phase current. Other, less ideal, waveforms may yield slightly different requirements, but the important result remains that a current shaper must store energy, and the minimum amount stored is limited by the line frequency and the processed power, regardless of internal switching frequency.

Consider a converter with 100% efficiency drawing an in-phase, sinusoidal current from the line and delivering constant power  $P$  to a load. The input voltage  $v_l$  and current  $i_l$  both vary as  $\sin \theta$ ,

$$v_l(\theta) = V_l \sin \theta \quad (15.1)$$

$$i_l(\theta) = \frac{V_l}{R_{em}} \sin \theta, \quad (15.2)$$

so that the input power is

$$P_{in}(\theta) = 2P \sin^2 \theta = P(1 - \cos 2\theta) . \quad (15.3)$$

The difference between the input power and the output power is absorbed by the converter. Since no energy can be lost, this power difference must alternately increase and decrease the stored energy of the converter. The change in stored energy is the integral of the absorbed power, plus some constant:

$$U(\theta) = \int -P \cos 2\theta dt = -\frac{P \sin 2\theta}{2\omega_l} + U(0) . \quad (15.4)$$

Since the stored energy must always be positive, the value of  $U(0)$  must be at least  $P/2\omega_l$ .

The peak stored energy is then

$$U_{peak} \geq \frac{P}{\omega_l} . \quad (15.5)$$

The converter must contain a set of inductors and/or capacitors that store at least this amount of energy at some point in each half cycle of the line voltage.

This restriction on stored energy does *not* apply to converters operating from a three-phase line, because three-phase sinusoidal currents draw constant power. With both input and load power constant, no power imbalance need be absorbed by the converter. Minimum stored energy can be a function of the switching, not the line frequency, and the reactive elements can therefore be smaller.

In dc-dc converters, energy stored in the converter itself (exclusive of any hold-up capacitors) can be reduced by raising the switching frequency. (This is one reason for the present interest in high-frequency resonant converters.) Converters used for single-phase current shaping, however, have an energy-storage requirement that is *independent* of switching frequency.

## 15.2 Energy Storage Methods

Every current-shaping power converter must satisfy the energy-storage requirement. Although the storage methods discussed here are illustrated on specific active shapers, the techniques will work with other fast-switching active circuits. Some of the storage techniques are applicable to passive shaping circuits as well.



### 15.2.1 Large Reactance

The simplest way to store energy under nearly constant voltage or current is to use a large capacitor or inductor, respectively. In the boost converter, for example, a large output capacitor is used to hold the output voltage constant, as in Fig. 13.5. With unity power factor, the current through this capacitor is a sinusoid at twice the line frequency. The capacitor takes up and releases energy to account for the difference between input and output power.

Define the ripple ratio  $\mathcal{R}$  as the ratio of one-half the peak-to-peak output ripple voltage to the average output voltage  $V$ . For a fast-switching current shaper with a voltage-fed load, the peak energy in the energy-storage capacitor is then given by

$$U_{pk} = \frac{P}{\omega_l} \frac{1}{2\mathcal{R}}. \quad (15.6)$$

Specifying a small output ripple voltage, and hence a small  $\mathcal{R}$ , demands a large value of  $C$  and excessive stored energy. The peak energy stored in the capacitor is much greater than that required by theoretical power balancing because of the large capacitance necessary to keep the ripple voltage small while a large sinusoidal current flows.

An energy-storage capacitor has a large rms ripple current at twice the line frequency. In boost-like active current shapers, the same capacitor also has large rms currents at the switching frequency and its harmonics. High-frequency rms current capability and large capacitance in the same package requires a large and expensive capacitor. An alternative would be to use two capacitors in parallel, one of large capacitance to handle the line-frequency current, and another of small capacitance to absorb the switching ripple. In either case, the energy-storage capacitor will be expensive.

The output inductor of a converter with current-fed output plays the same energy-storage role as the capacitor of a converter with voltage-fed load. The inductor maintains its current constant while under a sinusoidal voltage. Equation (15.6) also gives the stored energy in the inductor for the case of a current-fed load, but in this case the ripple ratio  $\mathcal{R}$  refers to the ripple in the output current, rather than in the output voltage.

The high rms current in the energy-storage capacitor of a voltage-fed load corresponds to a large rms voltage across the filter inductor of a topology with current-fed load. The switching-frequency rms voltage on the inductor is not a major stress, however.

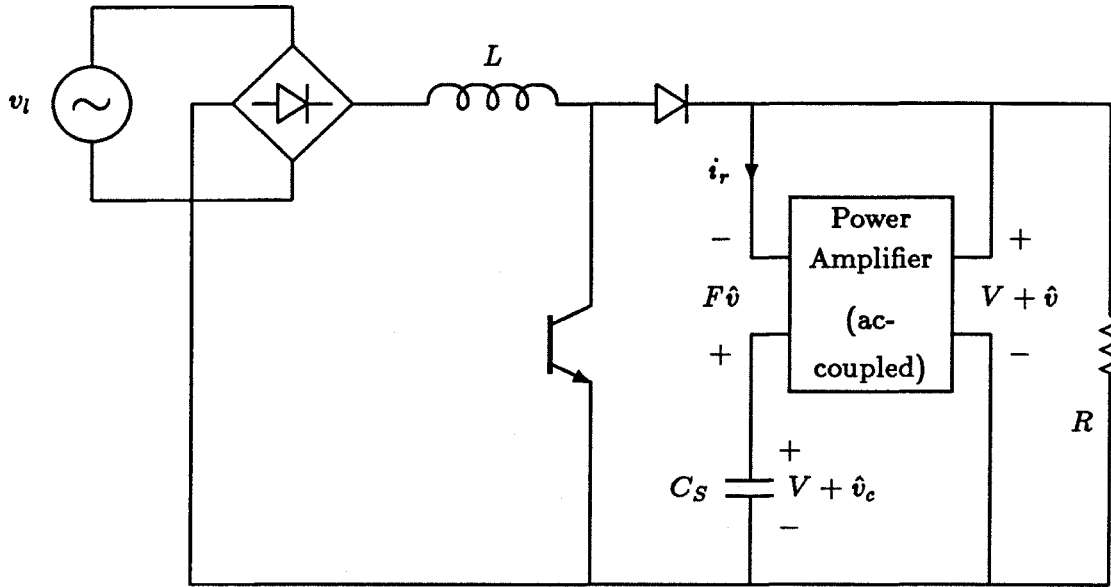


Figure 15.1: Super-capacitor filter in a boost current shaper.

### 15.2.2 Active Filter

A power amplifier can effectively multiply the value of a capacitance or inductance, producing the same ripple performance as a much larger reactance alone. The “super-capacitor” filter [45] is an example of this technique. A fast-switching inverter (power amplifier) and small capacitor  $C_S$  can replace the large capacitor in a current shaper with voltage-fed output, as in Fig. 15.1. If the voltage gain of the power amplifier is  $F$ , the ripple voltage  $\hat{v}_c$  on  $C_S$  is  $(1 + F)$  times the ripple at the output,  $\hat{v}$ . The ripple current  $i_r$  generated by current shaping is absorbed by the filter at the lower ripple voltage. While the impedance of the capacitor is  $Z_C = \hat{v}_c/i_r$ , the apparent impedance seen by the load is

$$\frac{\hat{v}}{i_r} = \frac{1}{1 + F} \frac{\hat{v}_c}{i_r} = \frac{1}{1 + F} Z_C . \quad (15.7)$$

A small capacitor  $C_S$  therefore simulates a much larger capacitance  $(1 + F)C_S$ , yet the peak voltage on  $C_S$  is still approximately  $V$ . A dual circuit for current-fed outputs could emulate a large inductance.

The peak energy stored in the capacitor is approximately

$$U_C = \frac{P}{\omega_l} \frac{1}{2F\mathcal{R}}, \quad (15.8)$$

where  $\mathcal{R}$  is the output-voltage ripple ratio. Compared to a capacitor alone (see Eq.(15.6)), the stored energy of the super-capacitor filter is smaller by a factor of  $F$ , a considerable improvement.

The super-capacitor filter offers only limited improvement, however. Closer study reveals that the filter must operate with  $F\mathcal{R} \ll 1$  for two reasons. First, if  $F\mathcal{R}$  exceeds this limit, the input current drawn by the power amplifier is no longer negligible. If this happens, the super-capacitor filter becomes a nonlinear circuit and draws a distorted current. Second, if  $F\mathcal{R}$  is not small then the power amplifier itself must store significant energy, a difficult task and one opposed to the purpose of the filter, which is to reduce the stored energy.

Although the super-capacitor filter offers a factor of  $F$  improvement over the stored energy of a capacitor alone, the restriction  $F\mathcal{R} \ll 1$  forces the stored energy to be much larger than the theoretical minimum value of  $P/\omega_l$ . Another drawback of the active filter is the expense of the power amplifier. The amplifier must be fast-switching and have a four-quadrant output. The amplifier need dissipate no power, however, since it operates in the switched mode.

The capacitance-multiplying effect of the super-capacitor filter is present only over a frequency range where  $|F|$  is large, that is, over the bandwidth of the power amplifier. The filter is therefore effective against the ripple-current component at  $2\omega_l$ , but unless the power amplifier's bandwidth exceeds the switching frequency, the components at and above the switching frequency see the actual capacitance  $C_S$  in series with the output impedance of the power amplifier. A small capacitor suitable for high-frequency currents may therefore be required in parallel with the super-capacitor filter to absorb the high-frequency currents produced by the "chopping" action of the semiconductor switch.

### 15.2.3 Resonant Filter

For fast-switching current shapers with near-unity PF, an alternative form of energy storage is the resonant filter, shown replacing the large capacitor of a boost shaper in

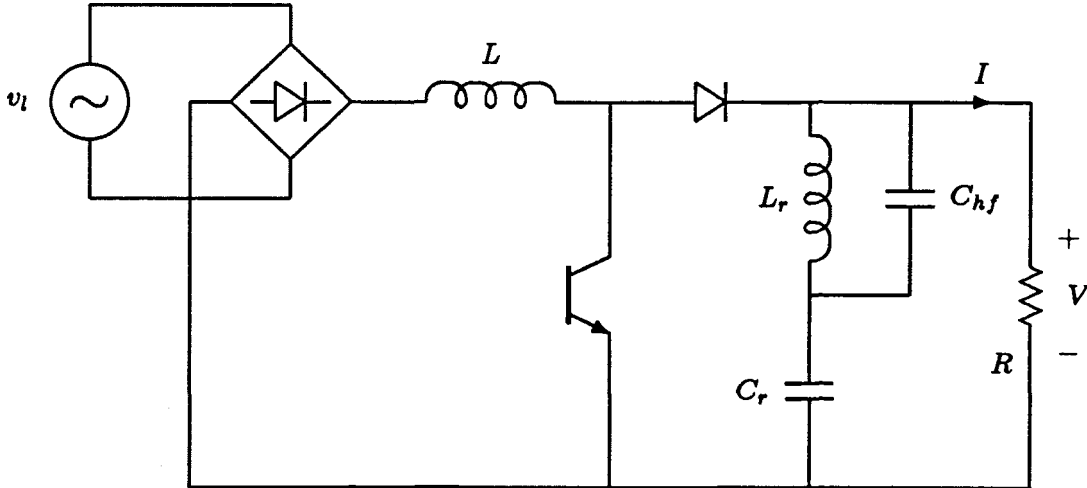


Figure 15.2: Resonant filter in a boost current shaper.

Fig. 15.2. This filter is discussed at length in [46], but the circuit is evidently widely known, judging by its mention in references [38] and [40].

Since the switching-frequency average of the current in the capacitor of a fast-switching boost shaper is sinusoidal at twice the line frequency, a resonant filter tuned to this frequency presents a low impedance to the current, providing small voltage ripple. The resonant capacitor  $C_r$  must see the same dc voltage as the single capacitor it replaces, but  $C_r$  can be much smaller for the same output voltage ripple. The small capacitor  $C_{hf}$  is necessary because the actual current in the filter is discontinuous as a result of switching, and a path must be provided around the resonant inductor for the high-frequency currents. (The capacitor  $C_{hf}$  effectively performs the switching-frequency average, leaving only a sinusoidal ripple current at frequency  $2\omega_l$  for the resonant filter to absorb.)

From the analysis in [46], the stored energy is a function of the  $Q$  of the filter and the allowable ripple voltage. To achieve a desired ripple ratio  $\mathcal{R}$  with a filter of quality factor  $Q$ , the resonant inductance must be

$$L_r = \frac{R}{2\omega_l Q \mathcal{R}} \quad (15.9)$$

with the resonant capacitor chosen to place the resonant frequency at  $2\omega_l$ . With these

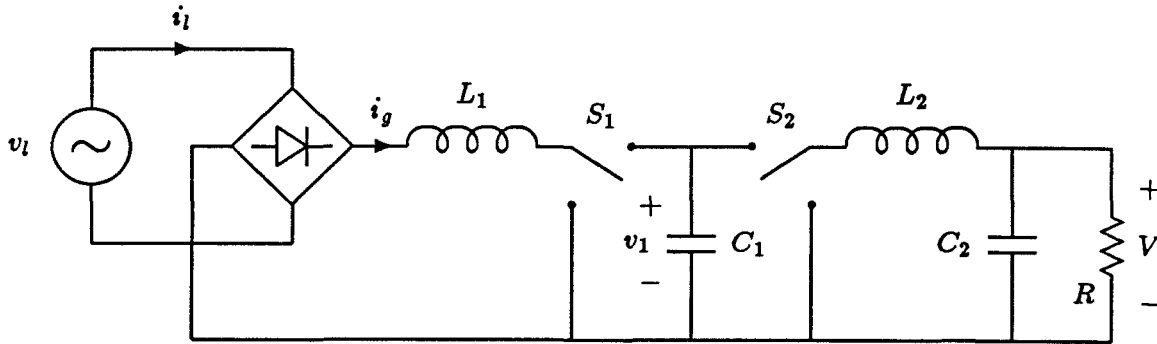


Figure 15.3: Topology used for directly controlling energy storage.

element values, the stored energies in the inductor and capacitor are

$$U_L = \frac{P (1 + Q\mathcal{R})^2}{\omega_l 4Q\mathcal{R}} \quad (15.10)$$

$$U_C = \frac{P Q\mathcal{R}}{\omega_l 4}. \quad (15.11)$$

The total stored energy is therefore a function of the product  $Q\mathcal{R}$ . The value  $Q\mathcal{R} = 1/\sqrt{2}$  produces the minimum total stored energy of about 1.2 times the theoretical minimum of Eq.(15.5). Note that a very small ripple ratio  $\mathcal{R}$  requires a correspondingly large  $Q$  to maintain a reasonable  $Q\mathcal{R}$  product and therefore keep the stored energy small.

The filter shown in Fig. 15.2 is applicable to any current-shaping topology with a voltage-fed output. For a fast-switching shaper with a current-fed load (the dual situation), a parallel-resonant filter can replace the output inductor, gaining the same advantages of less total stored energy.

#### 15.2.4 Active Control of Energy Storage

A recent approach confronts the energy-storage problem directly, choosing a topology and control scheme with the purpose of balancing the difference between input and output power [47]. An example of the proposed technique is shown in Fig. 15.3. The converter can be viewed as a boost shaper followed by a buck regulator. The inductor  $L_1$  is “small,” as in the boost current shaper, and stores insignificant energy if the switching frequency is far above the line frequency. Capacitor  $C_1$  provides the line-frequency energy storage.

Stored energy in this capacitor is “programmed” in the sense that its voltage is controlled to provide energy  $\frac{1}{2}C_1V_1^2$  that will balance the difference between the instantaneous input and output power with very little extra stored energy. The time-varying voltage across  $C_1$  is regulated by the buck post-converter so that the load voltage is dc.

In theory, the capacitor voltage changes to provide ideal energy storage while the switches on either side provide ideal input and output waveforms. However, to obtain precisely the theoretical minimum stored energy, the switch duty ratios must reach extreme values of 0 or 1, and the peak voltage across  $C_1$  (and hence the switch voltage stresses) must be arbitrarily large. For example, to obtain 1.21 times the theoretical minimum stored energy (the lowest value achievable by the resonant filter of Section 15.2.3), the circuit of Fig. 15.3 subjects its switches to voltage stresses of more than 2.5 times the line voltage when the conversion ratio is  $M = 1$  and the duty ratios are allowed to vary over the full range of 0 to 1.

An energy-controlled converter offers low stored energy at the expense of added complexity, large range of switch duty ratios, and increased voltage stress. However, the extra degree of freedom afforded by the second active switch allows improved output-voltage regulation, as discussed in the following chapter.

### 15.3 Implications of Stored Energy

As already mentioned, the drawbacks of storing large amounts of energy are the added volume, weight and cost, as well as the sluggish response of the converter. The problem of slow response is discussed further in the following chapter.

An energy-storage scheme is chosen by weighing the cost and complexity of the various energy-storage methods against the penalties of large storage. The quality of the dc voltage provided by the energy-storage circuit is also an issue.

Despite the high costs of extra stored energy, it is not always desirable to store only the minimum energy required by power balancing. Other functions of the ac-dc conversion system may call for stored energy apart from the requirements of shaping. For example, a common specification for off-line converters is a minimum hold-up time, the length of time the converter must continue to provide usable dc output after the

input ac power fails or is removed. The hold-up requirement calls for a large amount of stored energy. If the necessary hold-up time is  $h$  times the line period, then the minimum energy required for hold-up is  $2\pi h$  times the theoretical minimum energy required for shaping,  $P/\omega_l$ . For instance, if 50 msec of hold-up time is needed, and the line frequency is 60 Hz, then the hold-up energy is 19 times the energy required for shaping. Since the converter usually cannot extract the last remnants of stored energy while maintaining the output within specification, in practice even more energy must be stored.

If hold-up requirements call for significant stored energy, then there is no point in using the methods of this chapter to reduce the stored energy for shaping. For example, using a large capacitor in a boost shaper is not a waste of size and weight if the extra energy provides hold-up time for a post-regulator.

Another use of extra stored energy is meeting sudden changes in load demand. Suppose a minimum-energy scheme is employed and a sudden increase of load power is called for when the stored energy is at its minimum. Since the converter stores no energy at this instant, the increase in load power can only come directly from the line. The current-shaping function of the converter only allows the input power level to change slowly, however, as discussed in Chapter 16. Even if the line current could be changed quickly, the presence of reasonably large capacitors or inductors at the converter output makes it impossible to rapidly change the load power. The minimum energy stored in a current-shaping power converter must be such that load changes and hold-up specifications can be met during any portion of the line period.

The problems of stored energy are not solved simply by reducing the energy to a minimum. Practical designs must combine the methods of minimizing stored energy discussed in this chapter with system specifications for hold-up time, dynamic response, size, weight, and cost.





## Chapter 16

# Isolation and Voltage Regulation

Isolation from the power line and regulation of the output voltage are features required of nearly every ac-dc conversion system. Isolation helps solve noise and interference problems but is even more important as a safety feature. Close regulation of the output voltage is essential when the ac-dc converter supplies sensitive electronic loads.

Section 16.1 discusses different ways of regulating the output voltage while providing well-shaped input current. Although current-shaping converters with single control variables are capable of performing both functions, conflicting requirements severely limit the bandwidth of the voltage regulation. It is a little-known fact that this bandwidth limitation applies to all shaping converters with a single control, regardless of what control method is used.

The tradeoffs involved in introducing isolation to an ac-dc conversion system are discussed in Section 16.2. The size of the transformer and the stresses on the semiconductor switches depend upon the location of the transformer in the system—before, within, or after the shaping converter.

### 16.1 Output Voltage Regulation

Most ac-dc converter applications require that the voltage on the dc load be maintained within certain specifications. Since this voltage depends on uncontrollable line and load variations, closed-loop control is usually necessary. Figure 16.1 demonstrates three ac-dc systems including regulation. In the situation of Fig. 16.1(a), a current-shaping converter is followed by a post-regulator. The shaping converter has either no regulation or very slow regulation of its output voltage. The post-regulator ensures that the final load voltage is within specifications. In Fig. 16.1(b), a current-shaping converter with

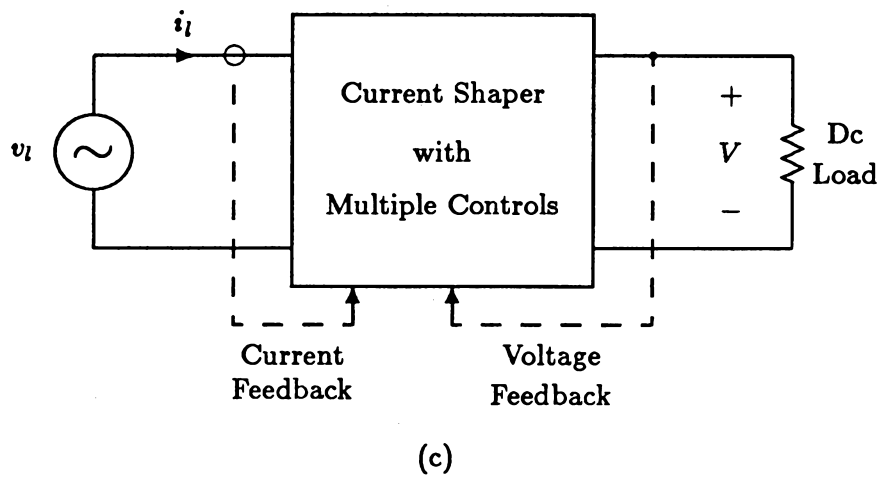
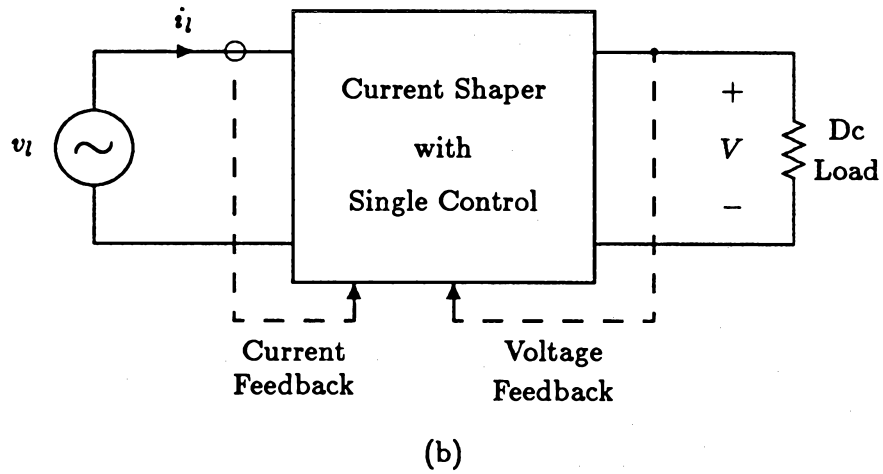
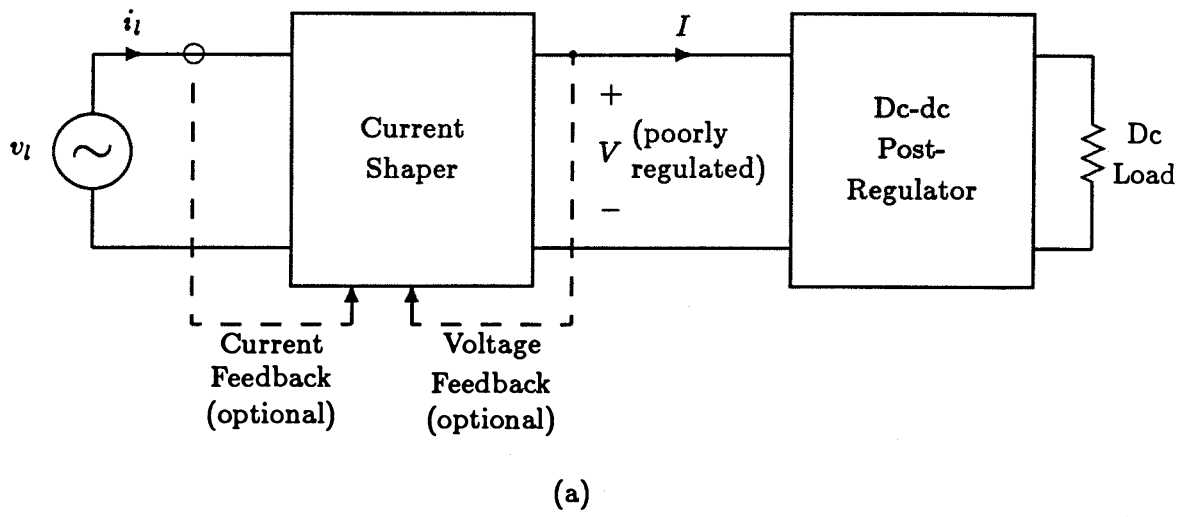


Figure 16.1: Three methods of providing regulation for an ac-dc conversion system.

a single control variable provides both input-current shaping and output-voltage regulation. Finally, in Fig. 16.1(c), a current shaper with multiple controls performs both shaping and regulation functions.

### 16.1.1 Separate Post-Regulator

A post-regulator, as shown in Fig. 16.1(a), provides several advantages. First, a dc-dc switching post-regulator is an excellent place to introduce isolation. The transformer in such a converter is small, sized according to the switching frequency. Second, with a high-bandwidth post-regulator the demands on the shaper's regulation are much less severe. Fluctuations and line-frequency ripple in the output voltage of the shaper are easily removed by the post-regulator, which can be thought of as a series active filter. Conversely, if the shaper provides some degree of regulation, the input-voltage range of the post-regulator is small, easing the design of the latter stage. Even a linear stage may give acceptable efficiency as a post-regulator if the current shaper can maintain the post-regulator input voltage within a narrow range.

A separate post-regulator has some drawbacks, of course. The extra components, size, and weight are unwelcome, as is the reduction in efficiency that results from "processing the same power twice," once in the current-shaper and once in the post-regulator. Another problem may arise from the fact that a switching dc-dc post-regulator supplying a load with constant power presents a negative resistance to the shaping converter at low frequencies. If the current-shaper's output voltage decreases, for example, the post-regulator must draw *more* current to maintain the same output power. The shaping converter may be difficult to stabilize with this negative resistance at its output.

### 16.1.2 Single-Control Shaper and Regulator

Figure 16.1(b) shows a system with only one converter: a current shaper with a single control variable, providing a regulated output voltage as well as a controlled input current. At first thought it may seem unlikely that a single control can perform both functions. In a current-shaper with closed-loop control of the input current, however, the control circuit has some reference current it tries to follow. If the amplitude of

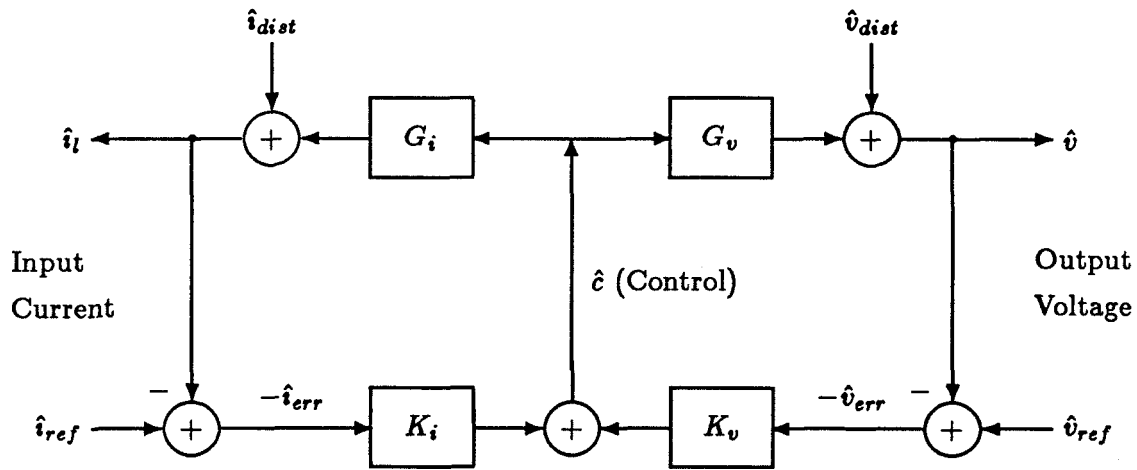


Figure 16.2: Block diagram of a current shaper with both the input current and the output voltage controlled by feedback loops.

the reference current is increased, the power drawn from the line must also increase, ultimately raising the voltage at the dc load. Circuits controlling both the input current and output voltage use two feedback loops, one closed around the input current, and one setting the reference current based on the output-voltage error. The block diagram of Figure 13.7 is representative of these techniques.

The single-converter approach of Fig. 16.1(b) has the advantage of only processing the power once, and the possibility of using a single active switch. (A converter can have multiple active switches, however, and yet have only one control variable. The resonant-pulse shaper of Chapter 13 is an example.) If such a system must be isolated from the line with a switching-frequency transformer, then the transformer must reside inside the shaping circuit. It will be shown in Section 16.2 that embedding the transformer in the shaper demands higher switch stresses and/or more switches than in a non-isolated shaper of the same topology.

The most important feature of the system of Fig. 16.1(b) is a limitation on the simultaneous control of input current and output voltage. Figure 16.2 shows a linearized (small-signal) model of a current-shaping converter with feedback loops closed around both the input (line) current  $\hat{i}_l$  and the output voltage  $\hat{v}$ . It is assumed that all quantities

have been normalized so that every parameter is dimensionless. Hats (^) denote small-signal variations. The transfer functions  $G_i$  and  $G_v$  give the dependence of  $\hat{i}_l$  and  $\hat{v}$ , respectively, on the single control variable  $\hat{c}$ . The feedback gains are  $K_i$  and  $K_v$ .

Disturbances are shown affecting the input current and output voltage. The input-current disturbance represents non-idealities of the shaping topology (which are especially prevalent near the cusp of the input voltage), variations of the line voltage, and the change in the current reference as a cycle of the line progresses. The output voltage inevitably contains ripple at twice the line frequency as a consequence of the time-varying power in the energy-storage circuit. Variations in the load also disturb the output voltage.

### Conflict Between Current and Voltage Control

From the block diagram of Fig. 16.2, the errors in the input current and output voltage,

$$\hat{v}_{err} = \hat{v} - \hat{v}_{ref} \quad (16.1)$$

$$\hat{i}_{err} = \hat{i}_l - \hat{i}_{ref}, \quad (16.2)$$

are determined to be

$$\hat{v}_{err} = \frac{(1 + G_i K_i) \hat{v}_{dist} - G_v K_i \hat{i}_{err}}{1 + G_v K_v} \quad (16.3)$$

$$\hat{i}_{err} = \frac{(1 + G_v K_v) \hat{i}_{dist} - G_i K_v \hat{v}_{err}}{1 + G_i K_i}. \quad (16.4)$$

Successful current shaping requires that the control circuit reject both current and voltage disturbances to keep  $\hat{i}_{err}$  small. This requirement is met when

$$\|G_i K_i\| \gg 1 \quad \text{and} \quad \|G_i K_i\| \gg \|G_v K_v\|. \quad (16.5)$$

Similarly, close regulation of the output voltage requires

$$\|G_v K_v\| \gg 1 \quad \text{and} \quad \|G_v K_v\| \gg \|G_i K_i\|, \quad (16.6)$$

so that disturbances do not reach the load. The requirements are obviously contradictory, and this is a consequence of the single control. Any change in the control variable  $\hat{c}$  intended to raise the output voltage inevitably increases the input current as well. In

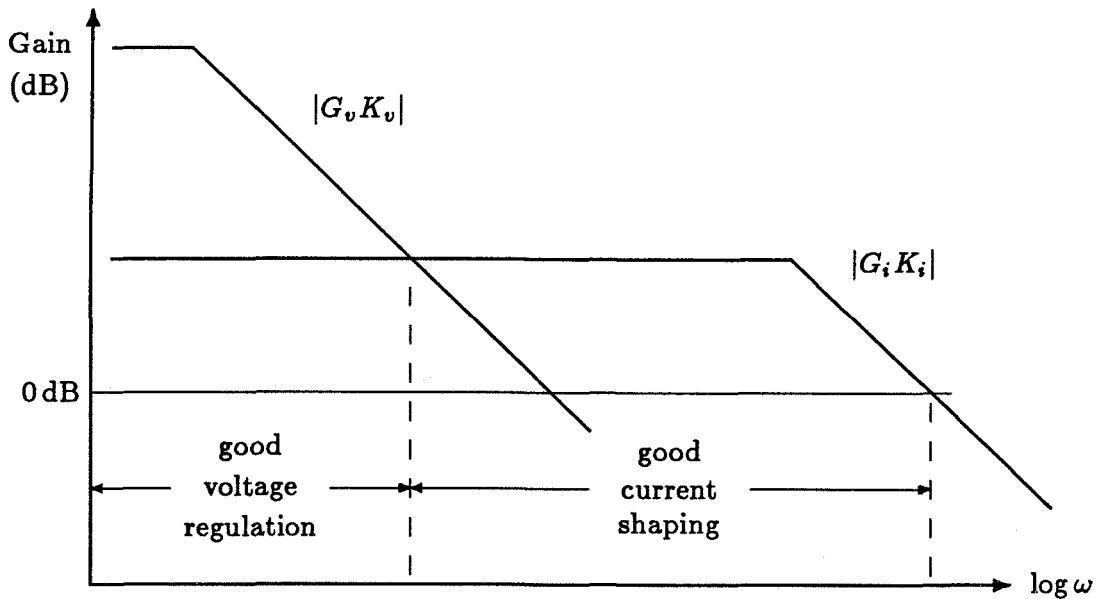


Figure 16.3: Typical loopgain magnitudes for a current shaper with both output-voltage and input-current feedback.

a sense, the converter “has no way of knowing” if a change in control is a command to correct the output voltage or the input current.

The usual solution to this problem of conflicting requirements is to satisfy Eq.(16.5) at some frequencies and Eq.(16.6) at others. In other words, one assigns different priorities to the voltage and current control loops at various frequencies, as illustrated in Fig. 16.3. It is important that the dc (that is, low frequency) output voltage be correct, so at very low frequencies  $\|G_v K_v\|$  is made large so that it dominates  $\|G_i K_i\|$ . At some frequency well below the line frequency,  $\|G_v K_v\|$  rolls off so that at the line frequency and above,  $\|G_i K_i\|$  is dominant, assuring an undistorted input-current waveform. In particular, the current loop must dominate at twice the line frequency, to avoid second-harmonic distortion of the input current from feedback of the output voltage ripple. Finally, at some high frequency, the current loop gain is rolled off to ensure stability.

Current-shaping converters with a single control are therefore able to regulate two independent quantities because these quantities are separated in frequency. Control of the input-current *waveshape* is a high-frequency function, while regulation of the dc

output voltage is a low-frequency requirement.

Current-programmed dc-dc power converters use a similar control scheme. The current-programming is a high-bandwidth function which yields desirable dynamics in the range near loop-gain crossover. At low frequencies, however, voltage feedback dominates the current loop so that the dc (low-frequency) output voltage is regulated. In effect, current-programmed converters have the same division of function according to frequency as found in current-shaping converters. A current-programmed converter “regulates” the peak of a transistor or inductor current, and this is a high-frequency function. Using the same duty-ratio control, the converter regulates the dc output voltage, a low-frequency function.

### Limitations of Stored Energy

The conflict between control of the input current and output voltage is one reason why the voltage feedback loop must have low bandwidth. Another limitation on the speed of the voltage control comes from the shaper’s requirement for stored energy.

Chapter 15 showed that a current-shaping power converter stores a significant amount of energy, at least  $P/\omega_l$  and usually much more. If the shaper has only a single control then this energy must be stored “adjacent” to the load, meaning that the voltage or current of the energy-storage circuit is identically the load voltage or current. To change the load voltage, the voltage or current of the energy-storage circuit must also be changed, a process that requires either great effort or considerable time.

To get a rough idea of the time constants involved, suppose the energy-storage network holds energy  $U$  and supplies the load with power  $P$ . The characteristic time of this combination is  $U/P$ . For a shaping converter with the minimum possible stored energy,  $P/\omega_l$ , the time constant is on the order of the line period. Shapers with a single control inevitably store more energy than this minimum and so have correspondingly longer time constants.

For example, the large energy-storage capacitor at the output of the boost converter of Fig. 13.5 produces a pole in the transfer function  $G_v$  at a (radian) frequency  $2\mathcal{R}\omega_l$ , where  $\mathcal{R}$  is the ripple ratio defined in Section 15.2.3. Reducing the output ripple therefore

slows down the converter's response. The active filter of Section 15.2.2 simulates a large output capacitor and produces the same low-frequency pole in  $G_v$ . The resonant filter of Section 15.2.3 yields a second-order transfer function  $G_v$ . With the resonant filter, the poles of  $G_v$  are centered around twice the line frequency. In all three of these energy storage methods,  $G_v$  is a "slow" transfer function. The resonant filter seems to offer the fastest response, not a surprising result since it stores the least energy of the three methods.

The requirement for stored energy thus leads to a slow response in the transfer function,  $G_v$ , and limits the bandwidth of the voltage control loop. In theory, a large feedback gain  $K_v$  can be used to make the closed-loop bandwidth—the frequency at which the loop gain  $G_v K_v$  crosses over unity gain—well above the line frequency. It is only the small-signal response that can be modified in this way, however. A large loop gain provides fast response by overcoming the sluggishness of  $G_v$  with tremendous swings of the control variable  $\hat{c}$ . The control circuit and power stage cannot tolerate extremely large variations of the control signal, however. For example, in a duty-ratio-controlled power converter, the control signal is the duty ratio  $d$ , which must lie between 0 and 1. The control circuit, whether analog or digital, faces similar limits if the gain  $K_v$  is too large. It is the *power* bandwidth rather than the *small-signal* bandwidth that really determines the capabilities of a power converter, and in the case of single-control current shapers, the power bandwidth is limited by the stored energy to approximately the line frequency or less.

### Voltage Control for Automatic Current Shapers

The converter topologies discussed in Section 13.3 shape the input current "automatically" and ideally do not require a current feedback loop. The absence of the current feedback loop does not remove the conflict between current and voltage control, however. Automatic current shaping requires that the control signal be held constant. If output-voltage regulation causes rapid changes in the control signal, the shaping properties are lost. Setting  $K_i$  to zero in Eq.(16.5) accounts for the absence of a current loop



in automatic shapers. The resulting error current,

$$\hat{i}_{err} = \hat{i}_{dist} - \frac{G_i K_v}{1 + G_v K_v} \hat{v}_{err} , \quad (16.7)$$

receives current disturbances unattenuated, while voltage disturbances are *amplified* by a gain of approximately  $\|G_i/G_v\|$  over the frequency range where the loop gain  $G_v K_v$  is large. The gain  $\|G_i/G_v\|$  is likely to be large because  $G_i$  is a high-bandwidth transfer function while  $G_v$  has the low-frequency dynamics of the energy-storage circuit. The only way to ensure good current shaping in an automatic current shaper is to roll off the feedback gain  $K_v$  at low frequency, so that at and above the line frequency the control signal is not perturbed by output-voltage errors.

In summary, then, a current-shaping converter with a single control variable can perform both current shaping and voltage regulation, provided these two functions are separated in frequency. Since the current shaping is a high-frequency function, voltage regulation is confined to frequencies well below the line frequency. A single-control shaper therefore can provide *dc* regulation of the output voltage, but it cannot provide the *fast* regulation needed by most electronic loads.

### 16.1.3 Shapers with Multiple Controls

Current-shaping power converters with two or more independent control variables have the potential to achieve both good current shaping *and* fast voltage regulation. Such a converter, represented in the block diagram of Fig. 16.1(c), must have its energy storage circuitry “inside” the converter with one active switch controlling the flow of energy between the storage circuit and the input and another switch controlling the connection between the storage and the load. The second active switch allows the load voltage and current to be independent of the input current, and independent of the sluggish voltage or current of the energy-storage circuit.

### Energy-Controlled Converters

Several examples of converters with two active switches and “central” energy storage are given in [47]. These topologies are actually offered in [47] as solutions to the problem

of excessive stored energy, but the extra active switch needed to control the energy storage can also be used for fast voltage regulation.

The circuits presented in [47], however, are equivalent to the cascade connection of a boost and a buck converter. The circuit shown in Fig. 15.3 of Section 15.2.4, for example, is simply a boost converter followed by a buck converter. Some of the topologies in [47] use bridge connections, instead of single-ended connections, but the same performance would be achieved by separate boost and buck converters with the same number of active switches.

What distinguishes the converters of [47] from the usual cascade connection of two dc-dc converters is that the “link” voltage, the voltage produced by the boost converter and used as the input for the buck converter, is allowed to vary widely, even down to zero. Except for this difference, the converters suggested in [47] might be considered as cascades of shapers and post-regulators, as in Fig. 16.1(a), instead of as a single converter with multiple controls, as shown in Fig. 16.1(c).

### Three Switched-Network Converters

Each position of the switches in a switching converter results in a linear circuit called a *switched network*. Converters with a single active switch usually have only two switched networks, and the single control determines the fraction of each period allotted to each switched network. An extra degree of control can be gained in these converters by adding a second active switch to produce a third switched network of controlled duration. Three switched-network (3SN) converters were presented in [48] as a means of regulating multiple-output converters.

The dual controls of a 3SN converter allow independent control of the input current and output voltage when the converter functions as a current-shaping ac-dc converter. The 3SN Čuk converter, shown in Fig. 16.4, is topologically equivalent to the converter of Fig. 15.3, and performs exactly the same functions. The only difference between the converters of Figs. 15.3 and 16.4 is the implementation of the switches. The 3SN Čuk converter can be isolated as described in [48], but when the converter is used as a shaper the isolation transformer is subject to line-frequency voltages and must be large. As

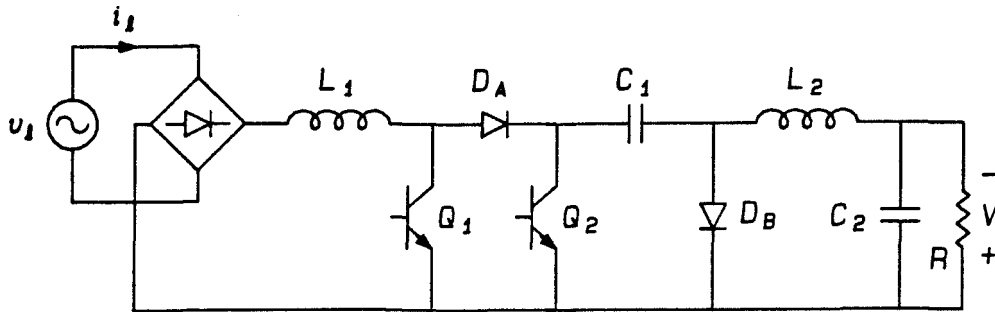


Figure 16.4: The three-switched-network (3SN) Ćuk converter.

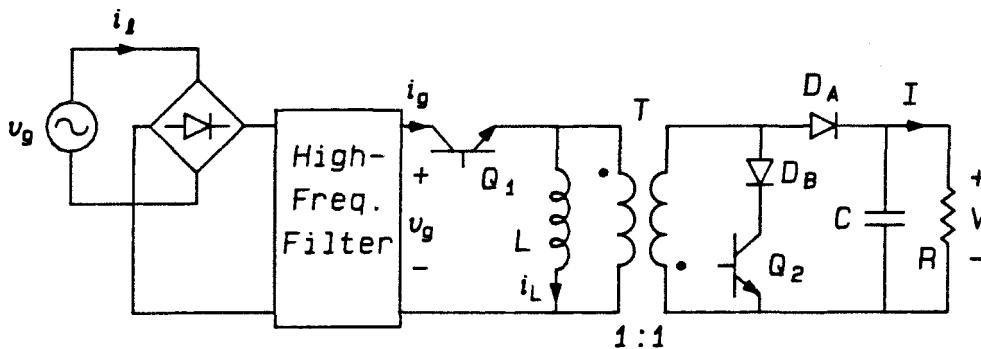


Figure 16.5: The three-switched-network (3SN) flyback converter.

a current-shaper, the isolated 3SN Ćuk converter holds no advantages over a separate boost shaper and buck post-regulator.

The 3SN flyback converter of Fig. 16.5, on the other hand, holds significant advantages as a current-shaper with fast voltage regulation. The transformer in this topology is still a line-frequency transformer, and hence fairly large, but in this case the magnetizing inductance of the transformer also serves as the energy-storage device for current shaping. Isolation is "free" in this topology since significant energy must be stored in the inductance whether or not isolation is present.

The operation of the active switches in the 3SN flyback topology is detailed in Fig. 16.6. During the interval designated  $d_1 T_S$ , the magnetizing inductance  $L$  is charged from the source voltage and the current  $i_L$  rises. The inductor is shorted during the "idle" interval  $d_2 T_S$ , and the current  $i_L$  (or equivalently, the core flux) remains constant. The energy stored in  $L$  is delivered to the load during the final interval,  $d_3 T_S$ . The

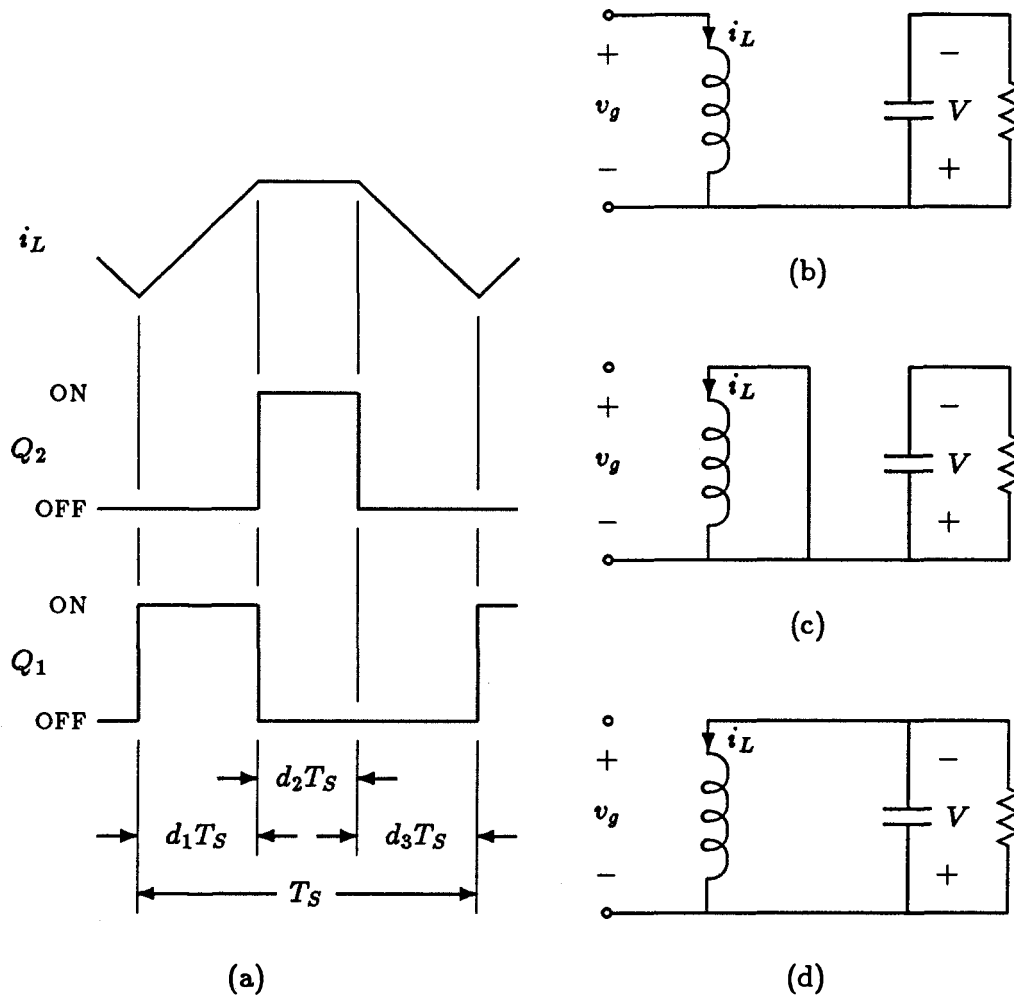


Figure 16.6: Operation of the 3SN flyback converter, showing (a) inductor-current waveform and switch duty ratios, and (b), (c), and (d) the three switched networks corresponding to  $d_1$ ,  $d_2$ , and  $d_3$ , respectively.

two independent controls are the fractions  $d_1$  and  $d_2$ . The length of the  $d_3$  interval is determined by the identity  $d_1 + d_2 + d_3 = 1$ . The sequence  $d_1$ - $d_2$ - $d_3$  shown in Fig. 16.6 can be changed to  $d_1$ - $d_3$ - $d_2$  without changing the average behavior of the converter. The latter sequence may yield a slightly higher efficiency [48].

The following analysis assumes that the high-frequency input filter can be neglected and that the output voltage  $V$  has negligible ripple. The switching frequency must lie far above the line frequency so that the concept of the switching-frequency average applies.

The input current  $i_g$  is non-zero only during the interval  $d_1$ , so the switching-

frequency-averaged input current is

$$\bar{i}_g(\theta) = d_1(\theta)i_L(\theta) . \quad (16.8)$$

Successful current shaping also enforces

$$\bar{i}_g(\theta) = \frac{V_l}{R_{em}} \sin \theta = 2MI \sin \theta . \quad (16.9)$$

Since the object is to have the inductor perform all the necessary energy storage and supply purely dc power to the output capacitor and load, the averaged output current must be constant:

$$\bar{i}' = d_3(\theta)i_L(\theta) = I . \quad (16.10)$$

Rather than deriving and solving differential equations for the circuit, an approach used in [47] gives the inductor-current waveform and duty ratios based on the requirement of stored energy. On the assumption that the converter generates the desired sinusoidal input current and creates no low-frequency harmonic currents in the output capacitor  $C_f$ , the energy stored in the inductor must obey Eq.(15.4) of Chapter 15, written here in a slightly different form,

$$U_L = \frac{1}{2} Li_L^2 = \left( \frac{U_0}{U_{0,\min}} - \sin 2\theta \right) \frac{P}{2\omega_l} . \quad (16.11)$$

The minimum energy offset,  $U_{0,\min}$ , was shown in Chapter 15 to be  $P/2\omega_l$ . With  $U_0/U_{0,\min} = 1$ , the stored energy reaches zero at some point in the cycle, so that  $U_0/U_{0,\min}$  must always be greater than unity.

When Eq.(16.11) is solved for  $i_L$  and the result substituted into Eqs.(16.8) through (16.10), the resulting expressions for the inductor current and the duty ratios are

$$i_L(\theta) = I \left[ \frac{1}{\pi K_l} \left( \frac{U_0}{U_{0,\min}} - \sin 2\theta \right) \right]^{1/2} \quad (16.12)$$

$$d_1(\theta) = 2M \sin \theta \left[ \frac{1}{\pi K_l} \left( \frac{U_0}{U_{0,\min}} - \sin 2\theta \right) \right]^{-1/2} \quad (16.13)$$

$$d_3(\theta) = \left[ \frac{1}{\pi K_l} \left( \frac{U_0}{U_{0,\min}} - \sin 2\theta \right) \right]^{-1/2} , \quad (16.14)$$

where  $K_l$  is the by now familiar conduction parameter  $\omega_l L / \pi R$ .

The parameter  $U_0/U_{0,\min}$  determines the amount of stored energy in the converter, and may be chosen independently of the conduction parameter  $K_I$ . Small values of  $U_0/U_{0,\min}$  allow size and weight savings, but extra stored energy may be needed to meet sudden load demands or to meet hold-up specifications, as discussed in Chapter 15. Equations (16.13) and (16.14) place another constraint on  $U_0/U_{0,\min}$ , however, because the sum of the duty ratios  $d_1$  and  $d_3$  must always be less than unity. It is not possible analytically to translate this condition into constraints on  $M$ ,  $K_I$ , and  $U_0/U_{0,\min}$ , but it is clear that small values of  $U_0/U_{0,\min}$  aggravate the problem of the limited duty ratio range. For instance,  $d_3 < 1$  implies that

$$\frac{U_0}{U_{0,\min}} > 1 + \pi K_I, \quad (16.15)$$

a necessary but certainly not sufficient condition for realizable duty ratios.

An interesting case is when the stored energy is large, and  $U_0/U_{0,\min} \gg 1$ . In this case the inductor current is nearly a constant,  $I_L$ , the stored energy is approximately  $\frac{1}{2}LI_L^2$ , and the ratio  $U_0/U_{0,\min}$  is  $(I_L/I)^2$ . The duty ratios are approximately

$$d_1 \approx \frac{I}{I_L} 2M \sin \theta \quad (16.16)$$

$$d_3 \approx \frac{I}{I_L}. \quad (16.17)$$

The sinusoidal duty ratio  $d_1$  is the same as the duty ratio  $d = D_m \sin \theta$  needed for a flyback converter with a single control (see Section 14.2 of Chapter 14). The average time spent in the first switched network, when the source current equals the inductor current, must vary sinusoidally. When the flyback converter has only two switched networks, the duration of the second network must therefore vary as  $1 - D_m \sin \theta$ . The product of this time varying duty ratio and the constant inductor current result in a time-varying current fed to the output capacitor. Thus a two switched-network flyback converter has *both* a large inductor and a large output capacitor.

The second active switch of a 3SN flyback converter permits both a sinusoidal duty ratio  $d_1$  to obtain current shaping *and* a constant duty ratio  $d_3$  to provide constant output power. The inductor is the only element that stores significant energy, and that energy can approach the theoretical minimum if desired. In a sense, intelligent control

becomes a substitute for “brute-force,” passive energy control when the second active switch replaces the large output capacitor as a means of ensuring dc voltage at the load.

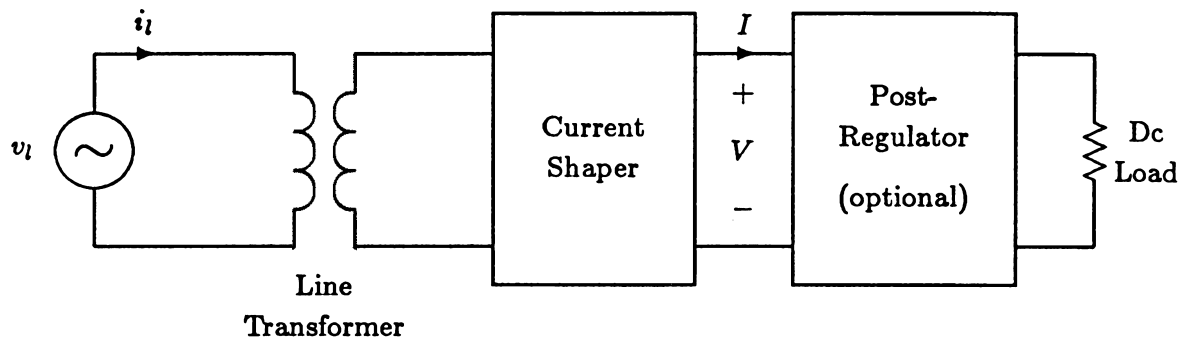
The 3SN flyback topology is very attractive for ac-dc power conversion at relatively low power levels. The converter offers the advantages of isolation, current shaping, fast voltage regulation, and minimum parts count. The stored energy is not excessive and can be made small at the expense of limiting the acceptable load and conversion ratio and increasing the dynamic range of the control variables. The only major drawback to this topology is that the semiconductor switches suffer stresses higher than those found in separate buck or boost shapers and post-regulators.

## 16.2 Isolation

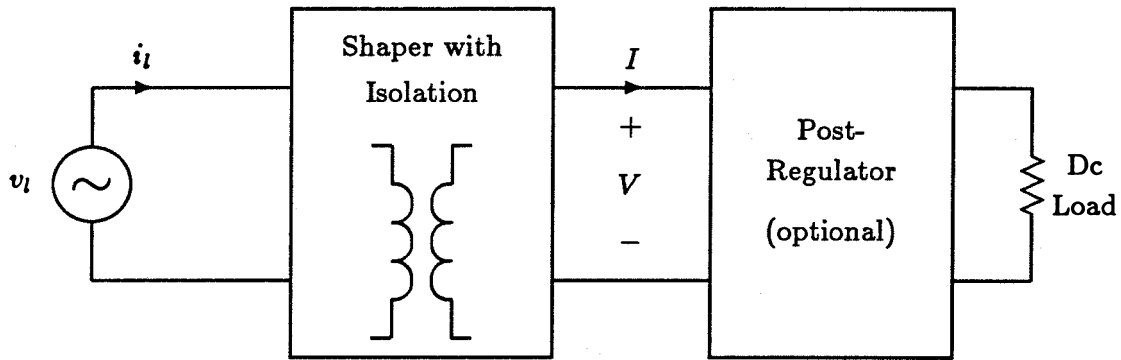
Many applications require an ac-dc power processor to isolate the dc load from the power line. This requirement is primarily a safety measure, and is always found in consumer products or other systems in contact with people. Isolation also provides electrical advantages, protecting low-voltage circuitry and eliminating circulating currents. Isolation is essential in the control of EMI (electromagnetic interference).

Figure 16.7 illustrates three basic isolation schemes. In Fig. 16.7(a), a transformer is inserted into the power line before any of the power processing circuits. This is an “ordinary,” *line-frequency* power transformer and is large because it operates at the line frequency. In Fig. 16.7(b), isolation is included in the current-shaping converter. In this case it is possible for the transformer to be a *switching-frequency* transformer and hence to be much smaller than the line transformer of Fig. 16.7(a). Finally, isolation can be included in a dc-dc post-regulator, as shown in Fig. 16.7(c).

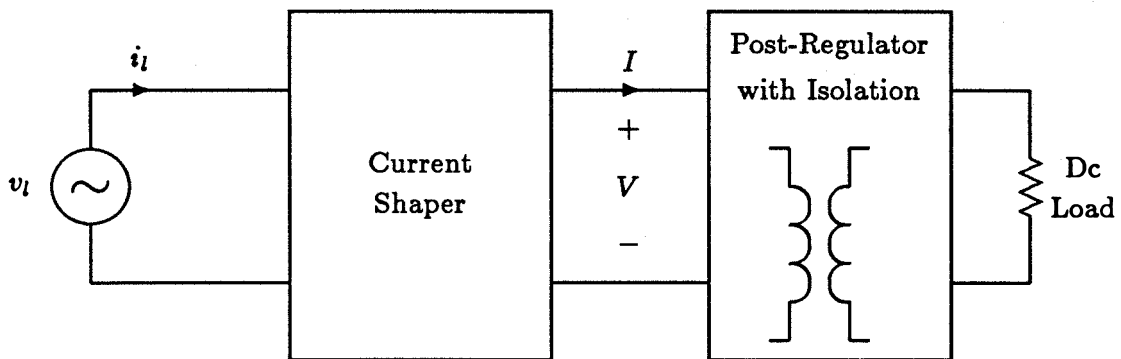
Each of these three transformer locations has certain advantages and drawbacks. The main considerations are the size of the transformer and the stress on the semiconductor switches in the power converters. Section 16.2.4 compares the transformer size and switch stresses for converters in each of the situations shown in Fig. 16.7.



(a)



(b)



(c)

Figure 16.7: Three ways to add isolation to an ac-dc power system.



### 16.2.1 Line Transformer

A transformer inserted between the utility line and a shaping converter, as shown in Fig. 16.7(a), is the simplest way to provide isolation between the ac source and the dc load. Line transformers are not without positive features: they are widely available and thoroughly understood, and their relatively high leakage inductance provides some degree of protection from transient line voltages. The transformer is large and expensive, however, because it must operate at the line frequency. The transformer typically reduces the efficiency of the system by 3% to 5%.

The line transformer ideally has no effect on the power-processing circuits that follow. Both the shaper and the dc-dc post-regulator are free to use non-isolated topologies with few switches and low stresses. In practice, however, the leakage inductance of the line transformer significantly increases the source impedance. The higher source impedance means the source voltage seen by the current shaper changes as the load changes, and any distortion of the shaper's input current results in a distorted input voltage. Moreover, some shaping circuits (for example buck-based active shapers and the inductor-input filter in continuous conduction mode) draw discontinuous input currents. With these circuits, a high-frequency filter is essential to shunt the high-frequency currents away from the transformer leakage inductance.

### 16.2.2 Shapers with Isolation

An isolation transformer can be built into a current-shaping power converter, and the transformer in this case might experience line-frequency voltages or only switching-frequency voltages. Only the case of a switching-frequency transformer is considered here. A line-frequency transformer can always be added between the line and the shaper, as in Fig. 16.7(a), with less impact on the operation and stresses of the shaping converter.

Figure 16.8 shows a representative isolated shaping converter, the full-bridge buck converter. The converter operates much like its non-isolated counterpart. When either pair of switches,  $Q_1$ - $Q_4$  or  $Q_2$ - $Q_3$  is ON, a current  $I$  is drawn from the source. When all the switches are OFF the source current is zero. Duty-ratio modulation produces a PWM input-current waveform that, when averaged by a small filter, approximates the desired

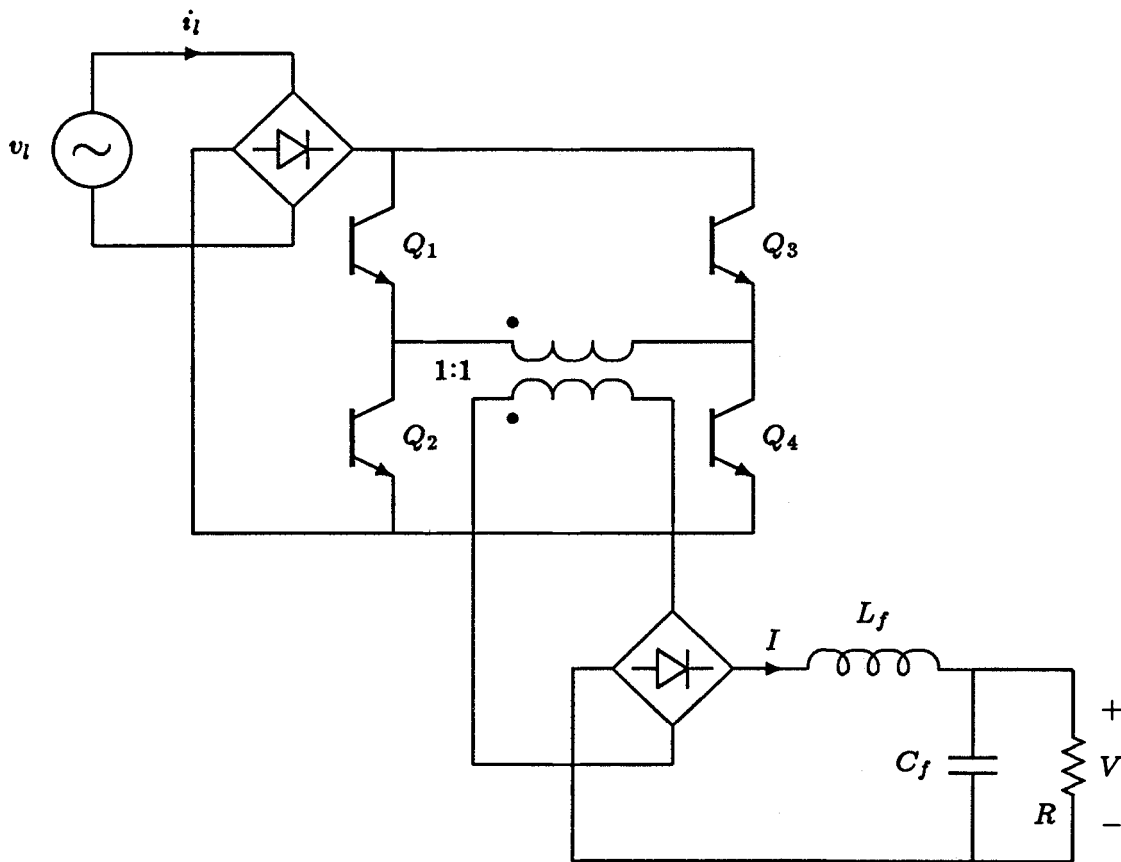


Figure 16.8: A full-bridge buck current shaper.

(rectified) sinusoidal line current. The switch pairs operate alternately in a symmetrical fashion so that the transformer is “reset” after every cycle.

Insertion of a transformer into a current shaper places additional demands upon the semiconductor switches, except in the case of flyback converters. For instance, in the full-bridge buck topology four switches are needed, and the voltage and current stress on each switch are the same as in the non-isolated buck topology of Fig. 13.1. A half-bridge topology could also be used for isolation. This alternative requires only two switches, but the current stress is twice that of the full-bridge configuration. Isolation of the buck topology with a single switch is also possible, using a forward converter, but the switch voltage stress is higher than in the non-isolated topology. Adding a high-frequency transformer to a buck current shaper therefore requires either more switches or higher-

rated switches. In addition, the leakage inductance of the high-frequency transformer complicates the switching process relative to the non-isolated case. Similar conclusions hold for isolated versions of the boost current-shaping topology, where a high-frequency transformer demands extra switches with higher voltage ratings.

The flyback topology is naturally isolated, however. When operating in the discontinuous conduction mode (DCM), the transformer is reset during every switching cycle and is therefore a switching-frequency device. If instead the flyback topology is operated as a current-shaper in the continuous mode (CCM), then the transformer sees line-frequency voltages and must be large.

### 16.2.3 Isolation in Post-Regulators

Isolated dc-dc converters are some of the most common power circuits. These converters have high-frequency transformers that are efficiently utilized. Some examples are the current-fed (or boost) push-pull converter, the isolated Ćuk converter, and a host of isolated buck-derived topologies, including the forward, push-pull, half-bridge, and full-bridge converters. The latter uses the same circuit as shown in Fig. 16.8, but the input voltage is dc and the duty ratio  $D$  is held constant. Resonant converters are another possibility for isolated post-regulators.

Isolated converters often require snubbers on their transistors to relieve the extra stress generated by the leakage inductance of the transformer. These snubbers are fairly easy to implement since the converter operates in a steady state: the duty ratio and switching frequency are essentially constant. In contrast, it is more difficult to design snubbers for a converter performing current shaping, where the conversion ratio and apparent load vary at twice the line frequency.

Another advantage to including isolation in the post-regulator is that an isolated dc-dc converter can easily support multiple loads.

### 16.2.4 Stress and Transformer Size Comparison

One indication of the size of a transformer is its core geometry factor,  $K_g$  [49]. The square root of  $K_g$  is proportional to the product of the volt-seconds experienced by

the transformer and a weighted sum of the rms currents in the primary and secondary windings. The weighting depends on how the window area is allocated between primary and secondary. At any operating point an optimal division exists giving a minimum  $K_g$ . The product of the volt-seconds and weighted rms currents is called the VA-seconds here, a quantity that provides a useful tool for comparing the sizes of transformers in different converters. Dimensional analysis reveals that the weight and volume of a transformer varies roughly as the  $3/5$  power of the factor  $K_g$ , and therefore as the  $6/5$  power of the VA-second rating. It is therefore reasonable to use the VA-second rating as a rough indication of the weight and volume of a transformer.

Table 16.1 compares the VA-second ratings of transformers and the transistor stresses in several converters, representing each of the three locations illustrated in Fig. 16.7. The table assumes for convenience that each transformer has a 1:1 turns ratio and an optimal division of window area between primary and secondary, and that all the transformers are designed for equal copper losses. Unity power factor operation is also assumed. The stresses of a non-isolated buck shaper are included for comparison.

Several features of the table merit discussion. "Switching-frequency" transformers are distinguished from "line-frequency" transformers by the factor  $\omega_l T_S$  in their VA-second rating. As the separation between the line frequency ( $\omega_l/2\pi$ ) and the switching frequency ( $1/T_S$ ) increases, the factor  $\omega_l T_S$  becomes small, as does the corresponding transformer. The size of line-frequency transformers, in contrast, is fixed by the power level and the line frequency, regardless of the switching frequency of the surrounding circuits.

The only advantage offered by the line transformer is simplicity. Although the transformer is large, it permits the use of a non-isolated shaper and post-regulator.

The CCM flyback shaper has a line-frequency transformer, one at least twice as large as a simple line transformer. The shaper also suffers from large stresses. The only merit of this circuit is that it provides isolation with a single transistor.

The DCM flyback shaper has a small, switching-frequency transformer and requires only a single transistor. The voltage stress is large, but the main drawback to this converter is the very high current stress. The current stress is smallest when the converter

Converter	Number of Switches	Transformer VA-seconds (units of $P/\omega_l$ )	Switch Voltage Stress (units of $V_l$ )	Switch Current Stress (units of $I$ )
Non-isolated Buck Shaper	1	—	1	1
Line Transformer	—	$2\sqrt{2}$	—	—
CCM Flyback Shaper	1	$\approx \frac{5}{\mathcal{R}} \text{ to } \frac{10}{\mathcal{R}}$	$(1 + M)$	$(1 + \frac{4M}{\pi})$
DCM Flyback Shaper	1	$\approx 1.5\sqrt{K_S}(\omega_l T_S)$	$(1 + M)$	$> 4(M + 1)$
Full-bridge Buck Shaper	4	$\sqrt{2D_m}(\omega_l T_S)$	1	1
Full-bridge Dc-Dc Buck	4	$\sqrt{D}(\omega_l T_S)$	(1)	(1)

*Table 16.1: Comparison of transformer size and switch stresses for several isolated converters. The quantity  $\mathcal{R}$  for the CCM flyback converter is the ripple ratio of the magnetizing current. For the full-bridge dc-dc buck converter, the voltage and current stresses equal the converter's input voltage and output current, respectively.*

just reaches the CCM/DCM boundary at the peak of the line voltage, as determined by Eq.(13.31). Even in this “best case,” the switch current stress is at least four times the dc output current and more than twice the peak of the line current. The transformer size can be reduced by making  $K_S$  smaller than the upper limit of Eq.(13.31), but only at the expense of even greater current stress. At low power levels, where component count is more important than stresses, the isolated DCM flyback shaper is attractive. The high stresses exclude the circuit from application at medium and high power levels.

The full-bridge topology has roughly the same stresses whether it appears as a dc-dc post-regulator or as an isolated shaper. In both cases the switch stresses equal the peak input voltage and dc output current. If a full-bridge shaper and dc-dc converter

shared the same conversion ratio, the transformer would be about twice as large in the shaper. In both the dc-dc and the shaping full-bridge converters, the transformer can be made arbitrarily small by operating at a lower duty ratio (and lower conversion ratio). Extreme reduction of the duty ratio, however, raises the current stresses in the semiconductor switches to intolerable levels.

Table 16.1 indicates that putting isolation in a dc-dc post-regulator instead of in the shaping converter results in the best combination of low stresses and small transformer size. Isolation is also preferred in the dc-dc post-regulator for two reasons not evident from the table. First, the switches in a dc-dc converter have fixed ON-time, whereas in the shaper the switch ON or OFF time must go to zero. The limited switching speed of transistors has a smaller impact on the dc-dc converter, so that its switching frequency can be somewhat higher than in a shaper processing the same power. Higher switching frequency of course corresponds to a smaller transformer. Furthermore, if the current shaper has a conversion ratio  $M < 1$ , as does the buck shaper, the post-regulator operates with a smaller input voltage than the shaper. The post-regulator can therefore use transistors with lower voltage ratings, which again implies higher switching speed and a smaller transformer.

Clearly, if transformer size is a major consideration, the line transformer should be avoided. If a post-regulator is included in the system, then this is the best place to introduce isolation. For cases where isolation is required but fast regulation is not, an isolated shaping converter is a good choice. At low power levels, shaping, isolation, and regulation are provided in a single circuit by the 3SN flyback topology.

## Chapter 17

# Conclusions

The delivery of power from a single-phase ac line to a dc load is a common and important problem in power electronics. It is becoming increasingly necessary that this function be performed while drawing a high-quality current waveshape from the power line. Inferior line currents lead to poor utilization of the power line, reduced efficiency, and interference problems. Line-current quality is reflected by several measures, including power factor. The most beneficial line current, from a system-wide viewpoint, is one proportional to the line voltage. At a given power level, this is the *only* current waveform yielding unity power factor, full utilization of the power line, and reduction of distortion caused by harmonic currents from nonlinear loads.

A first step to understanding and designing current-shaping circuits is to realize that all these circuits use one of just a few basic shaping methods. Shaping circuits fall into two broad categories—passive and active. Passive current-shapers circuits have the advantages of ruggedness and simplicity, but suffer from excessive size and weight if good power factor is needed. High power factor is more easily obtained using circuits with semiconductor switches, especially if those switches are operated at frequencies far above the line frequency.

Active current shapers are divided into three categories:

- Buck-like shapers, characterized by a PWM input-current waveform generated by switching the current in a stiff inductor.
- Boost-like shapers, which apply a PWM voltage across an input inductor to produce a desirable input-current.
- Automatic shapers, in which a converter operating in the discontinuous conduction mode draws a sinusoidal input current while operating with fixed duty ratio and

switching frequency.

In every case, increasing the switching frequency far above the line-frequency leads to smaller filters and a higher-quality input current.

Criteria were developed for deciding whether a given dc-dc converter topology is suitable for current shaping, and these criteria were applied to several resonant converters. Topologies that showed promise as current shapers were the parallel-resonant converter without an output inductor, and the zero-voltage-switching buck and zero-current-switching boost half-wave quasi-resonant converters. The full-wave quasi-resonant, series-resonant, and parallel-resonant converters all are undesirable topologies for current-shaping

All current shapers—active or passive—must satisfy a requirement of minimum stored energy. This limitation has a profound effect on the size of a shaping converter and on its ability to supply a well-regulated output voltage. Several methods of minimizing the stored energy were studied, but it was also noted that a system may require a significant amount of stored energy for purposes other than current shaping.

Output-voltage regulation can be provided by a shaping converter or by a post-regulator. If the shaper has only a single control, its control of the output voltage is restricted to low frequencies. This restriction is a result of the stored-energy requirement, and is effective regardless of the feedback arrangement or switching frequency. Shapers with multiple switches and multiple control variables can avoid this restriction and provide fast regulation of their output voltages.

An ac-dc conversion system can include isolation in any of several positions. The preferred location is in the post-regulator if the system contains one. A line transformer is unnecessarily heavy, and adding isolation to a current shaper places an extra burden on the switches.

The components of an ac-dc conversion system are chosen depending on the specifications of each application. For example, systems with high line frequencies tend toward passive current shaping. High-power systems are forced to use passive or slow-switching active shapers and have difficulty achieving high power factor. Low-cost, low-power systems place a premium on component count. The 3SN flyback converter—an “integrated”



topology providing shaping, isolation, and fast voltage regulation in one converter with only two switches—is a good candidate for such systems.

Every ac-dc conversion system must fulfill the functions of current shaping, energy storage, and—if called for—regulation and isolation. Dc-dc converters, performing similar functions, can reduce their stored energy, decrease input and output ripple, and improve regulation bandwidth, all simply by increasing the switching frequency. The demands on a current shaper, however, are imposed solely by the frequency of the single-phase power source. The requirement for significant stored energy and the impact of that requirement on the system performance is rigid and cannot be relieved by increasing the switching frequency or by any other means.

This part has studied single-phase ac-dc conversion from a system viewpoint. Examination of the required performance of the system has revealed common constraints on the “internal” workings of ac-dc converters and has led to a very general conclusion: all current shapers must perform the same basic functions, and in consequence they are all subject to the same inescapable performance limitations. With this forewarning, and the methods, circuits, and analysis of the preceding chapters, a designer is well-equipped to prevent his single-phase ac-dc power converter from polluting the power line.



## Appendix A

# Proofs of Topological Theorems

The graph theoretic terms and results used in the following proofs follow Seshu and Reed [20], with one exception: the term "loop" is used instead of Seshu and Reed's "circuit."

The following two lemmas are useful in proving Theorems 1 through 4.

**Lemma 1:** *If there exists a cut-set consisting of an element  $x$  and a set of elements  $y_i$ ,  $i = 1, 2, \dots, n$ , then every loop containing  $x$  must contain at least one of the  $y_i$ .*

**Lemma 2:** *If there exists a loop consisting of an element  $x$  and a set of elements  $y_i$ ,  $i = 1, 2, \dots, n$ , then every cut-set containing  $x$  must contain at least one of the  $y_i$ .*

The lemmas are duals of each other, so it is sufficient to prove Lemma 1. Consider Fig. A.1 showing the cut-set formed by  $x$  and the  $y_i$ . The cut-set by definition divides the original graph into two sub-graphs  $G_1$  and  $G_2$ . Since a loop containing  $x$  consists of  $x$  and a path connecting the endpoints of  $x$ , the path must connect the two sub-graphs of Fig. A.1. Clearly, such a path must contain at least one of the  $y_i$ , proving Lemma 1.

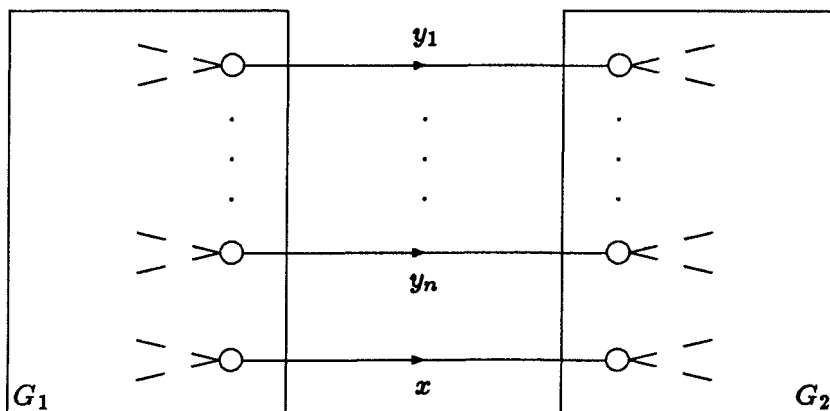


Figure A.1: Illustrating the cut-set formed by the elements  $x$  and  $y_i$ ,  $i = 1, 2, \dots, n$ .

To prove the theorems, begin by choosing a tree  $\mathcal{T}$  for the graph of a PWM converter satisfying Definition 1 of Chapter 3. Choose all capacitors and the voltage source  $V_g$  as tree branches and all inductors as chords. This is always possible unless a set of capacitors and possibly  $V_g$  form a loop. For example, two capacitors might be in parallel, or a capacitor might be across the input. In such a case, one of the capacitors is redundant and may be absorbed. Similarly, if a cut-set of inductors prevents one of the inductors from being assigned to a chord, then the inductor is redundant and may be absorbed.

Assign the diode  $D_2$  to a tree branch. This is possible unless  $D_2$  forms a loop with a subset of the capacitors and  $V_g$ . But if this were so, then Kirchhoff's voltage law (KVL) for this loop would require  $D_2$  to have small voltage ripple, and  $D_2$  could not perform its rectification function. By a similar argument, the transistor  $Q$  may be assigned to a chord. Any cut-set of  $Q$  and inductors prohibiting this would require  $Q$  to have small current ripple and prevent switching.

It is therefore possible to choose a tree  $\mathcal{T}$  of the graph with all the capacitors,  $V_g$ , and the diode  $D_2$  on the tree, and  $Q$  and all the inductors as chords.

**Proof of Theorem 1:** Consider the  $f$ -loop (of the tree  $\mathcal{T}$ ) containing  $Q$ . This loop by definition contains only  $Q$  and a subset of the tree branches. The diode  $D_2$  must be in this loop, otherwise Kirchhoff's voltage law for the  $f$ -loop would require  $Q$  to have small voltage ripple. It must be determined whether the load  $R$  is part of this  $f$ -loop. If  $R$  satisfies item 6 of Definition 1 by forming a loop with small ripple-voltage elements, then  $R$  must be a chord and cannot belong to the  $f$ -loop containing  $Q$ . If instead  $R$  and a set of inductors form a cut-set, then  $R$  will be a branch of the tree. By application of Lemma 1 to this case, every loop containing  $R$  must contain at least one inductor. The  $f$ -loop containing  $Q$  contains no inductors, however, so this loop cannot contain  $R$ . The  $f$ -loop therefore contains  $Q$ ,  $D_2$ , a set of capacitors and possibly  $V_g$ . The proof is completed by choosing the orientation of the loop such that the signed sum of voltages on the small ripple-voltage elements is positive, and by defining this voltage to be  $V_{off}$ .

**Proof of Theorem 2:** Consider the  $f$ -cut-set (of the tree  $\mathcal{T}$ ) containing  $D_2$ . This cut-set by definition contains only  $D_2$  and a sub-set of the chords of the tree. The transistor

$Q$  must be in this cut-set, otherwise Kirchhoff's current law for the  $f$ -cut-set would require  $D_2$  to have small current ripple. If  $R$  satisfies item 6 of Definition 1 by forming a cut-set with inductors, then  $R$  is a tree branch and is not a part of the  $f$ -cut-set under consideration. The load  $R$  will only be a chord if it satisfies Definition 1 by forming a loop with small ripple-voltage elements. By Lemma 2, however, every cut-set containing  $R$  must contain at least one capacitor or  $V_g$ , none of which is part of the  $f$ -cut-set. The  $f$ -cut-set therefore contains  $Q$ ,  $D_2$ , and a set of inductors. The cut-set orientation may be chosen such that the signed sum of inductor currents is positive. Defining this quantity to be  $I_{on}$  completes the proof of Theorem 2.

**Proof of Theorem 3:** Turning a PWM converter into a quasi-resonant converter adds the two elements  $L_r$  and  $C_r$  to the graph of the converter. The PWM converter had a tree  $\mathcal{T}$  with  $D_2$ , all the capacitors, and  $V_g$  on the tree, and  $Q$  and all the inductors as chords. When the resonant capacitor  $C_r$  is added, it must be a chord of  $\mathcal{T}$  because the loop of Rule 1 of Definition 2 prevents it belonging to the tree. Similarly, the cut-set of Rule 2 requires that  $L_r$  be a tree branch of  $\mathcal{T}$ .

Consider once again the  $f$ -loop of  $\mathcal{T}$  containing  $D_2$ . In the PWM converter, this loop contained only  $D_2$ ,  $Q$ , and the elements generating  $V_{off}$ . Apply Lemma 2 to this loop, using the cut-set of Rule 2. The lemma requires every loop containing  $S$  (the elements replacing  $Q$  of the PWM converter) to contain at least one inductor, either a "stiff" inductor or  $L_r$ . The  $f$ -loop cannot contain any of the small ripple-current inductors because they are chords. Therefore, the  $f$ -loop consists of  $S$ ,  $D_2$ , the elements generating  $V_{off}$ , and  $L_r$ . This completes the proof of Theorem 3.

**Proof of Theorem 4:** Consider the  $f$ -cut-set (of the tree  $\mathcal{T}$ ) containing  $S$ . Apply Lemma 1 to this cut-set, using the loop of Rule 1. The lemma requires every cut-set containing  $D_2$  to contain  $C_r$ ,  $V_g$ , or a small ripple-voltage capacitor. Since  $V_g$  and all the "stiff" capacitors are tree branches, only  $C_r$  can fulfill this requirement. The  $f$ -cut-set consists of  $S$ ,  $D_2$ , the inductors generating  $I_{on}$ , and  $C_r$ , proving Theorem 4.



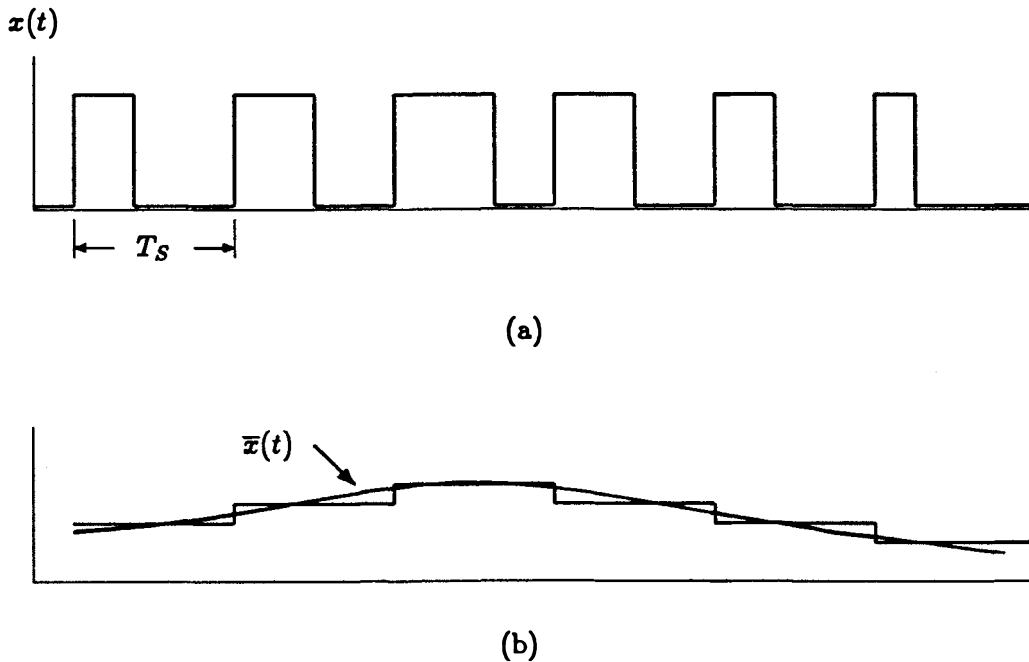
## Appendix B

# Averaging and Its Effect on Low-Frequency Information

This appendix studies the effects of “averaging” in the frequency domain. Averaging is used in both Parts I and II. In Part I, the switch waveforms  $i_S(t)$  and  $v_D(t)$  are replaced with the averaged waveforms,  $\bar{i}_S(t)$  and  $\bar{v}_D(t)$ . In Part II, averaging is used frequently in the analysis of fast-switching active current-shaping converters. For example, the duty-ratio-modulated input current of a buck-based current shaper is treated as a continuous waveform  $\bar{i}_g = d(\theta)I$ , the result of averaging the actual input current over the switching periods.

The purpose of averaging is to replace rapidly-varying, analytically difficult waveforms with new, analytically “easy” waveforms that contain the same low-frequency (slowly-varying) information. The ability of averaging to provide tremendous simplification of analytical models has made it a popular technique in the analysis of switching power converters. Averaging frequently makes the difference between a simple analytical model suitable for design and a set of equations so complicated that only numerical simulation can provide useful results.

In certain cases, however, applying averaging to a waveform destroys the low-frequency information. An analytical model that averages such a waveform will yield unreliable results. Although the waveforms for which averaging fails are infrequent, they can be found in power converters. An example from the quasi-resonant converters of Part I is discussed here.



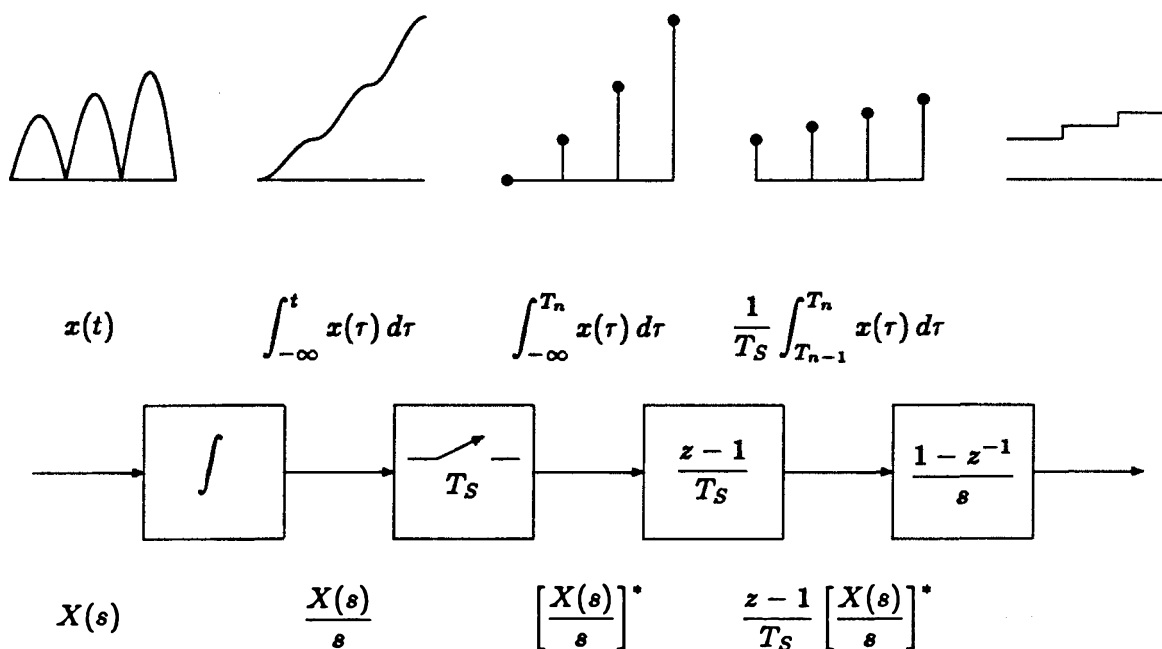
*Figure B.1: Application of averaging to a waveform. The original waveform  $x(t)$  (a) is averaged over each switching period and then low-pass filtered to obtain the slowly-varying averaged waveform  $\bar{x}(t)$  (b).*

## B.1 Definition of Averaging

Consider a waveform  $x(t)$  in a system for which a switching frequency is defined, as illustrated in Fig. B.1(a). The switching frequency serves to mark a series of time intervals, each referred to as a switching period. The switching frequency need not be constant; it can be modulated from interval to interval in a small-signal fashion. The spectrum of  $x(t)$  may contain components at and near the switching frequency and its harmonics, as well as low-frequency modulation components. The low-frequency information is said to be at the *modulation* frequency.

Averaging is defined by the process illustrated in Fig. B.1(b). The average of  $x(t)$  is calculated over each switching period. This sequence of averages produces a “stairstep” waveform. Then a new, slowly-varying waveform  $\bar{x}(t)$  is generated, as shown in Fig. B.1(b). This waveform has the same sequence of averages as  $x(t)$ , but almost no high-frequency components. In the limit that the switching frequency is much higher than the modulation frequency, the averaged waveform  $\bar{x}(t)$  is unique.





*Figure B.2: A block diagram of the process of averaging a waveform over a set of switching periods. The output of the system is a stair-step waveform with the height of each "step" equal to the average of the input waveform during the same period.*

The question to be answered now is whether or not the waveform  $\bar{x}(t)$  has the *same* low-frequency information as  $x(t)$ .

## B.2 Analysis of Averaging

The frequency-domain effects of averaging are now studied by means of a small-signal, sampled-data model of the averaging process. Since only small-signal perturbations are considered, the sampling process defined by the switching frequency is *almost periodic*. As shown in [21, pp. 91–93], the spectrum of a sampled waveform, neglecting noise, is the same whether the sampling is uniform (periodic) or almost periodic. It is therefore sufficient to consider only the case of uniform sampling.

Figure B.2 is a sampled-data model of the averaging process. Illustrative time-domain waveforms are shown above the block diagram for each step of the process, along with

time-domain expressions. Below the block diagram is the frequency-domain representation of the processed signal.

The signal  $x(t)$  is integrated, sampled, and then passed through a digital filter implementing a forward-difference operation. (Note that the forward-difference filter is not causal: it uses information from the entire switching period to generate the waveform's average at the *beginning* of the same period.) These three steps produce the average of  $x(t)$  over each switching period. The series of discrete average values is converted into a staircase waveform by the fourth block, a zero-order hold. Finally, a low-pass filter (not shown in Fig. B.2) with transfer function  $H(s)$  transforms the staircase waveform into the smooth, slowly-varying waveform  $\bar{x}(t)$ . The transfer function  $H(s)$  of the low-pass filter is not important, so long as  $H(s)$  is low-pass with a cut-off frequency below the switching frequency and well above the modulation frequency.

Let  $X(s)$  and  $\bar{X}(s)$  denote the Laplace transforms of  $x(t)$  and  $\bar{x}(t)$ , respectively. From the block diagram of Fig. B.2,  $\bar{X}(s)$  is given by

$$\bar{X}(s) = H(s) \left[ \frac{(z-1)(1-z^{-1})}{sT_S} \right] \left[ \frac{X(s)}{s} \right]^* , \quad (\text{B.1})$$

where the asterisk indicates sampling and  $z$  may be replaced by  $e^{sT_S}$ . For modulation frequencies much less than the switching frequency,  $H(s)$  approaches unity and the first term in brackets in Eq.(B.1) approaches  $sT_S$ . Near the modulation frequency, the spectrum of the averaged signal is therefore

$$\bar{X}(s) \approx sT_S \left[ \frac{X(s)}{s} \right]^* . \quad (\text{B.2})$$

The difference between this spectrum and that of the original signal is

$$\bar{X}(s) - X(s) \approx sT_S \left[ \frac{X(s)}{s} \right]^* - X(s) \quad (\text{B.3})$$

$$= s \left\{ T_S \left[ \frac{X(s)}{s} \right]^* - \frac{X(s)}{s} \right\} \quad (\text{B.4})$$

$$= s \left\{ \sum_{n=-\infty}^{\infty} \frac{X(s + jn\omega_0)}{s + jn\omega_0} - \frac{X(s)}{s} \right\} , \quad (\text{B.5})$$

where  $\omega_0 = 2\pi/T_S$ .

Equation (B.4) states that if the sampled version of the integral of  $x(t)$  doesn't differ at low frequencies from the unsampled signal, then averaging will preserve the

low-frequency information. Equation (B.5) reveals a sufficient condition for this to be true. If  $X(s)/s$ , the transform of the integral of  $x(t)$ , is sufficiently bandlimited, then  $X(s + jn\omega_0)$  will be negligibly small for  $n \neq 0$ . On the other hand, if  $x(t)$  and its integral are not sufficiently bandlimited, then the sampling inherent in the averaging process may corrupt the low-frequency content of  $\bar{x}(t)$  and yield false information at the modulation frequency.

The smoother a waveform is, therefore, the better the chance that averaging will preserve low-frequency information. This is only a sufficient condition, however. Some waveforms, such as the PWM input-current waveform of a buck-based current shaper, have strong high-frequency content yet yield valid low-frequency information after averaging. Bandlimited waveforms are uncommon in power converters, where the waveforms that call for averaging are usually discontinuous with strong components at the switching frequency and its harmonics.

### B.3 Example of Failed Averaging

One example of a case where averaging fails to preserve low-frequency information can be found in the quasi-resonant converters of Part I. Consider the current in the resonant capacitor  $C_r$  of the converter shown in Fig. 5.10(a). The current  $i_C$  is given by

$$i_C = C_r \frac{d}{dt} v_D . \quad (\text{B.6})$$

Since the diode voltage  $v_D$  always returns to zero at the end of every switching period, the average of the capacitor current is zero over every cycle. The averaged capacitor current is therefore zero for all time, and apparently contains no low-frequency information.

The voltage  $v_C$  on the resonant capacitor is the same as the diode voltage  $v_D$ . From Chapter 5, however, it is very clear that  $v_D$  *does* contain low-frequency information whenever the converter is modulated. Since the capacitor is linear, the transforms of the capacitor voltage and current are related by

$$I_C(s) = sC_r V_C(s) \quad (\text{B.7})$$

and the capacitor current must have low-frequency modulation components. Measurements with a current probe confirm that  $i_C$  carries low-frequency information even

though it has zero average over every switching interval.

In light of the previous discussion, it is not surprising that averaging fails when applied to the capacitor current. The integral of this waveform is the diode voltage  $v_D$ , a waveform shown in Fig. 5.2. The diode voltage has discontinuous slope and is obviously not bandlimited.

#### B.4 Example of Successful Averaging

As mentioned above, a bandlimited waveform is only a sufficient condition for successful averaging. The input-current of a buck-based current shaper, shown in Fig. 13.2, is certainly not bandlimited after integration. The analysis of [18] applies to this situation, however, and concludes that when the modulation and switching frequencies are sufficiently far apart, averaging will faithfully reproduce the modulation information.

#### B.5 Conclusion

Averaging includes a sampling process and is therefore subject to the problems of aliasing, in which high-frequency components corrupt the low-frequency portion of the spectrum. In some waveforms, such as the resonant capacitor current of a quasi-resonant converter, this aliasing completely destroys the desired low-frequency information, making averaging useless. In other waveforms, for example the input current of a buck-based current shaper, averaging yields valid results. It would be helpful to have a general criterion to decide whether or not averaging will “work” in a particular situation. Unfortunately, bandlimiting—the only condition arising from the analysis of this appendix—is only a sufficient condition and is unlikely to be found in a switching converter where most waveforms that are candidates for averaging have large components at the switching frequency.

## References

- [1] F. C. Schwarz, "An Improved Method of Resonant Current Pulse Modulation for Power Converters," IEEE Power Electronics Specialists Conference, 1975 Record, pp. 194–204 (IEEE Publication 75CH0-965-4 AES).
- [2] Dilip A. Amin, "Applying Sinewave Power Switching Techniques to the Design of High-Frequency Off-line Converters," Proc. Seventh National Solid-State Power Conversion Conference (Powercon 7), San Diego, CA, March 24–27, 1980, pp. A1.1–7.
- [3] R. Redl, B. Molnar, and N. O. Sokal, "Class-E Resonant Regulated Dc/Dc Power Converters: Analysis of Operation, and Experimental Results at 1.5MHz," IEEE Power Electronics Specialists Conference, 1983 Record, pp. 50–60 (IEEE Publication 83CH-1877-0).
- [4] K-H. Liu and F. C. Lee, "Resonant Switches—A Unified Approach to Improve Performances of Switching Converters," IEEE International Telecommunications Energy Conference, 1984 Proceedings, pp. 344–351 (IEEE Publication 84-CH-2073-5).
- [5] E. J. Miller, "Resonant Switching Power Conversion," IEEE Power Electronics Specialists Conference, 1976 Record, pp. 206–211 (IEEE Publication 76CH-1084-3 AES).
- [6] P. Vinciarelli, "Forward Converter Switching at Zero Current," U. S. Patent 4,415,959, Nov. 15, 1983.
- [7] K-H. Liu, R. Oruganti, and F. C. Lee, "Resonant Switches—Topologies and Characteristics," IEEE Power Electronic Specialists Conference, 1985 Record, pp. 106–116 (IEEE Publication 85CH2117-0).

- [8] K-H. Liu and F. C. Lee, "Zero-Voltage Switching Technique in Dc/Dc Converters," IEEE Power Electronics Specialists Conference, 1986 Record, pp. 58–70 (IEEE Publication 86CH2310-1).
- [9] T. Zeng, D. Y. Chen, and F. C. Lee, "Variations of Quasi-Resonant Dc-Dc Converter Topologies," IEEE Power Electronics Specialists Conference, 1986 Record, pp. 381–392 (IEEE Publication 86CH2310-1).
- [10] V. Vorpérian and S. Čuk, "A Complete Dc Analysis of the Series Resonant Converter," IEEE Power Electronics Specialists Conference, 1982 Record, pp. 85–100 (IEEE Publication 82CH-1762-4 AES).
- [11] R. D. Middlebrook and Slobodan Čuk, "A General Unified Approach to Modelling Switching Converter Power Stages," IEEE Power Electronics Specialists Conference, 1976 Record, pp. 18–34 (IEEE Publication 76CH1084-3 AES); also *International J. of Electronics*, vol. 42, no. 6, pp. 521–550, June 1977.
- [12] V. Vorpérian and S. Čuk, "Small Signal Analysis of Resonant Converters," IEEE Power Electronics Specialists Conference, 1983 Record, pp. 269–282 (IEEE Publication 83CH-1877-0).
- [13] R. Redl, B. Molnar, and N. O. Sokal, "Small-Signal Dynamic Analysis of Regulated Class-E Dc/Dc Converters," IEEE Power Electronics Specialists Conference, 1984 Record, pp. 62–71 (IEEE Publication 84CH-2000-8).
- [14] R. P. E. Tymerski, "Generation, Classification and Analysis of Switched-Mode Dc-to-Dc Converters by the Use of Converter Cells," IEEE International Telecommunications Energy Conference, 1986 Proceedings, pp. 181–195 (IEEE Publication 86CH2328-3).
- [15] R. D. Middlebrook, "Topics in Multiple-Loop Regulators and Current-Mode Programming," IEEE Power Electronics Specialists Conference, 1985 Record, pp. 716–732 (IEEE Publication 85CH-2117-0).
- [16] S. Čuk and R. D. Middlebrook, "A General Unified Approach to Modelling Switching Dc-to-Dc Converters in Discontinuous Conduction Mode," IEEE Power Electronics

- Specialists Conference, 1977 Record, pp. 36–57 (IEEE Publication 77CH-1213-8 AES).
- [17] W. M. Polivka, P. R. K. Chetty, and R. D. Middlebrook, “State-Space Averaging Modelling of Converters with Parasitics and Storage-Time Modulation,” IEEE Power Electronics Specialists Conference, 1980 Record, pp. 119–143 (IEEE Publication 80CH-1529-7).
- [18] R. D. Middlebrook, “Predicting Modulator Phase Lag in PWM Converter Feedback Loops,” Proc. Eighth International Solid-State Power Conversion Conference (Powercon 8), Dallas, TX, April 27–30, 1981, pp. H4.1–6.
- [19] A. R. Brown, “Topics in the Analysis, Measurement, and Design of High-Performance Switching Regulators,” PhD thesis, California Institute of Technology, May 1981, pp. 118–120.
- [20] S. Seshu and M. B. Reed, *Linear Graphs and Electrical Networks*. Reading, Mass.: Addison-Wesley, 1961.
- [21] Billy B. Y. Lau, “Small-Signal Frequency Response Theory for Ideal Dc-Dc Converter Systems,” PhD thesis, California Institute of Technology, June 1986.
- [22] W. Shepherd and P. Zakikhani, “Suggested Definition of Reactive Power for Nonsinusoidal Systems,” Proc. IEE, Vol. 119, no. 9, September 1972, pp. 1361–1362.
- [23] Institute of Electrical and Electronics Engineers, IEEE Std 519-1981, “IEEE Guide to Harmonic Control and Reactive Compensation of Static Power Converters,” 1981.
- [24] E. W. Kimbark, *Direct Current Transmission*, Vol. I. New York: John Wiley & Sons, 1971.
- [25] W. E. Simon and D. L. Nored, “Manned Spacecraft Electrical Power Systems,” Proc. of the IEEE, Vol. 75, No. 3, March 1987, pp. 277–307.
- [26] F. C. Schwarz, “A Time-Domain Analysis of the Power Factor for Rectifier System with Over- and Subcritical Inductance,” IEEE Trans. on Industrial Electronics and Control Instrumentation, Vol. IECI-20, No.2, May 1973, pp. 61–68.

- [27] S. B. Dewan, "Optimum Input and Output Filters for a Single-Phase Rectifier Power Supply," *IEEE Trans. on Industry Applications*, Vol. IA-17, No.3, May/June 1981, pp. 282-288.
- [28] J. K. Watson, *Applications of Magnetism*. New York: John Wiley & Sons, 1980.
- [29] J. J. Spangler, "A Power Factor Corrected, MOSFET, Multiple Output, Flyback Switching Supply," *Proc. PCI '85* (October 1985), pp. 19-32.
- [30] E. Destobbeleer, G. Segquier, and A. Castelain, "Ac-Dc Converter Minimizing Induced Harmonics in Industrial Power Systems," *IEEE Power Electronics Specialists Conference, 1985 Record*, pp. 573-580 (IEEE Publication 85CH2117-0).
- [31] T. Kataoka, K. Mizumachi and S. Miyairi, "A Pulse-Width Controlled Ac to Dc Converter to Improve Power Factor and Waveform of Ac Line Current," *Proc. IEEE International Semiconductor Power Converter Conference, Orlando Fl., March 1977*, pp. 334-339.
- [32] M. Mazzucchelli and G. Sciutto, "Improving Ac Line Current and Power Factor Using Converters Controlled by a Generalized PWM Method," *Proc. Eighth International Solid-State Power Conversion Conference (Powercon 8), Dallas, TX, April 27-30, 1981*, pp. D1-2.1-8.
- [33] R. L. Steigerwald and J. N. Park, "Power Circuits for Obtaining a High Power Factor Electronically," *U. S. Patent 3,913,002, Oct. 14, 1985*.
- [34] M. J. Kocher and R. L. Steigerwald, "An Ac to Dc Converter with High Quality Input Waveforms," *IEEE Power Electronics Specialists Conference, 1982 Record*, pp. 63-75 (IEEE Publication 82CH1762-4).
- [35] N. J. Barabas, "Simplified Control Algorithm for Active Power Factor Correction," *Proc. PCI '85* (October 1985), pp. 1-9.
- [36] W. E. Rippel, "Optimizing Boost Chopper Charger Design," *Proc. Sixth National Solid-State Power Conversion Conference (Powercon 6), Miami Beach, FL, May 2-4, 1979*, pp. D1.1-20.



- [37] R. Keller and G. Baker, "Unity Power Factor Off-Line Switching Power Supplies," Proc. Intelec '84, pp. 332-339 (IEEE Publication 84CH2073-5).
- [38] H. Knöll, "3 kW-Switch-Mode Power Supply Providing Sinusoidal Mains Current and Large Range of Dc-Output," International Powerconversion '80 (Sept. 1980, Munich, West Germany), pp. 2.6.1-17.
- [39] N. Mohan, T. M. Undeland, and R. J. Ferraro, "Sinusoidal Line Current Rectification with a 100kHz B-SIT Step-Up Converter," IEEE Power Electronics Specialists Conference, 1984 Record, pp. 92-98 (IEEE Publication 84-CH-2073-5).
- [40] H. Kull, "Mains Rectifier Providing Nearly Sinusoidal Mains Current and Constant Output Voltage," International Powerconversion '80 (Sept. 1980, Munich, West Germany), pp. 2.5.1-13.
- [41] D. Chambers and D. Wang, "Dynamic P.F. Correction in Capacitor Input Off-Line Converters," Proc. Sixth National Solid-State Power Conversion Conference (Powercon 6), Miami Beach, FL, May 2-4, 1979, pp. B3.1-6.
- [42] S. Čuk, "General Topological Properties of Switching Structures," IEEE Power Electronics Specialists Conference, 1979 Record, pp. 109-130 (IEEE Publication 79CH-1461-3 AES).
- [43] S. Čuk, "Discontinuous Inductor Current Mode in the Optimum Topology Switching Converter," IEEE Power Electronics Specialists Conference, 1978 Record, pp. 105-123 (IEEE Publication 78CH-1337-5 AES).
- [44] S. D. Johnson and R. W. Erickson, "Steady-State Analysis and Design of the Parallel Resonant Converter," IEEE Power Electronics Specialists Conference, 1986 Record, pp. 154-165 (IEEE Publication 86CH-2310-1).
- [45] T. Wolpert, "Active Filter Technique for the Attenuation of Ac Ripple in Dc Power Plants and Distribution," Proc. Intelec '84, pp. 461-467 (IEEE Publication 84CH2073-5).

- [46] M. F. Schlecht, "Novel Topological Alternatives to the Design of a Harmonic-Free Utility/Dc Interface," IEEE Power Electronics Specialists Conference, 1983 Record, pp. 206-216 (IEEE Publication 83CH1877-0).
- [47] I. A. Khan and R. W. Erickson, "Control of Switched-Mode Converter Harmonic-Free Terminal Waveforms through Internal Energy Storage," IEEE Power Electronics Specialists Conference, 1986 Record, pp. 13-26 (IEEE Publication 86CH2310-1).
- [48] R. Mahadevan *et al.*, "A Converter with Three Switched-Networks Improves Regulation, Dynamics, and Control," Proc. Tenth International Solid-State Power Conversion Conference (Powercon 10), San Diego, CA, March 22-24, 1983, pp. E1.1-19.
- [49] C. W. T. McLyman, *Magnetic Core Selection for Transformers and Inductors*. New York: Marcel Dekker, Inc., 1982.